Brain Markers of Cumulative Stress Response and Allostatic Load in the Ageing Whitehall II Cohort



Enikő Zsoldos

Linacre College
University of Oxford

A thesis submitted for the Degree of Doctor of Philosophy

Brain Markers of Cumulative Stress Response and Allostatic Load in the Ageing Whitehall II Cohort

Enikő Zsoldos
Linacre College, University of Oxford

The Whitehall II (Stress and Health) study is a prospective study based on originally 10,308 British civil servants. Since 1985, rich socio-demographic, health and life-style measures have been acquired every 2-5 years. Eight hundred participants were randomly selected from the remaining 6,308 participants of Phase 11 for magnetic resonance imaging (MRI) and further examination in Oxford (2012-14).

There is evidence of changes in brain anatomy and mental health following traumatic events, such as combat stress or sexual abuse, in patients with post-traumatic stress disorder, mood or personality disorders, but little is known about the association between everyday stress, brain structure and function, and mental health in the general population. The secondary stress markers, Allostatic Load (AL) index, Framingham Stroke Risk score (FSRS) and Metabolic Syndrome (MetS) were selected as potential predictors of brain changes at follow-up. This thesis focuses on measures of structural grey and white matter (GM, WM) integrity, collected with the Siemens 3T Verio scanner in the first 563 participants of the Oxford study.

As hypothesised, stress markers measured as early as 20 years prior to the scan, predicted lower GM and WM integrity in older age. Unique linear relationships remained even after controlling for socio-demographic confounders between each stress marker and GM density but not with measures of WM integrity. This suggests that some, if not most variance is shared between the stress markers and the usual correlates of general health, such as age and employment class.

The three markers did not have equal power to predict brain measures: AL added more unique predictive variance to GM density than MetS and FSRS. On the other hand, FSRS was the more powerful predictor of poor WM integrity compared with AL and MetS, and after removing confounding variable effects.

This thesis thus provides some empirical support for the concept of allostatic load, linking ‘everyday’ stress and features of the ageing human brain.

This thesis contains approximately 40,000 words

A thesis submitted in partial fulfilment of the requirements for the degree of Doctor of Philosophy in the University of Oxford

Trinity Term 2016

Copyright © Enikő Zsoldos, 2016. All rights reserved.

Table of Contents

Acknowledgements viii

List of Abbreviations ix

List of Figures xi

List of Tables xiv

List of Publications and Presentations xvii

List of Publications arising from this thesis project xvii

Other Publications during the time of my DPhil xvii

Presentations: xviii

Chapter 1: Preface 1

1.1 Background 1

1.2 Overall aims 4

1.3 Individual chapter aims 4

Chapter 2: Stress Concepts in the Context of Ageing Research 7

2.1 Introduction 7

2.2 Defining 'stress' 8

2.3 Common and extreme stressors 9

2.4 The stress response 10

2.4.1 The Autonomic Nervous System (ANS) 10

2.4.2 The Hypothalamus-Pituitary-Adrenal (HPA) axis 11

2.5 The allostatic load and overload model of chronic stress 13

2.5.1 Biological ageing 14

2.5.2 Primary and secondary markers of allostatic load (AL) 15

2.6 Tertiary markers of AL and central role of the brain 21

Chapter 3: The Whitehall II Study and Imaging Sub-study 29

3.1 Introduction 29

3.2 The Whitehall II cohort 31

3.2.1 Background and importance 31

3.2.2 Data collection and sample description 32

3.3 Whitehall II Imaging Sub-study 34

3.3.1 Background and importance 34

3.3.2 Participant recruitment 35

3.3.3 Data collection 37

Chapter 4: Subjects + Out-of-scanner Methods 38

4.1 Introduction 38

4.2 Participants 38

4.2.1 Recruitment 38

4.2.2 Demographics 39

4.3 Out-of-scanner materials 41

4.3.1 Assessment of secondary markers of stress 41

4.3.2 Nuisance variables 52

Chapter 5: Imaging Methods and Analysis 60

5.1 Introduction 60

5.2 Background 60

5.2.1 MRI safety 60

5.2.2 Principles of MRI 61

5.2.3 Whitehall II Imaging Sub-study 65

5.3 Sequence parameters and analysis 67
5.3.1 T_1-weighted 67
5.3.2 Fluid Attenuated Inversion Recovery (FLAIR) 71
5.3.3 Diffusion Tensor Imaging (DTI) 75
5.4 Statistical analysis 82
5.4.1 Nuisance variables 83
5.4.2 Atlases 84
Chapter 6: Framingham Stroke Risk and Brain Structure 85
6.1 Introduction 85
6.1.1 Background 85
6.1.2 Aims and hypotheses 86
6.2 Methods 87
6.2.1 Sample characteristics, inclusion/exclusion criteria 87
6.2.2 Assessment of Framingham Stroke Risk Score (FSRS) 87
6.2.3 Assessment of nuisance variables 88
6.2.4 MRI Methods 88
6.2.5 Statistical analysis 90
6.3 Results 92
6.3.1 Descriptive statistics 92
6.3.2 VBM Results 96
6.3.3 TBSS Results 102
6.4 Discussion 111
6.4.1 Whole-brain grey matter 111
6.4.2 Whole-brain white matter 115
6.4.3 Qualitative comparison of grey and white matter results 119
6.4.4 Methodological limitations 119

Chapter 7: Metabolic Syndrome and Brain Structure 121

7.1 Introduction 121

7.1.1 Background 121

7.1.2 Aims and hypotheses 122

7.2 Methods 123

7.2.1 Sample characteristics, inclusion/exclusion criteria 123

7.2.2 Assessment of Metabolic Syndrome (MetS) Score 123

7.2.3 Assessment of nuisance variables 124

7.2.4 Statistical analysis 126

7.3 Results 127

7.3.1 Descriptive statistics 127

7.3.2 VBM Results 134

7.3.3 TBSS Results 139

7.4 Discussion 146

7.4.1 Whole-brain grey matter 146

7.4.2 Whole-brain white matter 149

7.4.3 Qualitative comparison of grey and white matter results 151

7.4.4 Methodological considerations 152

Chapter 8: Allostatic Load Index and Brain Structure 153

8.1 Introduction 153

8.1.1 Background 153

8.1.2 Aims and hypotheses 154

8.2 Methods 155

8.2.1 Sample characteristics, inclusion/exclusion criteria 155

8.2.2 Assessment of Allostatic Load (AL) Index 155

8.2.3 Assessment of nuisance variables 156

8.2.4 MRI Methods 157
8.2.5 Statistical analysis 158
8.3 Results 159
8.3.1 Descriptive statistics 159
8.3.2 VBM Results 166
8.3.3 TBSS Results 172
8.4 Discussion 173
8.4.1 Whole-brain grey matter 173
8.4.2 Whole-brain white matter 178
8.4.3 Discussion 179
8.4.4 Methodological considerations 179
Chapter 9: The Unique Effect of Secondary Stress Markers on Brain Structure 181
9.1 Introduction 181
9.1.1 Background 181
9.1.2 Hypothesis 183
9.2 Methods 183
9.2.1 Sample characteristics, inclusion/exclusion criteria 183
9.2.2 Assessment of secondary stress markers 184
9.2.3 Assessment of nuisance variables 186
9.2.4 MRI Methods 187
9.2.5 Statistical analysis 188
9.3 Results 189
9.3.1 Descriptive statistics 189
9.3.2 VBM Results 197
9.3.3 TBSS Results 199
9.4 Discussion 206

9.4.1 Whole-brain grey matter 206

9.4.2 Whole-brain white matter 207

Chapter 10: Conclusions 208

10.1 Summary of findings 208

10.1.1 Grey matter density 208

10.1.2 White matter integrity 210

10.1.3 Underlying mechanisms 211

10.1.4 Future research 213

10.1.5 Key summary points 215

References 216

Appendix 238

Acknowledgements

First and foremost, I would like to thank every participant of this thesis project - most of whom have never had an MRI scan before - for their 30 years of continued dedication to socio-medical sciences; and the many personal stories and pearls of wisdom they would trust me with following our lengthy testing sessions.

I would also like to acknowledge the UK MRC "Lifelong Health and Wellbeing" Programme for funding the Whitehall Imaging Sub-study and thus my research assistant post organising this large-scale project, and the University of Oxford Staff Learning Scheme for help with my DPhil fees.

Furthermore, for longitudinal Whitehall II data provided by Prof Mika Kivimäki, Prof Archana Singh-Manoux, Aida Sanchez and the University College London team; assistance with recruitment, and data collection by Abda Mahmood and Mandy Pipkin; MRI scanner operation, which I was also thoroughly taught by the FMRIB team of Radiographers; image pre-processing by Dr Nicola Filippini, Dr Ludovica Griffanti and MRI scan quality checks by Prof Klaus Ebmeier; secondary supervision by Prof Clare Mackay.

Professor Mark Jenkinson generously taught me the secrets of F-tests, and provided help and advice on FSL designs, analysis and presentation of results.

Special thanks to my supervisor Professor Klaus Ebmeier for entrusting me with the *unique*[1] opportunity to tackle a project of my own, *especially the project of my choice*, while providing invaluable and *stress-free* support throughout my time in Oxford.

Last but not least, I would like to thank my family for their tireless patience, sacrifice, and unconditional support always and especially during my long journey abroad.

[1] Unique: (1) being the only one of its kind, unlike anything else, (2) the remaining variance of a (statistical) association once the variance explained by covariates of no interest has been removed.

List of Abbreviations

%GM	Percentage Grey Matter
3T	3 Tesla
AD	Axial Diffusivity
AF	Atrial Fibrillation
AL	Allostatic Load
BET	Brain Extraction Tool
BIANCA	Brain Intensity Abnormality Classification Algorithm
CHD	Coronary Heart Disease
CRP	C-Reactive Protein
CSF	Cerebrospinal Fluid
CUREC	University of Oxford Central University Research Ethics Committee
CVD	Cardiovascular Disease
dMRI	Diffusion MRI
DTIfit	FMRIB's Diffusion Toolbox
FA	Fractional Anisotropy
FMRIB	Oxford Centre for Functional MRI of the Brain, University of Oxford
FNIRT	FMRIB Nonlinear Registration Tool
FLIRT	FMRIB Linear Image Registration Tool
FSL	FMRIB Software Library
FSRS	Framingham Stroke Risk Score
GLM	General Linear Model
GM	Grey Matter
GMD	Grey Matter Density
^{1}H	Hydrogen
HDL	High-Density Lipoprotein (cholesterol)
JHU	John Hopkins University (white matter atlases)
IL-6	Interleukin 6
LDL	Low-Density Lipoprotein (cholesterol)
LVH	Left Ventricular Hypertrophy
M	net magnetic moment
MD	Mean Diffusivity
MEMPR	Multi-Echo MPRAGE
MetS	Metabolic Syndrome
MNI	Montreal Neurological Institute
MPRAGE	Magnetization-Prepared Rapid Gradient Echo
MRI	Magnetic Resonance Imaging
MRC	UK Medical Research Council
MSD-IDREC	Medical Science Division Interdisciplinary Research Ethics Committee
MTL	Medial Temporal Lobe
PE	Phase Encoding
RD	Radial Diffusivity

SCID-I	Structured Clinical Interview for DSM-IV-TR Axis I Disorders, Research version
RF	Radio Frequency
VBM	Voxel-Based Morphometry
T2D	Type-2 Diabetes (Diabetes Mellitus)
TBSS	Tract-Based Spatial Statistics
TFCE	Threshold Free Cluster Enhancement
WM	White Matter
WMH	White Matter Hyperintensity

List of Figures

2.0 Overview of stress response systems (allostasis)

3.0. Schematic representation of Whitehall II Imaging Sub-study recruitment and testing protocol

4.0 Cardiovascular risk measured by Framingham Risk scores in the general population and Whitehall II (W-II) cohort

4.1 The estimated nonlinear change of allostatic load over time in 7,007 Whitehall II participants

5.0 Scans acquired on a healthy 76-year-old male Whitehall Imaging Sub-study participant (no neurological, cognitive or psychiatric illness) with different image weighting used in this thesis

5.1 Example of a study-specific grey matter mask for VBM analysis

5.2 Example of a) periventricular white matter hyperintensities (WMH) and b) deep white matter lesions seen in the FLAIR image of a Whitehall II Sub-study participant.

5.3 Diffusion ellipsoids are modelled for each voxel to produce a measure of the magnitude and directionality of diffusion

6.0 Flowchart of participant exclusion before final VBM (N = 405) and TBSS (N=395) analyses, including missing or inadequate scans and missing FSRS values

6.1 Framingham Stroke Risk Score (FSRS) distribution across five Whitehall II phases (P) in VBM analysis

6.2 Framingham Stroke Risk Score (FSRS) dsitribution across five Whitehall II phases (P) in TBSS analysis

6.3 Association of Framingham stroke risk (FSRS), measured at five phases, with lower whole-brain grey matter density

6.4 Association of Framingham stroke risk (FSRS), measured at five phases across 20 years, with whole-brain white matter measures

6.5 Regression plot of individual mean FA values extracted from the significant tract volume (y-axis), against FSRS calculated at Phase 11, after controlling for FSRS at Phase 3, x-axis ($p < 0.05$; tfce)

6.6 Widespread lower FA was associated with FSRS at time of scan

6.7 Regression plot of individual means of MD values extracted from the significant tract volume on y-axis ($p < 0.05$; tfce), against FSRS calculated at Phase 11, after controlling for all confounders in model III (x-axis)

7.0 Flowchart of participant exclusion before final VBM (N = 426) and TBSS (N=412) analyses, including missing or inadequate scans and missing FSRS values
7.1 Histogram of total Metabolic Syndrome (sum across five Whitehall II phases) distribution in whole-brain grey matter analysis (VBM)
7.2 Histogram of total Metabolic Syndrome (sum across fice Whitehall II phases) distribution in whole-brain white matter analysis (TBSS)
7.3 Histogram of change in Metabolic Syndrome between the sum of Whitehall II Phases 3+5 and the sum of Phases 9+11 in whole-brain grey matter analysis (VBM)
7.4 Histogram of change in Metabolic Syndrome between the sum of Whitehall II Phases 3+5 and the sum of Phases 9+11 in whole-brain white matter analysis (TBSS)
7.5 Cumulative metabolic syndrome status (calculated as the presence of total MetS over five phases) and its significant association with lower grey matter
7.6 Regression plot of individual mean grey matter density values extracted from regions (y-axis) with which total MetS is significantly (p < 0.05, tfce) associated, after controlling for all confounders of Model III (x-axis)
7.7 Significant lower FA and higher MD with cumulative Metabolic Syndrome (MetS)
7.8 Significant association between percentage total GM volume (%GM) and lower FA values (top) and between white matter hyperintensities (%WMH) and lower FA (bottom), even after controlling for cumulative MetS
7.9 Regression plot of individual mean FA values extracted from the significant tract volume (y-axis), against total MetS, after controlling for all confounders (model III), x-axis (p < 0.05; tfce)
7.10 Regression plot of individual means of MD values extracted from the significant tract volume on y-axis (p < 0.05; tfce), against total MetS after controlling for all confounders in model III (x-axis)

8.0 Flowchart of participant exclusion before final VBM (N = 378) and TBSS (N = 366) analyses, including missing or inadequate scans and missing FSRS values
8.1 Histograms of Allostatic Load (AL) index at both Whitehall II phases
8.2 Histograms of total Allostatic Load (AL) index
8.3 Histograms of Allostatic Load (AL) index change
8.4 Allostatic Load (AL) index and whole-brain grey matter (GM) analysis results
8.5 Regression plot of individual mean grey matter density values extracted from regions (y-axis) with which Phase 3 AL index is significantly (p < 0.05, tfce) associated, after controlling for all confounders of Model III (x-axis)
8.6 Allostatic Load index measured at Phase 3 was associated with whole-brain lower FA values

9.0 Flowchart of participant exclusion before final VBM (N=349) and TBSS (N=337) analyses, including missing or inadequate scans and missing secondary stress markers
9.1 Percentage Total Framingham Stroke Risk Score distribution in VBM (top) and TBSS (bottom) analyses
9.2 Total Metabolic Syndrome Score distribution in VBM (top) and TBSS (bottom) analyses
9.3 Total Allostatic Load Index distribution in VBM (top) and TBSS (bottom) analyses
9.4 F-test 1 of unique Metabolic syndrome or Allostatic Load index association with grey matter
9.5 Significant association of Allostatic Load index with lower grey matter density after controlling for Metabolic Syndrome, Framingham Stroke Risk score, and demographic and socioeconomic variables (t2)
9.6 F-test 3 of unique Framingham Stroke Risk score or Metabolic Syndrome association with FA values
9.7 Significant association of Framingham Stroke Risk score with lower FA (t5) and higher MD (t3 = t5) values after controlling for Metabolic Syndrome, Allostatic Load index, and demographic and socioeconomic factors
9.8 F-test 2 (top) of unique Framingham Stroke Risk score or Allostatic Load index and F-test 3 (bottom) of unique Framingham Stroke Risk score and Metabolic Syndrome association with widespread MD values

List of Tables

2.0 Overview of primary and secondary markers of the stress response and allostatic load at the Whitehall II study

3.0 Overview of Whitehall II & Whitehall II Imaging Sub-study measures

4.0 Overview of Whitehall II Imaging Sub-study recruitment statistics in Dec 2014

4.1 Whitehall II participant demographics at baseline Phase 1 (P1; 1985-88), at Phase 11 (P11; 2012-13) and at Oxford (2012-14)

4.2 Overview of secondary stress markers and their individual components at Whitehall II

4.3 Overview of secondary stress markers derived from Whitehall II data, and their availability longitudinally

5.0 Acquisition parameters of T1-weighted, FLAIR and dMRI images

5.2 An overview of DTI measures

6.0 Overview of percentage Framingham Stroke Risk Scores used in whole-brain grey matter analysis (N = 405)

6.1. Framingham Stroke Risk Study sample characteristics

6.2. Framingham 10-year Stroke Risk Score characteristics across five Whitehall II phases (P)

6.3 Framingham Stroke Risk score (FSRS) and whole-brain grey matter (GM) analysis results

6.4 Chi-square test for cross-table relationship

6.5 Framingham Stroke Risk score (FSRS) and whole-brain grey matter (GM) analysis results after controlling for age, sex, and ethnicity (Model II)

6.6 Framingham Stroke Risk score (FSRS) and whole-brain grey matter (GM) analysis results after controlling for all confounders (Model III)

6.7 Framingham Stroke Risk score and whole-brain fractional anisotropy (FA) analysis results

6.8 Framingham Stroke Risk score and whole-brain mean diffusivity (MD) analysis results

6.9 Framingham Stroke Risk score and whole-brain mean diffusivity (MD) analysis results after controlling for age, sex and ethnicity.

6.10 Framingham Stroke Risk score and whole-brain mean diffusivity (MD) analysis results after controlling for all confounders

7.0 Metabolic Syndrome components

7.1 Total and Metabolic Syndrome (MetS) change used in whole-brain grey matter analysis (N = 426) marked with black for mean (SD)

7.2 Metabolic Syndrome study sample characteristics
7.3 Percentage of metabolic syndrome across five Whitehall II phases (P)
7.4 Total times of Metabolic Syndrome binary yes/no score across all Whitehall II phases
7.5 Metabolic Syndrome (MetS) change across all phases
7.6 Cumulative (total) Metabolic Syndrome score (MetS) and whole-brain grey matter (GM) analysis results
7.7 Cumulative (total) Metabolic Syndrome score (MetS) and whole-brain grey matter (GM) analysis results after controlling for age, sex and ethnicity (model II)
7.8 Cumulative (total) Metabolic Syndrome score (MetS) and whole-brain grey matter (GM) analysis results after controlling for age, sex and ethnicity and socioeconomic variables (model III)
7.9 Cumulative Metabolic Syndrome (MetS) status and whole-brain fractional anisotropy (FA) analysis results
7.10 Cumulative Metabolic Syndrome (MetS) status and whole-brain mean diffusivity (MD) analysis results

8.0 Allostatic Load (AL) Index component scores
8.1 Allostatic Load (AL) Index at Phases 3 and 7, as well as total and AL index change used in whole-brain grey matter analysis (N = 378)
8.2. Allostatic Load Index Study sample characteristics
8.3 Prevalence of Allostatic Load index at Whitehall II Phases 3 and 7 for VBM and TBSS analyses
8.4 Total Allostatic Load index (P3+P7) prevalence at Whitehall II
8.5 Allostatic Load (AL) index change between Phases 3 and 7
8.6 Allostatic Load (AL) index and whole-brain grey matter (GM) analysis results
8.7 Allostatic Load (AL) index and whole-brain grey matter (GM) analysis results controlling for demographic factors (model II)
8.8 Allostatic Load (AL) index and whole-brain grey matter (GM) analysis results controlling for demographic and socioeconomic factors (model III)
8.9 AL index measured at Phase 3 associated with lower FA and higher AD values

9.0 Comparison of Metabolic Syndrome and Allostatic Load Index composite measure cut-offs
9.1 Average (SD) Framingham Stroke Risk and Allostatic Load indices at Phases 3 and 7
9.2 Unique effects of secondary stress markers study sample characteristics
9.3 Total times of Metabolic Syndrome binary yes/no score across Whitehall II Phases 3 + 7
9.4 Total Allostatic Load index prevalence in VBM and TBSS analysis

9.5 F-test 1 of unique Metabolic syndrome (MetS) or Allostatic Load (AL) index association with grey matter density (GMD)

9.6 Significant association of Allostatic Load (AL) index with decreased grey matter density (GMD) after controlling for Metabolic Syndrome (MetS), Framingham Stroke Risk score (FSRS), and demographic and socioeconomic variables (t2)

9.7 F-test 3 of unique Framingham Stroke Risk score (FSRS) and Metabolic syndrome (MetS) association with Fractional Anisotropy (FA) values

9.8 Significant association of Framingham Stroke Risk (FSRS) with decreased FA values after controlling for Metabolic Syndrome (MetS), Allostatic Load (AL) index, and demographic and socioeconomic variables (t5)

9.9 F-test 2 (top) of unique Framingham Stroke Risk score (FSRS) or Allostatic Load (AL) index and F-test 3 (bottom) of unique Framingham Stroke Risk score (FSRS) and Metabolic Syndrome (MetS) association with Mean Diffusivity (MD) values

9.10 Significant association of Framingham Stroke Risk score (FSRS) with higher MD values after controlling for Metabolic Syndrome (MetS), Allostatic Load (AL) index, and demographic and socioeconomic variables (t3 = t5)

List of Publications and Presentations

List of Publications arising from this thesis project

Allan CL, **Zsoldos E,** Filippini N, Sexton CE, Topiwala A, Valkanova V, Singh-Manoux A, Tabák AG, Shipley MJ, Mackay CE, Ebmeier KP, Kivimäki M. Lifetime hypertension as a predictor of brain structure in older adults: a cohort study with a 28-year follow up. **Br J Psychiatry** 2015 Apr; 206(4): 308-15; **Chapters 2 & 6**

Allan CL, **Zsoldos E** & Ebmeier KP. Imaging and neurobiological changes in late-life depression. **Br J Hosp Med (Lond).** 2014 Jan;75(1):25-30; **Chapters 2 & 6**

Andersson JL, Graham MS, **Zsoldos E**, Sotiropoulos SN. Incorporating outlier detection and replacement into a non-parametric framework for movement and distortion correction of diffusion MR images. **Neuroimage**. 2016 Nov 1;141:556-72;**Chapters 5-9**

Ebmeier KP, Allan CL, Topiwala A & **Zsoldos E.** Psychosocial Factors, Mood Disorders and Risk of Cognitive Impairment and Dementia. Chapter 16 in: Kivimäki M, Batty CG, Kawachi I. & Steptoe A. **Handbook of Psychosocial Epidemiology**. Routledge, Taylor & Francis Group: London; 2017; **Chapter 2**

Ebmeier KP, Heise V & **Zsoldos E.** The biology of ageing. In Goodwin GM, Geddes J, & Andreasen N. **New Oxford Textbook of Psychiatry, Third Edition**, Oxford University Press, 2017; **Chapter 2**

Filippini N, **Zsoldos E**, Haapakoski R, Sexton CE, Mahmood A, Allan CL, Topiwala A, Valkanova V, et al, Kivimäki M & Ebmeier KP. Study protocol: The Whitehall II imaging sub-study. **BMC Psychiatry**. 2014 May 30; 14:159; **Chapters 4-9**

Zsoldos E & Ebmeier KP. Aging and Psychological Stress. Chapter in: G. Fink (ed.) **Handbook of Stress, 1st Volume**: Stress Concepts, Cognition, Emotion and Behavior. Elsevier, New York, 2016; **Chapter 2**

Zsoldos E, Mahmood A & Ebmeier KP. Occupational stress, bullying and resilience in old age. **Maturitas**. 2014 Jun; 78(2): 86-90; **Editor's Choice Award; Chapter 2**

Other Publications during the time of my DPhil

Allan CL, Sexton CE, Filippini N, Topiwala A, Mahmood A**, Zsoldos E**, Singh-Manoux A, Shipley MJ, Kivimaki M, Mackay CE, Ebmeier KP. A MRI study examining sub-threshold depressive symptoms within the Whitehall II cohort. **J Affect Dis** 2016 204, 219-225

Griffanti L, Salimi-Khorshidi G, Beckmann CF, Auerbach EJ, Douaud G, Sexton CE, **Zsoldos E**, Ebmeier KP, Filippini N, Mackay CE, Moeller S, Xu J, Yacoub E, Baselli G, Ugurbil K, Miller KL & Smith SM. ICA-based artefact removal and accelerated fMRI acquisition for improved resting state network imaging. **Neuroimage**. 2014 Jul 15; 95:232-47. Epub 2014 Mar 21.

Topiwala A, Allan CL, Valkanova V, **Zsoldos E**, Filippini N, Sexton CE, Mahmood A, Singh-Manoux A, Mackay CE, Kivimäki M, Ebmeier KP. Resilience and MRI correlates of cognitive impairment in community dwelling elders. **Br J Psychiatry** 2015 207(5): 435-439. Sep 3. Epub ahead of print

Presentations:

Zsoldos E et al (2015) Cumulative Framingham Stroke Risk in mid-life predicts poor brain integrity and memory performance in later life. Whitehall II 30th Anniversary Event, 8 December, University College London, London

Zsoldos E (2015) The Whitehall Imaging Study. Oxford Hungarian Society Young Researchers in Oxford guest speaker, 6 November, Oxford, UK; **Invited speaker**

Zsoldos E et al (2015) Framingham Stroke Risk Score: Biomarker of Biological Brain Aging in Community-Dwelling Older Adults. Organisation for Human Brain Mapping, 14-18 June, Honolulu, Hawaii, US; **Linacre House Trust Travel Grant Recipient**

Zsoldos E et al (2015) Chronological and Biological Ageing: Predicting grey matter density by age and Framingham Stroke Risk Scores in community-dwelling older adults. Society of Biological Psychiatry's 70th Annual Meeting, 14-16 May, Toronto, Ontario, Canada; **Guarantors of Brain Travel Award Recipient https://f1000research.com/posters/1098128**

Zsoldos E, Sexton CE, Filippini N et al (2014) Life events with contextual threat and brain structure in older adults. Society of Biological Psychiatry Annual Meeting, 9-11 May, NY, US: **https://f1000research.com/posters/1095552**

Zsoldos E, Sexton CE, Filippini N et al (2013) Reduced hippocampal size in old age after being a victim of violent crime or having financial difficulties. Society of Neuroscience Annual Conference, 9-13 November, San Diego, US

Chapter 1: Preface

1.1 Background

The *Whitehall II study, also known as the Stress and Health Study*, is an on-going prospective study conducted at University College London, based on 10,308 British civil servants aged 35-55 at baseline (Phase 1), of whom 6,895 were men. The cohort has been followed up at regular intervals since 1985 (Phase 1) to explore the relationship between socioeconomic factors, (occupational) stress and cardiovascular disease, and has made valuable contributions to clinical science and public policy in the UK and worldwide. Since Phase 1, self-administered questionnaires on lifestyle, psychosocial factors, behaviour, and physical, mental and social functioning, and clinical data of biological measures and mental and physical health have been collected every two to five years with a high rate of participation. 25 years after the study started, 74% of participants who took part in Phase 11 (2012-2013) were over 65 years old and retired, which shifted the focus on investigating age-related individual heterogeneity and its distribution by socioeconomic strata.

The *Whitehall II Imaging Sub-study* was set up in January 2012 to image 800 Whitehall II participants randomly recruited at Phase 11, by January 2017. The study combines some of the longitudinal data accumulated by the Whitehall II study with comprehensive information collected at the University of Oxford on cognitive, mental and physical functioning and brain structure and function using multi-modal magnetic resonance imaging (MRI) techniques. Accurate retrospective data are

typically not available in imaging studies, as participants tend not to remember information accurately and biological measures were not taken. Thus, the project provides an opportunity to study individual mid-life factors that contribute to or predict the non-universal decline seen in the ageing brain.

When I set out on defining a DPhil project within the Whitehall II Imaging Sub-study, an obvious and important topic was the *effect of stress on the ageing brain*. Since *'stress'* refers to multiple concepts, defining the term within the Whitehall II cohort was the first step. Adverse health effects of stressful or traumatic events are well established, e.g. in PTSD or major depression. A couple of pilot projects followed on the effects of childhood adversity and common or unexpected stressful life events on structural brain measures in older age (see for example: https://f1000research.com/ posters/%201095552). The majority of these yielded no findings, most likely because of plastic changes that might have taken place between the event and time of scan, which in some cases was taken as many as 80 years after the event. Thus, the next step was to identify biological markers that are said to directly capture the effects of stress (response) on the body and brain.

The repeated occurrence of *psychosocial stressors* leads to the *physiological dysregulation* of systems involved in the *stress response*. Effects of *cumulative* stress response can be summarised in the *allostasis* and *allostatic load and overload* model. Stressful (internal or external) events require temporary adaptations of the whole body (allostasis) in order to maintain homeostasis. Cumulative disturbance of homeostasis leads to syndromes that are triggered by the dysregulation of the stress response (allostatic load), and are represented by primary, secondary and tertiary

markers (allostatic overload). The model assumes the prominent role of certain *brain structures*, such as the amygdala, hippocampus and prefrontal cortex, as *regulators*, and sympathetic-adrenal-medullary axis release of catecholamines and hypothalamic-pituitary-adrenal axis secretion of glucocorticoids as *effectors*. Excessive adaptations to allostatic load can lead to peripheral organ damage and in *plastic changes in certain brain structures* (allostatic overload) that *perpetuate maladaptive responses.*

Secondary markers, such as the Framingham Stroke Risk score, Metabolic Syndrome and Allostatic Load index are composite measures of cardiovascular, metabolic and immune markers of the *chronic* stress response and allostatic load. They have an increased presence in association with adverse psychosocial stressors, such as low socioeconomic status or occupational stressors, thus *are related to stress upstream*; and are said to be better predictors of health outcomes and mortality than their individual components, therefore *are related to illness downstream*. The Framingham Stroke Risk score is an established multi-measure risk profile that gives the 10-year probability of a stroke, therefore is directly related to structural brain measures, and is routinely used in the clinic. The presence of metabolic syndrome is associated with an increased risk of cardiovascular disease and type-2 diabetes. Clinicians increasingly recognise its medically translational value, although slight variations in its computation exist. Allostatic load index is the least well-defined secondary marker, but it tends to be a combination of both primary- and secondary markers of the chronic stress response. Since the allostatic load model presumes the prominent role of certain brain structures in allostasis, which can also be damaged by the stress response, it provides a plausible theoretical framework for assessing

the effect of stress on brain structure in older age. Importantly, composite measures of Framingham Stroke Risk score, Metabolic Syndrome and Allostatic Load index are longitudinally available for the Whitehall II study.

1.2 Overall aims

Thus, this thesis aims to link longitudinally available secondary markers of the chronic stress response and allostatic load to cross-sectional structural brain integrity, i.e. measures of local grey matter density or volume, white matter microstructure, and volume of white matter lesions, on a voxel-wise basis across the whole brain, in ca. 500 community-dwelling older Whitehall II participants. It aims to examine: 1) whether these hypothesised markers in mid-life are able to predict patterns of abnormalities in grey and white matter in later life; 2) whether they are predictive of abnormalities in certain brain regions beyond standard confounding variables such as demographic and socioeconomic factors, and 3) whether they represent the same construct or have each a unique independent role beyond the two others.

1.3 Individual chapter aims

Chapter 2 introduces the stress concepts in the context of ageing (brain) research. It presents the definition and an overview of stress, common stressors, and the stress response before placing them within the allostatic load and overload model of chronic stress. Finally, primary, secondary and tertiary markers are described, with a focus on the human brain.

Chapter 3 provides a succinct introduction to the Whitehall II study, including its history, and description of sample and data structure.

Chapter 4 provides an introduction to the Whitehall II Imaging Sub-study, including participant recruitment and demographics, and the out-of-scanner methods, including the assessment of secondary stress markers at the Whitehall II study. It also aims to provide a summary of nuisance variables and their assessment, and the statistical concept of confounding and mediating variables.

Chapter 5 summarises the principles of MRI, as a non-invasive brain imaging method, the sequence parameters of the Whitehall II Imaging Sub-study scans and the statistical methods that are used in this thesis.

Chapter 6 examines whether there is an association between Framingham Stroke Risk score across five Whitehall II study phases and structural brain integrity at follow-up in older age, namely grey matter density and white matter microstructure, and if so, whether they remain associated even after the effects of demographic and socioeconomic confounding factors have been removed. Furthermore, it also aims to assess how far back in time Framingham Stroke Risk predicts brain structure. Finally, it tries to explore whether the association of white matter microstructure measures, namely fractional anisotropy, with Framingham Stroke Risk may be due to Wallerian degeneration or regional white matter changes.

Chapter 7 examines whether there is an association with Metabolic Syndrome across five Whitehall II study phases and grey matter density and white matter microstructure integrity at follow-up in older age, and whether this link remains

present after controlling for confounding variables. Finally, it aims to explore whether fractional anisotropy associated with Metabolic Syndrome may be due to Wallerian degeneration or regional white matter changes.

Chapter 8 examines whether there is an association between Allostatic Load index across two Whitehall II study phases and grey matter density and white matter microstructure integrity at follow-up in older age, and whether it remains present beyond the effect of confounding variables. Furthermore, it also aims to assess how far back in time Allostatic Load index predicts brain structure. Finally, it explores whether white matter microstructure measures, namely fractional anisotropy, associated with Framingham Stroke Risk may be due to Wallerian degeneration or regional white matter changes.

Chapter 9 examines, whether each secondary marker's unique variance not shared with the other two and with demographic or socioeconomic confounders explains a unique portion of structural brain integrity measures in older age.

Chapter 10, finally, summarises the main findings of this thesis and provides suggestions for future research.

Chapter 2: Stress Concepts in the Context of Ageing Research

> "Stress is the salt of life. The absence of stress is death. Only the dead has no stress." – János Selye, 1976
>
> "Any concept that covers such a broad scope of life circumstances as does this particular term is bound to be somewhat complex. Yet at its heart the notion of stress is also very simple. It unifies a vast array of human responses into a single concept with which people strongly identify." **-** John Kabat-Zinn, *Full Catastrophe Living (2004)* p. 235 (1))
>
> "If I could get back my youth, I'd do anything in the world except get up early, take exercise and be respectable." – Oscar Wilde, *The Picture of Dorian Gray*

The construct of Allostatic Load links ageing and psychological stress. It is based on the notion that a repeated and cumulative disturbance of homeostasis may lead to certain syndromes triggered by a dysregulation of the chronic stress response. Chapter 2 provides a summary of the markers of this hypothetical process at its primary, secondary and tertiary stages, with particular attention to brain mechanisms that are in this pathway or are even instrumental to such dysregulation and its pathological consequences. Since cumulative stress and allostasis are highly correlated with chronological age, the concept of biological ageing is also introduced.

2.1 Introduction

Chronic psychosocial stress leads to physiological dysregulation, worsening of disease trajectories and accelerated biological ageing (2-4). During extraordinary

(*stressful*) events the organism adapts its internal milieu to maintain homeostasis (*allostasis*). The repeated demand for allostasis and subsequent dysregulation of the stress response over time (*allostatic load*; the biological cost of adapting to stress (5)) leads to syndromes associated with peripheral organ damage, and plastic changes in brain structures that are regulators or targets of the stress response and may therefore perpetuate maladaptive responses (*allostatic overload*; (6)). Individual differences at any stage of these mechanisms may influence the vulnerability to or resilience against stress-related diseases (7).

2.2 Defining 'stress'

In popular perception and everyday life, the term '*stress'* has been frequently used to describe both an external environment and an internal state or feeling. This confusion is most likely due to the lack of clear academic definition of the concept. The endocrinologist János Selye was the first to coin the term (8). He described *stress* as the body's non-specific response to a *stressor*; a real or imagined stimulus that exerts demands on the organism, thus causing stress (9) Stressors can have either short or long-term effects. The former comprise acute, time-limited events, while the latter may have long-lasting effects that subside over time. Examples include certain life-events (10), changes that are chronic and require the restructuring of identity or social roles (e.g. becoming a caregiver (11)), or are traumatic with lasting physiological and psychological effects (e.g. childhood maltreatment (12, 13), sexual assault (14) or combat stress (15)). Stress can be negative (*distress*) or positive ('*eustress'*), the latter increasing performance. Albeit individual variability exists in

the perception of stress, both distress and eustress may pose a threat to the organism's internal steady state (homeostasis) (3, 16, 17).

2.3 Common and extreme stressors

Common stressful psychosocial and environmental factors, such as socioeconomic status and workplace stressors, are predictors of cardiovascular outcomes (18-20) and mortality (21). While attempts to relate specific stressors to certain medical problems have been unsuccessful, stress remains an underlying theme in the development and course of virtually all physical illness (8). The diathesis-stress model, combining predisposition with environmental impact (22, 23) and the allostatic load model (2), provide an explanatory framework for research into cumulative psychosocial factors and resulting illness. Distant predisposing childhood, environmental, personal or genetic factors act together with current stressors, to result in psychological disorder (24, 25). Distant or current risk factors may not lead to a disorder on their own, and in addition they often interact with protective factors, such as childhood attachment style (26), healthy self-esteem and a close network of friends, to increase resilience against developing disorders (20, 27).

Unexpected, traumatic events exerting acute, sudden or intense stress do not only overwhelm coping mechanisms (28), but may also be associated with psychopathology, such as posttraumatic stress disorder (PTSD) (29) or major depression (30). *Extreme* stressors can affect brain structures, such as the hippocampus, amygdala, anterior cingulate cortex, and medial frontal gyrus (10). In people with PTSD or major depression, early life events, such as childhood neglect or trauma, can result in structural and functional brain changes (31). Recent evidence

suggests that brain changes seen in psychopathology may be causal to its manifestation (32, 33).

2.4 The stress response

The amygdala evaluates stressors and relays relevant information to the hypothalamus, which delivers the *stress response*. This utilizes two major pathways, the *autonomic* component of the peripheral *nervous system (ANS)*, and the *hypothalamus-pituitary-adrenal (HPA) axis* of the central nervous system (7) (for an overview see Figure 2.0).

2.4.1 The Autonomic Nervous System (ANS)

The ANS supplies the internal organs of the body, hence the 'visceral nervous system'. It controls involuntary body functions, such as breathing, heartbeat, blood pressure, the dilation and constriction of blood vessels and bronchioles, and certain visceral reflex actions. It is associated with the fight-or-flight response, and responds to stressors via the catecholamine hormones and neurotransmitters adrenaline and nor-adrenaline, secreted by the adrenal medulla of the sympathetic-adrenal-medullary (SAM) axis (34, 35). The ANS consists of a sympathetic and parasympathetic branch. The *sympathetic ANS* is responsible for energizing the body for immediate mobilization through glucose and fat release, and the release of proteins from non-exercising muscle. At the same time it inhibits vegetative functions, such as long-term energy storage, through suppressing insulin levels, and growth, repair and reproduction. The parasympathetic ANS generally counteracts sympathetic ANS activity.

2.4.2 The Hypothalamus-Pituitary-Adrenal (HPA) axis

The HPA-axis is the slower, *neuroendocrine* pathway of the stress response system, and culminates in the production of glucocorticoids by the adrenal cortex (Figure 2.0). Neurons in the medial parvocellular region of the paraventricular nucleus of the hypothalamus produce and release corticotropin-releasing hormone (CRH) and arginine vasopressin (AVP) (7), which in turn trigger the release of adrenocorticotropic hormone (ACTH) from the anterior pituitary gland. The anterior pituitary gland acts on the adrenal cortex to release the glucocorticoids hydrocortisone (commonly known as cortisol) and corticosterone. Cortisol regulates cardiovascular function and it blocks the storage and aids the conversion of fats, proteins and carbohydrates to energy. Corticosterone regulates immune responses and acutely suppresses inflammation (36-38). Once a perceived stressor has subsided, the system returns to its baseline homeostasis via feedback loops triggered at various levels. Glucocorticoid receptors are expressed throughout the brain and the HPA-axis. They have the ability to regulate gene expression, and thus have potentially long-lasting effects on the brain regions that regulate their release (7).

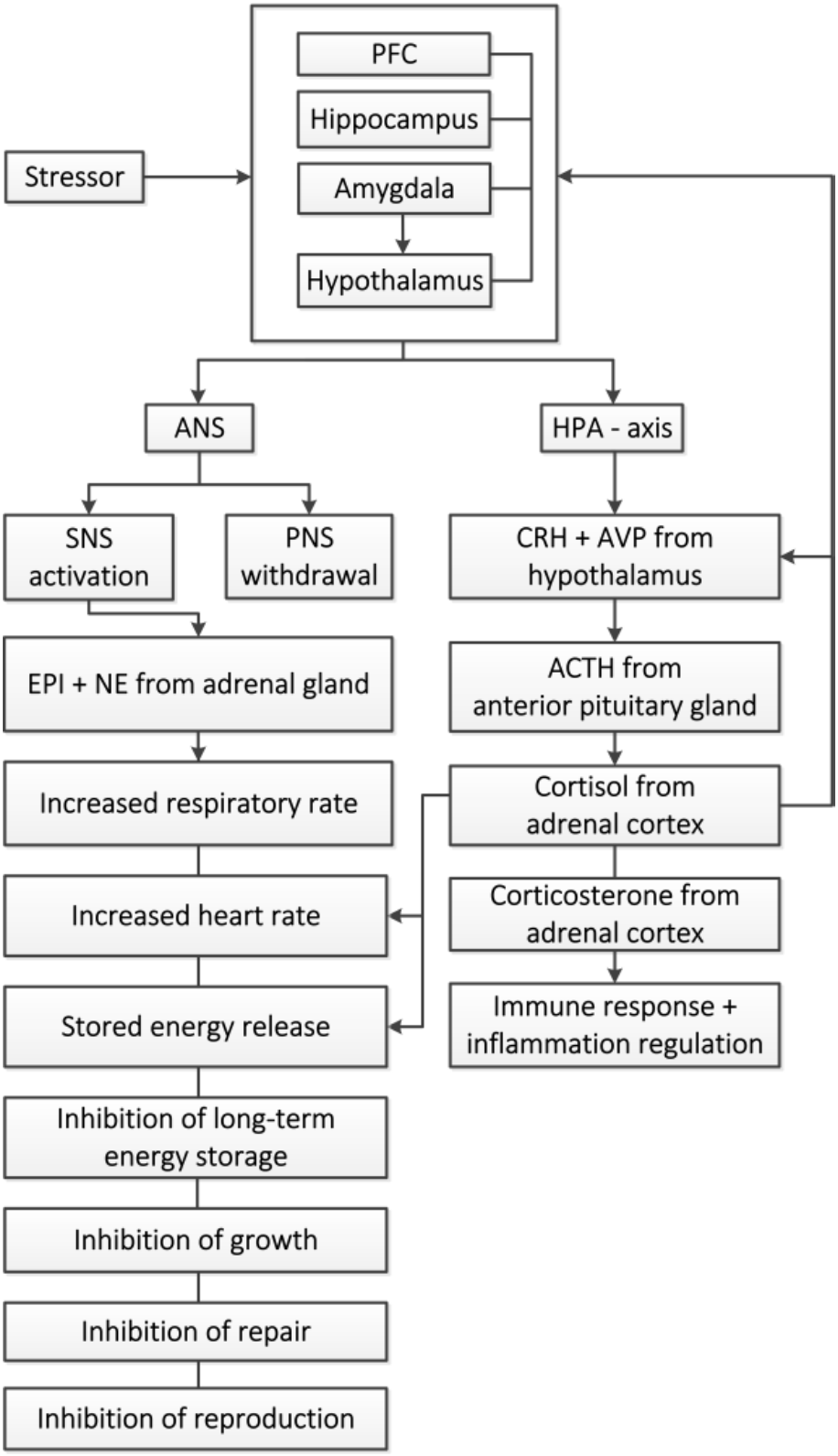


Figure 2.0 Overview of stress response systems (allostasis).

PFC: prefrontal cortex, ANS: autonomic nervous system, SNS: sympathetic nervous system, EPI: epinephrine (=adrenalin), NE: norepinephrine (=noradrenalin), HPA: hypothalamic-pituitary-adrenal, CRH: corticotropin-releasing hormone, AVP: argenine vasopressin, ACTH: adrenocorticotropic hormone. Reproduced from Zsoldos & Ebmeier (6) with the publisher's permission (Elsevier Books, License number: 3961920666436).

2.5 The allostatic load and overload model of chronic stress

Any stressor, no matter how small, requires temporary adaptations of the internal milieu and shift in its homeostasis. This process is termed *allostasis*, and it mainly affects systems involved in the stress response (4, 39). In response to a stressor components of the ANS and HPA-axis change their physiological response within a normal range of values. Markers of the stress response that participate in allostasis are able to regulate the activity of other markers, by linking together in a nonlinear regulatory network. Chronic allostasis, however, can be damaging, leading to wear and tear, in other words *allostatic load (AL)* and *overload* (3, 40).

This can result in damage to one or many parts of the body that are involved in the stress response and allostasis (3, 41, 42). Vulnerability or resilience against stress-related diseases will vary at the individual level (43). It is said that AL and overload occur when responses chronically deviate from the normal physiological range, because of *1)* repeated exposure to multiple stressors, *2)* lack of response adaptation, *3)* prolonged allostatic response even after the stressor subsided, or *4)* inadequate stress response (3, 42). Allostatic overload is refined as 'Type I allostatic overload', which occurs if "energy demands exceed energy income and what can be mobilized from body stores" and is said to be more common in developing countries (3). 'Type II allostatic overload' occurs if "energy demands are not exceeded and the organism continues to take in or store as much or even more energy than it needs. This may be a result of stress-related food consumption, choice of a fat-rich diet, or metabolic imbalances (pre-diabetic state) that favors fat deposition." (3)

The AL-model of chronic stress assumes the prominent role of certain brain structures, such as the hippocampus, amygdala, and prefrontal cortex as *regulators*, and the SAM-axis release of catecholamines and the HPA-axis secretion of glucocorticoids as *effectors* (2). Both an under- and overactive ANS and HPA-axis can be a feature of AL (38). Excessive adaptations to AL can lead to plastic changes in the brain structures that are said to be regulators of the stress response, and in turn perpetuate maladaptive responses.

2.5.1 Biological ageing

Although there is naturally no consensus about the age at which a person becomes 'old', in most western countries this is considered to be the retirement age of 60+ years. The percentage of the world's population over sixty will increase from 12% to 22% between 2015 and 2050 (44). While chronic diseases are generally associated with chronological age, the progressive loss of ability to deal with stress and the development of age-related distress occur at individually different rates. Psychological distress seems to accelerate the onset of age-related diseases, such as dementia and late-onset depression (first depressive episode over 60 years of age (45)), which might be due to the continued allostatic response even after the stressor has subsided (43). Both acute psychosocial stress in old age, such as workplace bullying (46), and chronic stress accumulated over the lifespan result in consequent physiological dysregulations, which has been described as "catalysts of accelerated aging and agitators of disease trajectories" (2). Chronic dysregulation of the stress response gives rise to *secondary markers of the stress response* (detailed in section 2.6), which in turn increase risk of pathological brain changes, impaired

cognitive function in late-life (47, 48) and Alzheimer's disease (49). Thus the gradual decline of homeostatic mechanisms that lead to physiological dysregulation and over time the wear-and-tear of the body can be thought of as *biological ageing* (50, 51).

2.5.2 Primary and secondary markers of allostatic load (AL)

Stress hormones and their antagonists, in conjunction with pro- and anti-inflammatory cytokines, such as interleukine-6 (IL-6) and tumor necrosis factor-alpha (TNF-α), form the *primary markers* (also referred to as stress response 'mediators' or 'biomarkers') of allostatic load (see Table 2.0) (3, 15). While their increase is adaptive in the short run, their prolonged secretion can damage both brain and body (42).

Markers of the stress response and allostatic load (AL)	
Primary	C-reactive protein, interleukin-6, cortisol, tumor necrosis factor-alpha
Secondary	Systolic BP, diastolic BP, prior cardiovascular diseases, hypertensive medication, diabetes mellitus, diabetes medication, fasting glucose, waist circumference, weight, fat mass, percentage body fat, serum triglycerides, low high-density lipoprotein cholesterol, high low-density lipoprotein cholesterol, blood cholesterol, BMI, glycated hemoglobin, age, cigarette smoking.

Table 2.0 Overview of primary and secondary markers of the stress response and allostatic load at the Whitehall II study (52)

Secondary markers of the stress response and allostatic load (Table 2.0) result from these primary stress responses, and increase risk of stress-related disease trajectories such as towards hypertension, coronary heart disease, stroke, angina pectoris, Type-2 diabetes, metabolic syndrome, autoimmune diseases, chronic fatigue syndrome or major depression (e.g. (4, 34). They include composite measures of cardiovascular, metabolic and inflammatory changes, e.g. *Framingham risk scores*, the *metabolic syndrome* or the *allostatic load index* that shift their operational ranges during allostasis, and may sustain allostatic load even at sub-clinical levels (6). Secondary markers are better predictors of physical, mental and cognitive health and mortality risk than individual markers of the stress response and allostatic load (53, 54). They are associated with low social status in child- and adulthood, capturing the long-term effect of chronic stressors, which have a higher prevalence in low socioeconomic strata (6) – for an overview see Appendix A. They can, therefore, be viewed as functional biomarkers of the biological ageing pathway from life stresses to Type II allostatic overload and ill health in epidemiological research (55).

2.5.2.1 Cardiovascular Health and Risk

Health effects of stressors have been most extensively researched in association with cardiovascular health and risk, including hypertension, and disease, especially at the work place (56). Job-strain, effort-reward imbalance, job insecurity, unfairness, overtime work, self-reported adverse effects of stress on health, cortisol secretion patterns, and depressive symptoms affect cardiovascular health negatively (Appendix A). High blood pressure reactivity in response to psychological stress (e.g. occupational stress including job structure and work environment (57) or laboratory stressors ("white coat syndrome" (58)) is associated with a higher risk of future

hypertension and an increased neural activation in response to a stress task in brain areas that control cardiovascular function (59). Furthermore, lifetime hypertension predicts brain structure and cardiovascular health 28 year later (60). Multifactorial cardiovascular and stroke risk scores, such as the *Framingham risk scores* (61) predict cognitive decline (62, 63), grey matter volume reduction (64), and white matter changes in the brain (65). Vascular risk factors measured by the Framingham stroke risk score in mid-life predict increased rates of vascular brain damage, global and hippocampal atrophy and decline of executive function over 10 years (62), and lower global cognition, memory and executive function at 4- and 8-years follow-up in middle-aged and older participants (64).

2.5.2.2 Metabolic syndrome

Metabolic syndrome conceptually links the cardiovascular and (neuro-) endocrine systems. It is defined by the following biomarkers of the stress response and allostatic load: increased abdominal circumference, increased levels of triglycerides, decreased levels of high-density lipoprotein (HDL) cholesterol, and elevated blood pressure (pre-hypertension) and fasting glucose levels (pre-diabetes). Metabolic syndrome is diagnosed if at least three of these markers are above defined thresholds (66). Low socioeconomic status, unfairness, and occupational stress (e.g. organisational justice, job strain) are predictors of metabolic syndrome (e.g. (67) see Appendix A). In turn, metabolic syndrome predicts diabetes, cardiovascular disease (68), telomere shortening (43), severe mental disorders (69), incident stroke (70) and mortality rates (71). Even if most biomarkers are at subclinical levels, they can increase the risk of heart disease, cognitive decline, decline of physical functioning, mortality and the onset of depressive symptoms (53).

Individual metabolic syndrome components are known to impact the human brain adversely. For instance, high normal fasting blood glucose levels are associated with lower grey and white matter volumes in the frontal cortex that correlate with cognitive performance in men (72). Little is known of their combined effect on the brain, or whether the number of components leads to a 'dose effect' and drive brain changes (73). In a single study of middle- to older aged participants with metabolic syndrome, significant grey matter volume reductions in the right nucleus accumbens as well as reduced cortical thickness in distinct areas of both hemispheres were present (74). Clinical vascular brain damage in the form of periventricular white matter hyperintensities and subcortical white matter lesions in middle-aged individuals (73), reduced white matter integrity in fronto-temporal regions (75), and silent brain infarction in older individuals (73) are also seen in metabolic syndrome.

2.5.2.3 Allostatic load (AL) index

There is no consensus about the exact combination of biomarkers that define the *allostatic load (AL) index* (2, 3) or the way it is computed (76, 77). It tends be a combination of both primary and secondary markers, including metabolic syndrome components (Table 2.0 and Appendix A). Psychosocial factors in combination, including those at work, predict high levels of the AL index (78). A recent systematic review of nine cross-sectional studies found that occupational stress was positively associated with AL index, in spite of the lack of consensus on its computation and the heterogeneity in study methods and quality (77). Low socioeconomic status is associated with higher AL index across the lifespan (79), due to the prevalence of stressors being higher in low socioeconomic groups. A recent community-based prospective cohort study of middle-aged adults found that material possessions,

such as car or house ownership, and smoking, but not other health behaviours (physical activity or alcohol consumption), or psychological factors, statistically mediated the relationship between low socioeconomic status and high AL index (80). Adversity-triggered chronic physiological dysregulation in childhood, such as living in a poor neighbourhood, has delayed negative effects on AL index levels in adulthood (81). However, an affluent environment in adulthood can attenuate this effect. Sex differences in the association of socioeconomic status and life-style with AL index have been found previously (82). Women with a low occupational position have higher AL (low vs. high OR = 3.99, 95%CI [1.22, 13.05]), while the opposite is true for men (middle vs. high OR = 0.48, 95%CI [0.23, 0.99]). Heavy drinking in men and abstinence in women is associated with higher AL index compared with moderate drinkers. Higher education level, physical activity and low salt intake seem to be protective against high AL in both sexes (82).

Combinations of physiological markers of wear-and-tear are usually better predictors of brain structure and function than any of the secondary markers on their own (53), see Appendix A, thus proving useful indicators of risk of subsequent poor health or function. There are, however, also conflicting reports. AL index is a significant predictor of total brain and white matter, but not grey matter volumes (83), general cognitive ability, but not memory (83), and physical decline, cardiovascular disease and mortality in older adults (53). Mechanisms in which primary and secondary markers come together to predict brain changes (84) or cognitive decline (85), and what role gender plays in these (86), needs further clarification (87).

2.5.2.4 Qualitative evaluation of the allostatic load / overload model

The *allostasis and allostatic load/overload model* provides a theoretical framework for individual adaptation under stress but it lacks empirical evidence. Delineating time-courses of dysregulation (40, 88) and quantification of AL at a biological level, let alone with respect to the multiplicity of psychosocial contributing factors (84) is a major challenge posed by the model. The complexity of AL as a construct has been demonstrated by research in the last decade (2). For example, cardiovascular outcomes have been linked to job strain and socioeconomic status (SES) in the Whitehall II cohort (Appendix A), but a cross sectional study of 972 individuals aged 54 years and older found no support "for the hypothesis that chronic stress, via sustained activation of stress-related autonomic and neuroendocrine responses, is an important mediator in the relation between SES and health outcomes. Most notably, "lower SES was not associated with higher basal levels of cortisol in either men or women" (89). The underlying allostatic processes that are said to link psychosocial stress to health need to be characterized in detail (90).

This lack of detailed mechanistic explanation has been used to argue that the AL concept does not add heuristic value to the currently used concept of stress (stressors, stress response, homeostasis) (91). Alternative models include the *adaptive calibration model*, which examines whether early life experiences need to be assessed as adaptive or maladaptive to the stress system (26, 92). In this case, stress is defined as an event or change in environment that elicits adaptive changes in both behavior and physiological systems. While allostasis is an attractive and plausible concept, it remains difficult to test and to make it stand out from other

models or explanation of stress (84, 87). Its translation into predictions within medical practice would make allostatic load a useful concept (55, 87).

The outcome of allostasis and allostatic load (known as *allostatic overload* or *tertiary markers of chronic stress response*) is disease, brain change or mortality. The association of AL index with in vivo brain structure forms the aspect of interest of this thesis, and is discussed below.

2.6 Tertiary markers of AL and central role of the brain

Tertiary markers of allostasis, *allostatic load (AL),* and *allostatic overload* include pathological brain changes (93). Key brain areas such as the hippocampus, amygdala and prefrontal cortex have an essential role in both the appraisal of stressors and the regulation of the physiological stress response of the periphery and accompanying behavioral changes. Therefore, their abnormal function changes the appraisal of future stressors and can lead to a deleterious cascade affecting the brain itself (94). Below is an overview of the effects of stress response on the brain, while Appendix A provides a succinct overview of key brain areas of the stress response and their involvement in allostasis and allostatic load (6).

2.6.1.1 Glucocorticoid neurotoxicity and vascular risk

The stress response and allostasis are regulated by the hippocampus, amygdala and prefrontal cortex (95). In the short-term, the formation of synapses and long-term potentiation to facilitate memory make these responses adaptive. In the long-term, neuronal damage caused by chronic elevated glucocorticoid levels can lead to further (hippocampal) neuronal death via further dysregulation of glucocorticoid secretion (96). Thus these responses can be deleterious to the very system that

produces them. Chronic stress and elevated glucocorticoid levels are associated with adverse brain changes, such as transient dendritic remodelling, weakening of synapses, inhibition of adult neurogenesis in the hippocampus, atrophy of hippocampal neurons (35), which further impair accurate (cognitive) evaluation of and response to stressors (2). This creates a vicious circle of damage through feedback loops, resulting in for example hippocampal neuron death, which also may affect memory performance. If the stressor is chronic the initial surge of glucocorticoid supplies to the hippocampus and cortex decreases, inhibiting energy storage by these neurons. Cutting back glucocorticoid energy supplies from neurons that are undergoing neurological insult is a stressor in its own right. Neurological insults such as hypoglycemia, hypoxia-ischemia, and seizures, can lead to neuronal death. "Glucocorticoid neurotoxicity" described above is also a feature of healthy aging in humans (97). In *rats,* additional stress in old age accelerates hippocampal degeneration and memory decline (35). Severe hippocampal volume loss and memory decline are often present with a continuous rise of resting glucocorticoid levels with age, although human findings are awaiting clarification (7). Elevated diurnal and reactive glucocorticoid levels in elderly males (N=90, 73-years) were also associated with an increase in adverse changes to white matter microstructure; white matter hyperintensities and decreased integrity (mean diffusivity), especially in anterior thalamic radiation, uncinate, arcuate and inferior longitudinal fasciculi (98). This is in line with previous in vitro post mortem studies, suggesting that "glucocorticoids potentially have negative effects on prefrontal cortex neurons' survival and function", due to the stimulating effects of low- and depressing effects of high glucocorticoid concentrations on axonal transport in prefrontal neurons (7).

Over time brain-regulated sympathetic ANS activity leads to the wear-and-tear of the cardiovascular system, which in turn affects brain regional vasodilation and vascular reactivity that are required for tasks and clearing of waste products. Increased rates of progression of vascular brain injury, global and hippocampal atrophy and decline of executive function over 10 years are predicted by mid-life vascular risk factors (98). *Framingham Stroke Risk Score* at baseline predicted lower global cognition, memory and executive function at 4- and 8-year follow-ups in middle-aged and older participants of the English Longitudinal Study of Ageing (62).

2.6.1.2 Metabolic Syndrome and the brain

Individual metabolic syndrome components have a negative impact on the human brain (73). For example, higher blood glucose levels in the normal range are associated with lower grey and white matter regional volumes in the frontal cortices that in turn predict poorer cognitive performance in men (72). The effect of metabolic syndrome on brain and cognitive health, particularly in ageing, has not been extensively studied, and results from existing studies are mixed (73, 74): ten studies assessed the effect of metabolic syndrome on cognition in older adults. Seven out of ten found that a higher metabolic syndrome score was associated with poorer cognition. No association was found in three studies. Four examined the effect of sex; two found a more pronounced negative effect of metabolic syndrome in men, one in women, and one did not find any sex differences. The studies found an association between metabolic syndrome and poorer memory, visuospatial skills, executive function, processing speed and overall IQ, even after controlling for CVD and CHD, Type 2 diabetes, silent brain infarcts, depression, education and socioeconomic (73). A magnetic resonance imaging (MRI) study found a dose effect

of metabolic syndrome in men, i.e. a higher number of metabolic syndrome markers was associated with poorer memory performance and executive function in men, but metabolic syndrome did not correlate with cognitive performance in women. There were no MRI differences, e.g. focal ischemic lesions or brain volumes that could have accounted for the cognitive differences (99).

As previously mentioned, one study examined cortical thickness and subcortical volumes in metabolic syndrome (74). Comparing participants with (N=40) and without metabolic syndrome (N=46), significant volume reductions in the right nucleus accumbens in participants with metabolic syndrome compared with controls were present even after controlling for socio-demographic factors and intracranial volume. Cortical thickness was significantly lower in participants with metabolic syndrome in both hemispheres, in the left insular, superior parietal, postcentral, entorhinal, and right superior parietal cortices.

In middle-aged individuals ischemic stroke, subclinical ischemic brain damage, intracranial arteriosclerosis, periventricular white matter hyperintensities and subcortical white matter lesions has been present with metabolic syndrome, and in both middle-aged and older individuals with silent brain infarction (73). Fifty to eighty-year-olds with metabolic syndrome compared with age-matched controls had reduced white matter integrity in frontal and temporal lobes (75). There was no relationship between any of the individual vascular risk factors and white matter integrity. Others have found a positive association between the number of metabolic syndrome components and the degree of white matter damage, which were driven by vascular risk factors (73). A small (N=14) diffusion tensor MRI study compared an

equal number of participants with and without metabolic syndrome to show decreased white matter integrity in participants with metabolic syndrome in the right external capsule, entire length of the corpus callosum, and part of the deep white matter in the right frontal lobe (100). Increased [myoinositol:creatine] and [glutamate:creatine] ratios in occipito-parietal regions of cognitively healthy middle-aged adults with metabolic syndrome suggest microglia- or neuroinflammation, which are also features of Type 2 diabetes (101). Such subclinical alterations in cerebral metabolism may be an early sign of brain damage associated with peripheral metabolic disturbances (73).

2.6.1.3 Allostatic Load Index and the brain

Few studies have examined the association of allostatic load indices (AL) with brain and cognitive health (2). A study of the Lothian birth cohort (N=658) reported a negative association of AL with total brain volume and white matter volume, a positive (sic!) association with hippocampal volume, and no association with grey matter volume (83). Higher AL was also associated with poorer general cognitive ability, processing speed, and knowledge, but not with memory or nonverbal reasoning. This dissociation between global and possibly hippocampal involvement may be the result of different pathways (cortisol-hippocampal cascade versus generalized peripheral vascular illness) in this cohort of 73 year-olds. The associations of AL with measures of cognitive impairment were not mediated by these brain volume measures, and AL did not predict cognitive change from age 11 to approximately age 73 (83).

2.6.1.4 Major depressive disorder

Major depressive disorder (MDD) is one of the most common examples of Type II allostatic overload associated with structural grey and white matter changes in the human brain. Prolonged HPA-axis dysregulation and elevated glucocorticoid levels are characteristics of early-onset MDD, and lead to volumetric decreases in the hippocampus, disruption of hippocampal neurogenesis and prefrontal cortex regulation, which in turn are associated with memory and concentration problems, and an increased risk of dementias (45). *Longer duration* of MDD is associated with a greater degree of hippocampal atrophy, amygdala, anterior cingulate cortex, and dorsomedial prefrontal cortex volume decline (62). Vulnerability for first time depressive episodes in later life (late-onset depression) is characterized by widespread "non-specific brain atrophy, consistent with evidence of generalized brain changes," and a *later onset* of MDD (31, 103). Ischemic changes are associated with white matter hyperintensities and deep white matter lesions, and in turn with reduced cognitive function and quality of life. Depression, particularly late-onset depression, is associated with changes in the integrity of white matter tracts in frontal-subcortical, temporal and limbic regions. Vascular disease and vascular risk factors, such as the Framingham Stroke Risk Score contribute to an increased risk of depression, which may be mediated by the effects of white matter lesions and integrity (45). The relationship between white matter changes and depressive symptoms might be since: 1) vascular damage leads to altered neural connectivity (disconnection hypothesis) or 2) vascular changes mediated by inflammatory markers cause altered brain function and subsequent clinical symptoms (inflammatory and hypoperfusion hypothesis (45)).

2.6.1.5 Cognitive impairment

Depression is a risk factor for dementia and dementia is a risk factor for depression (103). Both late-life depression and cognitive impairment are associated with hippocampal atrophy, white matter hyperintensities, and cardiovascular risk factors. It seems likely that depression thus acts as a marker of organic dysfunction, and contributes to progression towards Alzheimer's disease and vascular dementia via mild cognitive impairment.

2.6.1.6 Posttraumatic stress disorder

Higher sensitivity to glucocorticoids in posttraumatic stress disorder (PTSD) may similarly contribute to a reduction in hippocampal size (104). Although a lack of longitudinal studies makes it difficult to determine the mechanism for this, hippocampal atrophy may be caused by trauma. Alternatively individuals with smaller hippocampal size might be more vulnerable to developing PTSD (105).

2.6.1.7 Traumatic life events

There is some evidence for the negative effects of traumatic life stress on the hippocampus, amygdala, anterior cingulate cortex, and medial frontal gyrus (10) especially in people with MDD (88) and PTSD (104). Despite the obvious involvement of certain brain structures in the stress response, only a handful of studies have examined the effect of stressful life events on brain structure in adults *without* a clinical syndrome (e.g. 102, 106). While they all found deleterious effects on certain brain structures, some are difficult to interpret. There is some evidence that chronic perceived stress and the number of stressful life events is associated with decreased grey matter volumes in the limbic and prefrontal cortex: for example average chronic

perceived stress predicted decreased grey matter volume in the right orbitofrontal cortex and right hippocampus in healthy postmenopausal women, even after controlling for various demographic variables (107). Decreased grey matter volume in the left parahippocampal gyrus, the left and right anterior cingulate, and the right hippocampus, was also correlated with the number of stressful life events (10). Cumulative exposure to adverse life events was also associated with prefrontal and limbic grey matter volume reduction in a community sample of middle-aged adults (102).

2.6.1.8 Resilience

According to the match/mismatch model of stress response, mild or moderately aversive conditions during childhood can shape an individual to be optimally adapted to similar conditions later in life (108, 109). A large group of young adults who reported adverse childhood events was compared with those who did not (110). *Larger* hippocampi and amygdalae were found bilaterally in those who had experienced adverse life events. Interestingly, young adults who reported recent adverse events had smaller frontal anterior cingulate cortices (110). Although the findings have heuristic value due to the large participant numbers (111), their narrow age-range limits their wider relevance. While consistent with the notion that early adversity may confer resilience, and late adverse events are damaging, the absence of a crossover group did not allow for a direct test of the model. Large longitudinal prospective cohort studies are needed to address this issue, which would also help to clarify the definition of allostatic load and the adaptive calibration model mentioned above (112, 113).

Chapter 3: The Whitehall II Study and Imaging Sub-study

Chapter 3 presents an overview of two cohort studies on which analyses in the following chapters are based. In provides an overview of their background, strengths and limitations and the structure of the rich data that have been accumulated over three decades.

3.1 Introduction

People aged 65+ are the fastest growing section of the population worldwide (114), and it is estimated that the number of people aged 60+ is going to almost double by 2050 accounting for 21% of the population (115). By 2071 this number can reach 21.3 million and those aged 80+ could more than triple to 9.5 million (116). Since the pension paying younger population is decreasing, it is likely that retirement age will soon extend into the late 60s, making the older generation a substantial part of both the general as well as the working population. The ageing population thus poses both a scientific and political challenge to ensure that the prolonged working years of life are productive, of high quality and free from the mental, cognitive and physical disease often seen in old age (46, 116, 117). This will not be possible without identifying the causal mechanisms between structural and functional changes seen in the ageing brain and the deterioration of mental and cognitive functioning. For example, the reduction in incidence of dementia across the last decades is intriguing, but requires a 'mechanistic analysis' to help generate policies to sustain it (118). Identifying factors across the lifespan that account for resilience

against these changes is of equal importance. For instance, research on functional compensation and neural scaffolding has explored brain plasticity with ageing (119-122). Prospective cohort studies, such as the Whitehall II and the Whitehall II Imaging Sub-study provide an excellent resource to address some of these questions. They are a type of longitudinal studies that follow the same group of healthy individuals who share a certain aspect, for instance age or occupation, over a period of time. They are commonly used to understand the impact stressors can have on health, and to see why some people, but not others, become ill. They have the advantage of large participant numbers and can be used to study how multiple factors interact. As they are not interventional, however, they cannot answer questions about causation.

3.2 The Whitehall II cohort



3.2.1 Background and importance

The Whitehall II study, commonly known as the Stress and Health Study, is an on-going prospective occupational cohort study initiated in 1985 and conducted at the University College London (52). The study was originally set up to explore the biological pathways through which social circumstances influence and affect health, with a particular focus on stress that manifests as social inequalities at the workplace, and cardiovascular disease and mortality outcomes (19, 21). Findings from the study have had a major impact on understanding the social gradient of health (21, 123) and in the development of policies to address the social inequalities in health both nationally and internationally (116, 124).

Over the past thirty years the Whitehall II study has accumulated a rich longitudinal dataset of social circumstances and behaviour, biological measures, psychological factors and everyday functioning (Table 3.0). As on average participants reached retirement age, in recent years the study progressed into a longitudinal study of ageing and subsequently placed greater emphasis on the inequalities of successful ageing (125, 126) and measures which assess this and its contributing factors to cognitive and mental health, immune-function, socioeconomic and life style factors in older age (see Table 3.0). Initial results show for example, that physical functioning declines faster in low socioeconomic groups, who had a higher rate of lifetime stress (125). Thus, the effects of social gradient persist into old age.

3.2.2 Data collection and sample description

At baseline Phase 1 the Whitehall II study involved 10,308 British Civil Service workers aged 35-55 (born between 1932-1955), of whom 3,413 were women and 6,895 men, recruited between 1985-1988. Phase 1 assessment comprised of both a clinical health examination and questionnaire assessment. Follow-up questionnaire data were collected after each clinical health examination, approximately two years apart. Questionnaire administration for Phase 2 lasted between 1989-1990. Follow-up health examinations were conducted over the past 30 years to date, approximately every five years, at Phase 3 (P3, 1991-1994), Phase 5 (P5, 1997-1999), Phase 7 (P7, 2002-2004), Phase 9 (P9, 2007-2009), and Phase 11 (P11, 2012-2013). Phase 12 is underway at the writing of this thesis (P12, 2015-2016) and comprises of both a health examination and questionnaire assessment. By 2012-3013 74% of participants who took part in Phase 11 had reached or passed the statutory retirement age of 65. As Table 3.0 shows the Whitehall II study accumulated a rich longitudinal dataset on antecedent vascular and metabolic risk trajectories and morbidity, physical and mental activity, mood history, baseline cognitive performance, lifestyle and social factors.

Ethical approval was provided by the University College London / University College London Hospital Committees on the Ethics of Human Research (Committee Alpha, reference: 85/0938).

	Phase 1 1985-88	Phase 3 1991-93	Phase 5 1997-99	Phase 7 2003-04	Phase 9 2007-09	Phase 11 2012-13	Oxford* 2012-14	Phase 12 2015-16
Age range, *years*	35-55	39-64	45-69	50-74	55-79	60-85	**60-83**	64-88
Participants, *N*	10,308	8,637	7,830	6,967	6,755	6,308	**563**	In progress
Demographics	**X**	X	X	X	X	X	**X**	X
Behaviours: smoking, alcohol, exercise, sleep, diet	X	X	X	X	X	X	X	X
Biological measures: MRI brain scan							**X**	
Salivary cortisol				X	X			
Hair cortisol						X		X
Anthropometry		**X**	**X**	**X**	**X**	**X**	X	X
Cardiovascular/metabolic		**X**	**X**	**X**	**X**	**X**		X
Inflammatory markers		**X**	X	**X**			X	X
Genetic material				X				
Psychosocial factors: employment, retirement	**X**	X	X	X	X	X	X	X
Health & disease: CHD, stroke, diabetes, mortality	X	**X**	**X**	**X**	**X**	**X**	**X**	X
Medications	X	**X**	**X**	**X**	**X**	**X**	X	X
Functioning: physical, mental, social (questionnaire)	X	X	X	X	X	X	X	X
Mental health (clinic)							X	
Cognitive tests (clinic)			X	X	X	X	X	X
Physical tests (clinic)				X	X	X	X	X

Table 3.0 Overview of Whitehall II & Imaging Sub-study measures. Variables used in this thesis are marked with a black cross **x.** *data used in this thesis are from participants seen in Oxford between April 2012-December 2014 (N=563) due to MRI scanner change (projected end date is December 2016, N=800). CHD, coronary heart disease.

3.3 Whitehall II Imaging Sub-study



3.3.1 Background and importance

The Whitehall II Imaging Sub-study combines a multi-modal, non-invasive magnetic resonance imaging (MRI) brain scan, a rich clinical and cognitive dataset and immune parameters with thirty years of antecedent Whitehall II data in a projected number of 800 Whitehall II participants (127). Combining the two datasets presents a unique opportunity to explore the mechanisms that contribute to or protect against age-related decline and the temporal relation of damaging and protecting factors from mid-life into older life, such as secondary markers of stress accumulated from mid- to later life and brain changes seen in later life.

The Sub-study is funded by the UK Medical Research Council's "Lifelong Health and Well-being Phase 3 programme" (MRC-G1001354), the HDH Wills 1965 (English Charity Register: 1117747) and the Gordon Edward Small Charitable (Scottish Charity Register: SC008962) Trusts. The University of Oxford Central University and Medical Science Division Interdisciplinary Research Ethics Committee (CUREC/MSD-IDREC) provided ethical approval generally for the "Protocol for non-invasive magnetic resonance investigations in healthy volunteers" (Reference: MSD/IDREC/2010/P17.2) and specifically for the Whitehall Imaging sub-study, "Predicting MRI abnormalities with longitudinal data of the Whitehall II sub-study" (Reference: MSD-IDREC-C1-2011-71). The Health Research Authority National Research Ethics Service (NRES) Committee South Central – Oxford B. granted ethical approval for collection of blood samples and cheek swabs on "The Whitehall II Immune Function sub-study" (Reference: 13/SC/0072, IRAS project ID: 120516).

3.3.2 Participant recruitment

In order to make the sample as representative of the baseline cohort at Phase 1 (1985-88) as possible, a random sample of eight hundred Whitehall II participants were recruited from their Phase 11 clinic (2012-2013) and tested and imaged at the Oxford Centre for Functional MRI of the Brain (FMRIB) between April 2012 and December 2016. Whitehall II participants were approached and gave consent to be contacted by researchers at Oxford. Out of these participants' contact details of a random selection of a total of N = 1431 were sent to Oxford in order to achieve the targeted N = 800. Contact details were sent in batches of N = 100, apart from the first and last months, within two months of Phase 11 clinics at a given month in order to acquire a sub-sample of N = 185 participants who undergo an MRI scan within three months of their Phase 11 clinic appointment. Subsequently, where possible recruitment was in the order of Phase 11 clinic attendance to equalise time between clinic attendance and MRI scan acquisition.

Participants were contacted, provided with an overview of the study, and if interested, screened for MRI safety contraindications via phone. MRI safety was assessed based on a standard list of questions provided by the FMRIB Centre. Where applicable participants were assessed based on hospital records and with the aid of senior radiographers at the FMRIB Centre. Once suitability had been confirmed a time and date was agreed on the phone and confirmed in writing, along with study information, travel directions and a questionnaire, which participants were asked to complete within a week of their appointment. Participants were not invited if they had MRI safety contraindications such as a heart pacemaker, aneurysm clip or

certain coronary stents, or if they were unable to travel to Oxford unassisted and partake in neuropsychological testing. Figure 3.0 below provides a schematic representation of the recruitment process and testing protocol. For a more detailed depiction of the recruitment protocol see Appendix B.

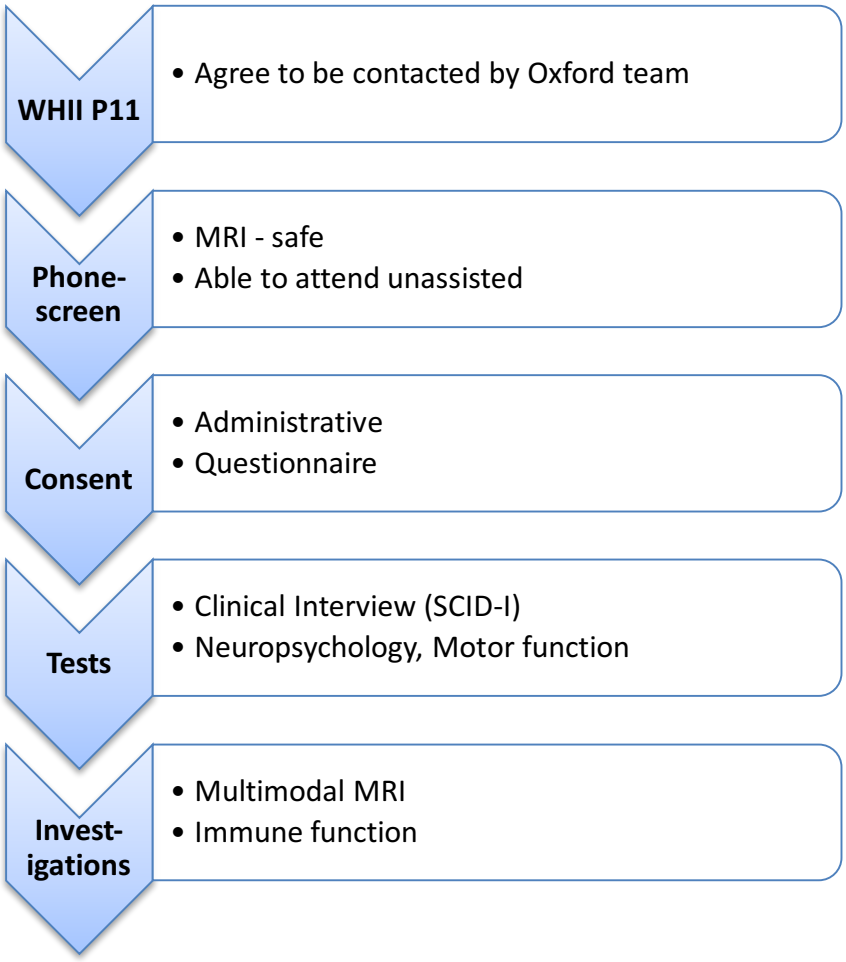


Figure 3.0. Schematic representation of Whitehall II Imaging Sub-study recruitment and testing protocol (P11, Phase 11; SCID-I, Structured Clinical Interview for DSM-IV-TR Axis I Disorders).

3.3.3 Data collection

Whitehall II participants attended the FMRIB Centre at the University of Oxford, Oxford UK, where they were given a chance to ask study-related questions, gave informed consent and were reimbursed for their time and expenses. In addition, a radiographer or trained MRI scanner operator screened them for MRI safety independent of their phone screening.

Before the MRI scan each participant recruited for the Whitehall II Imaging sub-study underwent a detailed clinical and cognitive assessment lasting up to two hours.

The clinical assessment is comprised of a psychologist or psychiatrist administered semi-structured psychiatric interview (SCID-I, Structured Clinical Interview for DSM-IV-TR Axis I Disorders (128)) and questionnaire on physical exercise, sleep, medical history, physical and mental health and general wellbeing, education, handedness and demographics, self-administered within a week of the appointment. Participants underwent a comprehensive neuropsychological battery, including paper pencil tests (cognitive screening test, language, visuospatial skills, short and long-term and working memory, premorbid intelligence), a computerised test to assess reaction and movement time and a motor function testing (Table 3.0, Figure 3.0). Following the MRI scan blood samples (3x8ml) and buccal mucosal epithelial samples (x2) are taken from participants, which are used in order to investigate immune function. Detailed data acquisition protocol and instruments used in the study have been published by Filippini, Zsoldos, Haapakoski, et al. (127). An overview of out-of-scanner protocol is included in Table 3.0, while a detailed description of the imaging protocol is presented in Chapter 5.

Chapter 4: Subjects + Out-of-scanner Methods

4.1 Introduction

Chapter 4 presents an overview of the sample of participants recruited and seen between April 2012 and December 2014 for the Whitehall Imaging sub-study. The key demographic data and description of the out-of-scanner variables on which analyses in Chapters 6 - 9 are based are outlined. Imaging methods are described in Chapter 5.

4.2 Participants

4.2.1 Recruitment

Analysis in the following chapters is based on data from Whitehall II Imaging sub-study participants who took part in the study between April 2012 and December 2014 inclusive, before the 3T Siemens Magnetom Verio MRI scanner was decommissioned.

Out of a total of 1431 contacts, 994 (69.5%) were contacted by telephone between April 2012 and December 2014. By the end of 2014, more than half of those contacted by telephone (N=563, 56.6%) had undergone the study protocol, and a further 148 (15%) had been MRI-safety screened and awaited MRI-safety confirmation and / or a study appointment. Out of those contacted via telephone 28.5% (N=283) were excluded; the majority declined participation due to the distance required to travel to Oxford, being unable to do the out-of-scanner tests due to health reasons (e.g. registered blind) or for reasons unspecified (N=233, 23%),

some had metallic implants such as a heart pacemaker, aneurysm clips or certain coronary stents, or surgeries that are an MRI contraindication (N=43, 4.3%) and a few died since the beginning of the study (N=7, <1%). 30.5% of all contacts (N=437) were still to be contacted via telephone at the end of 2014. An overview of the recruitment statistics is presented in Table 4.0.

	N	% Total contacted	% Total	% Total excluded
To be contacted	437	N/A	30.5	N/A
Phone-screened + awaiting confirmation	148	14.9	10.3	N/A
Complete	**563**	56.6	39.3	N/A
Excluded	283	28.5	19.8	100
Declined (far to travel, unable, other)	233	23.4	16.3	82.3
MRI contraindication	43	4.3	3.0	7.6
Deceased	7	0.7	0.5	2.5
Total contacted	**994**	100	69.5	N/A
Total	**1431**	N/A	100	N/A

Table 4.0 Overview of Whitehall II Imaging Sub-study recruitment statistics in Dec 2014.

4.2.2 Demographics

The following gives an overview of the Whitehall II cohort demographics at baseline (Phase 1, P1, N=10308), at Phase 11 (P11, N=6308) from which Whitehall Imaging sub-study participants were recruited, and at the Whitehall Imaging sub-study at Oxford (N=563; recruited by December 2014). The Oxford sample was representative of the whole Phase 11 cohort in terms of age and ethnicity. The imaged sample had more participants at the higher initial civil service grade (First) and fewer from the lower (Third). The Oxford sample had more males than the P11 cohort and included more participants with higher secondary education or a degree than the P11 cohort Table 4.1). Participants who attended at Oxford had on average 14 years of

education (SD: 3, range: 6-23 years). Their stroke risk at time of scan projected over a 10-year period (in percentage; measured by the Framingham Stroke Risk score (61)) was 1.4% lower than the average risk among Phase 11 attenders (see also 4.3.1).

	Phase 1 (N = 10,308)	**Phase 11** (N = 6,308)	**Oxford** (N = 563)
Age *[years]* *Mean (SD), range*	45.0 (6.05) 34-56	69.8 (5.87) 60-84	69.5 (5.3) 60-83
Sex, *N (%)*			
Male	6,895 (69)	4,459 (71)	454 (81)
Female	3,413 (33)	1,849 (29)	109 (19)
Ethnicity, *N (%)*	(N=10,216)	(N=6,298)	
White	9,181 (90)	5,833 (93)	525 (93)
Non-white	1,035 (10)	465 (7)	38 (7)
Grade at P1, *N (%)*			
Administrative	3,028 (29)	2,171 (34)	238 (42)
Professional/executive	4,943 (48)	3,181 (50)	277 (49)
Clerical/support	2,337 (23)	956 (15)	48 (9)
Education at P5, *N (%)*	(N=9,403)	(N=6,061)	
≥ Degree	3,325 (35)	2,269 (37)	237 (42)
Higher secondary	2,443 (26)	1,658 (27)	169 (30)
≤ Lower secondary	3,635 (39)	2,134 (35)	157 (28)
Continuous education, *[Years] mean (SD), range*	N/A	N/A	14.0 (3.0), 6-23 (N=562)
Framingham [10-year Stroke Risk] at Phase 11 *Mean (SD), range*	N/A	10.3% (8.5%), 1% - 88% (N=5,077)	8.9% (6.9%), 1% - 50% (N=534)

Table 4.1. Whitehall II participant demographics at baseline Phase 1 (P1; 1985-88), at Phase 11 (P11; 2012-13) and at Oxford (2012-14). Where N is indicated in brackets, this indicates the presence of missing data at a particular phase. The education variables were introduced only in later versions of the Whitehall II questionnaires (first at P5) and so is only known for about two third of the cohort. Education results peresented here are based on P5 and where missing, filled in with P1 education proxy variables. Where information was not available either at P5 or P1 for the Oxford sub-group, it was substituted by the same question answered by the sub-group when attending the Whitehall II Imaging sub-study. For similar reasons, continuous education was only complete at the Oxford study (calculated as total years of uninterrupted full-time

education not inclusive of part-time or later-life education). For a comparison of Framingham Stroke Risk scores within the general population see also 4.3.1.

4.3 Out-of-scanner materials

The association of 3 secondary stress markers with brain structure integrity in the Whitehall II Imaging sub-study is assessed in this thesis. Physiological and demographic measures that constitute these markers were acquired longitudinally during the Whitehall II study. Framingham Stroke Risk scores were derived at previous Whitehall II phases, while the metabolic syndrome score and allostatic load index were computed for participants attending an MRI brain scan in Oxford for the purpose of this thesis (Tables 4.1 and 4.2). Final sample size was based on maximum number of participants with available scores at each phase, and will be described in the individual analysis chapters. An overview of the marker scores and the structure of analyses follow below.

4.3.1 Assessment of secondary markers of stress

4.3.1.1 Framingham Stroke Risk Score (FSRS)

The *Framingham Stroke Risk Score* (FSRS) is a sex-specific stroke risk appraisal function that empirically relates cardiovascular risk factors to the probability of a stroke within 10 years. The original algorithm was developed predicting 427 first-time strokes in 2372 men and 3362 women aged 55 to 84 years, observed throughout a 10-year follow-up period (129). Since then it has been routinely used in clinical practice to predict the incidence of stroke and the need for prophylaxis (61). Whitehall II participants have on average similar vascular- and stroke risk to the

general population (Figure 4.0). FSRS has been shown to strongly predict the incidence of stroke amongst Whitehall II participants.

Age and sex adjusted odds ratio for 10% increment in stroke risk was 2.84 (95% [CI]: 1.66 - 4.88; (130)). Moreover, elevated stroke risk in midlife amongst Whitehall II participants free from previous stroke was found to be significantly associated with cognitive decline over a 10-year period (131).

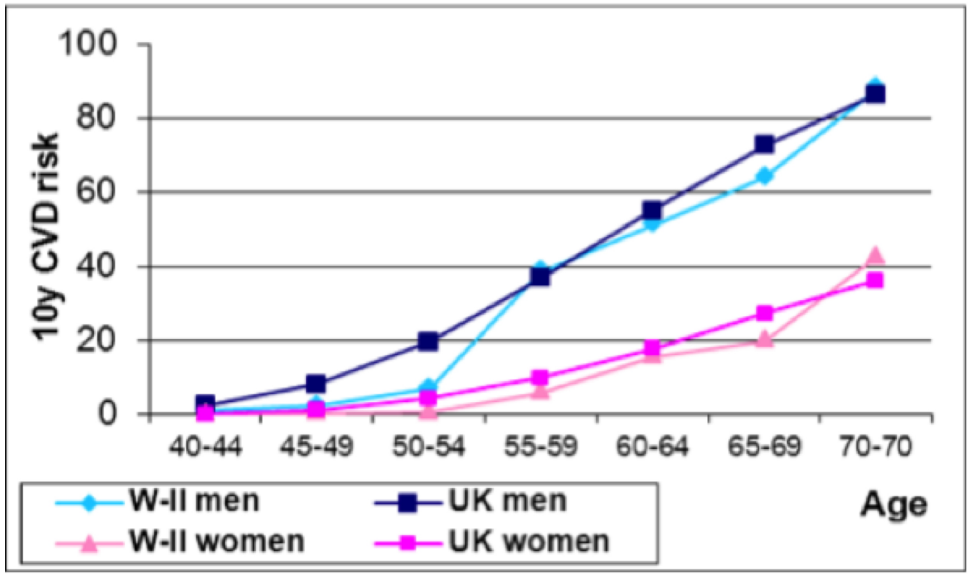


Figure 4.0 Cardiovascular risk measured by Framingham Risk scores in the general population and Whitehall II (W-II) cohort, provided by © Prof. Archana Singh-Manoux as part of the Whitehall II Imaging Sub-study application process. Graphs indicate that on average W-II participants have similar vascular risk to the general UK population. Up to the ages 50-54, W-II men have lower risk than British men, similar to W-II and British women. After the ages 50-54 W-II men have a similar risk profile to British men. The "delayed" increase in W-II men's risk reflects a cohort effect, whereby younger W-II men have a smaller risk than older W-II men.

The probability of stroke depends on an individual's presence and level of risk factors and is often expressed as a percentage score (61, 129). Risk factors include cardiovascular health (systolic blood pressure, prior cardiovascular disease, atrial

fibrillation, left ventricular hypertrophy), diabetes mellitus, smoking habits, gender and chronological age (Table 4.2, Appendix A).

FSRS in this thesis

Risk components were drawn from both questionnaires and clinical examinations at phases 3, 5, 7, 9, and 11 of the Whitehall II study (Tables 4.2, 4.3). The percentage stroke risk score was expressed as the predicted 10-year probability of a stroke at each phase. It was computed using beta coefficients based on the Cox proportional hazards regression model in the Framingham study (61, 129).

Biological measures and samples were collected according to standard operating protocols (130, 131). Systolic blood pressure was measured twice in sitting position after five minutes rest with a Hawskley random-zero sphygmomanometer (phases 3 and 5; Lynjay Services Ltd, Worthing, UK) and OMROM HEM 907 (phase 7 onwards; Omron, Milton Keynes, UK). The average of two readings was used in analysis. Atrial fibrillation (AF) and left ventricular hypertrophy (LVH) were identified on a standard 12-lead electrocardiogram analysis programme combined with manual review and the Minnesota code classification system for electrocardiographic findings (AF arrhythmias: 8-3-1; LVH high amplitude R-waves: 3-1) (132). History of prior cardiovascular disease (CVD) was based on electrocardiogram and angiogram examinations at phases 1, 3 and 5 as well as from general practitioner or hospital records. Hypertensive medication use was self-reported. Venous blood was taken in the fasting state or at least five hours after a light, fat-free breakfast before undergoing a standard 2h oral glucose tolerance test. Glucose was measured in fluoride plasma by an electrochemical glucose oxidase method (133) on YSI model

23A glucose analyser at Phase 3 (134) and YSI model 2300 STAT PLUS analyser at Phase 5 onwards (135) (YSI Corporation, Yellow Springs, OH, USA). Diabetes mellitus was defined by a fasting glucose level of ≥ 7.0 mml/L, a 2hr post-load glucose level of ≥ 11.1 mml/L, self-reported diabetes diagnosed by a doctor or use of diabetes medication (136). Participants were categorised as current cigarette smokers or past/non-smokers.

4.3.1.2 Metabolic Syndrome (MetS)

Metabolic Syndrome (MetS) is the clustering of central obesity, atherogenic dyslipidemia, arterial hypertension, dysglycemia and proinflammatory state (137). MetS therefore characterises the interconnection between the cardiovascular and neuroendocrine systems. At its root cause are chronic stress, ageing (138-140), overweight, obesity, physical inactivity, and genetic factors (141). It is closely related to a generalised metabolic disorder called insulin resistance, in which tissue responsiveness to the normal action of insulin is impaired (142). MetS is primarily a multivariate risk factor for CVD but in combination these metabolic factors increase the risk of diabetes mellitus (143), stroke (70), and have a negative effect on cognition and structural brain integrity (73). In the Whitehall II cohort presence of the syndrome was associated with depressive symptoms at a six-year follow-up (OR 1.38, 95% CI 1.02–1.96) after adjusting for confounders (144) but only persistent MetS (at least two of three screenings) was related to lower cognitive performance, which was further attenuated by occupational status (47). Furthermore, there was an increase in the proportion of 4,150 Whitehall II participants with MetS across three phases (8.3% at Phase 3, 8.9% at Phase 5 and 11% at Phase 7), and they were more likely to be men (67).

Because of their high association in one person the individual contribution of each factor to disease risk is difficult to dissect (66) but there is increasing evidence for using them in combination to define MetS rather than on their own (145, 146). The presence of MetS can be useful to complement the clinician's judgement to lower risk of cardio-metabolic illnesses through the direct (cholesterol and triglyceride-lowering drugs) and indirect (lifestyle changes such as physical inactivity and obesity) lowering of dyslipidemia levels (147, 148).

MetS in this thesis

Metabolic syndrome is defined by the linear combination of five physiological measures, at least three of which has to be above clinical thresholds to meet criteria for having the syndrome. MetS was defined at phases 3, 5, 7, 9, and 11 of the Whitehall II study using the National Cholesterol Education Program criteria (149), based on the presence of at least three of the following components: blood pressure: ≥ 130/85 mmHg or use of antihypertensive medication, waist circumference (abdominal obesity): men > 102 cm, women > 88 cm, fasting glucose: ≥ 6.11 mmol/L, HDL cholesterol: men < 1.03 mmol/L, women < 1.3 mmol/L, and serum triglycerides: ≥ 1.7 mmol/L. The same cut-off was used for all five phases. It is worth noting that overweight and obesity are associated with insulin resistance and the metabolic syndrome. However, the presence of abdominal obesity is more highly correlated with the metabolic risk factors than is an elevated body mass index (BMI), optionally used by the World Health Organisation (150) to define MetS. Therefore, the simple measure of waist circumference is recommended to identify the body

weight component of the metabolic syndrome. Most research studies involving Whitehall II metabolic data also rely on this protocol.

MetS was a binary (yes/no) score for each phase. To maximise the variance attributed to MetS in analysis, cumulative total MetS was defined as the number of times MetS was present across the five phases. In addition, change in MetS across the five phases was calculated as the difference between the sum of the first two (phases 3, 5) and the sum of the last two (phases 9, 11) statuses (Tables 4.2, 4.3). In analyses that used change in MetS the average status across five phases was included as a nuisance variable (nuisance variables are explained in section 4.3.2). Where a measure was missing at any given phase the overall MetS score was manually estimated. Where it was not possible (e.g. 2 scores met cut-off criteria + 2 scores did not meet cut-off criteria + 1 missing score) the participant was excluded from analysis. Participants were also excluded if their MetS scores were missing at all phases.

All measurements were carried out according to a standard protocol described in (67), (151), and (152). Blood pressure was measured as described for the Framingham Stroke risk score. Waist circumference was measured with the subject in the standing position and unclothed using a fibreglass tape measure at 600 *g* tension. The waist circumference was taken as the smallest circumference at or below the costal margin. Venous blood was taken from an antecubital vein in the fasting state or at least five hours after a light, fat-free breakfast before undergoing a standard 2h oral glucose tolerance test. Blood was coagulated with EDTA (viscosity) or citrate (homeostatic markers). Plain serum and plasma were stored at -80°C until

analysis. Serum cholesterol and triglycerides were measured in a centrifugal analyser by automated enzymic colorimetic methods. HDL cholesterol was determined using phosphotungstate precipitation. Glucose was measured in fluoride plasma by an electrochemical glucose oxidase method (133) on YSI model 23A glucose analyser at phase 3 (134) and YSI model 2300 STAT PLUS analyser at phase 5 onwards (135) (YSI Corporation, Yellow Springs, OH, USA).

4.3.1.3 Allostatic Load (AL) Index

As discussed in chapter 2, there is no consensus on the exact combination of biomarkers that define *Allostatic Load (AL) index* (2) but they often include a combination of both primary and secondary markers of the chronic stress response. In the Whitehall II study (52) the index is based solely on a combination of secondary markers of the stress response: cardiovascular, metabolic and inflammatory measures (153). A significant quadratic relationship between AL index and age was present in 7,007 Whitehall II participants (78), and as Figure 4.1 shows this nonlinear relationship becomes attenuated with age (roughly around the mid-60s). Although the index varies greatly in its components (2) the value of combining multiple physiological measures into one index of cumulative stress response system dysregulation is generally accepted. It provides a conceptual framework for stress researchers to work in and not least because in combination they are thought to be a better predictor of health outcomes and mortality than the individual components (51, 53). Therefore, it is of interest to examine its association with structural brain integrity.

The image originally presented here cannot be made freely available via ORA because of 'copyright' reason. The image was sourced at Dich N, Lange T, Head J, Rod NH. Work stress, caregiving, and allostatic load: prospective results from the Whitehall II cohort study. Psychosom Med. 2015;77(5):539-47.

Figure 4.1 The estimated nonlinear change of allostatic load over time in 7,007 Whitehall II participants. The trajectory is plotted for the average birth cohort born in 1943. Figure reproduced from Dich et al., 2015 (78) with the publisher's permission (Wolters Kluwer Health, Inc; license no. 3955631014713).

AL Index in this thesis

AL index in the Whitehall II study is defined by the linear combination of nine physiological measures. (78, 153). Following most common practices, AL index was defined as the number of physiological markers with values above a high-risk threshold (154, 155) Following another common practice, the 75th percentile distribution-based cut-off was used where such clinically relevant cut-off norms have not previously been established (here: fasting insulin and IL-6) (2). AL index was defined at phases 3 and 7 based on the following components and their cut-offs: blood pressure: ≥ 140/90 mmHg, BMI: ≥ 25 kg/mm², fasting glucose: ≥ 5.5 mmol/L, fasting insulin: ≥ 7.53 mcU/ml, high-density (HDL) lipoprotein cholesterol: < 1.03 mmol/L, low-density lipoprotein (LDL) cholesterol: ≥ 3.36 mmol/L, serum triglycerides: ≥ 1.7 mmol/L, C-reactive protein (CRP): and interleukin-6 (IL-6): ≥ 1.85 pg/ml. An elevated level of each measure carries more risk, except in case of HDL cholesterol.

The same cut-off values were used for both phases and distribution-based cut-offs were established based on phase 3 values. Each component was given the same weighting and was dichotomised (yes/no) based on their respective threshold. The dichotomised scores were summarised to form AL index at each phase. In addition cumulative total AL index was defined as the sum of AL index at both phases. Furthermore, change in AL index was calculated as the difference between Phase 3 and 7 (Tables 4.2, 4.3). In analyses that used AL index change the average index across the two phases was included as a nuisance variable (nuisance variables are explained in section 4.3.2). Where a measure was missing at either phase the participant was excluded from analysis. As indicated in Table 4.3, measures were acquired in Phase 5 as well; however, they were incomplete for > 50% of Whitehall II Imaging sub-study participants and in order to maximise the sample size this Phase had to be excluded from analysis.

The standard protocol for acquiring the biological measures was defined in (67), (151) and (152). Venous blood was taken as described under metabolic syndrome, as was the measurement of blood pressure, fasting glucose, serum triglycerides and HDL cholesterol. LDL cholesterol level was derived from the Friedewald equation (156). Serum insulin was measured with an in-house human insulin radioimmunoassay at phase 3 (157) and a DAKO insulin ELISA kit at phase 5 onwards (158) (DakoCytomation Ltd, Ely, UK).

Plasma C-reactive protein (CRP) was determined using automated turbidimetry at phase 3 (159) and with a high-sensitivity immunonephelometric assay in a BNProSpec nephelometer at phase 7 (Dade Behring, Milton Keynes, UK). Serum interleukin-6 (IL-6) was assayed using a high sensitivity two-site ELISA kit (R&D Systems, Oxford, UK). Body mass index was calculated by dividing the weight in kilograms by the square of the height in meters (160).

		Framingham Stroke Risk Score (129)	Metabolic Syndrome (149)	Allostatic Load Index (153)
CARDIO-VASCULAR	Systolic BP	X	X	X
	Diastolic BP		X	X
	Prior CVD	X		
	Atrial fibrillation	X		
	Left ventricular hypertrophy	X		
	Hypertensive medication	X		
METABOLIC	Waist circumference		X	
	Body mass index			X
	Diabetes mellitus	X		
	Diabetes medication	X		
	Fasting insulin			X
	Fasting glucose		X	X
	Low HDL cholesterol		X	X
	High LDL cholesterol			X
	Serum triglycerides		X	X
IMMUNE	CRP			X
	IL-6			X
OTHER	Age	X		
	Sex	X	X	
	Cigarette smoking	X		

Table 4.2. Overview of secondary stress markers and their individual components at Whitehall II. Framingham Stroke Risk Score is derived at Whitehall II. Metabolic Syndrome and Allostatic Load Index have been calculated based on published guidelines. BP, Blood pressure; CVD, Cardiovascular Disease; HDL, High-density lipoprotein; CRP, C-reactive protein; IL-6, interleukin 6. Adapted from Zsoldos & Ebmeier 2016 (6). An elevated level of each marker is damaging, except in case of HDL cholesterol.

	P3 '91-93	P5 '97-99	P7 '03-04	P9 '07-09	P11 '12-13	Total Derived	Slope Derived
Time to scan, *years*	20	15	10	5	0-2		
Age range, *years*	39-64	45-69	50-74	55-79	60-85		
Framingham Stroke Risk Score	X	X	X	X	X		
Metabolic Syndrome	X	X	X	X	X	X	X
Allostatic Load Index	X	X	X			X	X

Table 4.3. Overview of secondary stress markers derived from Whitehall II data, and their availability longitudinally. Binary metabolic syndrome variables marked with a blue cross X were used only to derive scores for analyses. Upto 50% of the variables that make up the Allostatic Load Index are missing at Phase 5, marked with a red cross X, hence not included in analysis.

4.3.2 Nuisance variables

4.3.2.1 Covariates of no interest

A nuisance variable is a ***covariate of no interest***, also termed a ***confounder***, if it is associated with both exposure and outcome variables, and is not on the causal chain leading from exposure to outcome. Ignoring a confounding variable in analysis leads to bias in the results such that they could suggest the existence of a difference or an association where there is none, or a difference or association in the opposite direction to the one that exists. Statistical associations in the data should not be the sole reason for including a variable as a confounder in analysis, and as such external knowledge is just as important (161). In statistical analysis we covary or control for a ***covariate of no interest***, in order to assess the ***unique effect of the exposure variable (of interest)*** (here: secondary stress markers) on the outcome variable (here: brain measures). When an exposure variable and a covariate of no interest are correlated, it is the component of the exposure variable that is not correlated with

(i.e. is orthogonal to) the covariate of no interest that is modelled within the GLM (general linear model). In other words, it is the association between the unique variance of the exposure and outcome variables that is being assessed. The unique variance is therefore not attributable to or shared with the covariates of no interest.

4.3.2.1.1 Confounders in present thesis

Demographic/potentially biological: age, sex, ethnicity

Since cerebral volumes and cortical thickness decrease with increasing age and men have larger volumes and smaller thickness than women, age and sex are routinely used as confounding variables in MRI analysis (111, 162). Gender differences exist in terms of ageing. For example, even though women have a higher life-expectancy, once they reach 65 years of age, they also have a higher incidence of disabling conditions than older men (163). Furthermore, cardiovascular responsiveness to stress increases with age in women but not in men (164), but the risk of incident stroke increases with age in both men and women (61).

Ethnicity and race are frequently controlled for in cohort and ageing studies (144, 165-167), often as a surrogate marker of race-specific social and cultural factors, such as educational attainment (168) or the higher prevalence of cumulative socioeconomic (169, 170) and environmental (171) disadvantage among ethnic minorities, rather than for biological reasons (168, 172). There is also emerging evidence however, that ethno-racial differences in biological, e.g. cardiovascular (173) and metabolic (174), as well as genetic (175) risk factors could explain the disparities often seen in the prevalence of vascular risk (176) and Alzheimer's disease (AD) between white and Hispanic/African-American decedents (177). Even though

the lack of population based and longitudinal cohort studies (177), and the inconsistent research methods and definition of minority groups (178) hinder the definite and consistent conclusions that can be drawn (179), according to the Alzheimer's Association the prevalence of AD above the age of 65 years is about twice the rate among African Americans and 1.5 times greater in Hispanic minorities than in whites (168, 174, 180). Findings that minority ethnic groups are disproportionately afflicted by AD compared to whites were presented in observational studies (181) and remained significant even after controlling for education level, and history of heart attack, stroke, and cardio- and cerebrovascular diseases (175). The incidence of vascular dementia is also reported to be higher among African Americans compared to whites (173, 182). Cardiovascular diseases such as hypertension, coronary heart disease (CHD), stroke, and diabetes are risk factors for dementias, including AD (183-185). CHD and cardiovascular risk factors are significantly more common in African Americans than any other ethnicities in the United States (176), and are often comorbid with high levels of other allostatic load measures (e.g. CRP, homocysteine (186)). The prevalence of diabetes mellitus is higher in both African Americans and Hispanics than in whites, and is therefore often implicated in accounting for some of the racial disparities in the prevalence of AD (174). In spite of existing population-based cohort studies the role of ethnicity in modifying the effects of genes, such as apolipoprotein E (APOE) gene polymorphisms, remains unclear, with contrasting findings of APOE ε4 allele known to increase the risk of AD in white ethnicities and might (187) or might not (175, 188) have the same effect among elderly African Americans. In this thesis ethnicity was considered as a demographic and potentially biological confounder.

Age at the time of the MRI scan was used in voxelwise analysis of brain measures in this thesis. Ethnicity was coded as white or non-white at Phase 1 of the Whitehall II study.

Socioeconomic

Being of higher social or occupational class is associated with lower stress, better health and lower mortality (189). A number of socioeconomic factors affect health and mortality, such as education level, social class (or parent's social class in childhood), occupational level, wealth (e.g. house or car ownership), household income and neighbourhood characteristics. For example, people with higher educational attainment are more likely to have healthy behaviours or change unhealthy ones after a heart attack (190). The Whitehall studies showed that other, psychosocial factors, such as work-related stress, link socioeconomic status with health outcomes both directly and indirectly (189). For example, low social position is associated with sustained activation of the stress response (51, 191), and a delayed recovery in cardiovascular function following mental stress (192).

Typically research focuses on pre-retirement socioeconomic status as socioeconomic differences are thought to diminish with age (193), while it is also challenging to measure socioeconomic status after retirement (194). Results from both the Whitehall study (125) and the more recent English Longitudinal Study of Ageing (195) showed however, that the effect of socioeconomic factors on health and mortality extend into older ages and increase with age in magnitude (196). For example, physical function declines faster in Whitehall II participants of low socioeconomic groups in older age (125). In addition, mid-life occupational grade in

male civil servants is a stronger predictor of post-retirement mortality than wealth although social differentials in mortality decrease to a greater degree based on work than non-work measures (196).

Education years were used as a proxy measure for socioeconomic status in young adulthood. It was self-reported by the participant at the time of the MRI scan and was calculated as the difference between the age at which the participant commenced primary school and the age at which (s)he first left full-time education. Mid-life socioeconomic status was defined as grade of employment at Phase 1 of the Whitehall II study: administrative (highest grade), professional or executive (medium grade), and clerical or support (lowest grade).

In initial analyses time between a phase and acquisition of MRI scan was included as a confounder, and did not have a significant effect on the results. Since longitudinal participant data was acquired at approximately equal time periods, the time to scan was not included as a confounder in the final analyses presented here.

4.3.2.2 Statistics

The association of each secondary stress marker and brain structure, grey matter density and white matter integrity, are examined. It is expected that higher stress marker scores are associated with more abnormal brain measures. In other words, stress markers measured in mid-life, are expected to predict or determine (= be associated with) lower or higher structural integrity measures, in older age. ***It should be noted, therefore, that the terms 'predict', 'determine', and 'brain changes' are used loosely to aid the flow of text. Although stress markers were measured longitudinally, MRI data were cross-sectional. Therefore, only the presence of a***

correlational association, not a causational change, can be assessed with the available data.

First, the raw (unadjusted) association between secondary stress markers and voxelwise brain measures was assessed (Model I). If the association was significant the unique association of stress markers with brain measures was assessed first controlling for the effect of 1) demographic/potentially biological (Model II) and then, 2) in addition to socioeconomic factors (Model III). A two-step model adjustment was taken to examine whether stress markers were associated with brain measures beyond the individual variability associated with chronological and some aspects of biological ageing (Model II). Model III represents any associations left between a stress marker and brain measure after the effects of socioeconomic, chronological and some biological aspects of ageing have been controlled for. It should be noted that based on the existing literature these confounders are expected to correlate and so any remaining association in Models II and III represent the unique variance explained by stress markers, not correlated with any of the confounders.

4.3.2.3 Mediation analysis

Mediation analysis is a type of process analysis often used in psychology, epidemiology and clinical trials to model and test intervening variable effects (197, 198). Although there are many methods available for testing hypotheses about intervening variables, i.e. mediation effects, the most widely used method is the causal steps approach popularised by Baron and Kenny (199). This approach requires the researcher to estimate the relationship between each variable (predictor,

mediator and outcome) of the model and then ascertain whether a variable functions as a mediator by seeing if certain statistical criteria are met (200, 201).

To test mediation effects, here it will be examined whether the effect of stress markers (predictor or causal variable) on fractional anisotropy (FA; outcome), an estimate of WM integrity derived from whole-brain white matter (WM) analysis, is mediated by total percentage grey matter (%GM) or by WM hyperintensity (%WMH) volumes. %GM is an estimate of cortical atrophy and thus could mediate the association via Wallerian degeneration. Wallerian degeneration is a type of neuronal degeneration where anterograde axon and myelin sheath degeneration occurs after connection with the cell body of the neuron is disrupted or lost (202). The disruption can be caused by axonal injury or an ischemic event. Equally, degeneration of the neuronal cell body leads to lack of axonal transport (203) and consequently axonal degeneration and permanent gliosis, death (204, 205). %WMH is a measure of small vascular lesions to the WM, showing up bright on T2-weighted MRI images. Following the presence of a significant relationship between stress markers and FA, i.e. an effect that can be mediated, the linear association between the stress marker and %GM volume (or hyperintensities) is assessed. Afterwards the effect of %GM volume on FA is assessed, covarying for the stress marker, since it is possible that %GM volume and FA are correlated because they are both an outcome of the stress marker. If %GM volume completely mediates the effect between a stress marker and FA, the effect of the stress marker on FA after controlling for %GM volume should be zero. If all the stages described are met, we are dealing with an example of complete mediation. If the effect of the stress marker on FA is reduced in absolute size but is

still different from zero when %GM volume is introduced as a nuisance variable, we have a case of partial mediation.

It should be noted that while the effect of stress markers on whole brain white matter FA was mediated by GM or WM hyperintensity volumes, depending on the marker (see below), the symmetrical mediation of stress markers effect on GM density loss by DTI and white matter hyperintensity measures, was not examined, because there were no specific hypotheses, specifically comparing the mediating effects of white matter integrity and white matter hyperintensity volumes on grey matter atrophy.

%GM and WMH measures are used as possible mediators in this thesis, and are described in sections 5.3.1.3 and 5.3.2.3.2, respectively.

Chapter 5: Imaging Methods and Analysis

5.1 Introduction

Chapter 5 provides an overview of the principles of magnetic resonance imaging (MRI) methods and structural MRI scans used in analyses in Chapters 6-9. It also outlines the imaging protocol for the first 563 participants of the Whitehall II Imaging sub-study, which was carried out on a 3 Tesla (3T) Siemens Magnetom Verio scanner with a 32-channel receive head coil (Erlangen, Germany). The MRI scanner was replaced between January and June 2015 with a 3T Siemens Magnetom Prisma (Erlangen, Germany), so that the imaging sequence parameters had to be changed. Systematic comparison of the sequences acquired on the different 3T scanners as well as any other systematic differences between scanners and optimisation of the analysis protocol were not completed in time for the submission of this thesis. Analyses in the following chapters (Chapters 6-9) therefore are based on the imaging protocol described below.

5.2 Background

5.2.1 MRI safety

Magnetic resonance imaging (MRI) is a non-invasive method of providing high-resolution in vivo images of the human body and brain. It is safe if care is taken to avoid the major hazards associated with MRI. These include magnetic attraction, torque effect, radio frequency (RF) heating and acoustic noise. Definite or potential contraindications such as certain implants and devices with vital function (pacemaker, aneurysm clip), which could immediately lose their function under

exposure to a strong magnetic field, orthopaedic or aesthetic implants and metal fragments that entered and were left in the body, and are either ferromagnetic (magnetic attraction) or could dislocate and cause tissue and organ damage (torque effect) or RF heating and burning, are investigated outside the 5 Gauss controlled area prior to scanning. RF heating and burns are prevented, and sufficient acoustic noise reduction is ensured during scanning set-up and image acquisition according to standardised procedures. MRI (head-) scans are well tolerated by the general population, with only about 1% having a claustrophobic reaction to them (206).

5.2.2 Principles of MRI

Magnetic resonance imaging (MRI) is the imaging of magnetic moments resulting from the quantum mechanical property of nuclear spins (207, 208).

5.2.2.1 Magnetic moment (spin)

Most clinical MRI utilises the prominent electromagnetic quality of hydrogen protons (^{1}H), which are in abundance in the water molecules of the human body and tissue[2]. About 80% of the body is made of water molecules, which are comprised of two hydrogen atoms plus an oxygen atom. ^{1}H nuclei consist of a single proton, and are orbited by a single electron. ^{1}H atoms have MR active nuclei with a net magnetic moment or spin (209). Each proton spins around its own axis, inducing an electrical current, and thus a magnetic field, called the magnetic moment or spin.

[2] Any element with a spin could potentially be used: ^{13}C, ^{19}F, ^{31}P, etc.

5.2.2.2 Spins in an external magnetic field (B_0)

^{1}H nuclei are randomly oriented in biological tissue, such as the brain. ^{1}H protons in water move randomly, equivalent to their thermal energy and with random orientation among their spins. The spins point in different directions and their respective magnetisation vectors cancel out, resulting in zero net magnetisation or magnetic moment (labeled as *M)* for the tissue sample. When protons are placed in an external magnetic field (B_0), such as within the bore of the MRI scanner, the spins align either in parallel or anti-parallel to B_0 (209). Since anti-parallel alignment requires more energy than parallel alignment a slight majority of spins align in parallel to B_0, and therefore the macroscopic net magnetisation *M* is parallel to B_0.

5.2.2.3 Larmor (resonance) frequency

When ^{1}H protons in a tissue sample are placed in an external magnetic field (B_0), the interaction of the magnetic moments of the nuclei and the external magnetic field B_0 described above causes protons to wobble or 'precess'. The frequency at which the precession occurs is called the Larmor or resonance frequency (ω_0), and is proportional to the strength of B_0. It is defined as: $\omega_0 = B_0 \times \gamma$, where ω_0 is the resonance frequency, B_0 is the external magnetic field strength measured in Tesla (here: 3T) and γ is the gyromagnetic ratio measured in MHz/T, which is a constant for every atom at any given magnetic field strength; for ^{1}H it is 42.58 MHz/T (210). The resonance frequency for a 3T scanner is about 128MHz. For ^{1}H the resonance frequency is in the radio frequency (RF) range, similar to that of an FM (frequency modulation) radiobroadcasting signal (88 – 128 MHz). For this reason it is also called an RF signal. This RF signal, and therefore the net *M* and the presence of ^{1}H can be detected with a device similar to an FM tuner.

5.2.2.4 Magnetic resonance effect

When the net magnetisation *M* is parallel to the external field B_0 its small size makes measuring it impossible. Therefore, using a transmit coil an RF pulse at Larmor frequency is applied to flip the net magnetisation vector *M* into the transverse (X, Y) imaging plane by a certain angle, termed flip angle. The direction of B_0 defines the imaging coordinate system, where the Z-axis is parallel to B_0 and is termed longitudinal magnetisation. As the protons resonate in phase of the transverse (X, Y) magnetisation around a receiver coil in accordance with Faraday's law of induction, a current is induced in the receiver coil (211). This current is the MR signal. By inducing brief temporary variations or gradients in B_0 in the X, Y plane protons at different locations along the gradient within a sample resonate at slightly different frequencies. Thus position along the gradient can be decoded by Fourier transform of signals, associating defined resonance frequencies with the known varying B_0 field strengths along the gradient. Protons behave differently in different tissue types such as grey matter (GM), white matter (WM), and cerebrospinal fluid (CSF), depending on their chemical and physical environment, e.g. the amount of water molecules within a tissue and free movement (more on this below). This is the basis of MR signal detection from a defined position in space, and is used for 3D MRI image formation (212, 213).

5.2.2.5 Signal decay

When the transmit coil and subsequently the RF pulse is turned off, the net magnetisation vector *M* realigns with the axis of B_0, during which the spinning protons realign with the main magnetic field B_0, and the longitudinal magnetisation (Z-axis) recovers or increases in magnitude. During this process protons release the

energy they absorbed during the RF pulse into the surrounding environment (lattice). This process is termed spin-lattice relaxation, T_1 relaxation or T_1 recovery. At the same time the interaction between spins causes the transverse magnetisation (X, Y axes) to dephase, which as a result decays or decreases in magnitude. As mentioned earlier, the transverse magnetisation induces a current in the receiver coil, but as protons spin out of phase the signal induced in the coil decreases. This is known as the spin-spin relaxation, T_2 decay and T_2* decay. In T_2* signal decay the transverse magnetisation is dephased because of magnetic field inhomogeneities, the spatial uniformity of the external magnetic field rather than due to the interaction between spins. T_2* is a parameter used in functional MRI imaging and since it does not constitute part of this thesis, it is not detailed here.

5.2.2.6 Repetition and echo time

GM, WM and CSF have different relaxation time properties, which are exploited to gain detailed information about these different tissue types within the brain. Differences in T_1, T_2 in various tissues are used to create differences in tissue contrast on MRI images (Figure 5.0). The process of how this is done is detailed below, under the relevant sequences used in this thesis (5.3.1, 5.3.2, 5.3.3). Repetition time (TR) and echo time (TE) have a key role in establishing these image contrasts. TR is the time (measured in milliseconds) between two RF excitation pulses. TE (in milliseconds) is the time between the application of the RF pulse and the peak signal (echo) detected.

5.2.2.7 Signal localisation and image formation

Gradient coils are used for the localisation of signal in different tissues. They are linear variations of B_0 in a selected region (214) and exist in the X, Y, Z planes. They are used for selecting the target of the RF excitation pulse, i.e. the section to be imaged (section selective gradient), and encode the phase shift in the spinning protons (phase encoding gradient) and the frequency at which they spin, enabling the detection of their location at TE (frequency encoding or readout gradient). The gradients are the main source of acoustic noise during scanning, which occurs during the rapid alterations of currents within the coils. Based on the phase and frequency, the exact location and amplitude of the signal is computed and stored in frequency- (k-) space (k is the symbol for wave number; Twieg (215)). The raw imaging data are Fourier transformed (see above) to obtain the final image in real 3D space.

5.2.3 Whitehall II Imaging Sub-study

The first 563 participants of the Whitehall II Imaging Sub-study were scanned at the Oxford Centre for Functional MRI of the Brain (FMRIB Centre) using a 3T Siemens Magnetom Verio (Erlangen, Germany) Scanner with a 32-channel receive head coil. The standard neuroimaging protocol lasted approximately 50 minutes and comprised of structural and functional sequences, and additional sequences, which were replaced after their acquisition on a sub-set of approximately N=100 participants, each. The following MRI sequences were acquired from every participant: a high-resolution T_1-weighted (T_1), a fluid attenuated inversion recovery (FLAIR), diffusion-weighted MRI (dMRI), resting state functional (rfMRI), and T2* scan. A full description of the MRI sequence parameters is provided in Appendix C.

Parameter	Sequence		
	T_1	FLAIR	dMRI
TR, *ms*	2530	9000	8900
TE, *ms*	1.79/3.65/5.51/7.37	73	91.2
Flip angle	7°	150°	n/a
Voxel, mm^3	1x1x1	0.9x0.9x3	2x2x2
FoV read	256	220	192
FoV phase	100%	100%	100%
Base resolution	256	256	96
Phase resolution	100%	100%	100%
TI, *ms*	1380	2500	n/a
Bandwith, *Hz/Px*	651	283	1680
Orientation	Sagittal	Transversal	Transversal
b-value, s/mm^2	n/a	n/a	1500
Directions, *N*	n/a	n/a	60 + 5 b=0
Acquisition T, *min*	6.02	4.28	9.93

Table 5.0 Acquisition parameters of T_1-weighted, FLAIR and dMRI images. FLAIR, fluid attenuated inversion recovery; dMRI, diffusion MRI; TR, repetition time; TE, echo time; FoV, field of view; TI, inversion time, Acquisition T; acquisition time.

T_1-weighted, FLAIR and dMRI images were used in this thesis and are described in detail below and their acquisition parameters are presented in Table 5.0. Each image was carefully inspected by a clinician (KPE) for structural abnormalities and by the imaging postdoctoral researcher (NF) for quality before inclusion in analysis. Exclusion numbers are detailed in Chapters 6-9 for each analysis.

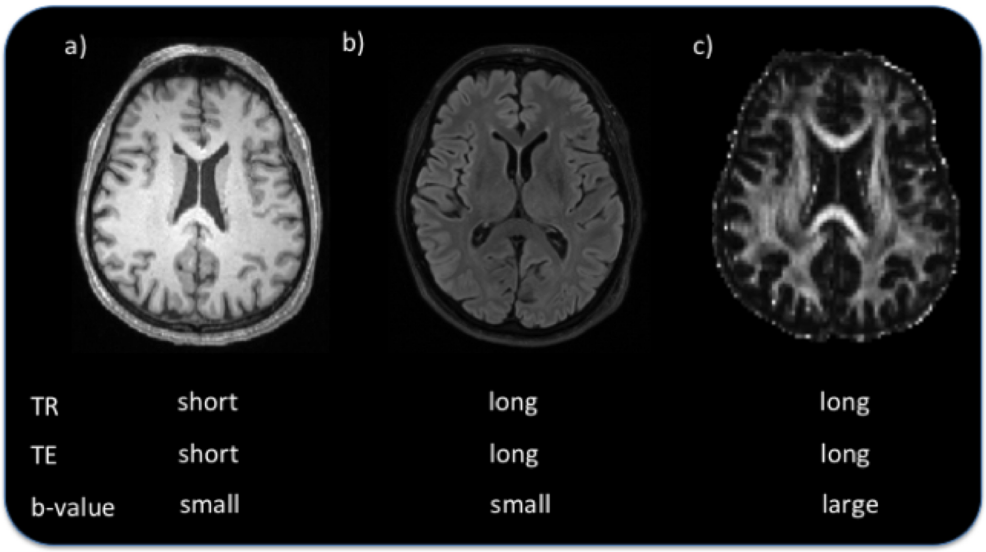


Figure 5.0 Scans acquired on a healthy 76-year-old male Whitehall Imaging Sub-study participant (no neurological, cognitive or psychiatric illness) with different image weighting used in this thesis. a) T_1-weighted image (WM in white, GM in grey, CSF in black), b) FLAIR image (WM in dark, GM in grey, CSF in black) c) FA map derived from diffusion-weighted image (WM in white, GM and CSF in black). TR, repetition time; TE, echo time.

5.3 Sequence parameters and analysis

5.3.1 T_1-weighted

5.3.1.1 Principles

GM, WM and CSF have different T_1 relaxation time, which are exploited on structural MRI images. For this reason structural MRI images are also called T_1-weighted images. As previously mentioned, during T_1 relaxation time protons release RF energy back into their environment. The amount of energy they transfer depends on how freely they can move within a certain tissue. Relatively unrestricted movement, such as in CSF, results in inefficient energy transfer and a long T_1 relaxation time, while restricted movement, such as due to myelin sheath in WM, leads to efficient energy transfer and short T_1 relaxation time: WM (800ms) < GM (1200ms) < CSF (4000ms). The difference in T_1 relaxation time between different tissues means that

when the RF pulse is removed, the net magnetisation *M* along B_0 is restored fastest in WM and slowest in CSF. A significant discrepancy in the signal intensity for each tissue can be achieved by applying another RF pulse before *M* is fully restored in all tissue types. If the repetition time (TR) between two RF pulses is long enough, *M* will be fully restored in all tissue types, making the strength of the MRI signal similar for each tissue, and consequently difficult to distinguish between them. Therefore, a typical T1-weighted image has a short TR in order to differentiate between WM, which has a high signal intensity and consequently appears bright on the image, CSF (low signal intensity = dark) and GM (intermediate intensity = grey) (Table 5.0, Image 5.0).

5.3.1.2 Whitehall II Imaging Sub-study T_1 sequence

Sequence properties

A 3-dimensional multi-echo magnetisation-prepared rapid acquisition (ME-MPRAGE) T_1-weighted structural sequence with online motion correction was employed, with TR 2530ms, TEs 1.79/3.65/5.51/7.37ms, flip angle 7°, a 256mm field of view (FOV) and 1mm isotropic voxel dimensions ((216, 217); Table 5.0). This sequence combines the properties of the standard MPRAGE sequence, which has excellent contrast properties for cortical segmentation, with multi-echo FLASH (hence multiple TEs) that provides better contrast for segmentation of subcortical structures across a number of automated segmentation tools. The ME-MPRAGE sequence results in 4 normalised and non-normalised images.

Sequence pre-processing

Sequence processing was performed using tools from FMRIB's Software Library (FSL version 5.0; www.fmrib.ox.ac.uk/fsl; (218)). The 4 normalised images were averaged to create a single image before running the anatomical pre-processing pipeline script using fsl_anat (http://fsl.fmrib.ox.ac.uk/fsl/fslwiki/fsl_anat). This image was corrected for spatial intensity variations (also known as bias field or radio frequency (RF) inhomogeneity) that arise due to some brain areas being closer to the head-coil channels, as part of FMRIB's Automated Segmentation Tool (FAST; (219), and brain extracted with –f 0.3 using FMRIB's Brain Extraction Tool (BET; (220)), which was visually checked afterwards to ensure sufficient neck removal.

5.3.1.3 Cortical atrophy

Brain tissues were segmented and the total GM, WM and cerebrospinal fluid (CSF) volumes were extracted using FAST with –g option, which is a binary segmentation option resulting in one image per tissue class (219). Images were visually inspected to ensure correct segmentation. Cortical atrophy was estimated by scaling the GM values for the total intracranial volume (GM + WM + CSF) resulting in percentage total GM volume, an estimate of cortical atrophy.

5.3.1.4 Grey matter density / Voxel based morphometry (VBM)

Image analysis was performed with FSL-VBM (http://fsl.fmrib.ox.ac.uk/fsl/fslwiki/FSLVBM; (221)) an optimised VBM protocol (222) using FSL tools (www.fmrib.ox.ac.uk/fsl; (218)) to assess the linear associations

between secondary markers of stress response and voxel-wise grey matter density[3], a measure highly correlated with grey matter volume (223), in an automated protocol. The advantage of VBM is that it does not require an a priori hypothesis about the localisation of results associated with a score or between study groups and thus reduces the likelihood of Type II error. It is also not operator-dependant.

Normalised bias-corrected brain extracted images were grey matter-segmented before being registered to the MNI 152 standard space using FMRIB's non-linear registration tool (FNIRT; (224)). The resulting images were averaged and flipped along the x-axis to create a left-right symmetric, study-specific grey matter template. Second, all native grey matter images were non-linearly registered to this study-specific template and "modulated" to correct for local expansion (or contraction) due to the non-linear component of the spatial transformation. The modulated grey matter images were then smoothed with an isotropic Gaussian kernel with a sigma of 3 mm. A study-specific grey matter mask was created using a combination of the VBM grey matter mask and thresholded (visual inspection based arbitrary threshold) MNI 152-based grey matter mask to enable accurate localisation of results in an ageing sample where atrophy is common (see Figure 5.1).

[3] Grey matter density here refers to the relative amount of grey matter and not cell-packing density (number of cells in a synaptically dense region with few cell bodies).

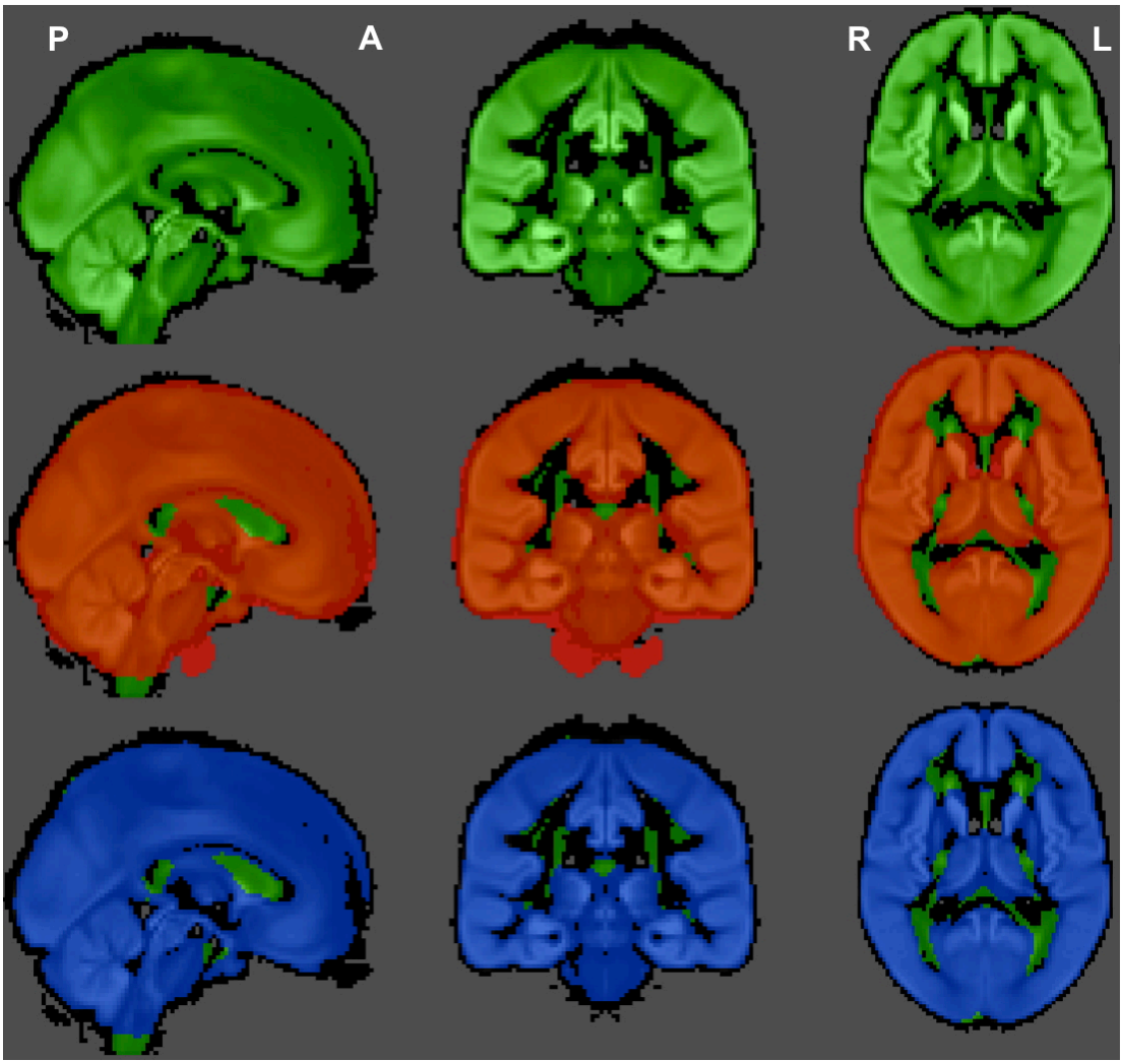


Figure 5.1 Example of a study-specific grey matter mask for VBM analysis. In green the VBM grey matter mask is shown on top of the study-specific grey matter template, which over-estimates the amount of grey matter, clearly extending into the ventricles and CSF. In red the thresholded MNI 152-based grey matter mask provides a better fit but over-estimates grey matter in the cortical areas and the neck. In blue the study-specific grey matter template is shown, which covers the areas common to both those shown in red and green providing a more accurate localisation of results in an ageing sample, only minimally extending into the CSF.

5.3.2 Fluid Attenuated Inversion Recovery (FLAIR)

Fluid attenuated inversion recovery (FLAIR) is a modified T_2-weighted sequence that is used to characterise white matter lesions. Most tissues that are involved in pathological processes have higher water content than healthy tissue, and the fluid

causes the affected areas, such as those with lesions, to appear brighter on T_2-weighted images (225, 226).

5.3.2.1 White matter lesions

White matter (WM) lesions are often seen on MRI scans of healthy and unhealthy older persons (183, 227, 228). WM lesions are of vascular origin, attributed to degenerative changes of small, deep penetrating arteries (cerebral small vessel disease; (229)) and can be divided into those present in subcortical and periventricular brain regions (230, 231). The presence of cerebral WM lesions increases with cardiovascular risk factors (232) and with age (233-236). In the older general population the prevalence of WM lesions ranges from 11-21% at around 64 years of age to 94% at age 82 (237, 238). In 1077 healthy men (N = 521) and women (N = 554) of the Rotterdam Scan Study aged between 60 and 90 years the prevalence and severity of WM lesions increased with age similarly for men and women; by 0.2% in subcortical and by 0.4% in periventricular regions even after adjusting for the vascular risk factors hypertension, diabetes and atherosclerosis. However, women tended to have more WM lesions of both types than men, as well as more severe, albeit difference in severity between the two groups was not statistically significant (236). WM lesions are also implicated in the pathogenesis of cognitive decline, dementia and mood disorders in later life. The presence and severity of periventricular WM lesions are associated with cognitive decline and dementia (239) and subcortical WM lesions are associated with late-onset depression (240, 241). Furthermore, WM lesions predict an increased risk of stroke and death (226).

5.3.2.2 Principles of T_2-weighted and FLAIR imaging

T_2-weighted

Similarly to T_1, T_2 relaxation times are different in GM, WM and CSF, which are exploited on T_2-weighted and FLAIR MRI images. As detailed above, T_2 relaxation time is measured from the interaction between proton spins after the RF pulse is removed and *M* is dephasing in the transverse plane. Similar to T_1, T_2 relaxation time varies based on microscopic tissue variations and the energy transfer is most efficient in WM where free movement of protons is most restricted: WM (70ms) < GM (80ms) < CSF (600ms). Therefore WM, which has a shorter T2 loses signal the fastest than GM and CSF.

T2-weighted imaging is normally achieved using a spin-echo sequence (242). This means that at a certain time after the first 90° RF pulse, i.e. at a certain time during dephasing, a second RF pulse is transmitted but this time at 180°. This refocusing reverses the phase angles but does not stop the dephasing. As tissue differences in T2 only become relevant when spins are left to dephase for some time, a long TR in combination with a long TE provides T2-weighted images. WM and CSF appear white, and GM grey in T_2-weighted images.

FLAIR

In FLAIR sequences an inversion-recovery pulse is used on the spin-echo sequence to suppress the signal from CSF, and consequently make it appear black on FLAIR images (Image 5.0). The preparatory pulse is applied to flip net magnetisation *M* vector by 180° and null the CSF signal. When the net magnetisation vector for water passes the transverse plane, i.e. the null point for water, the conventional 90° is

applied and the sequence continues. The time between the 180° and 90° pulse is the inversion time (TI). At TI the net magnetisation vector of water is weak whereas for other body tissues it is strong. As mentioned previously, flipping the net magnetisation vectors by the 90° pulse does not affect the dephasing of signal from other body tissues. This allows the detection of lesions that otherwise are not easily distinguishable or those that border fluid-containing spaces such as sulci or ventricles. (243, 244). White matter lesions are hyperintense on FLAIR images, therefore also called white matter hyperintensities (WMH) and mildly hypointense on T_1-weighted images (226) (Figure 5.2).

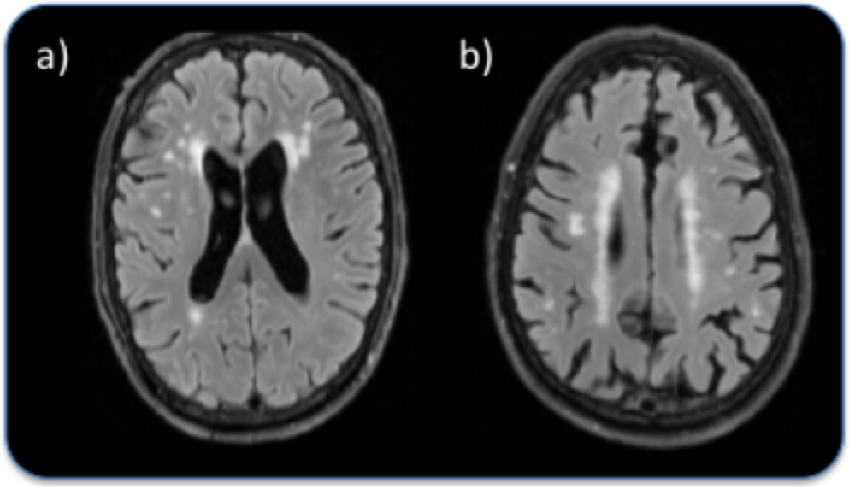


Figure 5.2 Example of a) periventricular white matter hyperintensities (WMH) and b) deep white matter lesions seen in the FLAIR image of a Whitehall II Sub-study participant. WMHs appear white (hyperintense) in FLAIR images.

5.3.2.3 Whitehall II Imaging Sub-study FLAIR sequence

Sequence properties

Fluid attenuated inversion recovery (FLAIR) images were acquired to characterise white matter hyperintensities (WMHs), with repetition time (TR) 9000ms, echo time

(TE) 73ms, field of view (FoV) 220mm and voxel dimensions 0.9 x 0.9 x 3.0mm (Table 5.0).

Sequence processing

WMHs were automatically segmented on FLAIR images with FMRIB's Brain Intensity AbNormality Classification Algorithm (BIANCA; (245)). BIANCA is a multimodal, automated, supervised method for WMH detection, based on the k-nearest neighbour algorithm. It classifies the image's voxels based on their intensity and spatial features, where the intensity features are extracted from FLAIR, T_1 and fractional anisotropy (FA) images. BIANCA offers options for weighting the spatial information, spatial intensity averaging and the choice of the number and location of training points. The following additional options were used: local average intensity within a 3D kernel of size = 3 voxels, MNI coordinates as spatial features, with a weighting factor of 2 and 24 manually segmented images as training dataset. The output image represents the probability per voxel of being WMH.

The total percentage WMH volume was calculated from voxels exceeding a probability of 0.9 of being WMH located within a white matter mask, and was adjusted for the total intracranial volume.

5.3.3 Diffusion Tensor Imaging (DTI)

5.3.3.1 Principles of diffusion tensor imaging (DTI)

Diffusion tensor imaging (DTI) is a useful MRI tool that assesses WM microstructure by quantifying the directionality and rate of diffusion of water molecules within different tissues (246-248). The diffusion of water molecules depends on the

structure and integrity of the tissue, and their interaction with barriers that restrict diffusion. When the movement of water is unrestricted in all directions, such as in CSF, the diffusion is isotropic and can be modelled with a sphere. When movement is restricted, such as in healthy WM, the diffusion is anisotropic and takes the form of an ellipsoid (Figure 5.3). Within WM a number of restrictive barriers can limit water diffusion perpendicular to (radial), but not along the length of the axon (axial). Such barriers include axonal membranes, myelin sheaths, and microtubules and neurofilaments (neurofibrils). The parallel organisation of membranes along the axon thus generates anisotropy, and myelin sheathes further increases the degree of anisotropy (249).

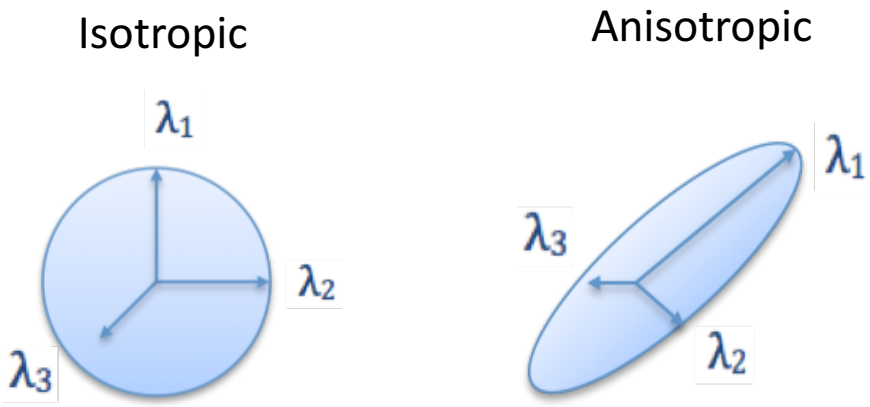


Figure 5.3 Diffusion ellipsoids are modelled for each voxel to produce a measure of the magnitude and directionality of diffusion. Where λ1 = λ2 = λ3, the tensor model is sphere-shaped and diffusion is said to be isotropic, such as in CSF and GM (left). Where λ1 >> λ2 ~ λ3, the tensor model is an elongated ellipsoid, and diffusion is anisotropic, such as in healthy WM. The image is created based on FMRIB Graduate Course lecture material.

In DTI the magnitude and direction of water diffusion is measured in each voxel in X, Y and Z dimension. A diffusion tensor ellipsoid is then fitted to each voxel with measurements that correspond to each axis. Three eigenvectors (ε_1, ε_2, ε_3) represent the orientation of major, medium and minor principal axes of the ellipsoid, while

three eigenvalues (λ_1, λ_2, λ_3) represent the direction of diffusivity in these dimensions (Figure 5.3). λ_1 denotes the largest axis and corresponds to the relative presence of CSF and extracellular water along axial direction of diffusivity (AD). It may reflect axon alignment in isolated fibre populations where pathological changes are reflected by an increasing amount of diffusion and consequently AD value (250). λ_2 and λ_3 are averaged to compute radial diffusivity (RD) along the minor axes. A higher RD is thought to reflect de- or dysmyelination (251). The average of all three eigenvalues is the mean diffusivity (MD) and reflect the relative presence of CSF in the voxel, providing a measure of membrane density. It is sensitive to cellularity, oedema and necrosis.

Fractional anisotropy (FA) is a ratio of axial and radial diffusivity, and is sensitive to microstructural changes (Figure 5.0). FA provides a measure of axonal orientation and coherent organisation of fibre tracts, membranes and myelination. Measured on a 0 to 1 scale, FA = 0 denotes isotropy and FA > 0 anisotropy. (252, 253). An overview is presented in Table 5.2.

Measure	Formula	Infers about
Fractional Anisotropy (FA)	$\sqrt{\frac{1}{2}}\frac{\sqrt{[(\lambda_1-\lambda_2)^2+(\lambda_2-\lambda_3)^2+(\lambda_3-\lambda_1)^2]}}{\sqrt{(\lambda_1^2+\lambda_2^2+\lambda_3^2)}}$	Fibre integrity
Mean Diffusivity (MD)	$(\lambda_1+\lambda_2+\lambda_3)/3$	Membrane density
Axial Diffusivity (AD)	λ_1	Axonal integrity
Radial Diffusivity (RD)	$(\lambda_2+\lambda_3)/2$	Myelin content

Table 5.2 An overview of DTI measures based on based on FMRIB Graduate course, (252) and www.diffusion-imaging.com/2013/01/relation-between-neural-microstructure.html. Lower FA and higher MD, AD and RD indicate white matter damage.

Mode (MO; (254, 255)) is another WM integrity measure. Rather than providing information about the restriction of diffusivity it informs about the shape of it, i.e. whether diffusion is primarily restricted in one (pancake shaped ellipsoid, suggesting one-fibre orientation) or two directions (cigar-shaped ellipsoid, suggesting crossing fibres). In conjunction with other diffusivity measures it may clarify the neurobiology underlying WM integrity differences (256). A combination of lower FA with higher MO might suggest reduced integrity in a WM tract, whereas the opposite could indicate macrostructural organisation of crossing fibres (255).

Although DTI is a popular diffusion-weighted model it is often criticised for its simplicity (257). Therefore, other alternative diffusion MRI analysis techniques exist such as diffusion kurtosis imaging (DKI; (258)), which provides a measure of tissue complexity, which is said to decrease with healthy ageing (259). Neurite orientation dispersion and density imaging (NODDI; (260)) quantifies the density and dispersion of neurites (axons and dentrites) but is yet to be applied to healthy ageing research. These alternative techniques could be used to provide complementary information about WM microstructure changes.

Diffusion-MRI estimates are highly sensitive to many microstructural changes but they lack specificity (261) and cannot directly assess myelin, which has an important role in ageing (252). Alternative MRI-based methods such as myelin water imaging (MWI), which uses T2 relaxation to infer myelin content, exist (262).

5.3.3.2 Principles of diffusion-weighted MRI (dMRI) sequence

In diffusion tensor imaging, image contrast is achieved by using diffusion weighting on the MRI sequence, hence called dMRI. dMRI sequences employ long TR and TE (Table 5.0 and Figure 5.0) and two gradient pulses, to first dephase the net magnetisation of protons in water and with a second pulse, to bring them back into phase, albeit not completely. Although the second pulse is of the same magnitude as the first one but in opposing direction the phases produced by the two gradient pulses do not cancel out. Rather, each proton has a different rate of movement along the direction of the diffusion gradient between pulses and so their signal in diffusing water molecules can be measured. Since the second pulse does not achieve perfect re-phasing, some MRI signal is lost, proportionally to the magnitude of diffusion. The signal loss is measured by comparing the diffusion-weighted image with an image that is acquired without diffusion weighting, the b0 image. The diffusion weighting b-value (measured in s/mm2) is determined by a combination of gradient pulse strength and duration, to determine how far water molecules can diffuse between two gradient pulses. Since not only the total amount of diffusion but also its directionality in each voxel is needed in order to compute the diffusion tensor for each voxel, multiple diffusion-weighted scans are acquired (here: 60; Table 5.0), each with the diffusion gradient applied in a different direction.

5.3.3.3 Whitehall II Imaging Sub-study dMRI sequence

Sequence properties

Diffusion-weighted MRI scans were acquired with an echo planar imaging sequence (60 diffusion weighted directions, b-value 1500 s/mm^2 and 5 non-diffusion weighted volumes, b-value 0 s/mm^2 (one b0 volume acquired in the reversed, posterior-

anterior, phase encode (PE) direction) with repetition time (TR) 8900ms, echo time (TE) 91.2ms, field of view (FOV) 192mm and 2mm isotropic voxel dimensions (Table 5.0). Monopolar diffusion encoding gradients with parallel imaging (GRAPPA) were used to minimise TE, which increases the signal to noise ratio (SNR), at the cost of a small increase in eddy-current distortion.

Sequence pre-processing

Despite its advantages in studying brain anatomy and structure, dMRI is susceptible to artefacts more than any other MRI technique used today (263, 264). These artefacts include image distortions (either due to inhomogeneities of the magnetic field (susceptibility) or eddy currents caused by rapid gradient switching during diffusion encoding), subject location within the field of view caused by subject motion (265) or signal dropout caused by bulk motion (subject or cardiac movement) during diffusion encoding (266).

Data correction was performed using FSL tools ((www.fmrib.ox.ac.uk/fsl; (218)). Data was corrected for susceptibility-induced distortions using two b=0 scans (b-value 0 s/mm^2) acquired with opposing PE directions that results in pairs of images with distortions going in opposite directions, estimating the susceptibility-induced off-resonance field, and combined into a single corrected image using the fsl_topup tool (267). Eddy current-induced distortions and subject movement within the FOV were corrected using the FSL tool eddy (268). In brief, a Gaussian Process was used to predict what each scan was supposed to look like and a second order polynomial model was used to transform each scan towards that prediction. This strategy also allowed for detection of outlier slices (dropout) caused by bulk subject movement

during the diffusion-encoding phase of the acquisition (266). The predicted slice replaced detected outliers, thus avoiding deleterious effects on derived parameters (e.g. FA or principal direction). Slices were classified as outliers if the signal was found to be more than 3 SD from the Gaussian Process predicted slice. The volume was removed if over 10 slices were identified as outliers within a volume. The scan was excluded from analysis if more than five volumes were removed.

5.3.3.4 White Matter Microstructure / Tract based spatial statistics (TBSS)

Voxelwise statistical analysis of Fractional anisotropy (FA), mean diffusivity (MD), axial diffusivity (AD) and radial diffusivity (RD) data was carried out using TBSS (Tract-Based Spatial Statistics, (269), part of FSL. A tensor model was fitted to the raw diffusion data using DTIFit part of FMRIB's Diffusion Toolbox (http://fsl.fmrib.oc.ac.uk/fsl/fdt) to create FA maps. This fits a diffusion tensor model to the raw diffusion data and then brain-extracts using BET (220). All subjects' FA data were then aligned into a common space using the FMRIB Nonlinear Registration Tool FNIRT (224), which uses a b-spline representation of the registration warp field (270). Next, the mean FA image was created and thinned to create a mean FA skeleton, which represents the centres of all tracts common to the group. Each subject's aligned FA data was then projected onto this skeleton and the resulting data fed into voxelwise cross-subject statistics. This method was repeated for mean diffusivity (MD), axial diffusivity (AD) and radial diffusivity (RD).

TBSS has improved sensitivity and interpretability of multi-subject diffusion imaging analysis by using nonlinear registration and addressing the arbitrariness of the level of spatial smoothing by projecting onto an alignment-invariant tract representation

(the mean-FA skeleton). However, its remaining disadvantage is its ability to assess diffusion patterns where WM fibres cross. Crossing fibre orientations should be estimated to improve TBSS measures, before performing probabilistic tractography to reconstruct white matter bundles and assess structural connectivity (271).

5.4 Statistical analysis

Voxelwise general linear model (GLM) was applied for the linear association of stress markers with MRI data using Randomise (272), correcting for multiple comparisons across space. Randomise is a permutation-based non-parametric statistical test, therefore is appropriate to be used where the outcome does not follow a normal distribution and contain outliers. For an arbitrary GLM, Randomise uses the method of Freedman & Lane (273). Based on the contrast (or set of contrasts defining an F test), the design matrix is automatically partitioned into tested effects and nuisance (confounding) effects. First, the data are fit to the nuisance effects alone to form nuisance-only residuals. These residuals are permuted (N = 5000), and then the estimated nuisance signal is added back on, creating an approximate realisation of data under the null hypothesis. This realisation is fit to the full model before the test statistic of choice (in Chapters 6-8: a t-statistic, and in Chapter 9: F-statistic) is computed as usual. This process is repeated to build a distribution of test statistics equivalent under the null hypothesis specified by the contrast(s). For simple models such as a correlation, this method is equivalent to the standard exact tests; otherwise, it accounts for nuisance variation present under the null hypothesis. The significance threshold was set at $p < 0.05$, using threshold-free cluster enhancement (TFCE; (274)). TFCE does not require a priori definition of an arbitrary cluster-forming

threshold and spatial smoothing, therefore is a sensitive thresholding option. Hence, cluster-like structures are enhanced while the image remains voxelwise. TFCE gives improved sensitivity and richer, more interpretable output than cluster-based thresholding (TFCE; (274)).

5.4.1 Nuisance variables

5.4.1.1 Covariates of no interest

The concept of different types of nuisance variables was discussed in section 4.2.2. Socio-demographic covariates of no interest were defined in section 4.3.2.1. In addition, motion correction during acquisition was applied on some (15%) of the MEMPRAGE T_1 scans. Since it affected both image quality and preliminary VBM results it was included as a standard covariate of no interest in every VBM-based analysis. To avoid repetition and confusion, as it is a methodological rather than experimental confounder, its inclusion will not be mentioned in the analysis chapters to follow.

5.4.1.2 Mediation analysis

The concept of mediation analysis was introduced in section 4.3.2.3. Percentage grey matter (%GM) and white matter hyperintensity (WMH) volumes are used as possible mediators in this thesis. Where a significant linear association between a stress marker and fractional anisotropy (FA) in Chapters 6-8 was found, %GM and WMH volumes were entered as nuisance variables to test whether the relationship between a secondary stress marker and FA decrease was mediated by %GM (i.e. an estimate of cortical atrophy due to Wallerian degeneration, section 5.3.1.3) or WMH

volume (i.e. lesion as opposed to homogenous white matter effect measured on FLAIR images using FMRIB's BIANCA, section 5.3.2.3.2).

5.4.2 Atlases

Results were localised using the Harvard-Oxford cortical and subcortical structural atlases for VBM. These atlases cover 48 cortical and 21 subcortical structural areas, based on T_1-weighted images of 37, 18-50 year-old healthy adults (21 males, 16 females) that were individually segmented by the Harvard Center for Morphometric Analysis then affine-registered to MNI152 space using FMRIB's Linear Image Registration Tool (FLIRT; (275, 276)). The transforms were applied to the individual labels before combining them across subjects to form population probability maps for each label (277).

John Hopkins University (JHU) DTI-based white matter atlases were used for identifying the location of TBSS results. In the ICBM-DTI-81 white-matter labels atlas, 48 white matter tract labels were created by hand segmentation of a standard-space average of diffusion MRI tensor maps of 81, 18-59 year-old healthy males (N=42) and females (N=39) (278). In the JHU white-matter tractography atlas, 20 structures were identified probabilistically by averaging the results of deterministic tractography on 28 healthy young males (N=17) and females (N=11) (279).

Chapter 6: Framingham Stroke Risk and Brain Structure

6.1 Introduction

6.1.1 Background

The effects of psychosocial stress have been most extensively studied in association with cardiovascular health and risk, including hypertension and disease, in the context of the workplace (56). Mid-life hypertension is associated with an increased risk of late-onset depression (54) and dementia (280). It has been linked to atrophy in both occipital and frontal cortical regions (281) and in hippocampus (282) in cognitively healthy older adults. Cumulative hypertension across mid-life also predicts structural brain changes in deep white matter in healthy older adults (60). Multifactorial cardiovascular and stroke risk scores, such as the Framingham Coronary Heart Disease (143) and Stroke risk (61) scores are associated with cognitive decline (62) (131), and structural brain changes such as grey matter volume reduction (64) and white matter hyperintensities (65). In turn, patterns of structural brain changes discriminate between those with high versus low coronary heart disease risk, as measured by the Framingham Coronary Heart Disease Risk score, even after accounting for genetic risk for Alzheimer's disease (283).

Framingham Stroke Risk score is a secondary marker of chronic stress and allostatic load and can be viewed as functional biomarker of the biological ageing pathway from life stresses to Type II allostatic overload and ill health in epidemiological research (55).

The Whitehall II (Stress and Health) Study was established in order to comprehensively assess the relationship between workplace stress and cardiovascular outcomes (52). Psychosocial workplace stressors have been extensively linked to both negative cardiovascular health and stroke risk and outcomes in the Whitehall II cohort (57, 284, 285). Moreover Framingham Stroke Risk has been shown to strongly predict the incidence of stroke (130) and cognitive decline (131) amongst Whitehall II participants. Chapter 6 examines whether there is a relationship between mid-life stroke risk and structural brain outcomes in older life.

6.1.2 Aims and hypotheses

6.1.2.1 Aims

Framingham Stroke multi-risk measure predicts the 10-year probability of a stroke but we know little about how it predicts brain integrity. Therefore the aims of the following analyses were:

1. To examine whether there is an association between the Framingham 10-year probability Stroke Risk Score (FSRS) across five study phases over a 20-year period and structural brain integrity at follow-up in older age, namely grey matter density and white matter microstructure
2. To examine how far back in time FSRS predicts brain structure.
3. To examine whether FSRS makes a unique contribution to grey and white matter integrity after accounting for the effects of demographic and socioeconomic factors.
4. To examine whether white matter microstructure measures, namely fractional anisotropy (FA), associated with FSRS may be due to Wallerian degeneration or regional white matter changes.

6.1.2.2 Hypotheses:

1. A strong association between FSRS and lower structural brain integrity in older age was hypothesised to be present after controlling for the effects of demographic or socioeconomic confounders.
2. Since FSRS represents the risk of stroke within 10 years it is assumed that its effects on the brain will take 10 years to manifest. Therefore, the strength of the association between FSRS and measures grey and white matter structure was expected to be the weakest 20 years before the scan and close to the time of the scan, and strongest 10 years before the scan, similar to an inverse U-shape.

6.2 Methods

6.2.1 Sample characteristics, inclusion/exclusion criteria

The sample of participants used in the analyses below was drawn from 563 Whitehall II Imaging Sub-study participants, described in section 4.1. Participants were excluded from analysis if they did not undergo an MRI scan, had noticeable structural abnormalities, such as a stroke, cyst or hydrocephalus, had poor image quality even after pre-processing and artefact correction, or had a missing Framingham Stroke Risk Score at any of the Whitehall II phases.

6.2.2 Assessment of Framingham Stroke Risk Score (FSRS)

Percentage Framingham Stroke Risk Score (FSRS) is a risk prediction algorithm that combines cardiovascular, metabolic and socio-demographic information to predict the 10-year probability of a stroke (61). FSRS was calculated at five Whitehall II Phases: 20 years (Phase 3), 15 years (Phase 5), 10 years (Phase 7) and 5 years (Phase 9) prior to MRI scan, as well as at follow-up (Phase 11), around the time of MRI scan

(Table 6.0). FSRS was composed of cardiovascular and metabolic risk factors detailed in section 4.2.1.1).

	P3 '91-93	P5 '97-99	P7 '03-04	P9 '07-09	P11 '12-13
Age, *years, Mean (SD)*	48.20 (5.2)	54.0 (5.2)	59.4 (5.2)	64.4 (5.2)	68.5 (5.2)
Framingham [10-year Stroke Risk] *Mean (SD)*	3.3% (1.4%)	3.9% (2.3%)	5.5% (4.8%)	6.8% (5.3%)	8.7% (6.4%)

Table 6.0 Overview of percentage Framingham Stroke Risk Scores used in whole-brain grey matter analysis (N = 405). P = Phase. Mean age at each phase (in blue) is not directly used in analysis. Follow-up at 2012-2014. See also Tables 6.1 and 6.2 for more details.

6.2.3 Assessment of nuisance variables

FSRS at Phase 3, percentage total GM volume (%GM), an estimate of cortical atrophy, and percentage white matter hyperintensities (%WMH), an estimate of WM lesions, described in chapters 5.3.1.3 and 5.3.2.3 respectively, were used as potential mediators. Subsequently, biological/demographic variables age at MRI scan, sex, ethnicity, and socioeconomic variables years of education and mid-life occupational status were identified from self-reported questionnaires at the Whitehall II Phase 1 clinic and in Oxford, which were used as covariates of no interest (detailed in section 4.2.2).

6.2.4 MRI Methods

6.2.4.1 Acquisition and analysis

Participants were scanned at the Oxford FMRIB Centre using a 3T Siemens Magnetom Verio (Erlangen, Germany) scanner with a 32-channel receive head coil.

T_1-weighted, FLAIR and diffusion-weighted MRI images were acquired as part of the protocol (see section 5.3, (127)). Image analysis was performed using tools from the FMRIB Software Library (FSL version 5.0, (218)).

6.2.4.2 Grey matter volume and density

Volumetric grey matter (GM), white matter (WM) and cerebrospinal fluid (CSF) were segmented and extracted from T_1-weighted images using FSL-FAST (219). Percentage total GM volume was calculated by scaling the GM value for total intracranial (GM + WM + CSF) volume.

In order to examine whole-brain GM density changes, T_1-weighted images were analysed with FSL-VBM (221) an optimised VBM protocol detailed in section 5.3.1.3 (222). Significant GM voxels were localised with the Harvard-Oxford cortical and subcortical structural atlases (277).

6.2.4.3 White matter hyperintensities and microstructure

White matter hyperintensities (WMHs) were automatically segmented on FLAIR images with FMRIB's BIANCA tool (245). The total percentage WMH volume was calculated from voxels exceeding a probability of 0.9 of being WMH, and was adjusted for the total intracranial volume (see section 5.3.2 in detail).

Voxelwise statistical analysis of microstructural WM was carried out on DTI measures, namely fractional anisotropy (FA), mean diffusivity (MD), axial diffusivity (AD) and radial diffusivity (RD), using FSL-TBSS (Smith, 2006) (detailed in section 5.3.2.3). JHU DTI-based white matter atlases were used for identifying the location of TBSS results (278, 279).

6.2.5 Statistical analysis

Voxelwise GLM was applied for the analysis of grey matter (GM) and DTI data using Randomise (272), a permutation-based non-parametric statistical test, running 5000 permutations and correcting for multiple comparisons across space. The significance threshold was set at $p < 0.05$, using threshold-free cluster enhancement (TFCE; (274), see also section 5.3.3).

6.2.5.1 Models I a) – c)

Linear associations between FSRS measured at five phases and voxelwise GM and DTI data were assessed (Model I).

Analyses with significant results for associations between FSRS at Phase 11 and voxelwise GM, FA and MD were repeated using FSRS at Phase 3 as a covariate of no interest, in order to remove the between-subject variability of baseline (Phase 3) risk, and thus examine the effect of new risk acquired over a 20-year period, between Phase 3 and scan time (follow-up). Controlling for the earliest available FSRS removes variance shared between the two scores, including between-subjects age and sex effects, which contribute to FSRS, thus providing a way to estimate biological ageing over the intervening period (see also section 2.5.1 and 4.2.2).

Subsequently, to assess whether the widespread association between FSRS and FA was mediated by percentage total GM or WMH volume, model I analysis was repeated covarying for these (model I b) and c) respectively).

6.2.5.2 Models II - III

Significant model I analyses were repeated including demographics (age, sex, ethnicity; model II) and demographics and socioeconomic variables (age, sex, ethnicity, education years, employment grade; model III) as covariates.

6.2.5.3 Plotting significant GMD, FA and MD values

The nature and directionality of the significant relationship between the unique variance explained by FSRS after controlling for the effect of age, sex, ethnicity, occupational position and education years (Model III)), and mean grey matter density (GMD), fractional anisotropy (FA) and mean diffusivity (MD) values was demonstrated by plotting these values for VBM and TBSS results respectively. First, a linear regression with age, sex, ethnicity, occupational position and education years as independent variables and FSRS as dependent variable was run and the standardised residuals saved in SPSS (IBM, version 22). A binarised mask was created based on the $p < 0.05$ thresholded (corrected for confounders) significant contrast, and used for the extraction of each participant's mean GMD, FA and MD values from the smoothed, modulated 4D grey matter image and the 4D image containing all the projected skeletonised FA and MD data, respectively. Correlation plots between the standardised residuals and individual mean GMD, FA and MD values were created.

Where Model III results were non-significant, values from Model I were plotted following the above steps.

6.3 Results

6.3.1 Descriptive statistics

6.3.1.1 Participant exclusion / inclusion

From the 563 total recruited, participants with no T_1 scan (N = 11), with structural abnormalities (N = 18) or inadequate T_1 scan (N = 2), missing Framingham Stroke Risk score at any of the five phases (N = 122), missing (N = 10) or un-useable DTI scan (N = 5) were excluded from analysis. VBM analysis was carried out on a final sample of N = 405 (72% of those attended), and TBSS on N = 395 (70% of those attended) participants. An overview is presented in Figure 6.0.

6.3.1.2 Participant demographics and nuisance variable characteristics

Participant characteristics used in analysis are shown in Table 6.1, and do not substantially differ from the total sample's presented in section 4.1.

	VBM (N = 405)	**TBSS (N = 395)**
Age *[years]* *Mean (SD), range*	69.6 (5.2) 60-83	69.6 (5.2) 60-83
Sex, *N (%)*		
Male	320 (79.0)	312 (79.0)
Female	85 (21.0)	83 (21.0)
Ethnicity, *N (%)*		
White	374 (92.3)	365 (92.4)
Non-white	31 (7.7)	30 (7.6)
Grade, *N (%)*		
Administrative (highest)	172 (42.5)	167 (42.3)
Professional/executive	197 (48.6)	194 (49.1)
Clerical/support	36 (8.9)	34 (8.6)
Education level *[years]* *Mean (SD), range*	14.0 (3.0) 6-23	14.0 (3.0) 6-23

Table 6.1. Framingham Stroke Risk Study sample characteristics

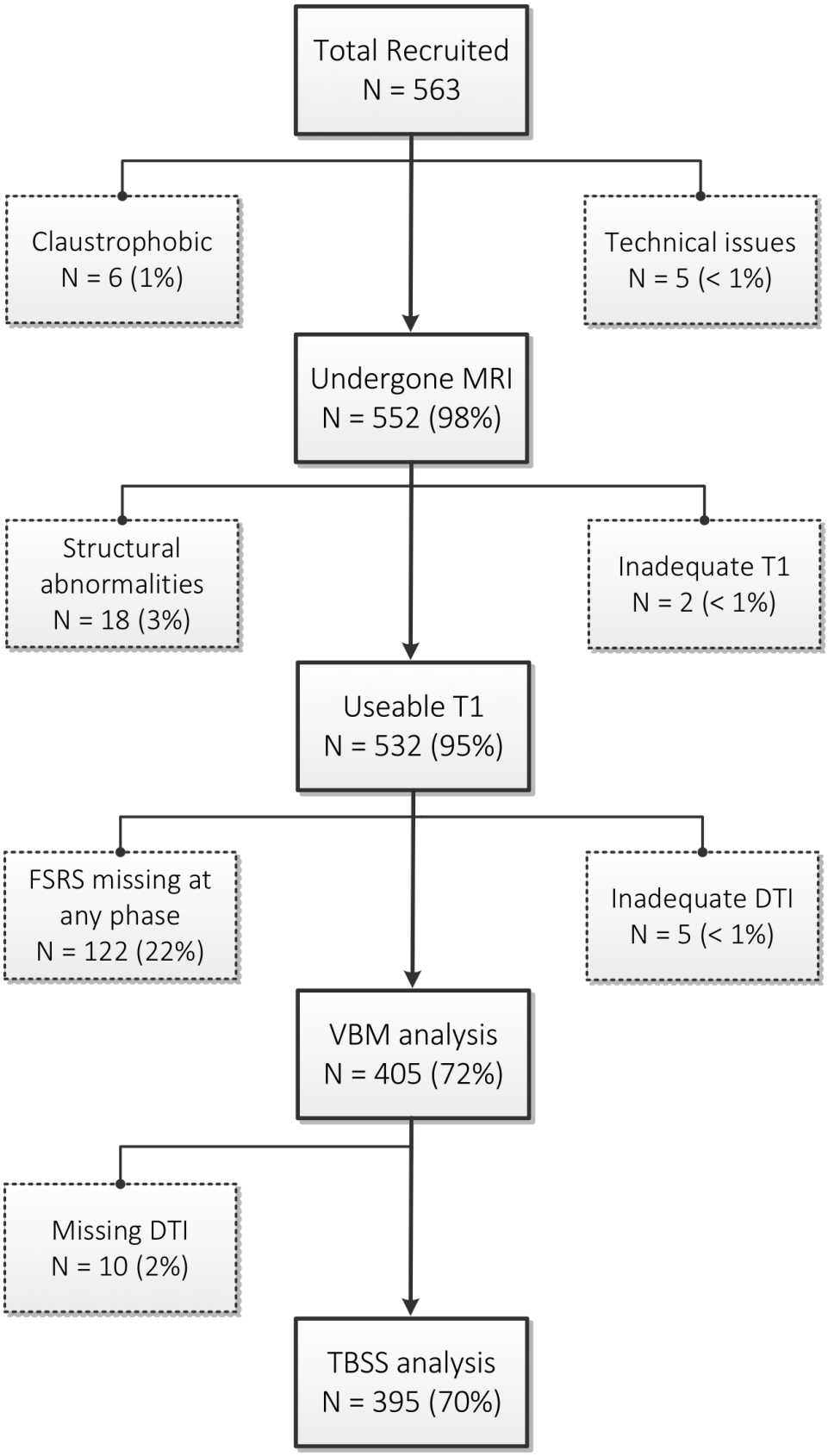


Figure 6.0 Flowchart of participant exclusion before final VBM (N = 405) and TBSS (N=395) analyses, including missing or inadequate scans and missing FSRS values.

6.3.1.3 Framingham Stroke Risk Score characteristics

Summary measures and distribution of FSRS over five Whitehall II phases is presented in Table 6.2 and Figures 6.1 and 6.2. Both the mean and spread of FSRS increased over the phases, on average by 1.4% every five years. The largest increase (1.9%) was between the most recent phase at the time of the scan and the one preceding it, when the cohort's age spread changed from 55 – 79 years to 60 – 85 years.

%, Mean (SD), range	**VBM (N = 405)**	**TBSS (N = 395)**
***P3** (1991 - 94)*	3.3% (1.4%) 1% -13%	3.3% (1.4%) 1% - 13%
***P5** (1997 - 99)*	3.9% (2.3%) 1% - %20	3.8% (2.2%) 1% - 20%
***P7** (2002 - 04)*	5.5% (4.8%) 1% - 52%	5.5% (4.7%) 1% - 52%
***P9** (2007 - 09)*	6.8% (5.3%) 1% - 52%	6.6% (4.7%) 1% - 37%
***P11** (2012 - 13)*	8.7% (6.4%) 1% - 47%	8.6% (6.2%) 1% - 47%

Table 6.2. Framingham 10-year Stroke Risk Score characteristics across five Whitehall II phases (P).

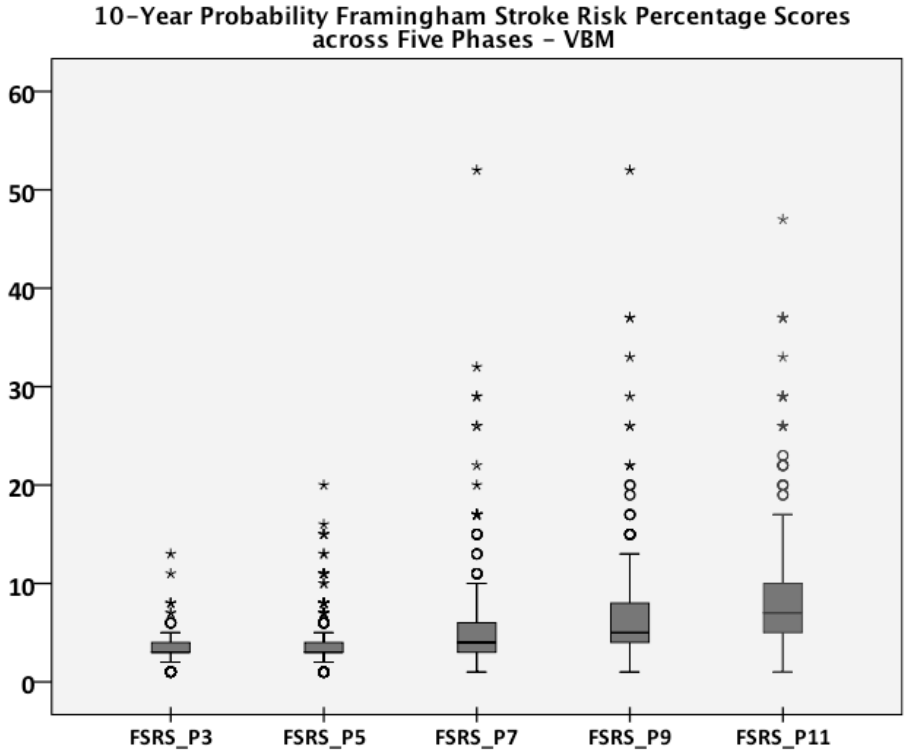


Figure 6.1. Framingham Stroke Risk Score (FSRS) distribution across five Whitehall II phases (P) in VBM analysis

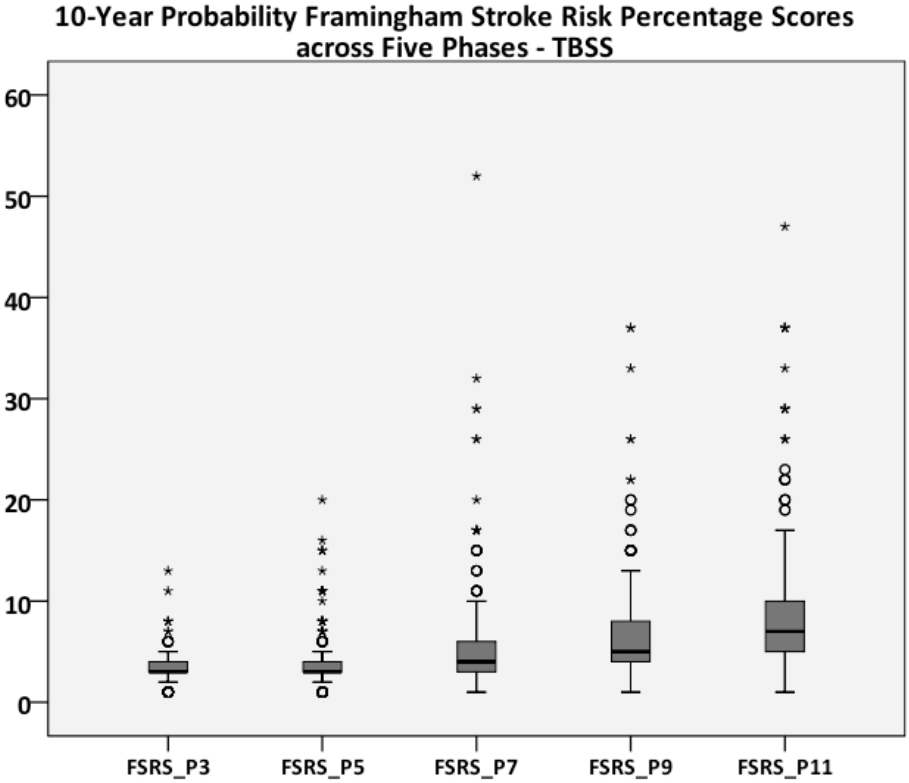


Figure 6.2. Framingham Stroke Risk Score (FSRS) distribution across five Whitehall II phases (P) in TBSS analysis

6.3.2 VBM Results

6.3.2.1 Model I

FSRS at each of the five phases, as early as 20 years preceding the scan was associated with widespread lower grey matter density at follow-up, across the cortex bilaterally, including higher cortical areas, the operculum and insular cortex, occipital cortex and medial temporal lobes (Figure 6.3 and Appendix D). Overall, FSRS measured in Phases 3, 5, and 9 was associated with lower GM than risk measured at follow-up, in Phase 11. Peak cluster locations were in the right frontal medial cortex (Phase 3: t (403) = 7.67, $p < 0.001$), right amygdala (Phase 5: t (403) = 8.02, $p < 0.001$; Phase 7: t (403) = 7.23, $p < 0.001$; Phase 9: t (403) = 7.79, $p < 0.001$) and left central opercular cortex (Phase 11: t (403) = 7.17, $p < 0.001$), see Table 6.3. The omnibus Chi-square test of independence was significant across the five phases: $\chi 2$ (4) = 7612.053, $p < 0.001$, $\phi = 0.075$. The Chi-square test between Phases 3 and 9 was also significant: $\chi 2$ (1) = 11.44, $p = 0.001$, $\phi = 0.001$ (Table 6.4).

Model I: FSRS 10yr probability								
	Cluster	Cluster size (voxels)	Max t	p-value	MNI coordinates (x, y, z)			Structure
P3	1	94680	7.67	< 0.001	6	40	-24	R frontal medial cortex
P5	1	98690	8.02	< 0.001	30	2	-16	R amygdala
P7	1	73602	7.23	< 0.001	30	2	-16	R amygdala
P9	1	93500	7.79	< 0.001	30	2	-18	R amygdala
P11	1	80718	7.17	< 0.001	-38	-16	22	L central opercular cortex
Ia: P11 (P3)	1	31454	5.52	< 0.001	46	4	-24	R temporal pole

Table 6.3 Framingham Stroke Risk score (FSRS) and whole-brain grey matter (GM) analysis results. FSRS at five Whitehall phases (P3 – P11) was associated with wide-spread lower GM bilaterally (Model I). Increase in risk over 20-years of the five phases (P11(P3)) was associated with lower GM bilaterally, predominantly in medial temporal lobes (Model Ia).

	P3	P5	P7	P9	P11	sum
Voxels in all significant clusters	94680	98690	73602	93500	80718	441190
Voxels in all non-significant clusters	171716	167706	192794	172896	185678	890790
Voxels in grey matter template	266396	266396	266396	266396	266396	

Table 6.4 Chi-square test for cross-table relationship.

6.3.2.2 Model I a)

Change in stroke risk between Phases 3 and 11, over a 20-year period, was associated with lower grey matter bilaterally, in cortical and subcortical areas. This association was about a third the size of the associations found with FSRS at any phase, e.g. 31454 voxels vs. 94680 voxels at Phase 3. Low GM was found in neocortical areas (including small parts of the orbitofrontal, somatosensory, motor strip, precuneus, and occipital cortex (Figure 6.3 and Appendix D), and more widespread in the operculum (including Heschl's Gyrus and planum polare), insular cortex, medial temporal areas, structures of the basal ganglia (including thalamus, putamen, nucleus accumbens, caudate and globus pallidus), and the temporal pole. Maximum t was located in the right temporal pole: t (402) = 5.52, $p < 0.01$ (Table 6.3).

6.3.2.3 Model II

After controlling for age, sex and ethnicity, FSRS measured in Phases 3 - 9 remained significantly associated with lower GM albeit markedly less so compared to Model I (Figure 6.3 and Appendix D). No association remained with FSRS measured in Phase 11. Results were localised in cortical areas within the right orbitofrontal cortex, along the supramarginal and temporal gyri, and in subcortical areas within the right medial temporal lobe. Most widespread results were associated with earlier phases (Phases 3 and 5) rather than the ones nearer the scan (Phases 7 and 9). Maximum t-values

were located in the right amygdala: Phase 3: t (400) = 4.72, p = 0.003; Phase 5: t (400) = 4.53, p = 0.008; Phase 7: t (400) = 4.72, p = 0.025; Phase 9: t (400) = 4.82, p = 0.004 (see Table 6.5).

6.3.2.4 Model III

After controlling the association further for socioeconomic variables, FSRS measured in Phases 3 to 9 remained significantly associated with lower GM values albeit further reduced (Figure 6.3 and Appendix D). Results were localised in the right ventromedial prefrontal cortex, right temporal pole and right medial temporal lobe. The associations followed a similar pattern to model II, whereby larger associations were found with stroke risk measured 20 and 15 years before the scan. Similarly to Model II, maximum t-values were located in the right amygdala: P3: t (398) = 4.71, p = 0.005; P7: t (398) = 4.82, p = 0.025; P9: t (398) = 4.94, p = 0.006; and in the right temporal pole: P5: t (398) = 4.78, p = 0.009 (see Table 6.6).

Model II: Model I + age, sex, ethnicity								
	Cluster	**Cluster size (voxels)**	**Max t**	**p-value**	**MNI coordinates (x, y, z)**			**Structure**
P3	1	1194	4.72	0.003	26	0	-20	R amygdala
	2	870	3.69	0.017	8	40	-16	R frontal medial cortex
	3	108	3.85	0.036	42	-46	54	R superior parietal lobule; supramarginal gyrus, posterior division
	4	90	3.39	0.038	30	50	12	R frontal pole
	5	88	3.8	0.031	22	50	26	R frontal pole
	6	25	3.04	0.046	32	24	-20	R frontal orbital cortex
P5	1	1075	4.53	0.008	30	0	-14	R amygdala
	2	217	3.56	0.031	46	-4	-2	R insular cortex; Heschl's gyrus
	3	186	3.83	0.031	-32	12	-20	L frontal orbital cortex; insular cortex
	4	105	3.43	0.038	50	-26	-10	R middle temporal gyrus posterior division
P7	1	99	4.72	0.025	22	0	-22	R amygdala
P9	1	703	4.82	0.004	24	0	-20	R amygdala
	2	312	3.64	0.027	48	2	-6	R planum polare
	3	140	3.89	0.026	52	-32	54	R supramarginal gyrus, anterior division; postcentral gyrus

Table 6.5 Framingham Stroke Risk score (FSRS) and whole-brain grey matter (GM) analysis results after controlling for age, sex, and ethnicity (Model II). FSRS measured at Phases 3, 5, 7 and 9 was associated with lower GM, smaller in volume than in Model I, primarily in right temporal areas.

Figure 6.4 shows mean grey matter density values extracted from the significant ($p < 0.05$, tfce) regions in which FSRS calculated at phase 3 is associated with lower grey matter density after controlling for age, sex, ethnicity, occupational position and education years in a non-parametric framework (model III). The plot demonstrates a negative linear relationship between FSRS and GM density, after controlling for the covariates of no interest.

Model III: Model II + socioeconomic status								
	Cluster	Cluster size (voxels)	Max t	p-value	MNI coordinates (x, y, z)			Structure
P3	1	428	4.71	0.005	26	0	-20	R amygdala
	2	271	4.22	0.015	42	24	-32	R temporal pole
	3	116	3.51	0.04	8	40	-16	R frontal medial cortex
P5	1	302	4.12	0.023	44	24	-28	R temporal pole
	2	260	4.78	0.009	30	0	-14	R amygdala
P7	1	82	4.82	0.025	22	0	-22	R amygdala
P9	1	297	4.94	0.006	24	0	-20	R amygdala

Table 6.6 Framingham Stroke Risk score (FSRS) and whole-brain grey matter (GM) analysis results after controlling for all confounders (Model III). FSRS at Phases 3, 5, 7 and 9 was associated with lower grey matter, smaller in volume than in Model I and II, in the right medial temporal lobe.

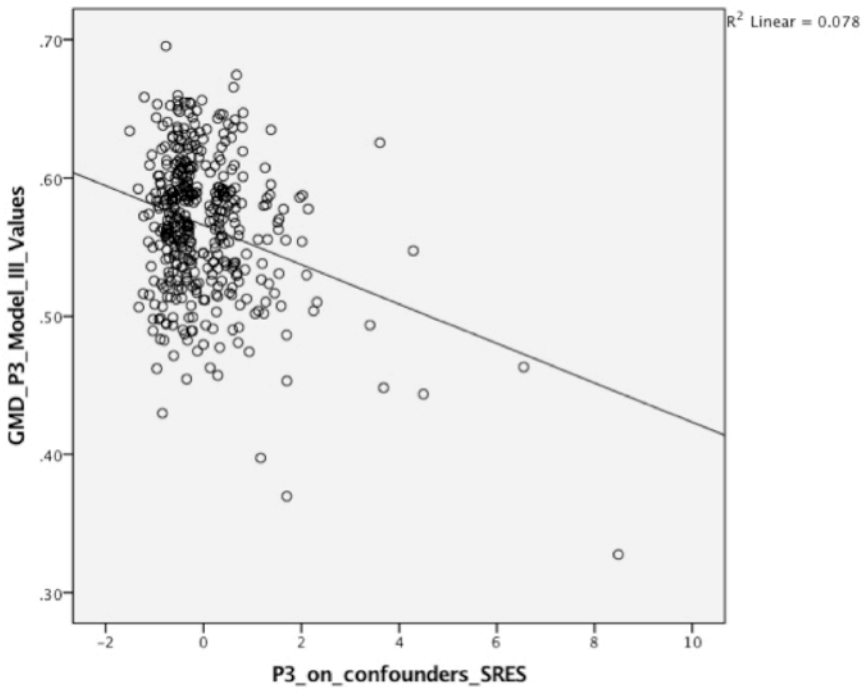


Figure 6.4 Regression plot of individual mean grey matter density values extracted from regions (y-axis) with which FSRS for Phase 3 is significantly (p < 0.05, tfce) associated, after controlling for all confounders of Model III (x-axis).

Stroke risk measured at any phase before or at scan was not associated with *higher* GM density in any of the models.

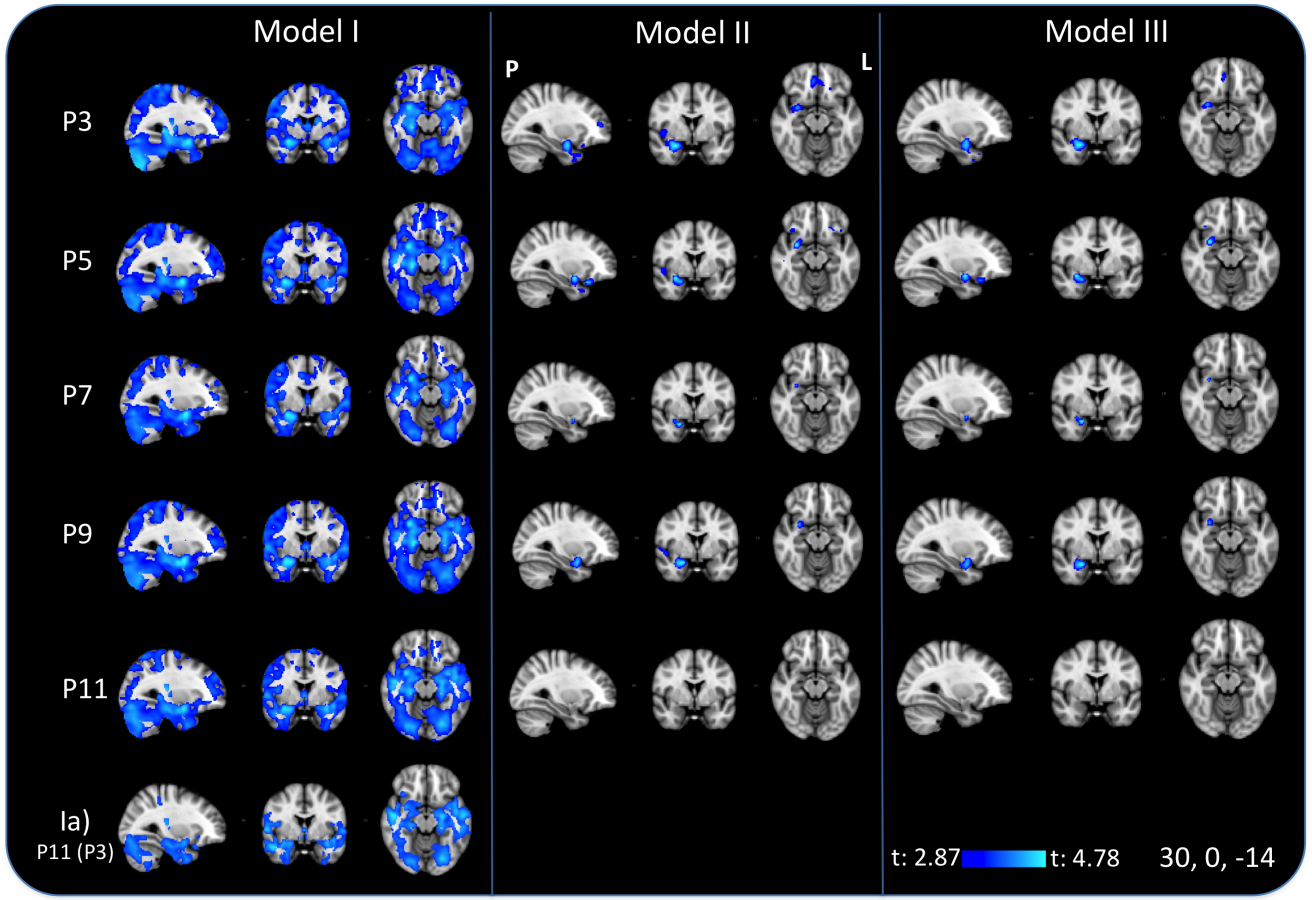


Figure 6.3 Association of Framingham stroke risk (FSRS), measured at five phases, with low whole-brain grey matter density. FSRS measured at each phase and new risk acquired between P3 and P11 (Ia) were associated with bilateral widespread grey matter (GM) (Model I). Significantly lower GM remained present with risk measured at Phases 3-9, but not at P11, after controlling for age, sex, ethnicity (Model II) and additionally socioeconomic factors (Model III), in right medial temporal lobe. Blue colour represents t-values significant at $p < 0.05$, tfce and multiple comparisons corrected.

6.3.3 TBSS Results

6.3.3.1 Fractional anisotropy

Model I

Whole-brain WM analysis revealed widespread lower FA values in association with FSRS measured at four phases, in Phases 5, 7, 9 and 11 (at follow-up). FSRS measured at follow-up was associated with lower FA in the most widespread areas, including anterior thalamic radiation, cingulum, anterior and superior corona radiata, corpus callosum, corticospinal tract, external capsule, forceps major, forceps minor, internal capsule, and superior longitudinal fasciculus. Peak cluster location was in the left forceps minor: t (394) = 7.39, $p < 0.001$. A smaller association followed this, 17-26% in comparison, with phases closer to and further away from the MRI scan respectively, in similar regions. Voxels with maximum t-values were also located in the left forceps minor: Phase9: t (394) = 7.1, $p < 0.001$; Phase 5: t (394) = 5.81, $p < 0.001$; and left forceps major: Phase 7: t (394) = 5.41, $p = 0.001$ (Table 6.7, Figure 6.4 and Appendix D).

Model I: FSRS 10yr probability								
	Cluster	Cluster size (voxels)	Max t	p-value	MNI coordinates (x, y, z)			Structure
P5	1	48846	5.81	< 0.001	-20	35	12	L forceps minor
P7	1	48762	5.41	0.001	-20	-79	15	L forceps major
P9	1	54427	7.1	< 0.001	-15	36	-4	L forceps minor
P11	1	65265	7.39	< 0.001	-18	37	11	L forceps minor
Ia: P11 (P3)	1	73048	6.86	< 0.001	-18	36	12	L forceps minor
Ib: P11 (%GM)	1	42269	5.71	0.002	-40	-54	41	L superior longitudinal fasciculus
Ic: P11 (%WMH)	1	5982	5.73	0.006	-18	37	11	L forceps minor
	2	174	5.01	0.04	24	-82	9	R inferior longitudinal fasciculus; forceps major
	3	60	3.55	0.047	-16	-11	52	L superior longitudinal fasciculus
	4	26	4.24	0.048	28	-55	21	R inferior longitudinal fasciculus
	5	13	3.83	0.049	29	-66	25	

Table 6.7 Framingham Stroke Risk score and whole-brain fractional anisotropy (FA) analysis results. FSRS at four Whitehall phases (P5 – P11) was associated with widespread lower FA values (Model I). Change in stroke risk over the five phases was also associated with widespread lower FA (Ia). The effect of FSRS at P11 on lower FA values was partially mediated by cortical atrophy (%GM; Ib) and almost completely mediated by total percent white matter hyperintensities (%WMH; Ic).

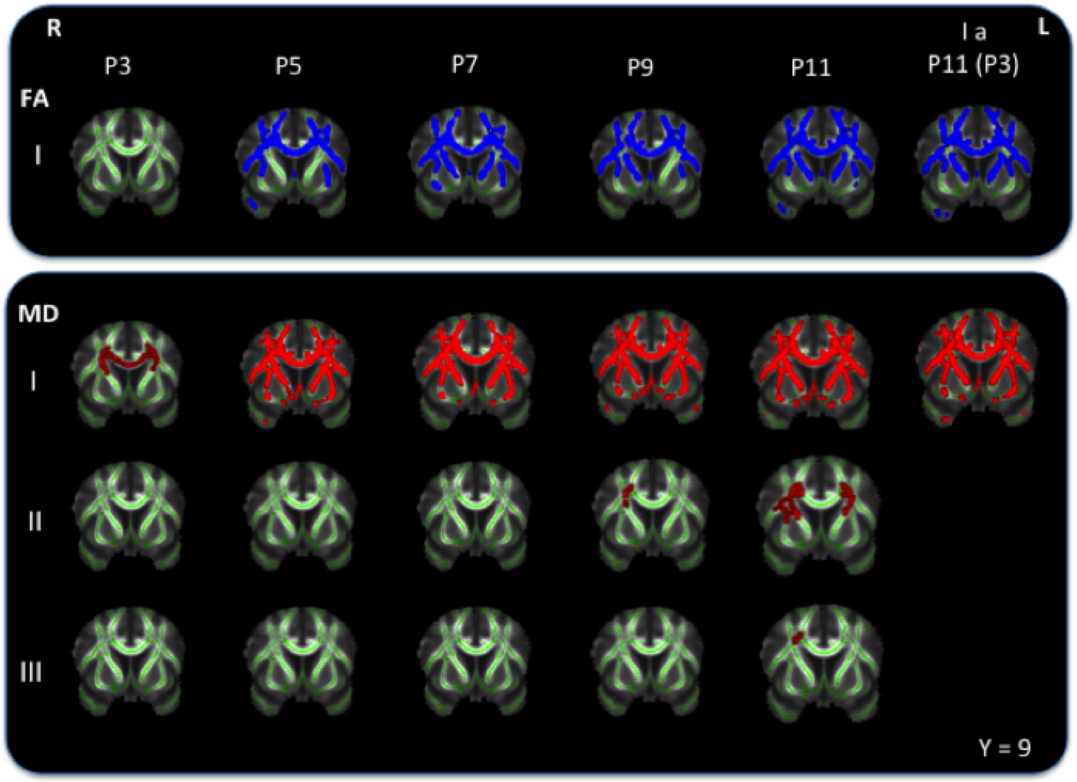


Figure 6.4 Association of Framingham stroke risk (FSRS), measured at five phases across 20 years, with whole-brain white matter measures. Significant regions (p < 0.05, tfce) are dilated for illustrative purposes, overlaid on a green skeleton.
Top panel in blue: FSRS at four Whitehall phases (P5 – P11) as early as 15 years prior to scan, as well as change in stroke risk over a 20-year period was associated with widespread lower FA values. No significantly higher FA was associated with FSRS at any point after controlling for confounders (Models II and III).
Bottom panel in red: FSRS at all phases and change in risk was associated with higher MD. Higher MD was associated with FSRS at P9 and P11 after controlling for age, sex, ethnicity (Model II) in the superior corona radiata (P9: right, P11: bilaterally) and with FSRS at P11 after controlling for all confounders (Model III), in right superior corona radiata.

Model I a), I b), I c)

Change in stroke risk between Phases 3 and 11 (Model I a)), was associated with widespread lower FA values in regions detailed above. This association was 11% larger than the largest association with FSRS, 73048 voxels vs. 65265 voxels at P11. Maximum t was located in the left forceps minor temporal pole: t (393) = 6.86, p < 0.001 (Table 6.7, Figure 6.4, and Appendix D).

Figure 6.5 shows mean FA values extracted from the significant ($p < 0.05$, tfce) tract volume in which change in FSRS is associated with lower FA. The plot demonstrates the negative linear association between mean FA values and FSRS calculated at Phase 3 after controlling for FSRS at Phase 11.

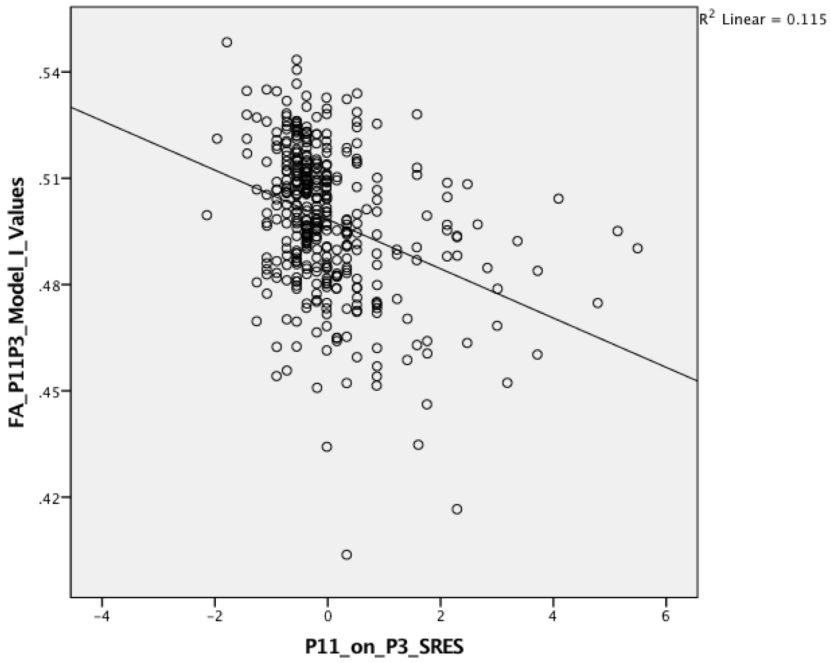


Figure 6.5 Regression plot of individual mean FA values extracted from the significant tract volume (y-axis), against FSRS calculated at Phase 11, after controlling for FSRS at Phase 3, x-axis ($p < 0.05$; tfce).

The mean percentage total GM (%GM) volume was 37% (SD = 2.1) and the mean percentage total white matter hyperintensities (%WMH) was 0.42% (SD = 0.27) in this sample of participants.

%GM as well as %WMH significantly correlated with lower FA values, even after controlling for FSRS measured at Phase 11. The association was more widespread with %WMH than %GM, the former including all major tracts and the latter localised primarily along the superior longitudinal fasciculus, corticospinal tract and anterior

thalamic radiation (Appendix D). Therefore both measures were entered in a regression analysis to reveal whether they mediate the effects of FSRS on lower FA.

The significant volume for the association between FSRS at follow-up (Phase 11) and lower FA values was reduced by 35% after covarying for %GM, from 65265 voxels to 42269 (Model I b)). The association between FSRS and lower FA was partially mediated by %GM, especially along the corticospinal tract, and anterior thalamic radiation. Peak cluster location was in the left superior longitudinal fasciculus (t (393) = 5.71, p = 0.002) (Table 6.7, Figure 6.6).

After controlling for percentage total white matter hyperintensities (%WMH) the volume of association of FSRS at Phase 11 with lower FA was reduced by over 90%, from 65265 voxels to 6255 (Model I c)). Therefore, the association between FSRS measured at Phase 11 and lower FA values, was almost completely mediated by white matter hyperintensities. The association was ***not*** mediated along the corticospinal tract, superior longitudinal fasciculus and anterior thalamic radiation. Peak cluster location was in the left forceps minor (t (393) = 5.73, p = 0.006) (Table 6.7, Figure 6.6).

Model II - III

No association between FSRS at any phase before or at the time of scan remained after controlling for age, sex, and ethnicity (model II), and socioeconomic variables (model III). No significant association was present between FSRS measured at any phase and *higher* FA in any model.

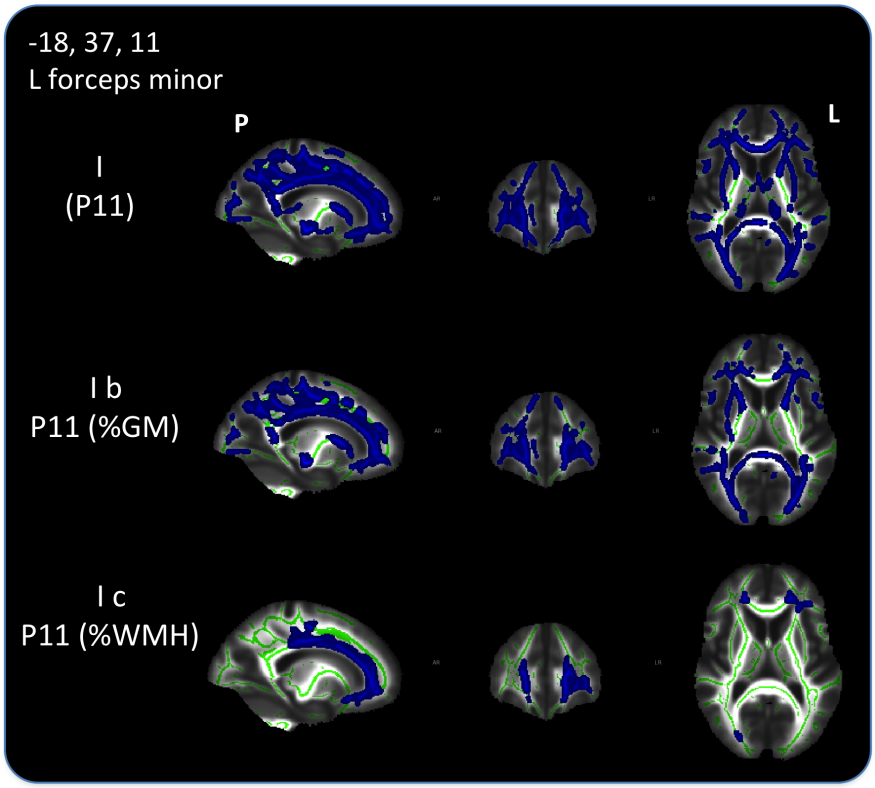


Figure 6.6 Widespread lower FA was associated with FSRS at time of scan. This association was partially mediated by cortical atrophy especially in the corticospinal tract, superior longitudinal fasciculus and anterior thalamic radiation (%GM; Ib) and almost completely mediated by total percent white matter hyperintensities, apart from along the corpus callosum (%WMH; Ic).

6.3.3.2 Mean diffusivity

Model I

Whole-brain WM analysis revealed widespread higher MD values in association with FSRS measured at five phases, as early as 20 years prior to follow-up (Phase 3) to follow-up (Phase 11), i.e. across Phases 3 to 11. FSRS measured at follow-up was associated with higher MD in most widespread regions also affected by lower FA. A 9-25% smaller association with higher MD was found with FSRS measured in phases 5-9, in similar regions. FSRS acquired 20 years prior to follow-up, in Phase 3, was the least associated with higher MD compared to FSRS at follow-up. This significant

association was contained in the right anterior limb of the internal capsule, body of corpus callosum, right forceps major, right forceps minor, and superior corona radiata. Voxels with maximum t-values were located in right superior corona radiata: Phase 3: t (394) = 5.61, $p = 0.035$; Phase 9: t (394) = 8.5, $p < 0.001$; Phase 11: t (394) = 8.22, $p < 0.001$; body of corpus callosum: Phase 5: t (394) = 7.71, $p < 0.001$; and right anterior thalamic radiation: Phase 7: t (394) = 7.7, $p = 0.001$ (Table 6.8, Figure 6.4 and Appendix D).

Model I a)

Change in stroke risk between Phases 3 and 11 (Model I a), was associated with widespread higher MD values in regions detailed above. This association was 11% larger than the largest association with FSRS at P11, 80869 vs. 71643 voxels. Maximum t was located in the left anterior thalamic radiation: t (393) = 7.83, $p < 0.001$ (Table 6.8, Figure 6.4, and Appendix D).

Model I: FSRS 10yr probability								
	Cluster	Cluster size (voxels)	Max t	p-value	MNI coordinates (x, y, z)			Structure
P3	1	2620	5.61	0.035	20	-3	34	R superior corona radiata
	2	601	4.47	0.043	27	3	32	R superior corona radiata
	3	208	4.29	0.048	25	-51	19	R forceps major
P5	1	60762	7.17	< 0.001	-18	8	31	Body of corpus callosum
P7	2	53630	7.7	0.001	21	13	9	R anterior thalamic radiation
P9	1	65603	8.5	< 0.001	22	0	33	R superior corona radiata
P11	1	71643	8.22	< 0.001	21	11	38	R superior corona radiata
Ia: P11 (P3)	1	80869	7.83	< 0.001	-18	7	11	L anterior thalamic radiation

Table 6.8 Framingham Stroke Risk score and whole-brain mean diffusivity (MD) analysis results. FSRS at five Whitehall Phases (P3 – P11) was associated with widespread higher MD values, as early as 20 years prior to scan (Model I). Change in stroke risk over the five phases was associated with widespread MD values (Ia).

Model II

No association remained with FSRS measured more than 5 years prior to scanning, in Phases 3-7, after controlling for demographic variables. FSRS measured 5 years prior to follow-up, in Phase 9, was associated with higher MD in the right corona radiata (peak in same location: t (390) = 4.81, p = 0.045) after controlling for age, sex, and ethnicity. A more widespread association with FSRS was measured at follow-up, primarily localised in the right hemisphere along the splenium of the corpus callosum, superior corona radiata (left, right), and superior longitudinal fasciculus (peak in right superior corona radiata: t (390) = 5.01, p = 0.034) (Table 6.9, Figure 6.5, Appendix D).

Model II: Model I + age, sex, ethnicity								
	Cluster	Cluster size (voxels)	Max t	p-value	MNI coordinates (x, y, z)			Structure
P9	1	235	4.81	0.045	25	6	23	R superior corona radiata
P11	1	2814	5.01	0.034	22	9	38	R superior corona radiata
	2	519	4.9	0.043	-25	12	32	L superior corona radiata
	3	515	4.21	0.048	38	-42	26	R superior longitudinal fasciculus
	4	35	3.98	0.049	-20	10	31	L superior corona radiata

Table 6.9 Framingham Stroke Risk score and whole-brain mean diffusivity (MD) analysis results after controlling for age, sex and ethnicity. FSRS 5 years prior to (P9) and at time of scan (P11) remained associated with higher MD values in right superior corona radiata (P9) and splenium, superior corona radiata, superior longitudinal fasciculus (P11).

Model III

FSRS at follow-up only remained associated with higher MD in the right superior corona radiata, after additionally controlling for socioeconomic variables (peak in right superior corona radiata: t (390) = 4.88, p = 0.047) (Table 6.10, Figure 6.5, Appendix D).

Model III: Model II + SES, education								
	Cluster	Cluster size (voxels)	Max t	p-value	MNI coordinates (x, y, z)			Structure
P11	1	118	4.88	0.047	22	9	38	R superior corona radiata

Table 6.10 Framingham Stroke Risk score and whole-brain mean diffusivity (MD) analysis results after controlling for all confounders. FSRS at at time of scan (P11) was associated with higher MD in the right superior corona radiata.

Figure 6.7 shows individual mean MD values extracted from the significant tract volume ($p<0.05$), against FSRS calculated at phase 11 positively associated with MD. The plot demonstrates the positive linear association between mean MD values and FSRS after controlling for all confounders: age, sex, ethnicity, occupational position and education years.

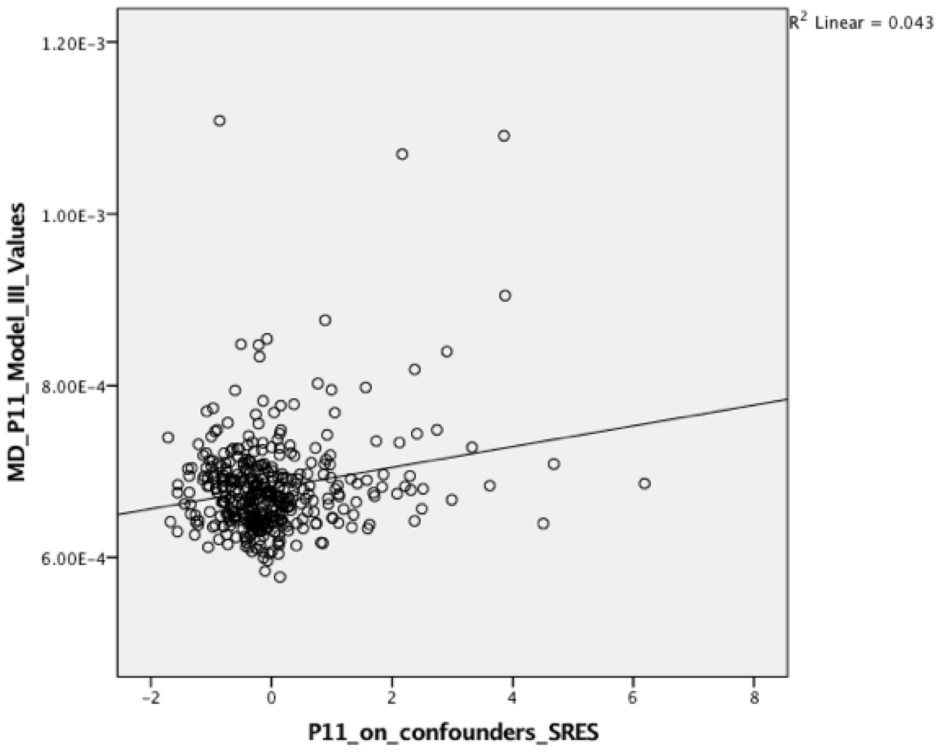


Figure 6.7 Regression plot of individual means of MD values extracted from the significant tract volume on y-axis ($p < 0.05$; tfce), against FSRS calculated at Phase 11, after controlling for all confounders in model III (x-axis).

No significant association was present between FSRS measured at any phase and decreased MD values in any model.

6.3.3.3 Axial and radial diffusivity

FSRS was associated with higher axial diffusivity (AD) in a pattern similar to the association seen in higher mean diffusivity results. The association of FSRS with higher radial diffusivity (RD) values mirrored the pattern seen in lower fractional anisotropy results. No association was revealed with lower AD and RD. Tables of AD and RD results are presented in Appendix D.

6.4 Discussion

In this chapter the linear association of Framingham Stroke Risk scores (FSRS, risk of stroke in % over the following 10 years) measured in five Whitehall II study phases, with whole-brain structural grey matter density and microstructural white matter integrity in older age was assessed.

6.4.1 Whole-brain grey matter

6.4.1.1 Summary of aims and hypotheses

FSRS in every study phase was associated with lower grey matter (GM) in widespread cortical and subcortical regions in older age, in line with ***Aim 1)*** of this study. This association was predicted as early as 20 years prior to the scan, in Phase 3 (***Aim 2)***). In addition, change in stroke risk over the 20-year period was associated with lower GM density, but this was mainly confined to sub-neocortical structures, i.e. medial temporal lobes, basal ganglia and temporal pole (***Aim 2)***).

Hypothesis 1) was supported through examining ***Aim 3)****:* FSRS was associated with lower GM even after controlling for demographic and socioeconomic variables. However, this association was substantially reduced 20, 15, 10, and 5 years before the scan, and was no longer significant for risk measured at the time of scan. Demographic factors removed most of the variance shared between FSRS and GM, while socioeconomic variables weakened the remaining effects of stroke risk. Demographic confounders removed association primarily in cortical and some temporal areas, while socioeconomic factors attenuated the ones not removed by demographic factors in medial temporal areas of the right hemisphere.

FSRS estimates the probability of a stroke in the subsequent 10 years, thus the fact that stroke risk measured at the time of scan was no longer associated with concurrent GM density might be, because the risk projected for a 10-year period had not manifested as GM density measurable by VBM techniques. This lends partial support to ***Hypothesis 2)***. Moreover, both controlled and uncontrolled associations were more widespread with FSRS measured earlier (15-20 years prior) than closer (≤10 years prior) to the scan. Change in stroke risk had the least widespread association with lower GM.

6.4.1.2 Unique FSRS effects

These findings suggest that the unique effects of 10-year probability stroke risk, which are not accountable for by age, sex, ethnicity, socioeconomic status or education levels, impact GM density in right medial temporal structures up to 5 years prior to the scan. This means that FSRS does not only predict established clinical stroke but also "subclinical" GM atrophy, interestingly particularly in medial

temporal lobe (MTL) structures that may be of relevance in the development of cognitive impairment (286) and dementias, e.g. Alzheimer's disease (287, 288) and dementia of vascular type (289). The effects of risk are present beyond chronological ageing, which itself is predictive of GM atrophy (290) and related cognitive decline in the general population (291, 292) as well as the Whitehall II cohort (126). Both Framingham Stroke and Cardiovascular Risk scores have been linked with impaired executive function (293) and global cognition (294, 295). This may be driven by the type-2 diabetes (T2D) and smoking components, as shown in a stroke free cohort of Framingham Offspring participants (N=1755, mean age=54±9 years) (293) as well as in a large group of individuals at risk across the lifespan (N=3778, mean age=54 years, range=35-82 years) (294). In the Whitehall II cohort higher FSRS at baseline predicted faster decline in verbal fluency, vocabulary and global cognition, but not in memory and reasoning, over a 10-year period (131). Furthermore both Framingham Stroke and Cardiovascular Risk scores were better at predicting the rate of decline in the aforementioned domains except for memory, than a multifactorial dementia risk score based on demographic, cardio-metabolic and genetic factors (63). In both studies T2D independently predicted global cognitive decline. One of the common risk factors of stroke and dementia is T2D. It predicts lower cognitive performance (296) and increased occurrence of cognitive impairment in older individuals (297), which might be due to underlying diabetes-associated atrophy seen particularly in medial temporal lobe structures (298-300).

6.4.1.3 FSRS, an estimate of biological ageing risk

Since FSRS was predictive of widespread lower GM as early as 20 years prior to scan, we might conclude that the effects of stroke risk do not change between 20 years

prior to and at the time of scan. However FSRS is a composite score, and is incremental with age, which makes it difficult to estimate at what time it starts to affect GM and at which point its effects become evident. By removing the variance shared between FSRS 20 years prior to the scan and at the time of scan, the between-subject variability of age and sex are removed, thus providing an estimate of cardio-metabolic biological ageing over 20 years. This estimate of biological ageing risk was associated with widespread lower GM density bilaterally in the opercular cortex, insular cortex, medial temporal areas, basal ganglia structures, and the temporal pole. This may mean that stroke risk already defines neocortical areas 20 years prior to the scan in older age, while sub-neocortical areas remain sensitive to change of risk over the 20-year period. This is consistent with the knowledge that hippocampi remain plastic in adulthood and can regenerate (301, 302).

The above regions are located in middle cerebral artery (MCA) vascular territories (303). The middle cerebral artery (MCA), which is the largest branch of the internal carotid and most often occluded by embolism, provides these areas with blood supply (304). This would provide a vascular explanation of results. As detailed above, stroke and dementia have common risk factors, and there is good evidence from epidemiological studies about the link between vascular risk factors and cognitive impairment (305, 306). However, the Baltimore Longitudinal Study of Ageing Autopsy Program (N=179; (307)) found that silent and clinically manifest hemispheral infarcts, but not deep subcortical infarcts, were responsible for dementia pathology. In this study clinical risk factors for stroke did not predict dementia (307). One voxel-wise grey matter study compared two groups of ischemic

stroke patients: a group free of cognitive impairment (N=51) and the other impaired in at least one cognitive domain (N=40). Those with impaired cognition in comparison with the cognitively healthy group demonstrated significant GM density reductions in areas also significant in the present study: in the thalamus, and smaller reductions in the cingulate gyrus, and frontal, temporal, parietal and occipital lobes (308).

Population-based (309) and prospective studies with imaging components, such as the Rotterdam study (310), Cardiovascular Health Cognition Study (311) and Whitehall II cohort, should provide further clarification. For instance, the present GM findings in the Whitehall II cohort could be extended by additionally controlling for white matter hyperintensities, a measure of vascular damage to WM. Nevertheless, to my knowledge, this study is the first to find an association between FSRS and GM decrease in voxel-wise analysis, even in the absence of past stroke, and thus has predictive value of GM atrophy and consequently cognitive impairment.

6.4.2 Whole-brain white matter

6.4.2.1 Summary of aims and hypotheses

FSRS in most phases was associated with widespread lower microstructural white matter (WM) integrity, in line with ***Aim 1)*** of this study. FSRS measured 20 years prior to scan, in Phase 3, was associated with higher mean diffusivity (MD) and axial diffusivity (AD) values only in the body of corpus callosum, superior corona radiata and their associated tracts in the right hemisphere. FSRS measured in four phases, up to Phase 5 ≤15 years before the time of scan, was associated with widespread lower fractional anisotropy (FA), and higher radial diffusivity (RD), MD and AD (***Aim***

2)). In addition, change in stroke risk over a 20-year period was associated with lower FA and higher MD values, in all major tracts (***Aim 2)***.

Hypothesis 1) was only partially supported through examining ***Aim 3).*** On the contrary to the expected FSRS no longer predicted lower FA and RD after controlling for demographic variables. Risk at the time of scan remained associated with higher MD and AD values in a few tracts mostly along the splenium and neighbouring tracts of the right hemisphere, and 5 years prior to the scan (Phase 9) in the right corona radiata, only. After controlling for socioeconomic variables, only FSRS at the time of scan predicted higher MD and AD values in the right corona radiata.

Interestingly, the strength of association with WM integrity measures showed an opposite pattern to that seen with GM, which suggests that stroke risk manifests more quickly as DTI detectable microstructural WM changes than VBM detectable GM density change. Uncontrolled associations were most widespread with change in risk over a 20-year period and closer to the scan (≤10 years prior), but were hardly present 20 years prior to scan. This result does not support ***Hypothesis 2)*** that the strength of association with FSRS across five phases followed an inverted U-shape.

In line with ***Aim 4),*** the effect of FSRS on FA is probably mediated by the extent of widespread WM changes that are visible in FLAIR images. The mediating effects of GM volume were small, suggesting that one-to-one connections between white and grey matter changes, such as found in Wallerian degeneration, are not of great importance.

6.4.2.2 Unique FSRS effects

The findings that WM integrity was no longer predicted by FSRS after controlling for demographic variables (apart from a slight association with MD close to the time of scan) suggests that a large amount of variance is shared between TBSS measures of WM integrity and demographic factors, in this sample of participants. Ageing is accompanied by decline in composition and integrity of WM, which compromise cognitive performance and is implicated in late-life depression (246). Contrary to findings in the present study, vascular and stroke risk effects in depression and on TBSS measures of WM integrity have been reported even after controlling for age and sex. For example, diagnosed vascular disease was associated with an increased risk of depressive symptoms in the Whitehall II cohort after adjusting for age and sex (130). Among those without manifest vascular disease however, the Framingham risk scores were associated with depressive symptoms before but not after age 65 (130). In a study comparing 36 older (72 ±7 years) depressed participants with age-matched controls, FSRS was correlated with lower FA values in the body, genu and splenium of corpus callosum and the corticospinal tract. In controls this relationship was only present in the body of corpus callosum (65).

6.4.2.3 An estimate of biological ageing risk and the mediating effect of WMHs

The estimate of biological ageing risk over 20 years (see above) was associated with widespread lower FA in all major tracts. This means that FA values in all areas remain sensitive to vascular risk, contrary to GM density in certain neocortical regions, where no further changes could be observed linked to new risk over 20 years before the scan (see above).

The effect of FSRS on fibre integrity was mediated by the extent of widespread WM changes that are visible in FLAIR images, which are generally interpreted clinically as micro-vascular changes (226). FSRS was predictive of WM hyperintensities in the present and past studies (312). WM hyperintensities affect cognitive abilities in healthy individuals (313) and may be related to late-onset depression and the maintenance of impaired cognitive function in late-life depression (314). In a small group (N=35) of people of 60+ years with major depression compared with a group of healthy individuals (N=19), WM hyperintensities rather than cortisol levels and GM atrophy appeared to underlie these deficits (314). However, some findings suggest that glucocorticoids-related neurodegeneration in temporal lobes and WM hyperintensities contribute to depression in old age via independent pathways (315).

The associations of grey matter volumes with WM fibre integrity were small, suggesting that one-to-one connections between white and grey matter changes, as found in Wallerian degeneration, are not of great importance, except maybe in the corticospinal tracts, where Wallerian degeneration is most common (316, 317), and often follow middle cerebral artery ischemic stroke (318). Since distal axonal and myelin damage is evident within weeks following Wallerian degeneration of the corticospinal tract (319), future research could assess whether vascular incidents are associated with change in DTI measures that indicate axonal and myelin structure, such as axial and radial diffusivity, developing with Wallerian degeneration.

6.4.3 Qualitative comparison of grey and white matter results

Stroke risk across five Whitehall II phases showed a different effect on grey matter and microstructural white matter integrity.

Widespread lower GM density was present with FSRS measured in earlier phases (up to 20 years) but not at the time of scan, while the most widespread lower WM integrity were present with FSRS at the time of scan and were absent in the earliest phase. While demographic and socioeconomic confounders limited this association to sub-neocortical GM structures, they removed all stroke risk effects on TBSS measures. In other words, FSRS gives added information beyond standard socio-demographic and economic variables in grey matter, while particularly age seems to be tightly linked to white matter microstructural changes that are therefore less specific. Furthermore, results suggest that stroke risk affects neocortical structures as early as 20 years prior to scan and continues in structures that show plasticity, such as medial temporal lobe and white matter, throughout the 20-year period. This suggests that WM and sub-neocortical structures are more reactive to stroke- and cardio-metabolic risk than neocortical GM.

6.4.4 Methodological limitations

The study had a number of strengths and limitations. Strengths were the large sample size, which is representative of the general population (e.g. see Figure 4.0) repeated FSRS measures, and up-to-date imaging techniques. The main limitation is that longitudinal imaging data are not available along with the repeated measures of FSRS. However, the fact that results are predicted two decades prior to the scan in older age highlights the potential for targeting modifiable risk factors in mid-life.

Only such interventional studies will be able to establish causal relationships. Future research will also have to examine further the association between stroke risk and cognitive performance in older age is mediated by structural brain integrity.

Findings in this chapter show that the Framingham 10-year Probability Stroke Risk score may be used in primary prevention not only for the assessment of stroke risk itself, but also for subclinical grey matter atrophy as early as 20 years in advance. These brain areas often implicated in cognitive impairment and dementias, thus preserving them into older age is of importance. Targeting modifiable risk factors throughout adulthood may be tracked using imaging results in the future.

Chapter 7: Metabolic Syndrome and Brain Structure

7.1 Introduction

7.1.1 Background

Metabolic syndrome (MetS) is a secondary marker of the chronic stress response (allostatic load), and is a combination of cardiovascular and neuroendocrine factors (66). It is defined by a number of biomarkers: increased abdominal circumference, increased levels of triglycerides, decreased levels of high-density lipoprotein (HDL) cholesterol, elevated blood pressure (including pre-hypertension) and fasting glucose levels (including pre-diabetes). A diagnosis of MetS is given, if at least three of these markers are above their defined thresholds. Low socioeconomic status (67) and workplace psychosocial stress have been shown to manifest as MetS (320). In turn, MetS is associated with a risk of stroke (70), cardiovascular disease mortality (321), telomere shortening (43) and poor mental and cognitive functioning (47, 69, 144, 322). Individual metabolic syndrome components are known to adversely impact the human brain (e.g. (72)) but our understanding of structural or functional brain associations with MetS is limited (73). Reduced cortical thickness in distinct areas of both hemispheres, as well as volume reductions in the right nucleus accumbens of middle- to older aged participants with metabolic syndrome have been documented (74). Vascular brain damage in the form of periventricular white matter hyperintensities and subcortical white matter lesions in middle-aged individuals (73), reduced white matter integrity in fronto-temporal regions (75) and silent brain infarction in older individuals (73) have also been reported.

Due to the limited research concerning metabolic syndrome and brain structure, Chapter 7 examines the association of MetS measured across five Whitehall II study phases in mid-life with voxel-wise grey and white matter structure in older age.

7.1.2 Aims and hypotheses

7.1.2.1 Aims

The aims of the following analyses are:

1. To examine whether there is an association with cumulative Metabolic Syndrome (MetS) across five study phases over a 20-year period, and structural brain integrity at follow-up in older age, namely grey matter density and white matter microstructure.
2. To examine whether MetS makes a unique contribution to grey and white matter integrity after accounting for the effects of demographic and socioeconomic factors.
3. To examine whether a change in MetS across the five study phases is associated with structural brain integrity in older age.
4. To examine whether white matter microstructure fractional anisotropy FA measure associated with MetS may be due to Wallerian degeneration or regional white matter changes.

7.1.2.2 Hypotheses:

1. A strong association between cumulative MetS and decreased structural brain integrity in older age was hypothesised to be present after removing the effects of demographic or socioeconomic confounders.
2. Furthermore, it was hypothesised that an increase in MetS across the five phases is associated with decreased structural brain integrity in older age.

7.2 Methods

7.2.1 Sample characteristics, inclusion/exclusion criteria

The sample of participants used in this chapter was drawn from 563 Whitehall II Imaging Sub-study participants, described in section 4.1. Participants were excluded from analysis if they did not undergo an MRI scan, had noticeable structural abnormalities, such as a stroke, cyst or hydrocephalus, had poor image quality that pre-processing and artefact correction did not fix, and had a missing Metabolic Syndrome Score at any of the Whitehall II phases.

7.2.2 Assessment of Metabolic Syndrome (MetS) Score

Metabolic Syndrome (MetS) characterises the interconnection between the cardiovascular and neuroendocrine systems. It is defined by the linear combination of five biological measures (biomarkers), at least three of which have to be above their respective clinical cut-offs to meet the criteria of having metabolic syndrome. MetS was defined at Phase 3 (1991-1994), Phase 5 (1997-1999), Phase 7 (2002-2004), Phase 9 (2007-2009) and Phase 11 (2012-2013) using the National Cholesterol Education Program criteria (149). For individual marker cut-offs see Table 7.0 and section 4.3.1.2, the latter for a description of laboratory measures protocol as well. At each Whitehall II phase participants met MetS criteria if ≥ 3 markers were above their respective cut-offs at that phase. Cumulative (total) MetS reflected scores across the five phases. The number of times participants had been classified as having a metabolic syndrome was calculated. In addition, change in MetS across the five phases was calculated as the difference between the sum of the first two (Phases 3, 5) and the sum of the last two (Phases 9, 11) statuses (Table 7.1).

Participants were also excluded if their MetS scores could not be computed or were missing at all phases.

7.2.3 Assessment of nuisance variables

Percentage total grey matter (%GM) volume, an estimate of cortical atrophy, and percentage white matter hyperintensities (%WMH), an estimate of WM lesions, described in chapters 5.3.1.3 and 5.3.2.3 respectively, were used as potential mediators of the association of metabolic syndrome on white matter microstructure. Demographic variables age at scan, sex, ethnicity, and socioeconomic variables years of education along with mid-life occupational status were used as covariates of no interest (detailed in section 4.2.2). In addition, where the association of MetS change with grey or white matter integrity was assessed, average MetS across the five phases was also included as a confounder (see 7.2.5).

	Cut-off
Blood pressure	≥ 130/85 mmHg
	Antihypertensive
Waist circumference	
Men	> 102cm
Women	> 88cm
Fasting glucose	≥ 6.11 mmol/L
HDL cholesterol	
Men	< 1.03 mmol/L
Women	< 1.3 mmol/L
Serum triglycerides	≥ 1.7 mmol/L

Table 7.0 Metabolic Syndrome component

	P3 '91-93	P5 '97-99	P7 '03-04	P9 '07-09	P11 '12-13	Total Derived	Change Derived
Age *[years] Mean (SD)*	48.2 (5.3)	54.0 (5.3)	59.4 (5.3)	64.4 (5.3)	68.5 (5.3)	69.6 (5.3)	
Metabolic Syndrome, *Yes [%] CI*	9.4 (6.8-12.6)	8.9 (6.4-12.0)	9.2 (6.6-12.3)	9.2 (6.6-12.3)	10.8 (8.0-14.1)	0.5 (1.1)	0 (0.5)

Table 7.1. Total and Metabolic Syndrome (MetS) change used in whole-brain grey matter analysis (N = 426) marked with black for mean (SD). Binary frequency [%, yes] and 95% exact binomial confidence intervals (CI) of MetS not directly used for analysis in blue. P = phase. Follow-up at 2012-2014. More information in Tables 7.1 and 7.2. MRI Methods

7.2.3.1 Acquisition and analysis

Scanning was carried out at the Oxford FMRIB Centre using a 3T Siemens Magnetom Verio (Erlangen, Germany) scanner with a 32-channel receive head coil. T_1-weighted, FLAIR and diffusion-weighted MRI images were acquired as part of the protocol (127). Image analysis was performed using FSL v.5.0, (www.fmrib.ox.ac.uk/fsl, (218)). Process detailed in section 5.3.

7.2.3.2 Grey matter volume and density

Volumetric grey matter (GM), white matter (WM) and cerebrospinal fluid (CSF) were segmented and extracted from T_1-weighted images using FSL-FAST (219). %GM volume was calculated by scaling the GM value for total intracranial (GM + WM + CSF) volume.

Voxelwise analysis of whole-brain grey matter density was performed on T_1-weighted images using FSL-VBM (221), which was detailed in section 5.3.1.3. Significant GM voxels were localised with the Harvard-Oxford cortical and subcortical structural atlases (277).

7.2.3.3 White matter hyperintensities and microstructure

WMHs were automatically segmented on FLAIR images with FMRIB's BIANCA tool (245). The total %WMH volume was calculated from voxels exceeding a probability of 0.9 of being WMH, and was adjusted for the total intracranial volume (detailed in section 5.3.2).

Voxelwise statistical analysis of fractional anisotropy (FA), mean diffusivity (MD), axial diffusivity (AD) and radial diffusivity (RD) data was carried out on DTI data using FSL-TBSS (Smith, 2006) (see section 5.3.2.3). JHU DTI-based white matter atlases were used for identifying the location of TBSS results (278, 279).

7.2.4 Statistical analysis

Voxelwise GLM was applied for the analysis of grey matter (GM) and DTI data using Randomise (272), a permutation-based non-parametric statistical test, running 5000 permutations and correcting for multiple comparisons across space. The significance threshold was set at $p < 0.05$, using threshold-free cluster enhancement (TFCE; (274), see section 5.3.3).

7.2.4.1 Models I a) – b)

Linear associations between total MetS and voxelwise GM and DTI data were assessed (Model I). This was also repeated with change in MetS, controlling for average MetS.

Subsequently, to assess whether the widespread association between total MetS and FA was mediated by percentage total GM or WMH volume, model I analysis was repeated covarying for these (model I a) and b) respectively).

7.2.4.2 Models II - III

Significant model I analyses were repeated including demographics (age, sex, ethnicity; model II) and demographics and socioeconomic variables (age, sex, ethnicity, education years, employment grade; model III) as covariates of no interest.

7.2.4.3 Plotting significant GMD, FA and MD values

The nature and directionality of the significant relationship between the unique variance explained by total metabolic syndrome after controlling for demographic and socioeconomic confounders (Model III)), and mean grey matter density (GMD), fractional anisotropy (FA) and mean diffusivity (MD) values was demonstrated by plotting these values for VBM and TBSS results. MetS and corresponding significant values were extracted following the procedures outlined in section 6.2.5.3.

7.3 Results

7.3.1 Descriptive statistics

7.3.1.1 Participant exclusion / inclusion

Between April 2012 and December 2014 a total of 563 Whitehall II participants attended the Whitehall II sub-study. Participants with no T_1 scan (N = 11), with structural abnormalities (N = 18) or inadequate T_1 scan (N = 2), missing MetS at all five phases (N = 72), MetS cannot be calculated (N = 34), missing (N = 10) or un-useable DTI scan (N = 5) were excluded from analysis. Voxel-based morphometry (VBM) analysis was based on a final sample of N = 426 (76% of those attended), and tract-based spatial statistics (TBSS) on N = 412 (73% of those attended) participants. An overview is presented in Figure 7.0.

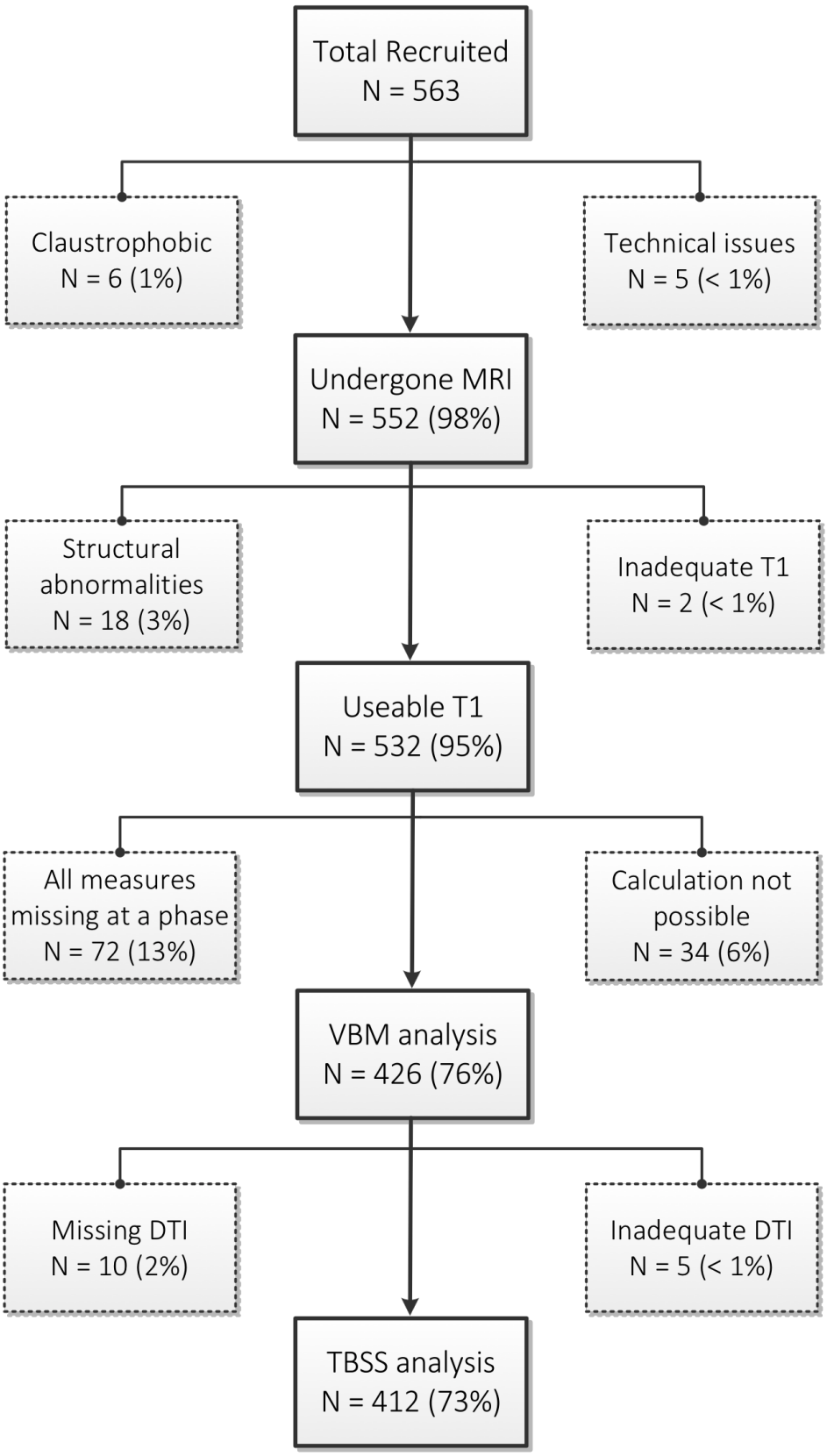


Figure 7.0 Flowchart of participant exclusion before final VBM (N = 426) and TBSS (N=412) analyses, including missing or inadequate scans and missing FSRS values.

7.3.1.2 Participant demographics and nuisance variable characteristics

Participant characteristics used in analysis are shown in Table 7.2, and do not substantially differ from the total sample's presented in section 4.1.

	VBM (N = 426)	TBSS (N = 412)
Age, *years, Mean (SD), range*	69.6 (5.3), 60-83	69.6 (5.3), 60-83
Sex, *N (%)*		
Male	338 (79.3)	327 (79.4)
Female	88 (20.7)	85 (20.6)
Ethnicity, *N (%)*		
White	401 (94.1)	388 (94.2)
Non-white	25 (5.9)	24 (5.8)
Grade, *N (%)*		
Administrative	180 (42.3)	173 (42.0)
Professional/executive	211 (49.5)	206 (50.0)
Clerical/support	35 (8.2)	32 (7.8)
Education level, *years, Mean (SD), range*	14.0 (3.0) 6-23	14.0 (3.0) 6-23

Table 7.2 Metabolic Syndrome study sample characteristics

Ethnicity and cumulative MetS were weakly correlated (ρ (424) = 0.154, p = 0.001). Non-white participants had higher cumulative MetS scores than white participants (t (424) = 3.19, p = 0.001). MetS was not correlated with age (r (424) = 0.35, p = 0.471), sex (ρ (424) = -0.014, p = 0.77; men had higher MetS than women), years of education (r (424) = -0.133, p = 0.002) and socioeconomic status (ρ (424) = 0.55, p = 0.26).

7.3.1.3 Metabolic Syndrome characteristics

Distribution of metabolic syndrome (MetS) over five Whitehall II phases is presented below. Table 7.3 shows that the majority of the recruited sample was free of cardio-metabolic risk factors; about 9% of participants had metabolic syndrome at a given phase, even in later phases despite its prevalence increasing with age in the general

population. A slight increase in the proportion of MetS over the five phases was observed, albeit the proportion of MetS at each phase was smaller than in 4,150 Whitehall II participants at Phases 3-7 (8.3% at Phase 3, 8.9% at Phase 5 and 11% at Phase 7; in section 4.3.1.2 (47)).

	VBM (N = 426)	**TBSS (N = 412)**
Phase	*Yes (%) 95% CI*	*Yes (%) 95% CI*
Phase 3	9.4 (6.8-12.6)	8.7 (6.2-11.9)
Phase 5	8.9 (6.4-12.0)	8.3 (5.8-11.3)
Phase 7	9.2 (6.6-12.3)	8.5 (6.0-11.6)
Phase 9	9.2 (6.6-12.3)	9.2 (6.6-12.4)
Phase 11	10.8 (8.0-14.1)	10.4 (7.7-13.8)

Table 7.3 Percentage of metabolic syndrome across five Whitehall II phases (P). 95% exact binomial confidence intervals of ratios.

Table 7.4 shows that 77.2% of the final sample was free from MetS at any phase, 20.9% of them met criteria for MetS at minimum 1 phase and only 1.9% had persistent MetS across five phases. Therefore, the majority of participants were free from MetS. This is further demonstrated by the histograms plotted in Figures 7.1 and 7.2. These are positively skewed confirming that most observations are toward the lowest value, i.e. no MetS at any phase.

N (%)	**VBM (N = 426)**	**TBSS (N = 412)**
0	329 (77.2)	320 (77.7)
1	42 (9.9)	41 (10.0)
2	25 (5.9)	25 (6.1)
3	18 (4.2)	16 (3.9)
4	4 (0.9)	3 (0.7)
5	8 (1.9)	7 (1.7)

Table 7.4 Total times of Metabolic Syndrome binary yes/no score across all Whitehall II phases. Percentage shows prevalence within the sample.

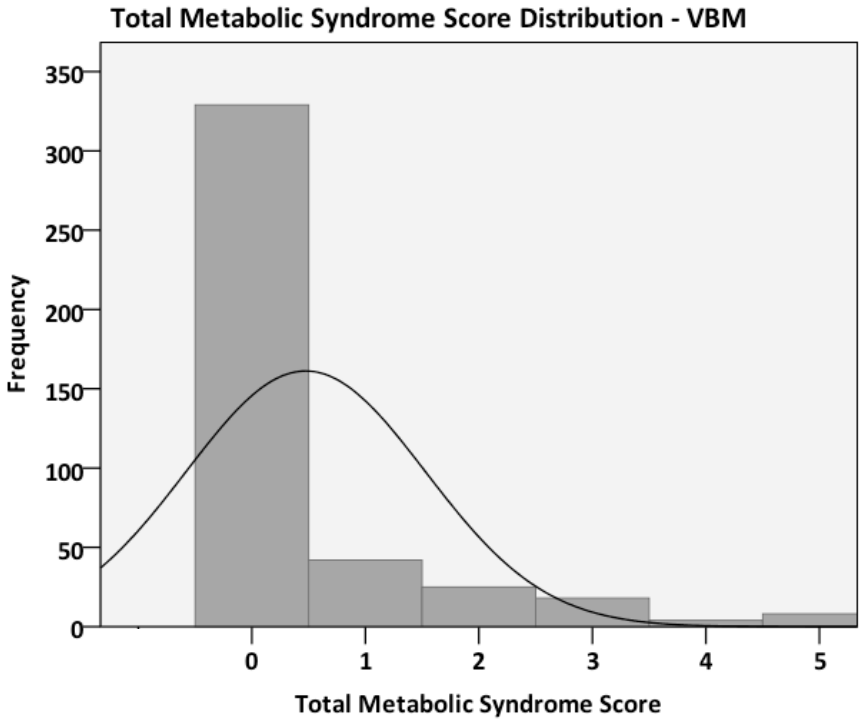


Figure 7.1 Histogram of total Metabolic Syndrome (sum across five Whitehall II phases) distribution in whole-brain grey matter analysis (VBM). This demonstrates that the majority had no Metabolic Syndrome.

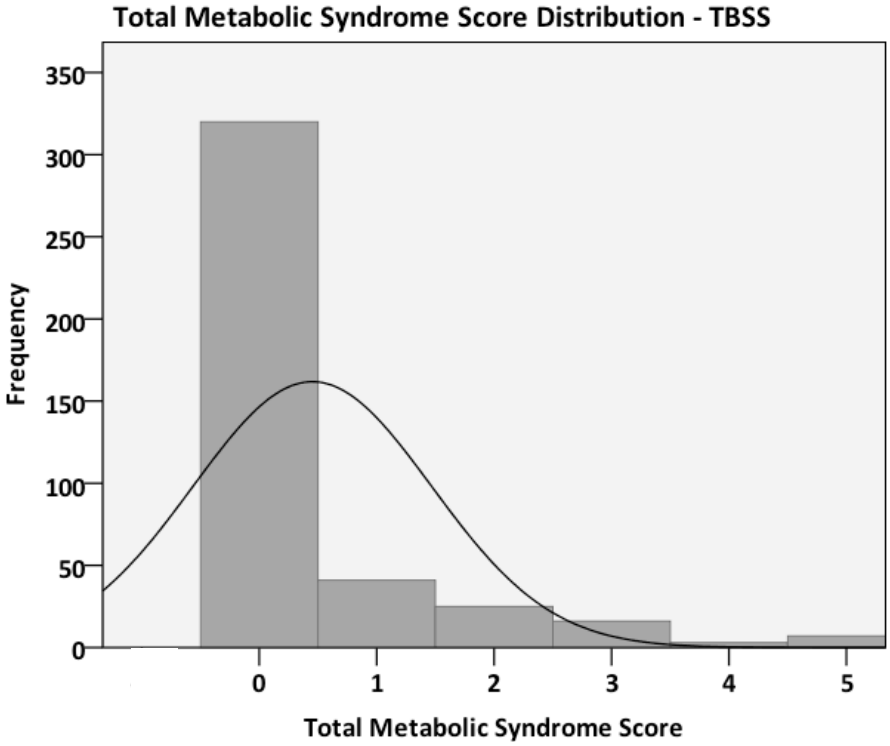


Figure 7.2 Histogram of total Metabolic Syndrome (sum across fice Whitehall II phases) distribution in whole-brain white matter analysis (TBSS). This demonstrates that the majority of participants had no Metabolic Syndrome.

Table 7.5 and Figures 7.3 - 7.4 show the distribution of change in MetS between the first two (Phases 3, 5) and last two (Phases 9, 11) Whitehall II phases. Although this method of calculating change does not capture change between the middle (Phase 7) and any other phase, due to the overall healthy status of the sample change in MetS in phase 7 would be unlikely to have a large effect on score distribution characteristics. 84% participants' MetS score on average did not change across the five phases. Approximately 9% (N=38) no longer had MetS and only 7.5% (N=32) developed MetS in Phases 9 and 11 compared to Phases 3 and 5. This is further demonstrated by the histograms plotted in Figures 7.3 and 7.4. These have positive kurtosis confirming that the most frequent observation is zero, i.e. no change in MetS score.

N (%)	**VBM (N = 426)**	**TBSS (N = 412)**
-2	8 (1.9%)	6 (1.5%)
-1	24 (5.6%)	23 (5.6%)
0	356 (83.6%)	346 (84.0%)
1	29 (6.8%)	28 (6.8%)
2	9 (2.1%)	9 (2.2%)

Table 7.5 Metabolic Syndrome (MetS) change across all phases. Distribution of change in MetS score between the sum of Phases 3+5 and Phases 9+11. Positive values depict a decrease, and negative ones an increase in score. Percentage shows prevalence of MetS within the sample.

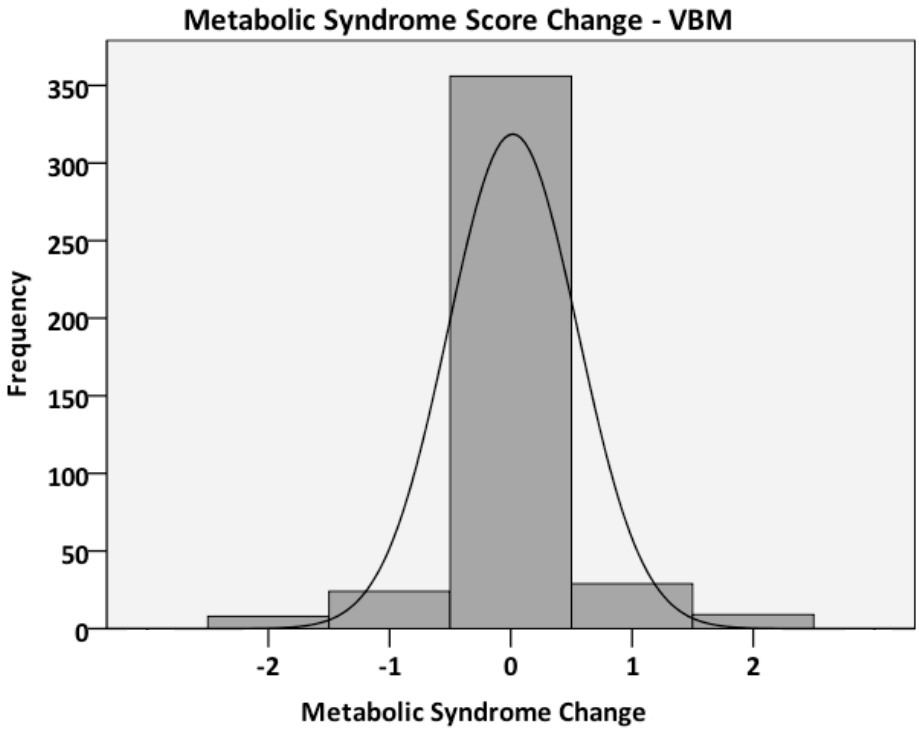


Figure 7.3 Histogram of change in Metabolic Syndrome between the sum of Whitehall II Phases 3+5 and the sum of Phases 9+11 in whole-brain grey matter analysis (VBM). It shows that most participants' Metabolic Syndrome did not change.

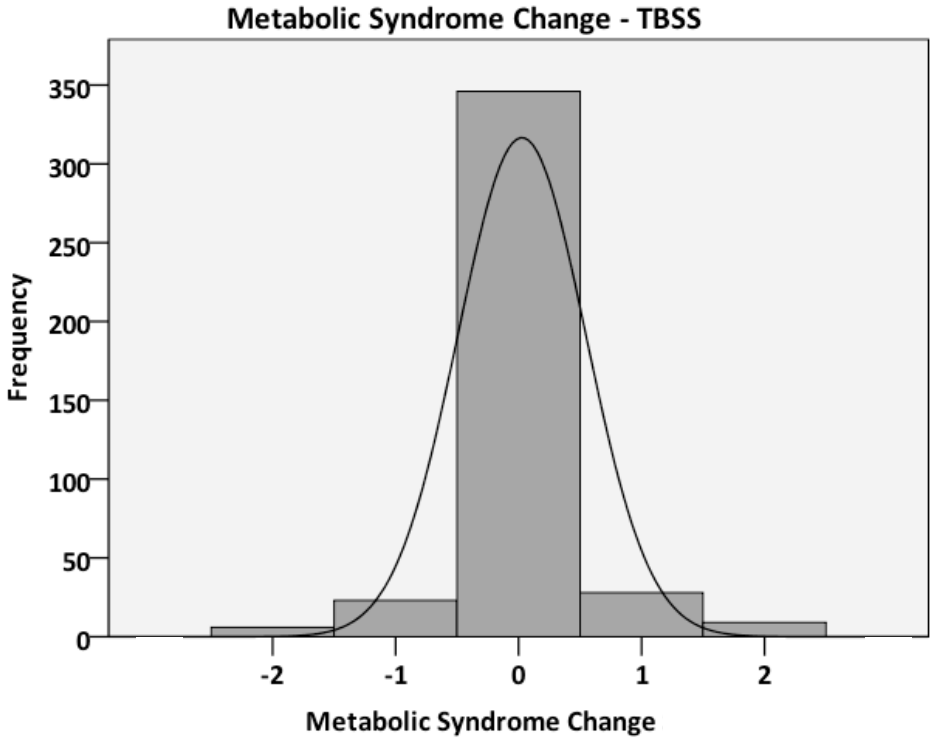


Figure 7.4 Histogram of change in Metabolic Syndrome between the sum of Whitehall II Phases 3+5 and the sum of Phases 9+11 in whole-brain white matter analysis (TBSS). It shows that most participants' Metabolic Syndrome did not change.

7.3.2 VBM Results

Change in MetS between the sum of Phases 3 and 5, and the sum of Phases 9 and 11, *was not significantly associated* with whole-brain grey matter (GM) density. Below is a detailed presentation of results for cumulative MetS, defined as the sum of MetS scores across Phases 3 to 11.

7.3.2.1 Models I

Cumulative metabolic syndrome (MetS) score was associated with significant lower grey matter density. This means that the more times MetS criteria were met across the five phases, the lower GM density was in the affected areas. Significant voxels were mostly located in neocortical areas of the parietal and temporal lobes, i.e. in the precuneus, right postcentral gyrus, precentral gyrus, supramarginal gyrus, central opercular cortex, cingulate gyrus, superior temporal cortex, fusiform cortex, left frontal pole, and in subcortical structures, i.e. the thalamus and medial temporal lobes (Table 7.6, Figure 7.5.). Peak cluster location (maximum t-value) was in the right postcentral gyrus: t (424) = 5.44, $p < 0.001$).

7.3.2.2 Models II-III

The above associations were slightly reduced but remained significant in regions that were affected bilaterally in model I, after controlling for age, sex, ethnicity (model II; Table 7.7, Figure 7.5). Fewer significant voxels were present in the left precentral gyrus, supramarginal gyrus, and medial temporal lobe. Significant voxels were no longer present in the left frontal pole, precuneus, and cingulate gyrus and left half of the thalamus. Overall there was a 32% reduction in the number of significant voxels

from model I. Maximum t-value was located in the right medial temporal lobe: t (421) = 5.43, $p < 0.001$).

Model I : Total Metabolic Syndrome							
Cluster	**Cluster size (voxels)**	**Max t**	**p-value**	**MNI coordinates (x, y, z)**			**Structure**
1	17236	5.44	< 0.001	50	-30	52	R postcentral gyrus
2	7462	4.35	0.001	-56	-4	2	L planum polare, central opercular cortex
3	1261	3.68	0.017	-34	-74	50	L lateral occipital cortex
4	529	4.91	0.003	-26	-82	-14	L occipital fusiform gyrus
5	495	4.35	0.008	12	-76	30	R cuneal cortex
6	136	4.23	0.022	14	60	26	R frontal pole
7	112	3.03	0.04	10	12	-4	R accumbens, caudate
8	24	2.96	0.046	-62	-46	40	L supramarginal gyrus
9	21	3.49	0.045	-10	-74	-2	L lingual gyrus
10	21	3.38	0.045	0	56	22	L frontal pole, superior frontal gyrus

Table 7.6 Cumulative (total) Metabolic Syndrome score (MetS) and whole-brain grey matter (GM) analysis results. MetS calculated as the sum of MetS over five phases was associated with lower GM density primarily in neocortical areas of the parietal and temporal lobes and in sub-neocortical structures such as the thalamus and medial temporal lobes.

Model II : Total Metabolic Syndrome + age, sex, ethnicity							
Cluster	**Cluster size (voxels)**	**Max t**	**p-value**	**MNI coordinates (x, y, z)**			**Structure**
1	13137	5.43	< 0.001	32	2	-14	R amygdala
2	4433	4.17	0.002	-54	-4	2	L planum polare, central opercular cortex
3	379	3.48	0.023	-48	-50	52	L supramarginal gyrus
4	215	4.56	0.008	-24	-82	-14	L occipital fusiform gyrus
5	173	4.16	0.016	12	-76	30	R cuneal cortex, precuneous
6	43	3.01	0.042	-30	18	-22	L frontal orbital cortex
7	33	3.51	0.036	-34	-76	48	L lateral occipital cortex

Table 7.7 Cumulative (total) Metabolic Syndrome score (MetS) and whole-brain grey matter (GM) analysis results after controlling for age, sex and ethnicity (model II). The association between MetS and lower GM was present primarily in structures of the left hemisphere.

There was no noticeable reduction (only 1%) in the number of significant voxels or affected regions after additionally controlling for socioeconomic variables (model III; Table 7.8, Figure 7.5). Similarly, maximum t-value was located in the right medial temporal lobe: t (419) = 5.4, $p < 0.001$.

Model III : Model II + SES, education							
Cluster	**Cluster size (voxels)**	**Max t**	**p-value**	**MNI coordinates (x, y, z)**			**Structure**
1	13261	5.4	< 0.001	32	2	-14	R amygdala
2	4238	4.17	0.002	-54	-4	2	L planum polare, central opercular cortex
3	204	4.51	0.01	-24	-82	-14	L occipital fusiform gyrus
4	190	3.48	0.027	-34	-44	48	L superior parietal lobule
5	182	4.16	0.016	12	-76	30	R cuneal cortex, precuneous
6	81	3.46	0.036	-48	-50	52	L supramarginal gyrus
7	42	3.02	0.045	-30	18	-22	L frontal orbital cortex
8	24	3.55	0.043	-34	0	44	L middle frontal gyrus

Table 7.8 Cumulative (total) Metabolic Syndrome score (MetS) and whole-brain grey matter (GM) analysis results after controlling for age, sex and ethnicity and socioeconomic variables (model III). Results did not substantially differ from model II.

Figure 7.6 shows mean grey matter density values extracted from the significant ($p < 0.05$, tfce) regions in which total MetS was associated with lower grey matter after controlling for age, sex, ethnicity, occupational position and education years (model III). The plot demonstrates a negative linear relationship between MetS and GM density, after controlling for the covariates of no interest.

No association was found between total MetS and higher GM density.

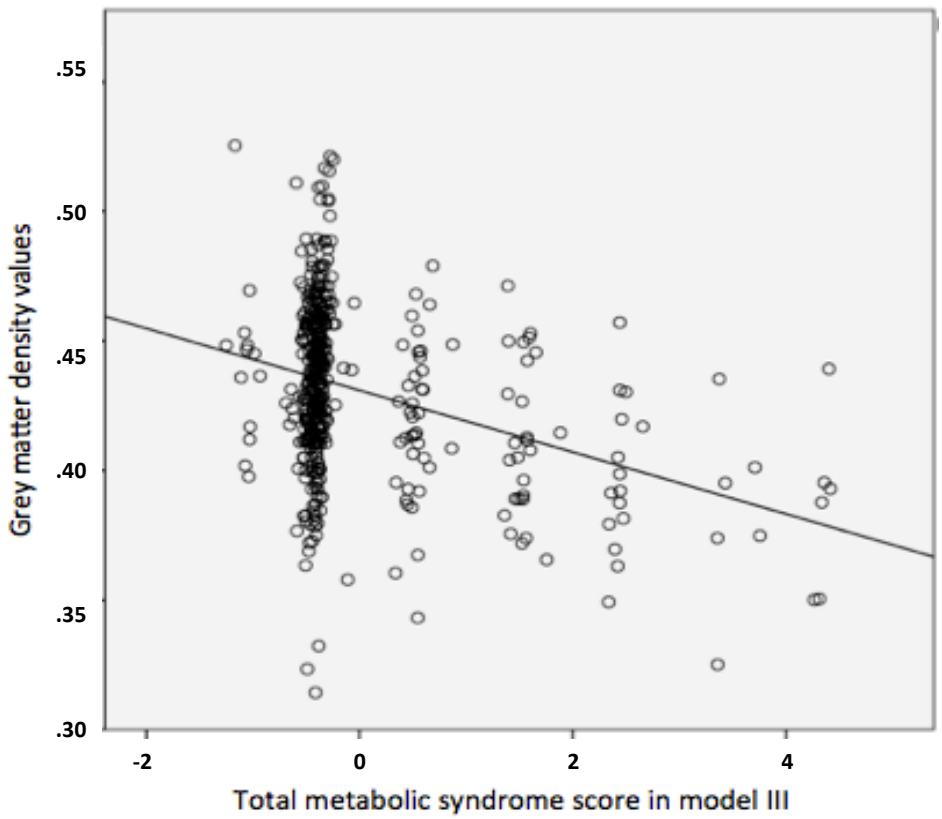


Figure 7.6 Regression plot of individual mean grey matter density values extracted from regions (y-axis) with which total MetS is significantly ($p < 0.05$, tfce) associated, after controlling for all confounders of Model III (x-axis).

Caption for Figure 7.5 on the following page:

Cumulative metabolic syndrome status (calculated as the presence of total MetS over five phases) and its significant association with lower grey matter. It was mainly present in neocortical areas of the parietal and temporal lobes and in sub-neocortical structures, the thalamus and medial temporal lobes (Model I). After controlling for age, sex, ethnicity (Model II) plus socioeconomic status (Model III) the association was reduced or disappeared primarily in left hemisphere structures. Locations represent maximum t values at model III. Colours represent t-values significant at $p < 0.05$, threshold free cluster enhancement and multiple comparisons corrected.

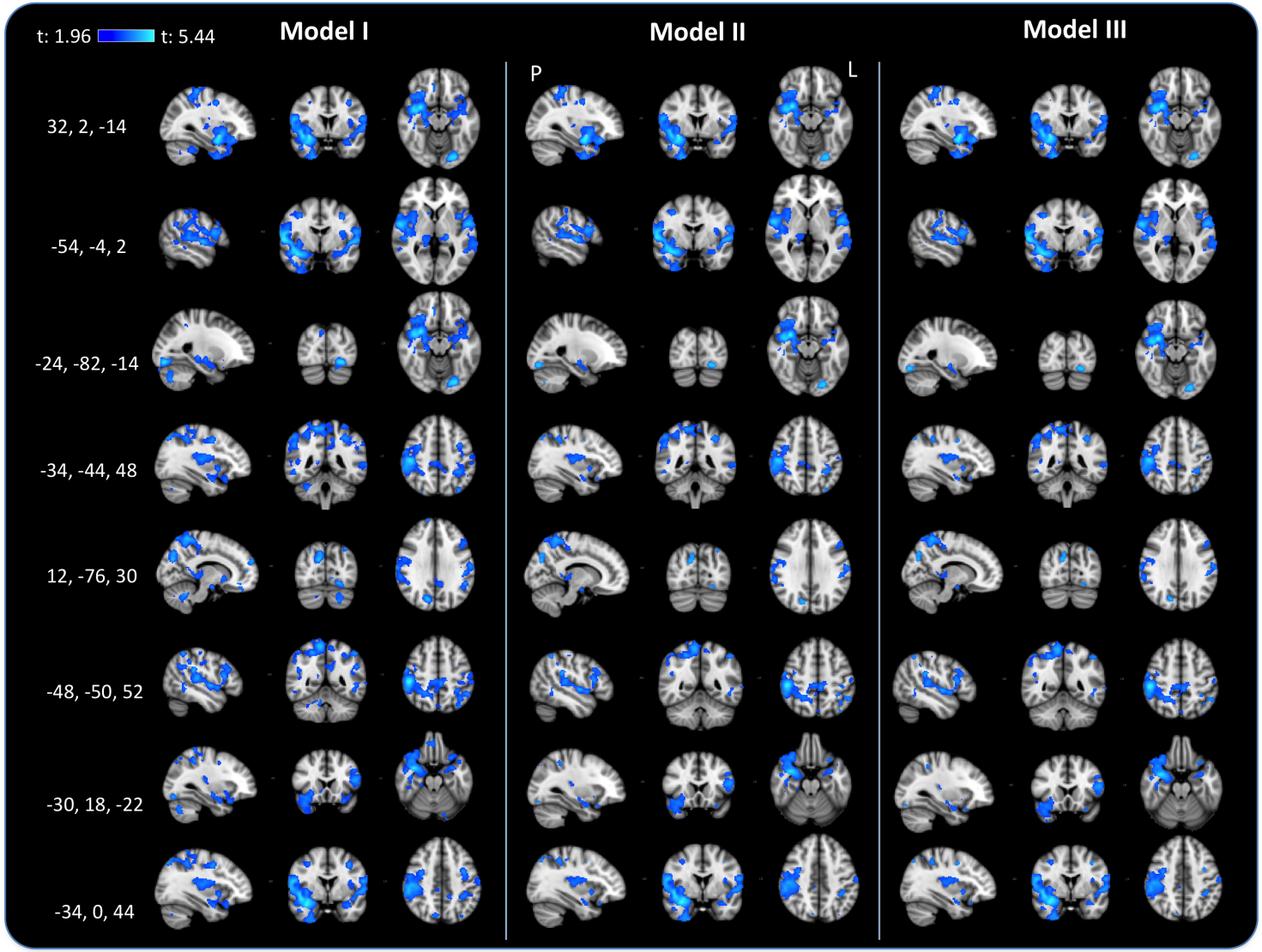

t: 1.96
t: 5.44
Model I
Model II
Model III
P
L
32, 2, -14
-54, -4, 2
-24, -82, -14
-34, -44, 48
12, -76, 30
-48, -50, 52
-30, 18, -22
-34, 0, 44

Figure 7.5

7.3.3 TBSS Results

Change in MetS between the sum of Phases 3 and 5, and the sum of Phases 9 and 11, *was not significantly associated* with whole-brain microstructural measures in white matter. Below is a detailed presentation of results for cumulative MetS score.

7.3.3.1 Fractional anisotropy

Model I

Whole-brain WM analysis revealed widespread lower FA values in association with cumulative MetS, defined as the sum of MetS scores across five phases (P3 to P11). Significant voxels were found in the cingulum, corona radiata, corpus callosum (apart from the splenium), corticospinal tract, external capsule, forceps major, inferior fronto-occipital fasciculus, superior corona radiata, and superior longitudinal fasciculus, as well as in parts of the left anterior thalamic radiation right anterior corona radiata, inferior longitudinal fasciculus, and internal capsule. Peak cluster location was in the right superior longitudinal fasciculus: t (411) = 5.31, p = 0.009. (Table 7.9, Figure 7.7).

Total Metabolic Syndrome and FA reduction								
Model	**Cluster**	**Cluster size (voxels)**	**Max t**	**p-value**	**MNI coordinates (x, y, z)**			**Structure**
I	1	32922	5.31	0.009	50	-2	17	R superior longitudinal fasciculus
II	1	23805	4.41	0.015	41	-54	45	R superior longitudinal fasciculus
	2	197	3.76	0.045	-48	-54	2	L superior longitudinal fasciculus
	3	97	3.16	0.049	-42	-47	6	
	4	31	3.53	0.049	14	-73	5	R inferior fronto-occipital fasciculus
III	1	23362	4.52	0.012	41	-54	45	R superior longitudinal fasciculus
	2	55	3.06	0.048	-11	29	47	L superior longitudinal fasciculus
	3	38	2.86	0.049	23	6	37	R superior longitudinal fasciculus

Table 7.9 Cumulative Metabolic Syndrome (MetS) status and whole-brain fractional anisotropy (FA) analysis results. The association was present in widespread tracts bilaterally (model I) and reduced or no longer present in anterior thalamic radiation, external and internal capsule and right anterior corona radiata after controlling for confounders (models II, III).

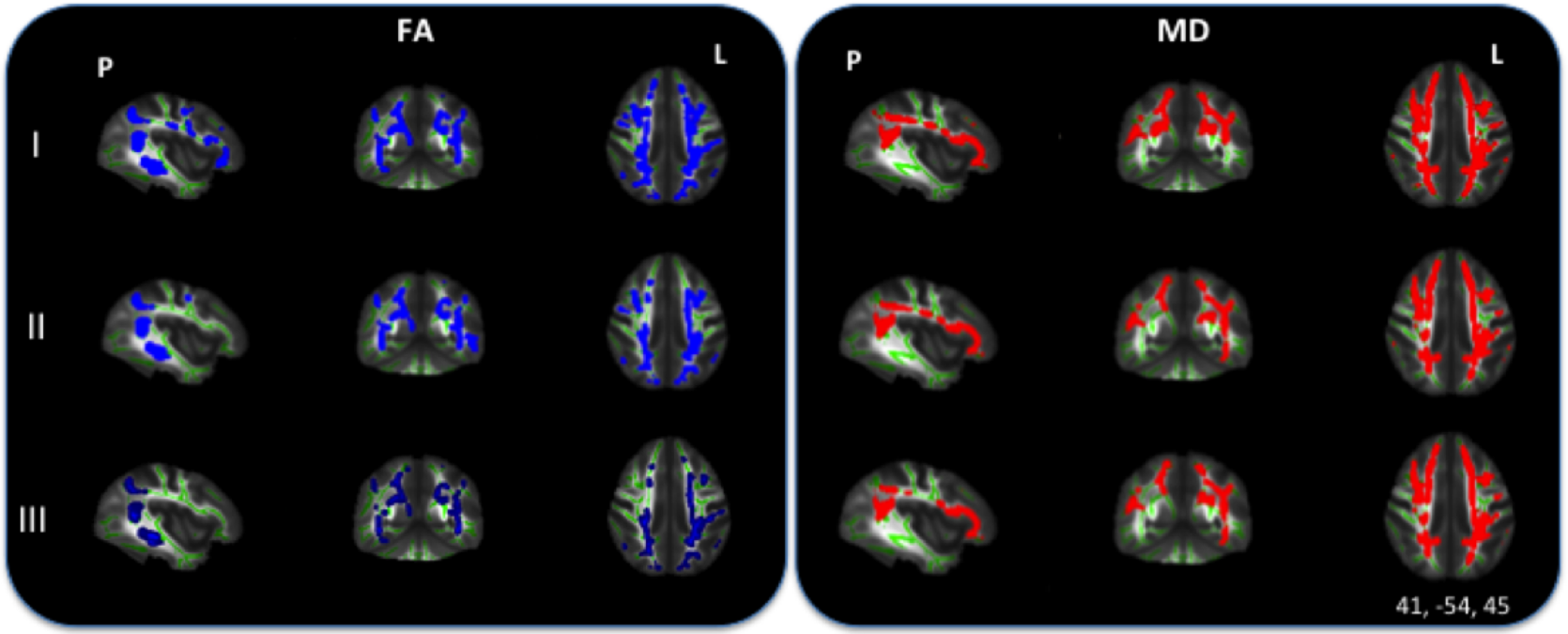


Figure 7.7 Significant lower FA and higher MD association with cumulative Metabolic Syndrome (MetS). Voxel location (41, -54, 45) placed at highest t-value FA in model III. Significant regions are dilated for illustrative purposes, overlaid on a green skeleton.

Left (blue): Lower whole-brain fractional anisotropy (FA) association was present in widespread tracts bilaterally (model I) and reduced in anterior thalamic radiation, external and internal capsule and right anterior corona radiata after controlling for confounders (models II + III). **Right (red):** Higher whole-brain mean diffusivity (MD) association was present in widespread tracts similar to association with lower FA (model I). Results were no longer widespread in similar areas to those seen in FA after controlling for condounders (models II + III) apart from the inferior fronto-occipital fasciculus where higher MD values were present even after confounders were added to the model. Furthermore, model II confounders reduced the effect of MetS on MD to a smaller extent than did the effect of MetS on FA.

Model I a), I b)

Mean percentage total GM (%GM) volume was 37% (SD = 2) and mean percentage total white matter hyperintensities (%WMH) was 0.41% (SD = 0.27) in this sample of participants.

%GM volume as well as %WMH significantly correlated with lower FA values, even after controlling for total MetS. The association was more widespread with %WMH than %GM, the former including all major tracts and the latter localised primarily along the superior longitudinal fasciculus, corticospinal tract and anterior thalamic radiation (Figure 7.8). Therefore both measures were entered in a regression analysis to reveal whether they mediate the effects of cumulative MetS on lower FA values. This association was no longer significant after controlling for either %GM or %WMH, which suggests that both cortical atrophy and regional white matter changes can completely mediate the effect of MetS on fractional anisotropy.

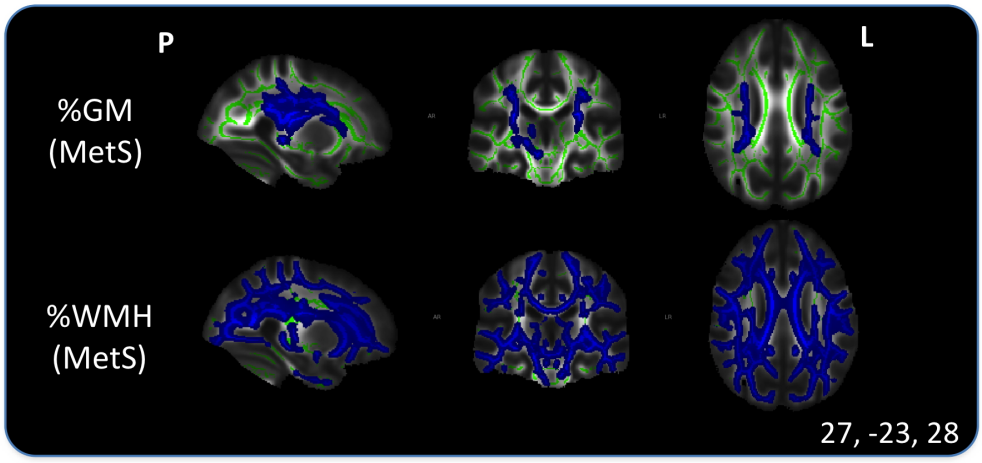


Figure 7.8 Significant association between percentage total GM volume (%GM) and lower FA values (top) and between white matter hyperintensities (%WMH) and lower FA (bottom), even after controlling for cumulative MetS. Significant regions ($p < 0.05$, tfce) are dilated for illustrative purposes, overlaid on a green skeleton.

Models II – III

These associations were significant in slightly fewer voxels but remained present in the same areas apart from the anterior corona radiata, anterior thalamic radiation, external capsule, inferior fronto-occipital fasciculus and internal capsule, after controlling for age, sex, ethnicity (Model II) and occupational position and education years (Model III; Table 7.9, Figure 7.7). Overall there was a 27% reduction in the number of significant voxels from model I. Maximum t value was located in the right superior longitudinal fasciculus: t (408) = 4.41, p = 0.015). There was minimal reduction (2%) in the number of significant voxels when additionally controlling for socioeconomic variables (peak cluster location unchanged: t (406) = 4.52, p = 0.012).

Figure 7.9 shows mean FA values extracted from the significant ($p < 0.05$, tfce) tract volume in which cumulative MetS is associated with lower FA. The plot demonstrates the negative linear association between mean FA values and total MetS after controlling MetS for age, sex, ethnicity and socioeconomic variables (model III).

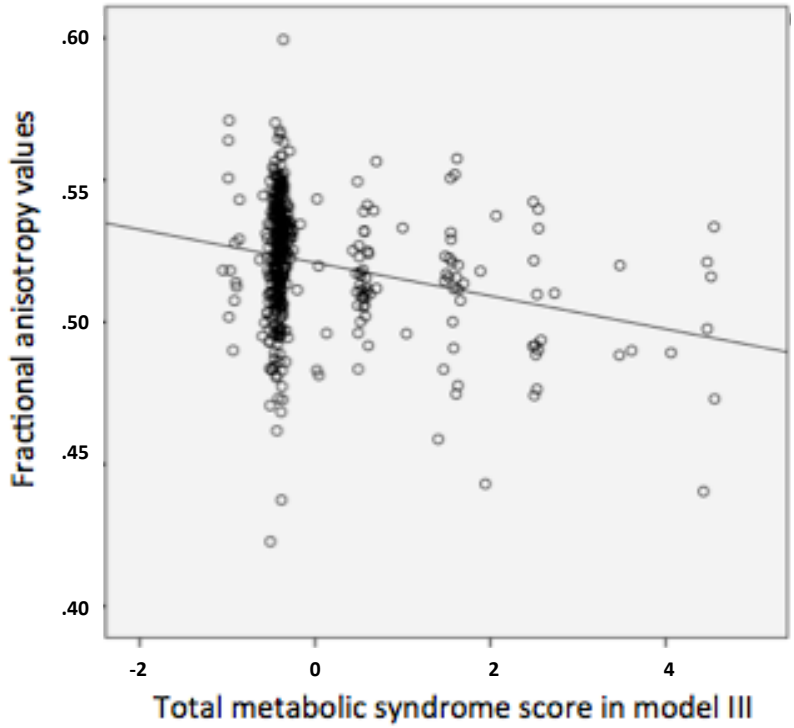


Figure 7.9 Regression plot of individual mean FA values extracted from the significant tract volume (y-axis), against total MetS, after controlling for all confounders (model III), x-axis ($p < 0.05$; tfce).

7.3.3.2 Mean Diffusivity

Model I

Whole-brain WM analysis revealed higher MD values in association with cumulative MetS measured across five phases, in regions where significant lower FA was found, apart from the inferior longitudinal fasciculus where association was weaker. Peak cluster location was in the left superior longitudinal fasciculus: t (411) = 5.78, p = 0.013. (Table 7.10, Figure 7.7).

Total Metabolic Syndrome and MD increase								
Model	**Cluster**	**Cluster size (voxels)**	**Max t**	**p-value**	**MNI coordinates (x, y, z)**			**Structure**
I	1	29939	5.78	0.013	-52	-34	38	L superior longitudinal fasciculus
II	1	25819	5.71	0.013	-52	-34	38	
III	1	25621	5.69	0.015	-52	-34	38	

Table 7.10 Cumulative Metabolic Syndrome (MetS) status and whole-brain mean diffusivity (MD) analysis results. The association was present in widespread tracts bilaterally similar to that seen with FA (model I) and reduced / no longer present in anterior thalamic radiation, external and internal capsule and right anterior corona radiata after controlling for confounders (models II + III).

7.3.3.2.1 Model II –III

The presence of this association reduced in size in regions where FA was also affected, apart from the inferior fronto-occipital fasciculus, and otherwise remained significant, after controlling for age, sex, ethnicity (Model II), occupational position and education years (Model III; Table 7.10, Figure 7.7). Furthermore, the association between MetS and MD was affected by confounders to a smaller extent than the association between MetS and FA. Overall there was a 14% reduction in the number of significant voxels from model I. Similarly to model I, maximum t value was located in the left superior longitudinal fasciculus: t (408) = 5.71, p = 0.013). There was a minimal reduction (2%) in the number of significant voxels when additionally controlling for socioeconomic variables (peak cluster location unchanged: t (406) = 5.69, p = 0.015). Therefore the addition of demographic confounders reduced the significant association to a greater extent than the addition of socioeconomic variables.

Figure 7.10 shows individual mean MD values extracted from the significant tract volume ($p < 0.05$), against cumulative MetS 11 positively associated with MD. The plot demonstrates the positive linear association between mean MD values and total MetS after controlling for all confounders at model III.

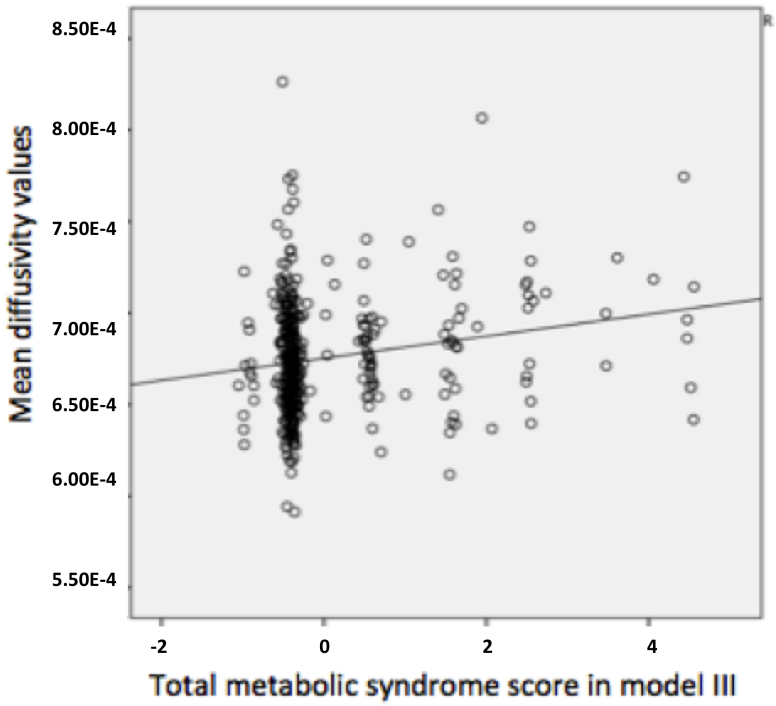


Figure 7.10 Regression plot of individual means of MD values extracted from the significant tract volume on y-axis ($p < 0.05$; tfce), against total MetS after controlling for all confounders in model III (x-axis).

7.3.3.3 Axial and radial diffusivity

Cumulative MetS was associated with higher axial diffusivity (AD) in a small number of voxels along the forceps minor, left inferior fronto-occipital fasciculus and anterior thalamic radiation: t (411) = 4.38, p = 0.046. This association was no longer significant after controlling for demographic and socioeconomic variables (models II – III).

A significant association of cumulative MetS with higher radial diffusivity (RD) values was also present in regions seen in FA and MD results. The association reduced in number of voxels with the addition of demographic confounders to the same extent it did with controlling for socioeconomic confounders (17%). Therefore, demographic confounders had a similar effect on the MetS and RD association as on the MetS and MD association. Socioeconomic confounders had a larger effect on the MetS and RD association than on MetS association with FA and MD. Tables of AD and RD results are presented in Appendix E.

No association was found between total MetS and higher FA or lower MD, AD and RD values.

7.4 Discussion

In this chapter the linear association of cumulative Metabolic Syndrome (MetS) with whole-brain structural grey matter density and microstructural white matter integrity in older age was assessed. Cumulative MetS was defined as the number of times participants fulfilled criteria for MetS across five Whitehall II study phases over a 20-year period.

7.4.1 Whole-brain grey matter

7.4.1.1 Summary of aims and hypotheses

Cumulative MetS was associated with lower grey matter (GM) bilaterally in neocortical areas of the parietal and temporal lobes, and in sub-neocortical structures, i.e. thalamus and medial temporal lobes, in line with ***Aim 1)***. Results of ***Aim 2)*** supported ***Hypothesis 1)***, i.e. although the effect of MetS was reduced in

some neo-cortical and sub-neocortical structures of the left hemisphere, e.g. precuneus, cingulate gyrus and thalamus, the same regions remained strongly affected beyond demographic and socioeconomic factors. On the contrary to the expected, ***Hypothesis 2)*** (***Aim 3)***) was not supported: an increase in MetS over phases was not associated with lower GM density, probably because only 7.5% (N = 32) of the sample developed MetS after Phase 5, fifteen years prior to the MRI scan. In other words, in the Whitehall Imaging Sub-study sample recruited on the 3T Verio scanner, MetS was relatively stable throughout the duration of the study.

7.4.1.2 Unique MetS effects

The unique effects of MetS, which are not accountable for by age, sex, ethnicity, socioeconomic status or education, predicted lower GM density predominantly in the right hemisphere, in neocortical areas of the temporal and parietal lobes, i.e. pre- and postcentral gyri, supramarginal gyrus, opercular cortex, and superior temporal cortex, and sub-neocortical structures, i.e. the thalamus and medial temporal lobes. Demographic confounders removed most of the variance shared between MetS and GM probably due to ethnicity, which was the only confounder correlating with MetS. In this sample non-white participants had a higher cumulative MetS score than white ones, which is in line with the general evidence that European-white and Chinese populations have lower clustering of all metabolic disturbances (323). Contrary to previous research suggesting that the prevalence of MetS increased with age, on average that was not the case in the present study (324). Moreover men had higher cumulative MetS than women, which is in line with some (324) but not other (325) studies of adults >50 years of age. In the Whitehall II

cohort mid-life employment status attenuated the negative effect of cumulative MetS on cognitive performance over a 10-year period by up to 68% (47). In the present study socioeconomic variables did not confound the effects of MetS on GM density.

7.4.1.3 MetS effects on MTL structures

The above findings suggests that MetS might predict GM atrophy in medial temporal lobe (MTL) structures, which may be of relevance to increased risks of future depressive symptoms and cognitive performance. In the Whitehall II cohort the presence of MetS in mid-life (41-61 years of age) was associated with an increased risk of depressive symptoms 6 years later (144). In white Whitehall II participants cumulative MetS across Phases 3, 5 and 7 predicted lower cognitive performance in Phase 7, compared with those who never had MetS (47). However, in a study of 819 subjects poorer memory and executive performance in those with MetS (N = 232, 28.3%) was not supported by differences in total grey and white matter volumes between the two groups (99).

While individual MetS components are known to have negative GM consequences (297, 326-328), literature on MetS as a constellation of risk factors is limited and mixed, and voxelwise analysis of GM or ROI analysis of MTL structures do not exist. In a community-based longitudinal sample of 130 participants (*M* = 66.2 years (6.7)) MetS did not predict GM volume (329) and in the study detailed above no total brain (GM + WM) volume differences were found between those with and without MetS (99). A recent study of GM atrophy in MetS (N=84; N=40 with MetS) found lower GM volume in the right nucleus accumbens and higher GM volume in the right thalamus

in the MetS group compared with controls (74). The MetS group also showed reduction in mean cortical thickness and volume in both hemispheres, and had reduced cortical thickness in the left insular, superior parietal, postcentral, entorhinal and right superior parietal cortices. Apart from the entorhinal cortex reduced GM density was present with MetS in the present group.

7.4.1.4 MetS effects on MCA vascular territories

Regions showing lower GM density with MetS are supplied by the middle cerebral artery (MCA) and lateral lenticulostriate arteries, which branch off the MCA to serve subcortical areas such as the thalamus (303). MCA is often occluded by embolisms and LLAs is a common site of lacunar strokes (304). MetS is a known risk factor for stroke (70, 330) and vascular reactivity under demand, e.g. during cognitive activity, among individuals with MetS might be dysfunctional in these areas. Insulin resistance, obesity, and consequent inflammation negatively impact the microvasculature and vascular reactivity, which may, in turn, lead to an inability to maintain energy-dependent processes and clear metabolic waste during increased demand. When coupled with other potentially damaging influences, such as HPA-axis dysregulation, dysfunctional vascular reactivity may damage the brain, particularly in vulnerable regions (73).

7.4.2 Whole-brain white matter

7.4.2.1 Summary of aims and hypotheses

Cumulative MetS was associated with lower white matter (WM) integrity bilaterally in *commissural fibres* (e.g. corpus callosum, forceps major), *association fibres* (e.g. cingulum, inferior and superior longitudinal fasciculus, inferior fronto-occipital

fasciculus (IFOF)), and *projection fibres* (e.g. corona radiata, corticospinal tract, internal and external capsule, left anterior thalamic radiation) in line with ***Aim 1)***. Results of ***Aim 2)*** supported ***Hypothesis 1)***: the same regions remained strongly affected after controlling for demographic or socioeconomic factors, albeit associations were no longer widespread with fractional anisotropy (FA) in association fibres in anterior tracts, and with mean diffusivity (MD) in commissural fibres. On the contrary to the expected, ***Hypothesis 2)*** (***Aim 3)***) was not supported: an increase in MetS was not associated with microstructural lower WM integrity, probably because only 7.1% (N = 29) of the sample developed MetS since Phases 3 and 5, at least 15 years prior to the MRI scan.

In line with ***Aim 4)*** the effect of MetS on FA was completely mediated by GM volume as well as regional WM changes. This suggests that both one-to-one connections between GM and WM changes as well as the extent of widespread WM changes that are measured on FLAIR images are of great importance.

7.4.2.2 Unique MetS effects

Voxel-wise microstructural WM studies of MetS are limited, and prospective cohort studies to do not exist. In a small group of middle-aged Japanese men (N=7, 42.3 years (5.3)) and their age-matched controls those with the presence of MetS showed lower FA in the right external capsule, IFOF and the corpus callosum in its entirety (100). In the present study cumulative MetS across 20 years in mid-life predicted lower FA and higher MD in regions including those found by Shimoji (100), but these regions were only significant for MD values after controlling for the effects of demographic factors. Both studies show some association of lower microstructural

WM integrity with MetS in mid-life but further research including larger sample size, women and other ethno-racial individuals (323) is needed. A Dutch community-based study of 130 participants (61 men, mean age 66 (6.7) years) found no unique effects of current MetS or total number of MetS components on whole-brain FA or MD after controlling for age and sex (329).

7.4.2.3 Underlying mechanisms

TBSS results indicate that MetS involves an alteration in WM microstructure, but the underlying pathophysiological mechanisms are unclear, especially since both GM volume and the volume of WM changes in FLAIR images completely mediate the relationship between MetS and fractional anisotropy. Previous studies have linked isolated components of the syndrome with WM damage, for example hypertension (331), central obesity (332), and type-2 diabetes (300). As mentioned above, MetS is a risk factor for stroke (70, 330), presumably due to its effect on large arteries (333). It is associated with atherosclerosis, which in turn can contribute to small-vessel disease and lead to microstructural alterations (334). Lesions are presumed to arise through chronic hypoperfusion and leakage of plasma into WM (231, 335). White matter hyperintensities have been commonly linked with cardiovascular risk factors, cerebrovascular disease (336) and metabolic syndrome (337), and in turn predict an increased risk of stroke, dementia and death (313).

7.4.3 Qualitative comparison of grey and white matter results

MetS had widespread effects on both structural grey and white matter integrity even after controlling for demographic and socioeconomic variables. Socioeconomic

confounders did not substantially affect the association of MetS with either grey or white matter integrity after removing the effects of demographic factors.

7.4.4 Methodological considerations

Peripheral vascular and metabolic disturbances throughout mid-life may lead to subclinical alterations in cerebral metabolism and cerebrovascular reactivity in older age (73), resulting in anatomical changes, as presented in this study.

Intervention studies incorporating protective factors, such as healthy diet, physical and mental exercise, and prospective cohort studies exploring the effect of individual metabolic syndrome risk factors, will help identify mechanisms and contribute to the development of preventative treatment. Nevertheless, the present results could point to the benefit of combining a combination of risk factors in one syndrome.

Chapter 8: Allostatic Load Index and Brain Structure

8.1 Introduction

8.1.1 Background

The exact combination of markers that define the allostatic load (AL) index is subject to debate (2) as is the way it is computed (76, 77). It tends to include a combination of primary and secondary markers of chronic stress and allostatic load, i.e. stress hormones, pro-inflammatory cytokines, inflammatory-, cardiovascular-, metabolic-, dyslipidaemia- and neuroendocrine markers. In combination these are said to be better predictors of health outcomes and mortality than on their own (338). High levels of AL index are predicted by the combination of psychosocial factors and negative emotional response to stressful life events (78, 153). The combination of measures in an AL index is a significant predictor of cognitive and physical decline, cardiovascular disease and mortality in older adults (53), and mental disorders, such as schizophrenia and bipolar disorder (339). A single birth-year cohort reported a negative association of AL index with total brain and white matter volumes, a positive association with hippocampal volume, and no association with grey matter volume in participants aged seventy-three (83). The index was negatively associated with general cognitive ability, processing speed, and knowledge, but not with memory or nonverbal reasoning. Although it is argued that the AL indices of wear-and-tear are better predictors of brain structure and function than any one of the AL markers (53), the mechanisms in which primary and secondary markers come

together to predict brain structure (84) and consequent cognitive decline are yet to be understood (85, 87).

Despite the proposed central role of brain in the chronic stress response and allostatic load, apart from the birth-year study mentioned above (83), no other studies investigated the effect of AL index on brain structure in (ageing) humans. Chapter 8 examines the associations between AL index levels in mid-life and brain structure in older age.

8.1.2 Aims and hypotheses

8.1.2.1 Aims

The aims of the following analyses were:

1. To examine whether there is an association between the Allostatic Load (AL) index across two study phases and in accumulation over a 10-year period in mid-life, and structural brain integrity at follow-up in older age, namely grey matter density and white matter microstructure.
2. To examine whether AL index makes a unique contribution to grey and white matter integrity after controlling for demographic and socioeconomic factors.
3. To examine how far back in time AL index determines brain structure.
4. To examine whether change in AL index between the two study phases is associated with structural brain integrity in older age.
5. To examine whether white matter microstructure fractional anisotropy (FA) measure associated with AL index may be due to Wallerian degeneration or regional white matter changes.

8.1.2.2 Hypotheses:

1. A strong association between AL index and decreased structural brain integrity in older age was hypothesised to be present after controlling for the effects of demographic or socioeconomic confounders.

2. The strength of the association was expected to be stronger cumulatively and 10 years than 20 years before the scan.
3. Furthermore, it was hypothesised that an increase in AL index over 10 years, between the two phases, is associated with lower grey and white matter integrity in older age.

8.2 Methods

8.2.1 Sample characteristics, inclusion/exclusion criteria

The sample of participants used in this chapter was drawn from 563 Whitehall II Imaging Sub-study participants, described in section 4.1. Participants were excluded from analysis if they did not undergo an MRI scan, had noticeable structural abnormalities, e.g. stroke, cyst or hydrocephalus, or poor image quality that pre-processing and artefact correction did not fix, and had a missing AL index component at either phase.

8.2.2 Assessment of Allostatic Load (AL) Index

AL index was defined at phases 3 and 7 of the Whitehall II study as the linear combination of nine physiological measures with values above a high-risk threshold (78, 153). For composite score cut-off see Table 8.0 and section 4.3.1.3, and the latter also for the standard protocol used for acquiring laboratory measures. Each component was given the same weighting and dichotomised based on their respective threshold. The dichotomised scores were summarised to form the AL index at each phase. Cumulative (total) AL index was defined as the sum of AL index at both phases. Furthermore, change in AL index was calculated as the difference between phase 3 and 7 (Table 8.1).

	Cut-off	Description
Blood pressure	≥ 140/90 mmHg	≥ Stage 1 hypertension
Body mass index	≥ 25 kg/mm²	Overweight
Fasting insulin	≥ 7.53 mcU/ml	
Fasting glucose	≥ 5.5 mmol/L	Pre-diabetes
HDL cholesterol	< 1.03 mmol/L	Low
LDL cholesterol	≥ 3.36 mmol/L	Borderline high
Serum Triglycerides	≥ 1.7 mmol/L	Borderline high
CRP	≥ 3 mg/L	
IL-6	≥ 1.85 pg/ml	

Table 8.0 Allostatic Load (AL) Index component scores. An elevated level of each measure carries more risk, except in case of HDL cholesterol. LDL, Low-density lipoprotein; HDL, High-density lipoprotein; CRP, C-reactive protein; IL-6, Interleukine-6.

	Phase 3 1991-1993	Phase 7 2003-2004	Total Derived	Change Derived
Age *[years] Mean (SD)*	48.3 (5.3)	59.5 (5.3)	69.8 (5.3)	
AL Index *Mean (SD)*	2.65 (1.7)	2.91 (1.8)	5.56 (3.0)	0.26 (1.7)

Table 8.1 Allostatic Load (AL) Index at Phases 3 and 7, as well as total and AL index change used in whole-brain grey matter analysis (N = 378). Marked with black for mean and SD. Follow-up at 2012-2014. More information in Tables 8.2 – 8.4.

8.2.3 Assessment of nuisance variables

Percentage total grey matter (%GM) volume, described in section 5.3.1.3, and percentage white matter hyperintensities (%WMH), described in section 5.3.2.3 respectively, were used as potential mediators of the association of AL index on white matter microstructure. Demographic variables age at scan, sex, ethnicity, and

socioeconomic variables years of education along with mid-life occupational status were used as covariates of no interest (detailed in section 4.2.2). In addition, in analyses that used AL index change the average index across the two phases was included as a confounder (see 8.2.5).

8.2.4 MRI Methods

8.2.4.1 Acquisition and analysis

Scanning procedure is detailed in section 5.3. Image acquisition was carried out at the Oxford FMRIB Centre using a 3T Siemens Magnetom Verio (Erlangen, Germany) scanner with a 32-channel receive head coil. T_1-weighted, FLAIR and diffusion-weighted MRI images were acquired as part of the protocol (127). Image analysis was performed using FSL v.5.0, (www.fmrib.ox.ac.uk/fsl, (218)).

8.2.4.2 Grey matter volume and density

Volumetric grey matter (GM), white matter (WM) and cerebrospinal fluid (CSF) were segmented and extracted from T_1-weighted images using FSL-FAST (219). %GM volume was calculated by scaling the GM value for total intracranial (GM + WM + CSF) volume.

Voxelwise analysis of whole-brain grey matter density was performed on T_1-weighted images using FSL-VBM (221), which was detailed in section 5.3.1.3. Significant GM voxels were localised with the Harvard-Oxford cortical and subcortical structural atlases (277).

8.2.4.3 White matter hyperintensities and microstructure

WMHs were automatically segmented on FLAIR images with FMRIB's BIANCA tool described in section 5.3.2 (245). The total %WMH volume was calculated from voxels exceeding a probability of 0.9 of being WMH, and was.

Voxelwise statistical analysis of fractional anisotropy (FA), mean diffusivity (MD), axial diffusivity (AD) and radial diffusivity (RD) data was carried out on DTI data using FSL-TBSS (Smith, 2006) (section 5.3.2.3). JHU DTI-based white matter atlases were used for identifying the location of TBSS results (278, 279).

8.2.5 Statistical analysis

Voxelwise GLM was applied for the analysis of grey matter (GM) and DTI data using Randomise (272), a permutation-based non-parametric statistical test, running 5000 permutations and correcting for multiple comparisons across space. The significance threshold was set at $p < 0.05$, using threshold-free cluster enhancement (TFCE; (274), see section 5.3.3).

8.2.5.1 Models I a) – b)

Linear associations between AL indexes measured at phase 3 and 7, as well as cumulative AL index and voxelwise GM and DTI data were assessed (Model I). This was also repeated with change in AL index, controlling for average AL index.

Subsequently, if significant association between AL indexes and FA was found, I assessed whether this association was mediated by percentage total GM or WMH volume. In this case model I analysis was repeated covarying for these (model I a) and b) respectively).

8.2.5.2 Models II - III

Significant model I analyses were repeated including demographics (age, sex, ethnicity; model II) and demographics and socioeconomic variables (age, sex, ethnicity, education years, employment grade; model III) as covariates of no interest.

8.2.5.3 Plotting significant GMD, FA and MD values

The nature and directionality of the significant relationship between the unique variance explained by total metabolic syndrome after controlling for demographic and socioeconomic confounders (Model III)), and mean grey matter density (GMD), fractional anisotropy (FA) and mean diffusivity (MD) values was demonstrated by plotting these values for VBM and TBSS results. AL index and corresponding significant values were extracted following the procedures outlined in section 6.2.5.3.

8.3 Results

8.3.1 Descriptive statistics

8.3.1.1 Participant exclusion / inclusion

Between April 2012 and December 2014 a total of 563 Whitehall II participants attended the Whitehall II sub-study. Participants with no T_1 scan (N = 11), with structural abnormalities (N = 18) or inadequate T_1 scan (N = 2), missing AL index at either of the two phases (N = 154), missing (N = 9) or un-useable DTI scan (N = 3) were excluded from analysis. Voxel-based morphometry (VBM) analysis was based on a final sample of N = 378 (67% of those attended), and tract-based spatial statistics (TBSS) on N = 366 (65% of those attended) participants. An overview is presented in Figure 8.0.

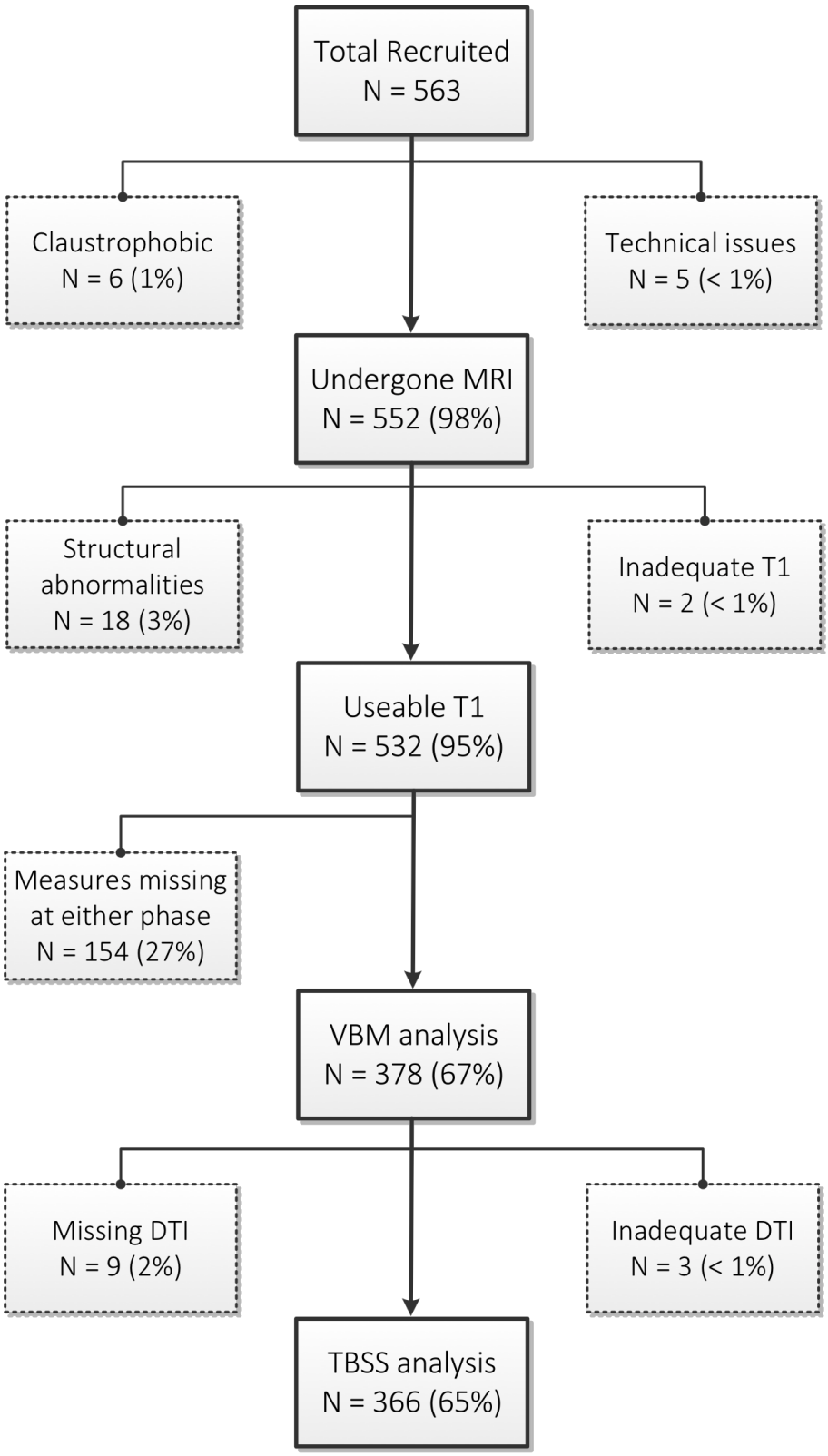


Figure 8.0 Flowchart of participant exclusion before final VBM (N = 378) and TBSS (N = 366) analyses, including missing or inadequate scans and missing FSRS values.

8.3.1.2 Participant demographics and nuisance variable characteristics

Participant characteristics are shown in Table 8.2, and do not substantially differ from the total sample's presented in section 4.1.

	VBM (N = 378)	TBSS (N = 366)
Age, *years, Mean (SD), range*	69.8 (5.3), 60-83	69.8 (5.3), 60-83
Sex, *N (%)*		
Male	305 (80.7)	295 (80.6)
Female	73 (19.3)	71 (19.4)
Ethnicity, *N (%)*		
White	353 (93.4)	341 (93.2)
Non-white	25 (6.6)	25 (6.8)
Grade, *N (%)*		
Administrative (highest)	163 (43.1)	156 (42.6)
Professional/executive	186 (49.2)	182 (49.7)
Clerical/support	29 (7.7)	28 (7.7)
Education level, *years, mean (SD), range*	13.9 (3.0) 6-23	14.0 (3.0), 6-23

Table 8.2. Allostatic Load Index Study sample characteristics

8.3.1.3 Allostatic Load (AL) index characteristics

Distribution of allostatic load (AL) index at both Whitehall II phases is presented below. Table 8.3 shows that the majority (71%) of the sample had only the third of the markers at Phase 3, but this decreased to 63% by Phase 7. Therefore, allostatic load increased with age in this sample of participants, in line with the Whitehall II cohort (Figure 4.1 in section 4.3.1.3). This is further demonstrated by the histograms plotted in Figures 8.1. Histograms for Phase 3 AL index are positively skewed confirming that most observations are toward the lowest value, i.e. small AL index.

Histograms for Phase 7 resemble normal distribution, i.e. equal spread of high and low AL index among sample participants. The distribution was almost identical for scores used in VBM and TBSS analysis (both Phase 3 and 7 TBSS analyses had one participant with a lower AL index than in VBM).

N (%)	**VBM (N = 378)**	**TBSS (N = 366)**
Phase 3 *(1991 - 94)*		
0	21 (5.5)	21 (5.7)
1	81 (21.4)	81 (22.1)
2	103 (27.2)	98 (26.8)
3	64 (16.9)	61 (16.7)
4	42 (11.1)	41 (11.2)
5	42 (11.1)	40 (10.9)
6	17 (4.5)	16 (4.4)
7	7 (1.9)	7 (1.9)
8	1 (0.3)	0 (0)
9	0 (0)	1 (0.3)
Phase 7 *(2002 - 04)*		
0	27 (7.1)	27 (7.4)
1	68 (18.0)	64 (17.5)
2	62 (16.4)	61 (16.7)
3	85 (22.5)	83 (22.7)
4	56 (14.8)	54 (14.8)
5	45 (11.9)	43 (11.7)
6	26 (6.9)	26 (7.1)
7	6 (1.6)	5 (1.4)
8	3 (0.8)	3 (0.9)
9	0 (0)	0 (0)

Table 8.3 Prevalence of Allostatic Load index at Whitehall II Phases 3 and 7 for VBM and TBSS analyses. Percentage shows prevalence within sample.

Total AL index further confirms the distribution of AL index at each phase, shown in Table 8.4. 38% had a total AL index of less than 5, 50% between 5-9 and only 12% had 10 to 15 total markers across phases 7 and 9. No one had 14 or more than 15 markers in total. Figure 8.3 depicts these scores in a histogram, possessing a normal distribution, showing that summing the index across phases normalised the scores.

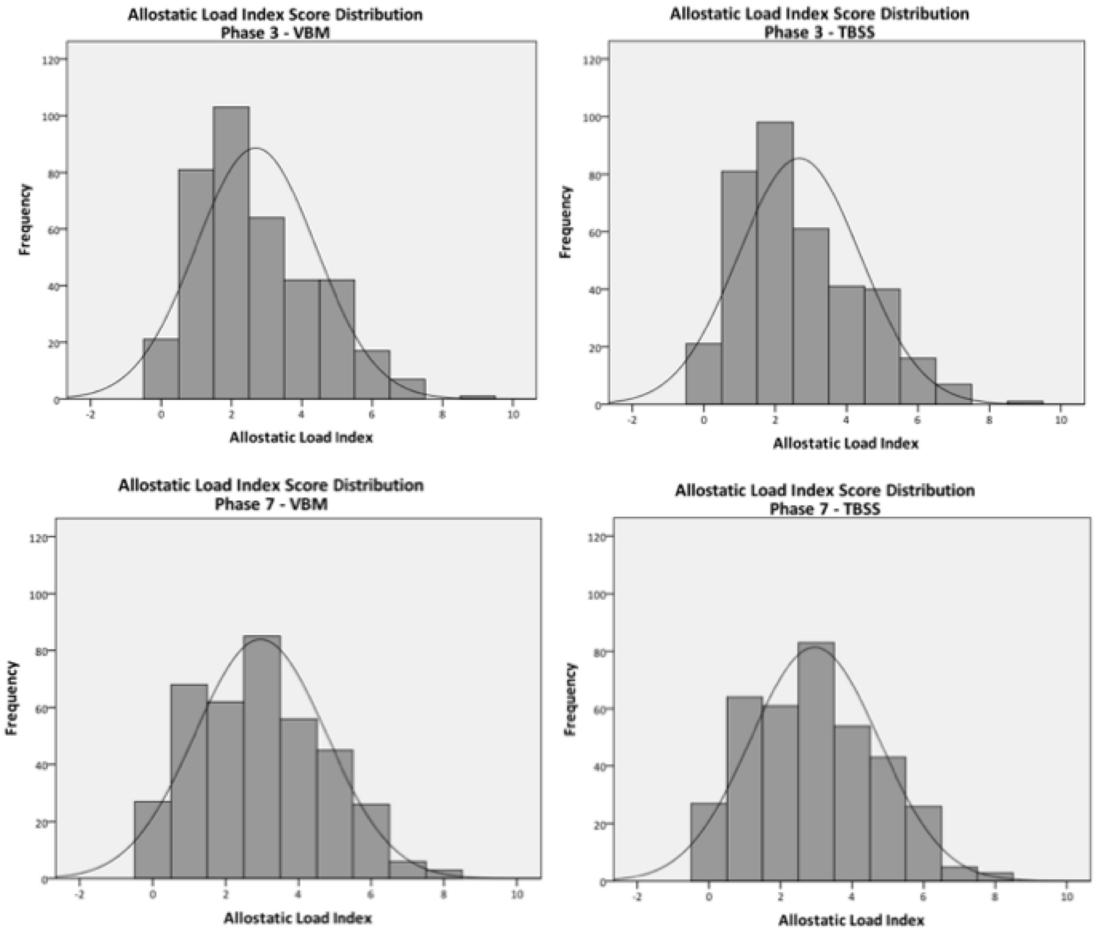


Figure 8.1 Histograms of Allostatic Load (AL) index at both Whitehall II phases. At Phase 3 (top) AL index are positively skewed confirming that most observations are toward small AL. AL at Phase 7 (bottom) show more resemblance with normal distribution. Left: VBM, Right: TBSS.

N *(%)*	VBM (N = 378)	TBSS (N = 366)
0	8 (2.1)	8 (2.2)
1	20 (5.3)	20 (5.5)
2	32 (8.5)	32 (8.5)
3	38 (10.1)	35 (9.3)
4	51 (13.5)	49 (13.0)
5	49 (13.0)	48 (13.0)
6	40 (10.6)	40 (10.9)
7	39 (10.3)	36 (9.8)
8	31 (8.2)	31 (8.5)
9	25 (6.6)	25 (6.8)
10	18 (4.8)	16 (4.4)
11	12 (3.2)	12 (3.3)
12	7 (1.9)	7 (1.9)
13	7 (1.9)	6 (1.6)
15	1 (0.3)	1 (0.3)

Table 8.4 Total Allostatic Load index (P3+P7) prevalence at Whitehall II.

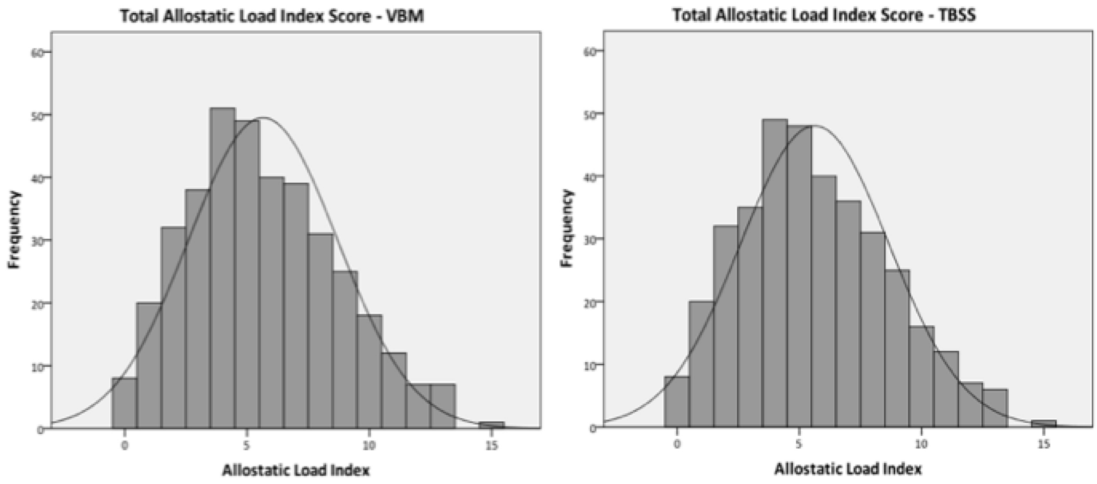


Figure 8.2 Histograms of total Allostatic Load (AL) index. The most frequent total AL index was 4. (left: VBM, right: TBSS)

Table 8.5 and Figures 8.3 show the distribution of AL index change between the phases 3 and 7. 27% participants' AL index remained unchanged between the phases. 41% had a between 1-7 scores smaller, while 32% had a between 1-4 scores larger AL index at phase 7 than at phase 3. This is further demonstrated by the histogram plotted in Figure 8.3, showing normal distribution with unchanged AL

index being the most frequent. This is also in line with AL index distribution in the Whitehall II cohort, which found that effect of age attenuated on AL index towards the end of mid-life (Figure 4.1 in section 4.3.1.3).

N *(%)*	**VBM (N = 378)**	**TBSS (N = 366)**
-4	3 (0.8)	3 (0.8)
-3	18 (4.8)	18 (4.9)
-2	27 (7.1)	26 (7.1)
-1	75 (19.8)	71 (19.4)
0	102 (27.0)	99 (27.0)
1	68 (18.0)	64 (17.5)
2	45 (11.9)	45 (12.3)
3	27 (7.1)	27 (7.4)
4	10 (2.7)	10 (2.7)
5	2 (0.5)	2 (0.6)
7	1 (0.3)	1 (10.3)

Table 8.5 Allostatic Load (AL) index change between Phases 3 and 7. Positive values depict a decreases and negative ones an increase in score. Percentage shows prevalence of AL index change within the sample.

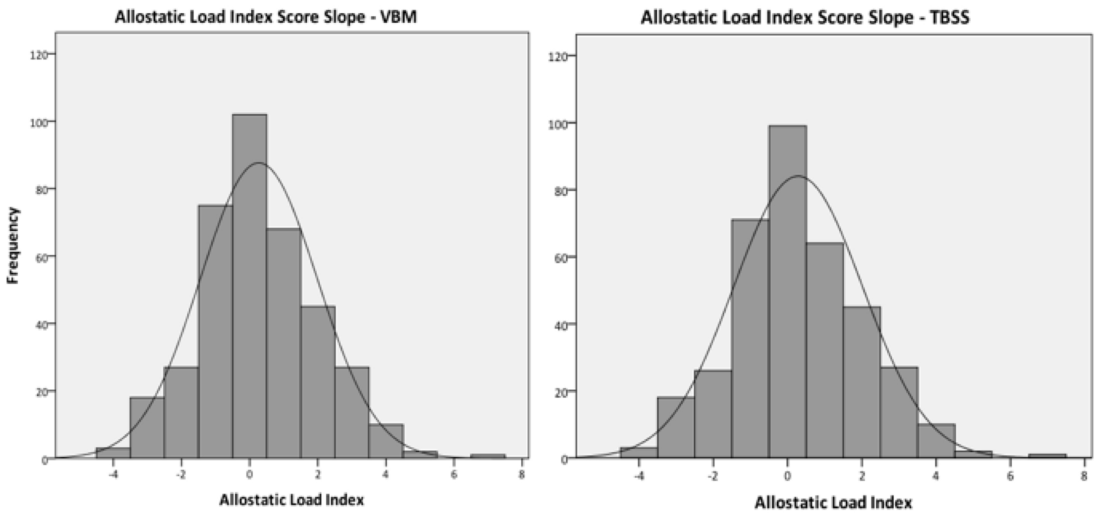


Figure 8.3 Histograms of Allostatic Load (AL) index change. Histograms show that most frequent count is of unchanged AL index, second most frequent is a reduction in score, followed by an increase in score between phases (left: VBM, right: TBSS).

8.3.2 VBM Results

Change in AL index *was not significantly associated* with whole-brain grey matter (GM) density. Below is a detailed presentation of results for AL indices.

Model I

Whole-brain analysis revealed a significant association between AL index at Phase 3 and 7, as well as the cumulative score, with lower GM (Figure 8.4). AL index measured at Phase 3 and as a cumulative score across mid-life was associated with lower GM bilaterally, in the superior frontal gyrus, in superior parietal lobe (precuneus), in the superior edge of the temporal lobe (postcentral gyrus, supramarginal gyrus), and thalamus as well as in the left supplementary motor cortex. Measured in Phases 3 and 7, as well as across the two, lower GM was predicted in the supramarginal gyrus, in the opercular cortex (planum polare, Heschl's gyrus) and medial temporal lobes bilaterally, and in the right medial frontal cortex and temporal pole.

AL index as a cumulative score was associated with low GM in most widespread regions at follow-up, with peak cluster location in the right planum polare: t (376) = 5.51, $p < 0.001$. In comparison, AL index measured at Phase 3 was associated with 15% fewer significant voxels (max t (376) = 5.35, $p < 0.001$; right planum polare), and Phase 7 with 67% less GM reduction (max t (376) = 5.05, $p = 0.001$; right planum polare), as shown in Table 8.6. Clusters associated with AL index were localised to regions already associated with either Phase 3 or 7, while they tended to be larger in size in the right hemisphere (Figure 8.4).

8.3.2.1 Model II - III

After controlling for age, sex and ethnicity (model II), remaining associations were stronger in the right hemisphere. Results with AL index at Phases 3 and 7, and in accumulation were localised in the precentral gyrus, central opercular cortex (including planum polare at phase 3) and temporal pole (Figure 8.4). Lower GM in the thalamus was predicted by total AL index only.

Compared to uncorrected associations, the variance removed by demographic confounders resulted in a 91% smaller association with AL index measured at Phase 3, a 78% smaller association with phase 7 AL index, and an 83% reduction with cumulative AL index. Peak cluster location was in the right planum polare: P3: t (373) = 4.82, p = 0.002; P7: t (373) = 4.97, p = 0.004; total: t (373) = 5.37, p < 0.001 (Table 8.7).

In addition to demographic variables only a minor reduction in the association was present with the further addition of socioeconomic confounders (Figure 8.4). Compared with uncorrected associations the variance removed by both demographic and socioeconomic factors resulted in a 93% smaller association with AL index measured at Phase 3, a 79% smaller association with AL index at Phase 7, and an 84% reduction with cumulative AL index (Table 8.8). Thus socioeconomic confounders do not substantially explain the association beyond the effect of demographic variables.

Model I: AL Index								
	Cluster	Cluster size (voxels)	Max t	p-value	MNI coordinates (x, y, z)			Structure
P3	1	13770	5.35	< 0.001	44	2	-12	R planum polare
	2	3790	4.78	0.001	-40	-20	8	L Heschl's gyrus; insular cortex
	3	907	3.76	0.015	22	-86	-16	R occipital fusiform gyrus
	4	386	4.74	0.007	6	42	-24	R frontal medial cortex
	5	274	3.77	0.023	-20	-30	-6	L hippocampus; thalamus
	6	143	3.78	0.03	-12	-8	-20	L hippocampus; amygdala
	7	53	3.85	0.035	-18	26	-18	L frontal orbital cortex
	8	41	3.47	0.039	14	50	-4	R frontal medial cortex
P7	1	5100	5.05	0.001	48	4	-4	R planum polare; central opercular cortex
	2	857	4.7	0.006	4	44	-24	R frontal medial cortex
	3	632	4.11	0.014	-54	-26	18	central opercular cortex
	4	431	3.74	0.028	-50	-28	50	L postcentral gyrus
	5	311	3.66	0.027	-50	-4	0	
	6	76	3.11	0.043	12	16	4	R caudate
	7	48	4.35	0.034	-18	-6	-20	L amygdala; hippocampus
	8	30	3.92	0.042	-28	16	-12	L insular cortex
	9	28	3.56	0.039	46	-52	58	R angular gyrus
TOTAL	1	14611	5.51	< 0.001	44	0	-10	R planum polare; insular cortex
	2	6817	4.88	< 0.001	-40	-20	10	L Heschl's gyrus; insular cortex
	3	1240	5.29	0.002	6	42	-24	R frontal medial cortex
	4	987	4.36	0.017	-12	18	68	L superior frontal gyrus
	5	286	3.9	0.025	-28	18	-18	L frontal orbital cortex
	6	271	3.49	0.029	-40	-30	-22	L temporal fusiform cortex
	7	220	3.93	0.029	2	-88	38	R cuneal cortex
	8	107	3.43	0.033	-58	-30	-16	L middle temporal gyurs.
	9	34	3.37	0.044	-16	-76	24	L cuneal cortex
	10	33	2.74	0.048	-12	14	2	L caudate
	11	21	4.23	0.046	-20	-80	-14	L occipital fusiform gyruss

Table 8.6 Allostatic Load (AL) index and whole-brain grey matter (GM) analysis results. Lower GM density was present bilaterally with AL index acquired at phase 3 (top), phase 7 (middle) and cumulatively (bottom). Largest number of significant voxels at follow-up were associated with cumulative AL index and AL index acquired in early midlife at phase 3.

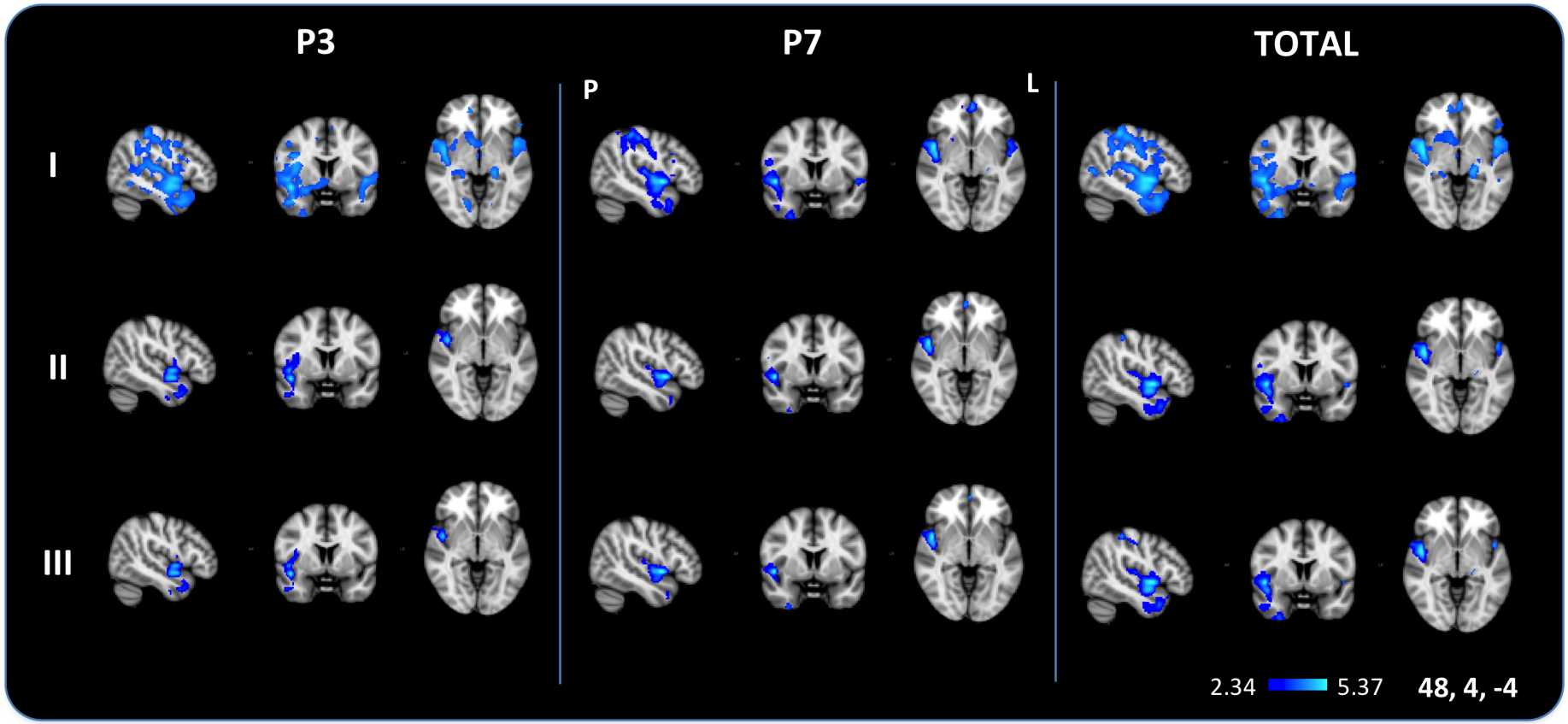


Figure 8.4 Allostatic Load (AL) index and whole-brain grey matter (GM) analysis results. Lower GM density in superior frontal, parietal, temporal and medial temporal, medial frontal regions and thalamus was present bilaterally with AL index acquired at phase 3 (P3), 7 (P7) and cumulatively (total), with largest number of significant voxels associated with P3 and cumulative AL index (model I). Significant association was found primarily in the precentral gyrus, central opercular cortex and temporal pole (P3, P7) and thalamus (total) after controlling for demographic factors (model II). Socioeconomic factors did not substantially reduce this association further (model III). Colours represent t-values significant at $p < 0.05$, threshold free cluster enhancement and multiple comparisons corrected.

Model II: AL Index + age, sex, ethnicity								
	Cluster	Cluster size (voxels)	Max t	p-value	MNI coordinates (x, y, z)			Structure
P3	1	1713	4.87	0.002	46	2	-12	R planum polare
P7	1	798	4.97	0.004	48	4	-4	R planum polare
	2	563	4.49	0.011	36	24	-20	R frontal orbital cortex
	3	163	4.47	0.021	2	50	-24	R frontal medial cortex
	4	52	3.67	0.042	36	-2	-44	R temporal fusiform cortex
	5	47	4.25	0.034	-2	56	-2	L frontal pole
TOTAL	1	3517	5.37	< 0.001	48	2	-2	R planum polare
	2	121	4.31	0.03	-48	8	-4	L central opercular cortex
	3	118	3.56	0.041	10	-30	6	R thalamus
	4	95	4.08	0.033	-56	-26	20	L parietal operculum cortex
	5	39	3.85	0.041	-42	-20	8	L Heschl's gyrus
	6	25	4.07	0.041	48	-34	54	R supramarginal gyrus
	7	16	4.21	0.045	-20	-26	-2	L thalamus

Table 8.7 Allostatic Load (AL) index and whole-brain grey matter (GM) analysis results controlling for demographic factors (model II). Significant lower GM was found in precentral gyrus, central opercular cortex and temporal pole (P3, P7) and thalamus (total).

Model III: Model II + SES, education								
	Cluster	Cluster size (voxels)	Max t	p-value	MNI coordinates (x, y, z)			Structure
P3	1	1266	4.75	0.003	46	2	-12	R planum polare
P7	1	772	4.77	0.006	48	4	-4	R planum polare; central opercular cortex
	2	521	4.3	0.013	36	24	-20	R frontal orbital cortex
	3	146	4.54	0.023	2	50	-24	R frontal medial cortex
	4	89	3.73	0.036	36	-2	-46	R temporal fusiform cortex
	5	19	4.19	0.043	-2	56	-2	L frontal pole; paracingulate g
TOTAL	1	3311	5.15	0.001	48	2	-2	R planum polare; central opercular cortex
	2	112	4.05	0.033	48	-34	54	R supramarginal g
	3	51	4.1	0.036	-56	-26	20	L parietal operculum cortex
	4	27	4.19	0.04	-48	8	-4	L parietal operculum cortex
	5	25	3.85	0.044	-42	-20	8	L insular cortex
	6	15	4.19	0.045	-20	-26	-2	L thalamus

Table 8.8 Allostatic Load (AL) index and whole-brain grey matter (GM) analysis results controlling for demographic and socioeconomic factors (model III). Significant lower GM was found in precentral gyrus, central opercular cortex and temporal pole (P3, P7) and thalamus (total), not substantially different from association found in model II (Table 8.6).

Figure 8.5 shows mean grey matter density values extracted from the significant (p < 0.05, tfce) regions in which AL index measured at Phase 3 is associated with lower grey matter density after controlling for age, sex, ethnicity, occupational position and education years (model III). The plot demonstrates a negative linear relationship between AL index and GM density, after controlling for the covariates of no interest.

No association was found between any measure of AL index and higher GM density.

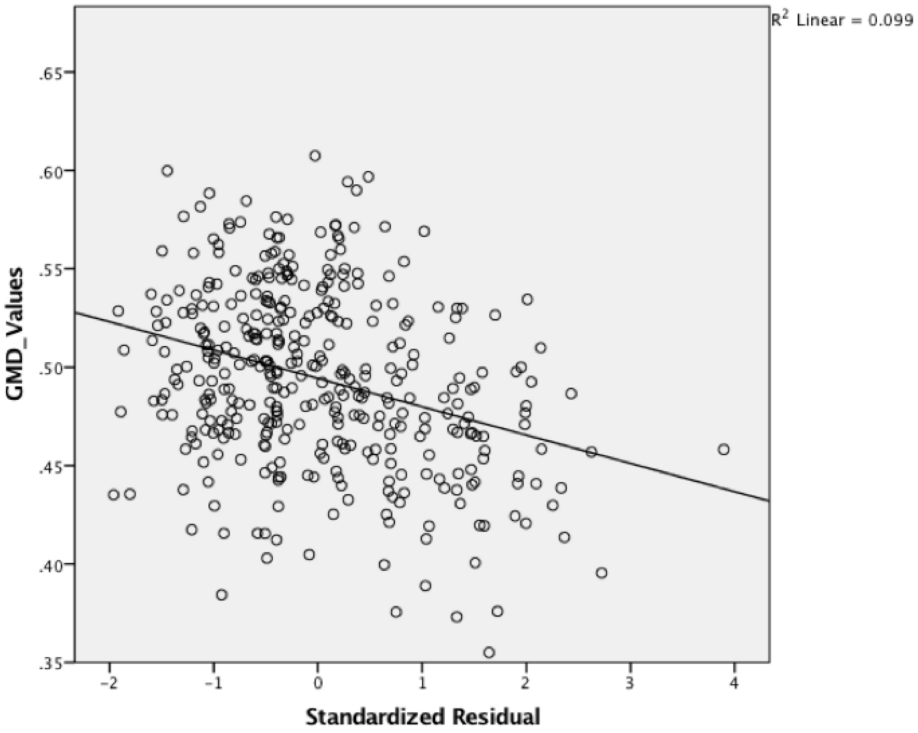


Figure 8.5 Regression plot of individual mean grey matter density values extracted from regions (y-axis) with which Phase 3 AL index is significantly (p < 0.05, tfce) associated, after controlling for all confounders of Model III (x-axis).

8.3.3 TBSS Results

Change in AL index between Phases 3 and 7, *was not significantly associated* with whole-brain white matter microstructure measures. Below is a detailed presentation of results for AL indices.

8.3.3.1 Models I

Only Allostatic Load index at Phase 3 was significantly associated with lower FA (left inferior longitudinal fasciculus; Figure 8.6, Table 8.9) and higher AD (right superior corona radiata, thalamic radiation; Table 8.8). No association with %GM and %WMH were examined, due to the small number of significant voxels, in which lower FA values were associated with AL index (Model I a) and I b)).

These associations were no longer significant after controlling for demographic factors. No significant association between any AL index measure and higher FA or lower AD values were found. No association was present with either MD or RD.

AL Index and FA reduction at Phase 3								
Model	**Cluster**	**Cluster size (voxels)**	**Max t**	**p-value**	**MNI coordinates (x, y, z)**			**Structure**
I	1	331	4.73	0.045	-33	-63	4	L inferior longitudinal fasciculus

AL Index and AD increase at Phase 3								
Model	**Cluster**	**Cluster size (voxels)**	**Max t**	**p-value**	**MNI coordinates (x, y, z)**			**Structure**
I	1	1509	4.77	0.02	29	-20	22	R superior corona radiata
	2	63	2.83	0.049	23	18	10	
	3	21	2.72	0.05	15	5	9	R anterior thalamic radiation
	4	14	2.45	0.05	19	11	9	

Table 8.9 AL index measured at Phase 3 associated with lower FA and higher AD values. Lower FA values were present in left inferior longitudinal fasciculus (top) and higher AD valus in right superior corona radiata and thalamic radiation.

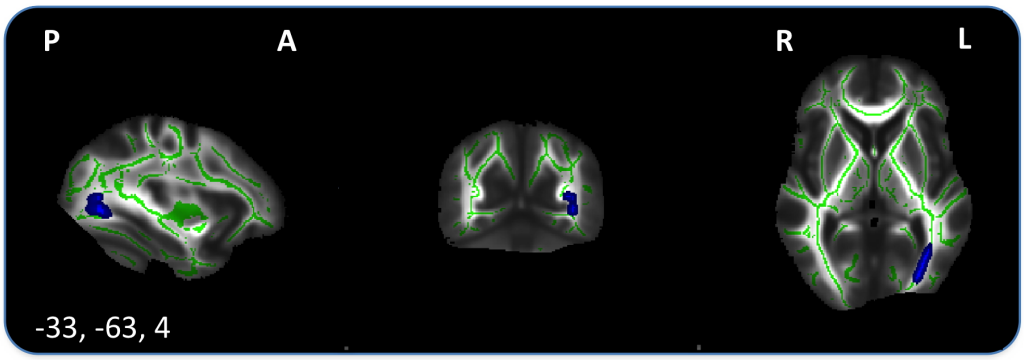


Figure 8.6 Allostatic load index measured at Phase 3 was associated with whole-brain lower FA values in the left inferior longitudinal fasciculus. Significant regions ($p < 0.05$, tfce) are dilated for illustrative purposes, overlaid on a green skeleton

8.4 Discussion

In this chapter the linear association of Allostatic Load (AL) index at two phases in mid-life and cumulative AL index with whole-brain structural grey matter density and microstructural white matter integrity in older age was assessed. Cumulative AL index was defined as the total number of AL index markers across two Whitehall II study phases over a 10-year period.

8.4.1 Whole-brain grey matter

8.4.1.1 Summary of aims and hypotheses

AL index affected brain structure as early as 20 years prior to the MRI scan, in Phase 3 (***Aim 3)***. A higher AL index in both phases and as a cumulative score was associated with lower grey matter (GM) density in neocortical areas of the superior parietal and temporal lobes and in neo-subcortical structures, i.e. the thalamus, medial temporal lobes, and temporal pole, in line with ***Aim 1)*** of this study. ***Hypothesis 1)*** was supported through examining ***Aim 2)***: AL index made a unique

contribution to lower GM after controlling for demographic and socioeconomic factors.

Demographic factors removed shared variance between AL index and GM primarily in the neo-cortex and the left parietal lobe, while controlling for socioeconomic factors weakened the remaining effects of AL index. The association with AL index at Phases 3 and 7, and with cumulative AL index remained localised in the right precentral gyrus, and bilaterally in central opercular cortex and temporal pole. Lower GM in the thalamus was in addition predicted by cumulative AL index.

As predicted, the strength of both controlled and uncontrolled associations was strongest with cumulative AL index. Contrary to ***Hypothesis 2)*** the uncontrolled effect of AL index 20 years prior to the MRI scan was stronger than 10 years prior to the scan. The effect of AL index 10 years prior to the scan, controlling for demographic and socioeconomic factors was slightly stronger than the effect of AL index 20 years prior to the scan. Therefore, ***Hypothesis 2)*** was partially supported.

On the contrary to the expected, ***Hypothesis 3)*** (Aim ***4)***) was not supported. An increase in AL index score from Phase 3 to Phase 7 was not associated with lower GM, possibly because in the majority of the cases AL index did not change between the two phases, leading to a lack of statistical power.

8.4.1.2 Changes of AL over time

Allostatic load (AL) is conceptualised as the accumulation of stress responses over time, and it theoretically represents the accumulated damage of the allostatic process on the body over the life course (51) (see also Chapter 2). Although there is

no consensus on the exact biological markers that constitute the AL index, there is a noted overlap between its markers and a suggested list of biomarkers of ageing (89). Unlike other secondary markers of the stress response, such as the Framingham Stroke Risk score, age is not incorporated in the index (2). Rather, it is often assumed, and is deemed *plausible* to assume, that AL index increased with the passage of time, even if it was low in early adulthood (83). On the other hand, a cross-sectional study using National Health and Nutrition Examination Survey data found that, whereas AL index increased from the 20s into the 60s, levels of the index stabilised in the 70s and 80s (340). Although conclusions about the general population should be drawn from Crimmins and colleagues' study with caution, in case this was a reflection of those with lower AL index surviving into older age.

AL index, defined the same way as in the present study, was previously measured in 7,007 Whitehall II participants across Phases 3, 5, and 7. AL index increased with age, "but as expected, the increase was nonlinear (*p* value for the quadratic term < 0.001), becoming attenuated with age", starting in the mid-60s (78) (see also Figure 4.1 in section 4.3.1.3). This is in line with both Crimmins and colleagues' study, and the current study, as in the majority of cases AL index was stable throughout the 10-year period of Phases 3 and 7. Prospective studies, that longitudinally and concurrently assess AL index and brain structure, are needed in order to identify critical periods where the ageing brain is particularly sensitive to AL index change, as well as studies that examine the structural brain markers of AL index change from early adulthood to mid-life. In fact, a recent review by Gallo and colleagues highlighted that the need for additional longitudinal research on the AL load

framework has been emphasised repeatedly (87). As they pointed out, only a few prospective studies support the applicability of the AL framework to date (341, 342).

8.4.1.3 Cumulative AL index

Findings of this chapter suggest that AL index is associated with lower grey matter in the right precentral gyrus, central opercular cortex, temporal pole and thalamus, even after controlling for confounding variables, with the strongest effect seen with cumulative AL index.

Since allostatic load is theorised to represent accumulated stress over the life course (51) AL index is assumed to represent a cumulative process, and is therefore often used as a cross-sectional measure at a single time-point in order to predict functional outcomes in ageing (e.g. (83, 338, 343)). Based on this theory we can conclude that AL index measured in two phases in mid-life, 10 years apart, predicts lower GM 10 and 20 years later in older age. However, after controlling for confounders, AL index measured 10 years prior to the MRI scan appeared more widely associated with lower GM values than AL index measured 20 years prior to the scan. A much stronger association was present the opposite way around before controlling for confounding variables, which may reflect a lack of statistical power to detect an association in the presence of limited AL index change between the two phases (see above). The association with cumulative AL index, both controlled and uncontrolled for confounding variables, was consistently stronger than with AL index measured at either phase. This could be because averaging reduces measurement error. Thus, findings of this chapter provide further evidence for the benefit of measuring allostatic load longitudinally (see above) and using it as a cumulative index.

8.4.1.4 Location of results

The AL model of chronic stress not only assumes the prominent role of certain brain structures, such as the hippocampus, amygdala, and prefrontal cortex as regulators and the hypothalamus as an effector (part of the HPA-axis) of the stress response, but also that over time they become damaged by chronic stress (6, 34). AL is theorised as a putative biological pathway between various types of psychological stressors that exert their effect in the life course and the brain structures mentioned above, in both healthy and ill (for review: (93, 344). For instance, low subjective socioeconomic status is associated with reduced GM in the prefrontal cortex in healthy (345) and temporal lobe shrinkage has been observed in relation to both chronic stress (107) and posttraumatic stress disorder (105). Yet the relationship between AL index and brain structure has not been scientifically established. Apart from a recent single birth-year study of the Lothian Birth cohort (83), no other studies investigated the effect of AL index on brain structure or function in (ageing) humans.

Using structural equation modelling Booth and colleagues (83) found that AL index in 633 members of the Lothian Birth cohort (72.5 (0.7) years) was inversely related to total brain volume, positively related to hippocampal volume and not related to grey matter volume. They also found an inverse relationship with cognitive ability, processing speed and knowledge but no relationship with memory or nonverbal reasoning. More importantly, the effects of AL index on cognition were not mediated by brain volume measures. These findings are not in line with findings of the current study, which might be due to the differing methods of image analysis, that the

Lothian birth cohort is possibly more homogenous than the Whitehall II cohort in terms of allostatic load, and that its results are based on contemporary as opposed to longitudinal cross-sectional measures.

In the present study, AL index did not affect the prominent brain structures theorised to be affected by allostatic load, such as hippocampal formation and prefrontal cortex. Rather, the location of the present findings point to the middle cerebral artery (MCA) territories (303), and so the underlying biological mechanisms might be of vascular nature. As pointed out above, prospective cohort studies that longitudinally and concurrently assess stressors, AL index and brain structure are needed in order to tease apart the allostasis and allostatic load mechanisms.

8.4.2 Whole-brain white matter

8.4.2.1 Summary of aims and hypotheses

AL index 20 years prior to the scan, in Phase 3, predicted lower FA values in the forceps major and in the inferior fronto-occipital fasciculus and superior longitudinal fasciculus in the *left* hemisphere. It also predicted higher AD values in the corticospinal tract, inferior fronto-occipital fasciculus and superior longitudinal fasciculus in the *right* hemisphere (***Aim 3)***). These associations were no longer present after controlling for the confounder variables. No WM association was found with AL index 10 years prior to the scan (in Phase 7), with cumulative AL index, and with increase in AL index between the two study phases, which was not in line with ***Aims 1), 2)*** and ***4).*** Therefore all ***hypotheses*** were rejected.

8.4.3 Discussion

In this study AL index was very weakly associated with white matter (WM) integrity, regardless of whether the association was or was not controlled for confounders. Furthermore, cumulative AL index, which was the most widely associated with grey matter, was not associated with microstructural WM measures. As predicted by their above reported results, Booth and colleagues found a strong, inverse relationship between WM volume and AL index even after controlling for age and sex (83).

The current findings imply that voxel-wise WM integrity measures are more related to demographic confounders, such as age, than AL index. AL index, at least in its present form, is not a good measure to predict WM integrity in older age.

8.4.4 Methodological considerations

The present study appears to be the first to examine the effect of AL index on structural integrity. The same strengths and limitations apply as in previous chapters. AL index defined at the Whitehall II studies does not contain primary markers of the stress response, e.g. cortisol. While cortisol has been acquired at the Whitehall II studies, it was not collected across phases using the same methods and was available for analysis only in some participants. There is no agreed rule for calculating the AL index, so that primary markers of stress response, such as cortisol, corticotropin or Tumour Necrosis Factor α, are not routinely included (e.g. (2, 87)). The effects of cortisol on brain areas, such as the prefrontal cortex and hippocampus, have a key role in initiating and delivering the stress response (e.g. (7)). Future research therefore needs to address, whether the combination of

primary and secondary markers of the stress response gives valuable information about the ageing brain.

Chapter 9: The Unique Effect of Secondary Stress Markers on Brain Structure

9.1 Introduction

9.1.1 Background

Chapters 6, 7 and 8 examined whether secondary markers of the stress response measured in mid-life, namely ***Framingham Stroke Risk, Metabolic Syndrome*** and ***Allostatic Load index***, predict an effect on structural brain integrity in later life. If an effect was found, it was also examined whether any effects remained significant after controlling for demographic and socioeconomic confounders.

Each marker had a unique linear association with lower ***grey matter (GM) density*** values in similar areas after controlling for age, sex, ethnicity (i.e. demographic confounders) and years of education and employment grade (i.e. socioeconomic confounders). Framingham Stroke Risk score (FSRS) was associated with lower GM values in the right medial temporal lobe (Chapter 6). Cumulative Metabolic Syndrome (MetS) predicted lower GM values predominantly in the right hemisphere, in neocortical areas of the temporal and parietal lobes, i.e. pre- and postcentral gyri, supramarginal gyrus, opercular cortex, as well as superior temporal cortex, and sub-neocortical structures, i.e. the thalamus and medial temporal lobes (Chapter 7). Cumulative Allostatic Load (AL) index was associated with lower GM values in the neo-cortex in the right precentral gyrus, and bilaterally in central opercular cortex and in sub-neocortical structures, i.e. the thalamus and temporal pole.

White matter (WM) integrity results showed more variability with stress markers than GM results. After controlling for demographic and socioeconomic confounders FSRS was not associated with substantial effects on WM integrity, apart from higher mean diffusivity (MD) values in the right superior corona radiata. Cumulative MetS was associated with lower FA and higher MD values bilaterally in anterior thalamic radiation, external and internal capsule and right anterior corona radiata, as well as with higher MD in the inferior fronto-occipital fasciculus. Cumulative AL index was not associated with WM integrity values after the addition of confounding variables.

The overlap in significant results between the three stress markers might be explained by a shared underlying mechanism. This might be due to the fact that the markers are made of similar composite measures. FSRS, MetS and AL index all contain cardiovascular and metabolic measures. While FSRS is primarily composed of cardiovascular risk factors, MetS and AL index have more metabolic risk factors, with similar cut-offs. Furthermore, AL index, in its current form in the Whitehall II studies (78, 153), is the only stress marker that contains immune function measures (see Table 4.2 and 9.0).

As detailed in the previous chapters, the above stress markers are better predictors of health outcomes than their individual components (e.g. (53, 145, 148). The present chapter, therefore, examines whether they are associated with the same structural brain integrity measures in older age.

9.1.2 Hypothesis

The following analysis examines whether there is a unique effect of any of the three secondary stress markers measured across two study phases in mid-life, namely Framingham Stroke Risk score (FSRS), Metabolic Syndrome (MetS) and Allostatic Load (AL) index, on structural brain integrity, namely grey matter (GM) density and white matter (WM) microstructure, at follow-up, having controlled for the effects of other stress markers, and demographic or socioeconomic factors.

The null hypothesis was that, as the three secondary stress markers measure the same construct in identical phases (Phases 3 and 7), none of them will have a unique association with structural brain integrity after controlling for the effects of the other stress markers, and demographic or socioeconomic factors.

9.2 Methods

9.2.1 Sample characteristics, inclusion/exclusion criteria

The sample of participants used in this chapter was drawn from 563 Whitehall II Imaging Sub-study participants, described in section 4.1. Participants were excluded from analysis if they did not have a MRI scan, had noticeable structural abnormalities or poor image quality that pre-processing and artefact correction did not fix, or had a missing FSRS, MetS or AL index value at either Whitehall II phase included in analysis.

9.2.2 Assessment of secondary stress markers

For this comparison, Framingham Stroke Risk Score (FSRS), Metabolic Syndrome status (MetS) and Allostatic Load (AL) Index were defined at Phase 3 (1991-1994) and Phase 7 (2002-2004) of the Whitehall II study were used. Protocols for acquiring and deriving the scores have been detailed in sections 6.2.2, 7.2.2 and 8.2.2 respectively. In order to make the three secondary stress markers comparable, each marker derived at Phases 3 and 7 was summed to create a total (cumulative) mid-life score.

In short, ***FSRS*** is a risk prediction algorithm that ***combines cardiovascular, metabolic and socio-demographic information*** to predict the 10-year percentage probability of a stroke. It was computed at Phases 3 and 7 using beta coefficients based on the Cox proportional hazards regression model in the Framingham study (61). Stroke risk scores computed at both phases were summed to create the total mid-life stroke risk score (Table 9.1).

MetS is defined as the linear combination of ***five cardiovascular and metabolic measures***, at least three of which have to be above a high-risk clinical cut-off (149). For individual marker cut-offs see section 4.3.1.2 and Table 9.0, the latter also indicates overlapping components between MetS and AL index. Participants who met MetS criteria at Phases 3 or 7 of Whitehall II were given a binarised (yes/no) score, if ≥ 3 markers were above their respective cut-offs at that phase. The total (cumulative) MetS score was calculated by summing the binary scores of Phases 3 and 7 (Table 9.1).

AL index was defined at Phases 3 and 7 of the Whitehall II study as the ***linear combination of nine physiological measures*** with values above a high-risk threshold (78, 153). For composite score cut-off see Table 9.0 and section 4.3.1.3. Each component was given a dichotomised (yes/no) score based on their respective threshold. The dichotomised scores were summarised to form the AL index at each phase. Total (cumulative) mid-life AL index was defined as the sum of AL index at both phases (Table 9.1).

	Metabolic Syndrome	**Allostatic Load Index**
Blood pressure	≥ 130/85 mmHg Antihypertensives	≥ 140/90 mmHg
Waist circumference		N/A
Men	> 102cm	
Women	> 88cm	
Fasting glucose	≥ 6.11 mmol/L	≥ 5.5 mmol/L
HDL cholesterol		
Men	< 1.03 mmol/L	< 1.03 mmol/L
Women	< 1.3 mmol/L	
Serum triglycerides	≥ 1.7 mmol/L	≥ 1.7 mmol/L
Body mass index	N/A	≥ 25 kg/mm²
Fasting insulin	N/A	≥ 7.53 mcU/ml
LDL cholesterol	N/A	≥ 3.36 mmol/L
CRP	N/A	≥ 3 mg/L
IL-6	N/A	≥ 1.85 pg/ml

Table 9.0. Comparison of Metabolic Syndrome and Allostatic Load Index composite measure cut-offs. An elevated level of each measure carries more risk, except in case of HDL cholesterol. LDL, Low-density lipoprotein; HDL, High-density lipoprotein; CRP, C-reactive protein; IL-6, Interleukine-6.

	Phase 3 1991-1993	Phase 7 2003-2004	Total *Mean, SD*
Age *[years]* *Mean, SD*	48.2 (5.2)	59.4 (5.2)	69.6 (5.2)
Framingham [10-year Stroke Risk] *Mean, SD*	3.3 % (1.4%)	5.2% (3.7%)	8.5 % (4.5%)
Metabolic Syndrome *95% CI*	8.0% (5.4% – 11.3%)	10.9% (7.8% – 14.6%)	0.19 (0.5)
Allostatic Load *Mean, SD*	2.69 (1.7)	3.0 (1.8)	5.7 (3.0)

Table 9.1. Average (SD) Framingham Stroke Risk and Allostatic Load indices at Phases 3 and 7, as well as binary frequency [%, yes] and 95% exact binomial confidence intervals (CI) of Metabolic Syndrome not directly used for analysis in blue and total scores across both phases used in whole-brain grey matter analysis (N = 349) marked with black for mean and SD. Follow-up at 2012-2014. See also Tables 9.3 and 9.4.

9.2.3 Assessment of nuisance variables

Secondary stress markers FSRS, MetS and AL index were included in a series of analyses, variably as either exposure variables (of interest) or confounding (nuisance) variables. This was required to identify each of the secondary stress markers' (i.e. as exposure variable of interest) unique association with brain structure integrity, having controlled for the variance it shares with the other markers (i.e. the confounding variables) taking into account the other confounding variables.

The other confounding variables were: demographic variables, i.e. age at scan, sex, ethnicity, and socioeconomic variables, i.e. years of education along with mid-life occupational status. These were used as confounding variables in all analyses (their assessment was detailed in section 4.2.2).

9.2.4 MRI Methods

9.2.4.1 Acquisition and analysis

Image acquisition was carried out at the Oxford FMRIB Centre using a 3T Siemens Magnetom Verio (Erlangen, Germany) scanner with a 32-channel receive head coil. T_1-weighted, FLAIR and diffusion-weighted MRI images were acquired as part of the protocol (127). Image analysis was performed using FSL v.5.0, (www.fmrib.ox.ac.uk/fsl, (218)). Image acquisition and analysis were detailed in section 5.3.

9.2.4.2 Whole-brain grey matter analysis

Voxelwise analysis of grey matter density, detailed in section 5.3.1.3, was performed on T_1-weighted images using FSL-VBM (221). Significant GM voxels were localised with the Harvard-Oxford cortical and subcortical structural atlases (277).

9.2.4.3 Whole-brain microstructural white matter analysis

Voxelwise statistical analysis of fractional anisotropy (FA) and mean diffusivity (MD) data was carried out on DTI data using FSL-TBSS (Smith, 2006) (section 5.3.2.3). JHU DTI-based white matter atlases were used for identifying the location of TBSS results (278, 279).

9.2.5 Statistical analysis

Voxelwise GLM was applied for the analysis of grey matter (GM) and diffusion tensor imaging (DTI; FA, MD) data using Randomise (272), a permutation-based non-parametric statistical test, running 5000 permutations and correcting for multiple comparisons across space. The significance threshold was set at $p < 0.05$, using threshold-free cluster enhancement (TFCE; (274), see section 5.3.3).

The null hypothesis was that the three markers, namely FSRS, MetS, and AL index, measure the same construct, thus none of them will have a unique association with structural integrity after controlling for the effects of the other markers, as well as demographic and socioeconomic factors.

Linear associations of FSRS, MetS and AL index with voxelwise GM and DTI data were assessed, including demographic and socioeconomic variables as covariates of no interest. First, a series of F-tests were run on pairs of stress markers, controlling for the third stress marker, as well as demographic and socioeconomic covariates of no interest. Whenever a significant F-test was found, further post-hoc tests were run to see if controlling for two of the three stress markers also yielded a result.

More specifically, the following F-tests were run: **F-test 1** on MetS and AL index controlling for FSRS and demographic and socioeconomic confounders, **F-test 2** on FSRS and AL index controlling for MetS and demographic and socioeconomic confounders, and **F-test 3** on FSRS and MetS controlling for AL index and demographic and socioeconomic confounders. For instance, the results of **F-test 1** indicate whether MetS and/or AL index is correlated with voxelwise GM and DTI data, after controlling for FSRS, demographic and socioeconomic variables. If **F-test 1**

was significant, two post-hoc tests were run. Namely, the linear association of MetS with voxelwise GM and DTI measures, controlling for AL index, FSRS, demographic and socioeconomic confounders (**t1**); and the linear association of AL index with voxelwise GM and DTI measures, controlling for MetS, FSRS, and demographic and socioeconomic variables (**t2**). If **F-test 2** was significant, the following post-hoc tests were run: the linear association of FSRS with voxelwise GM and DTI measures, controlling for AL index, MetS, demographic and socioeconomic confounders (**t3**); and the linear association of AL index with voxelwise GM and DTI measures, controlling for FSRS, MetS, and demographic and socioeconomic variables (**t4**). Finally, if **F-test 3** was significant, the following post-hoc tests were run: the linear association of FSRS with voxelwise GM and DTI measures, controlling for MetS, AL index, demographic and socioeconomic confounders (**t5**); and the linear association of MetS with voxelwise GM and DTI measures, controlling for FSRS, AL index, and demographic and socioeconomic variables (**t6**).

9.3 Results

9.3.1 Descriptive statistics

9.3.1.1 Participant exclusion / inclusion

Between April 2012 and December 2014 a total of 563 Whitehall II participants attended the Whitehall II sub-study. Participants with no T_1 scan (N = 11), with structural abnormalities (N = 18) or inadequate T_1 scan (N = 2), missing Framingham Stroke Risk score (N = 25), Metabolic Syndrome score (N = 4) or Allostatic Load index (N = 154) at either of the two phases, missing (N = 9) or un-useable DTI scan (N = 3) were excluded from analysis. VBM analysis was based on a final sample of N = 349

(62% of those attended), and TBSS on N = 337 (60% of those attended) participants. An overview is presented in Figure 9.0.

9.3.1.2 Participant demographics and nuisance variable characteristics

Participant characteristics are shown in Table 9.2, which do not substantially differ from the total sample's characteristics presented in Table 4.1.

	VBM (N = 349)	**TBSS (N = 337)**
Age, *years, Mean (SD), range*	69.6 (5.2) 60-83	69.5 (5.2) 60-83
Sex, *N (%)*		
Male	281 (80.5)	271 (80.4)
Female	85 (24.4)	66 (19.6)
Ethnicity, *N (%)*		
White	325 (93.1)	313 (92.9)
Non-white	24 (6.9)	24 (7.1)
Grade, *N (%)*		
Administrative (highest)	149 (42.7)	142 (42.1)
Professional/executive	171 (49.0)	167 (49.6)
Clerical/support (lowest)	29 (8.3)	28 (8.3)
Education level, *years, Mean (SD), range*	13.9 (3.0) 6-23	14.0 (3.0) 6-23

Table 9.2 Unique effects of secondary stress markers study sample characteristics.

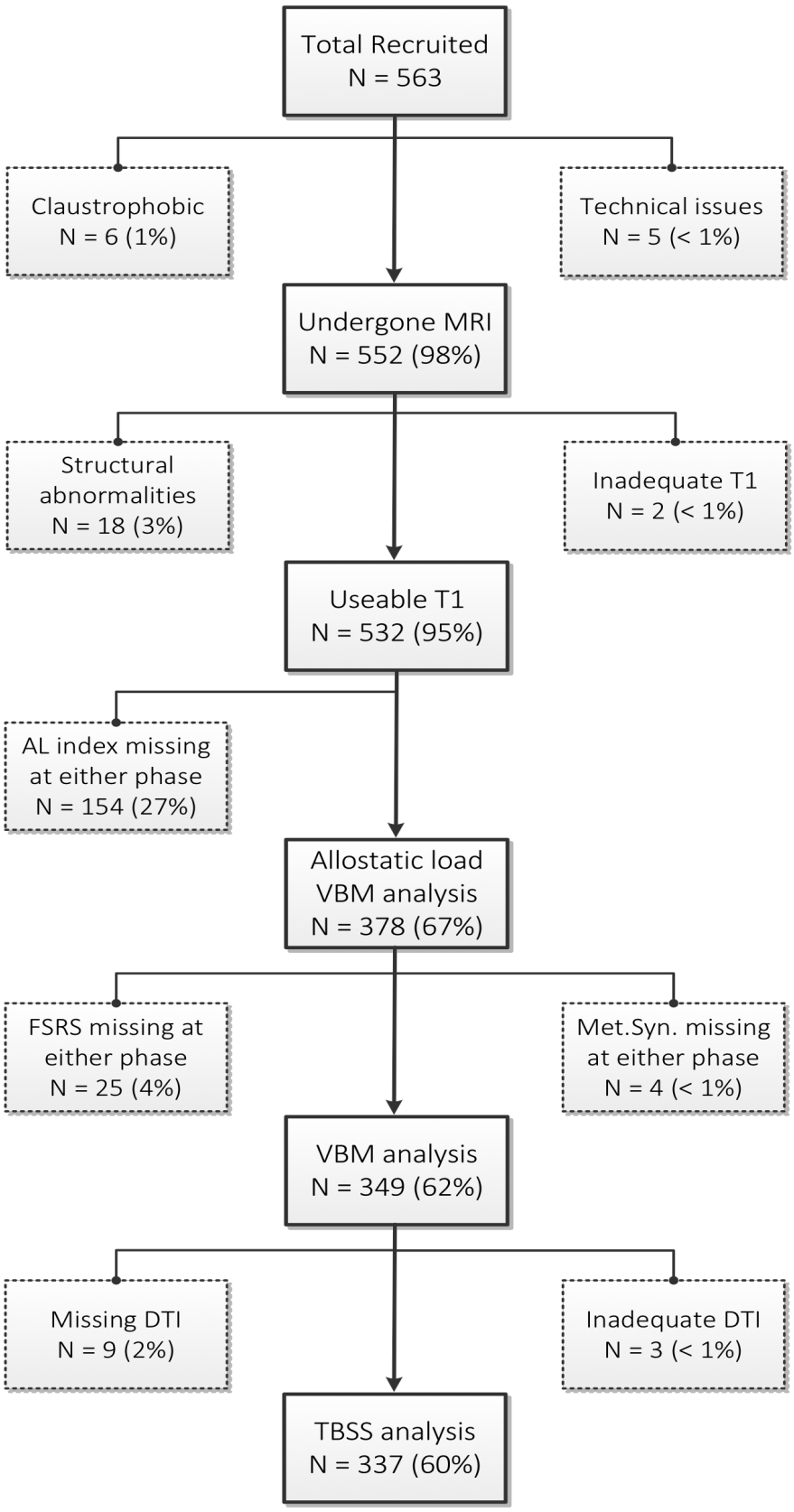


Figure 9.0 Flowchart of participant exclusion before final VBM (N=349) and TBSS (N=337) analyses, including missing or inadequate scans and missing secondary stress markers.

9.3.1.3 Characteristics of secondary stress markers

The three secondary stress markers were positively correlated. Participants with a high FSRS had a high MetS score (Pearson's r (347) = 0.409, p = 0.001) and a high AL index (r (347) = 0.413, p = 0.001). Participants with a high MetS score also had a high AL index (r (347) = 0.584, p = 0.001).

Mean total percentage ***Framingham Stroke Risk score (FSRS)*** used in whole-brain grey matter (GM) analysis (N = 349) was 8.5% (SD = 4.5), and in whole-brain white matter (WM) analysis (N = 337), 8.4% (SD = 4.4). Scores ranged between 2 – 42% in both analyses. Distribution of FSRS scores for both GM and WM analysis are shown in Figure 9.1.

Mean total ***Metabolic Syndrome (MetS)*** *score* used in whole-brain GM analysis was 0.19 (SD = 0.5), and 0.18 (SD = 0.5) in whole-brain WM analysis. Total MetS ranged between 0 – 2 in both analyses. Table 9.3 and the positively skewed histograms of Figure 9.2 show that the majority (approx. 85%) of the sample in both whole-brain GM and WM analysis was free from MetS.

N (%)	**VBM (N = 349)**	**TBSS (N = 337)**
0	295 (84.5)	286 (84.9)
1	42 (12.0)	42 (12.5)
2	12 (3.4)	9 (2.7)

Table 9.3 Total times of Metabolic Syndrome binary yes/no score across Whitehall II Phases 3 + 7. Percentage shows prevalence within the sample.

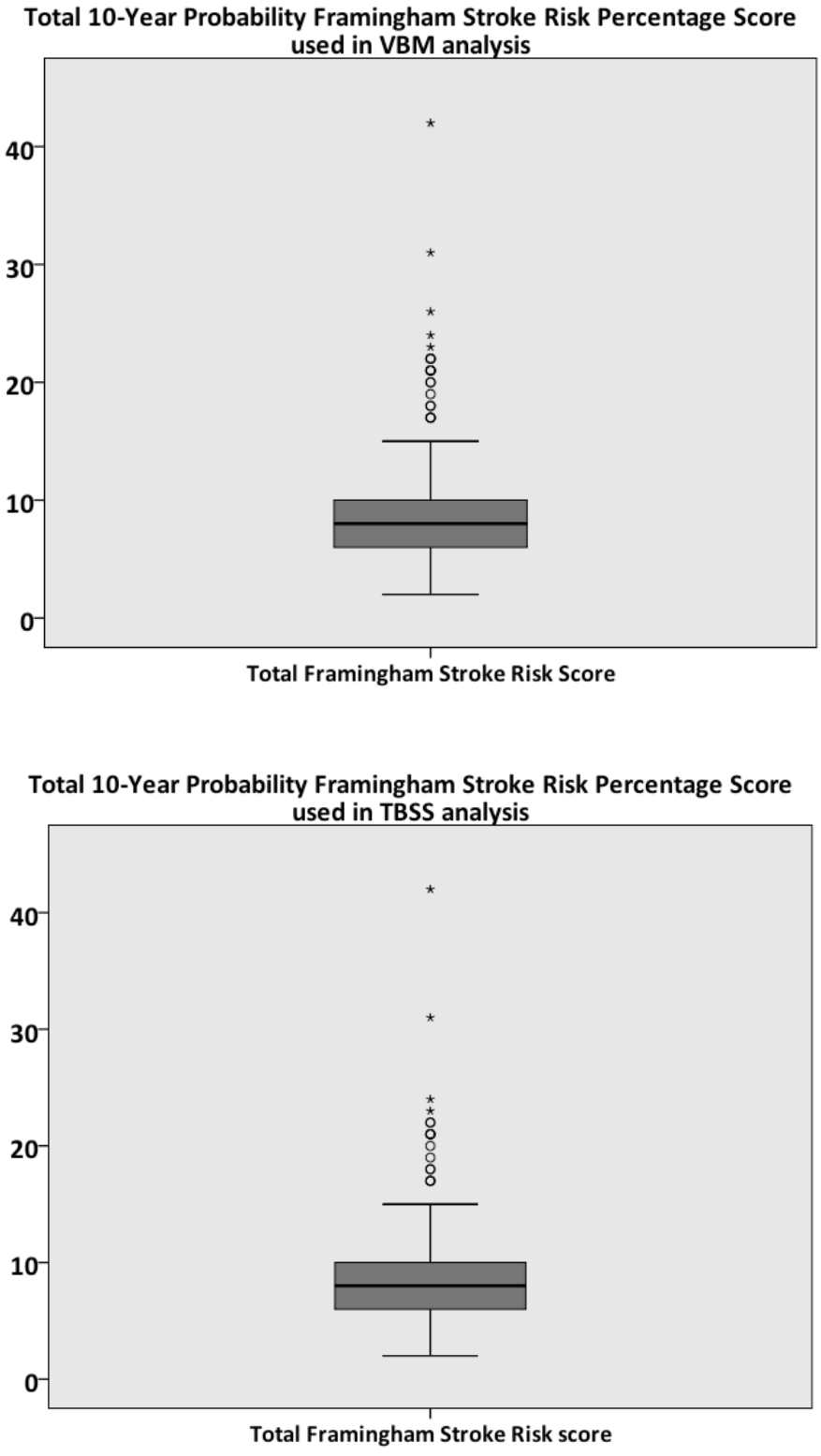


Figure 9.1 Percentage Total Framingham Stroke Risk Score distribution in VBM (top) and TBSS (bottom) analyses.

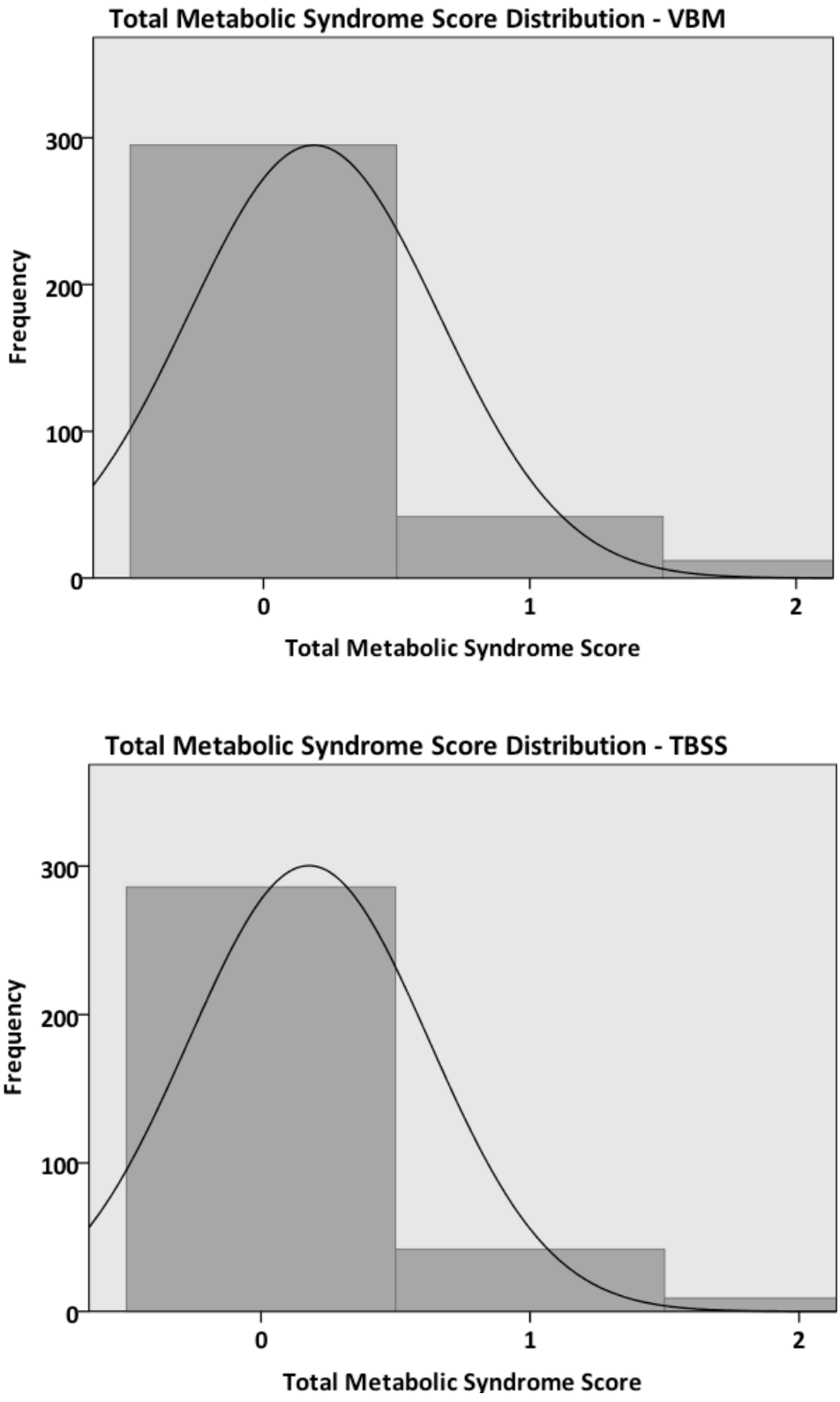


Figure 9.2 Total Metabolic Syndrome Score dsitribution in VBM (top) and TBSS (bottom) analyses.

Mean total ***Allostatic Load (AL) index*** used in whole-brain GM analysis was 5.65 (SD = 3.03), and in WM analysis, 5.62 (SD = 3.02). Total AL index ranged between 0 -15 in both analyses. Table 9.4 shows that 38.7% of participants used in whole-brain GM analysis had a total AL index of less than 5, 50.2% between 5-9 and only 19.8% had 10 to 15 total AL index across Phases 3 and 7. This is further demonstrated in Figure 9.3

N *(%)*	**VBM (N = 349)**	**TBSS (N = 337)**
0	8 (2.3)	8 (2.4)
1	17 (4.9)	17 (5.0)
2	30 (8.6)	30 (8.9)
3	35 (10.0)	32 (9.5)
4	45 (12.9)	43 (12.8)
5	47 (13.5)	46 (13.6)
6	37 (10.6)	37 (11.0)
7	38 (10.9)	35 (10.4)
8	29 (8.3)	29 (8.6)
9	24 (6.9)	24 (7.1)
10	14 (4.0)	12 (3.6)
11	12 (3.4)	12 (3.6)
12	5 (1.4)	5 (1.5)
13	7 (2.0)	6 (1.8)
15	1 (0.3)	1 (0.3)

Table 9.4 Total Allostatic Load index prevalence in VBM and TBSS analysis. Percentage shows prevalence within the sample.

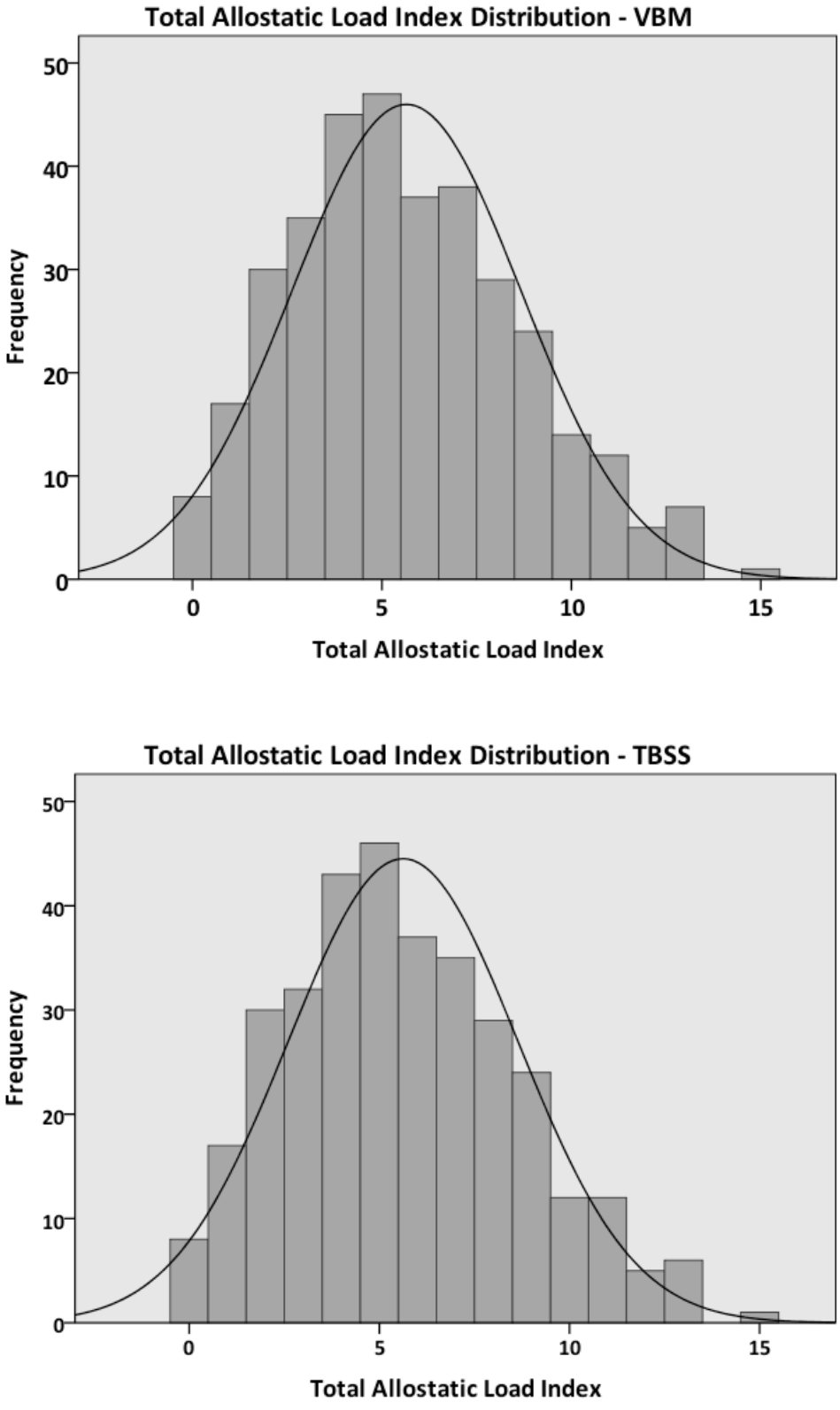


Figure 9.3 Total Allostatic Load Index distribution in VBM (top) and TBSS (bottom) analyses.

9.3.2 VBM Results

F-tests 2 and 3 showed no significant unique associations with whole-brain grey matter (GM) density. Below is a detailed presentation of significant **F-test 1** and follow-up post-hoc test results.

9.3.2.1 F-test 1

The F-test of MetS and AL index, controlling for FSRS, demographic and socioeconomic confounders, revealed significant unique associations between GM values in the right insular cortex and opercular cortex (including parts of the planum polare and Heschl's gyrus) and MetS or AL index. Maximum F-statistic was located in the right insular cortex: F (1, 340) = 11.7, p = 0.042 (Figure 9.4, Table 9.5).

GMD: MetS or AL index (+ FSRS, age, sex, ethnicity, SES, education)							
Cluster	**Cluster size (voxels)**	**Max F**	**p-value**	**MNI coordinates (x, y, z)**			**Structure**
1	38	11.7	0.042	46	2	-12	R insular cortex

Table 9.5 F-test 1 of unique Metabolic syndrome (MetS) or Allostatic Load (AL) index association with grey matter density (GMD). Results are localised in the right hemisphere along the insular and opercular cortex.

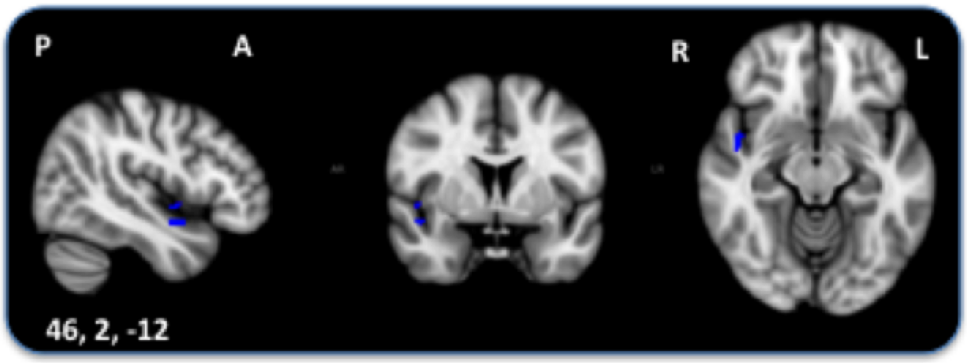


Figure 9.4 F-test 1 of unique Metabolic syndrome or Allostatic Load index association with grey matter. Results are localised in the right hemisphere along the insular and opercular cortex, with peak cluster location in the insular cortex (x=46, y=2, z=-12). Blue represents regions significant at $p < 0.05$, tfce and multiple comparisons corrected.

9.3.2.2 Post-hoc tests

A significant linear association between AL index and lower GM density was present after controlling for MetS, FSRS, and demographic and socioeconomic confounders (**t2**). Significant voxels were located in the right hemisphere in regions along the insular cortex, opercular cortex (planum polare, Heschl's gyrus), superior temporal gyrus, and temporal pole (Figure 9.5, Table 9.6). Maximum t-statistic was located in the right planum polare: t (340) = 4.61, p = 0.009.

No association of higher GM was found with AL index, and no significant GM association was present with MetS (**t1**). In summary, secondary stress markers could be ranked in terms of unique contribution to grey matter density as follows:

FSRS < MetS < AL.

GMD decrease: AL index (+ MetS, FSRS, age, sex, ethnicity, SES, education)							
Cluster	**Cluster size (voxels)**	**Max t**	**p-value**	**MNI coordinates (x, y, z)**			**Structure**
1	280	4.61	0.009	50	-4	-10	R planum polare
2	17	4.03	0.046	46	10	-24	R temporal pole

Table 9.6 Significant association of Allostatic Load (AL) index with lower grey matter density (GMD) after controlling for Metabolic Syndrome (MetS), Framingham Stroke Risk score (FSRS), and demographic and socioeconomic variables (t2). Results are localised in the right hemisphere along the insular and opercular cortex, and the superior temporal gyrus.

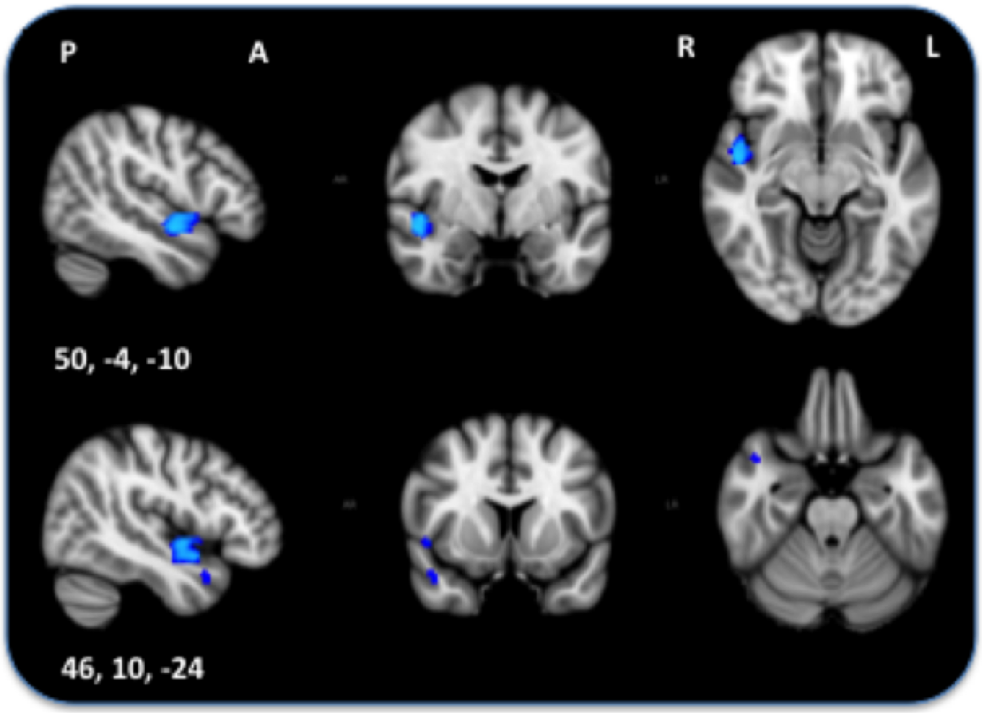


Figure 9.5 Significant association of Allostatic Load index with lower grey matter density after controlling for Metabolic Syndrome, Framingham Stroke Risk score, and demographic and socioeconomic variables (t2). Significant voxels are in the right hemisphere, along the insular cortex, opercular cortex (planum polare, Heschl's gyrus), superior temporal gyrus, and temporal pole. Blue represents regions significant at $p < 0.05$, tfce and multiple comparisons corrected.

9.3.3 TBSS Results

9.3.3.1 Fractional Anisotropy

F-tests 1 and 2 showed no significant unique associations with whole-brain fractional anisotropy (FA). Below is a detailed presentation of the significant **F-test 3** and follow-up post-hoc test results.

F-test 3

The F-test of FSRS and MetS, controlling for AL index, demographic and socioeconomic confounders, revealed significant unique associations between FA values in the body of corpus callosum and FSRS or MetS: F (1,329) = 11.4, $p = 0.045$ (Table 9.7, Figure 9.6).

FA : FSRS or MetS (+ AL index, age, sex, ethnicity, SES, education)					
Cluster	**Cluster size (voxels)**	**Max F**	**p-value**	**MNI coordinates (x, y, z)**	**Structure**
1	67	11.4	0.045	14 -19 30	Body of corpus callosum

Table 9.7 F-test 3 of unique Framingham Stroke Risk score (FSRS) and Metabolic syndrome (MetS) association with Fractional Anisotropy (FA) values. Results are localised in the body of corpus callosum.

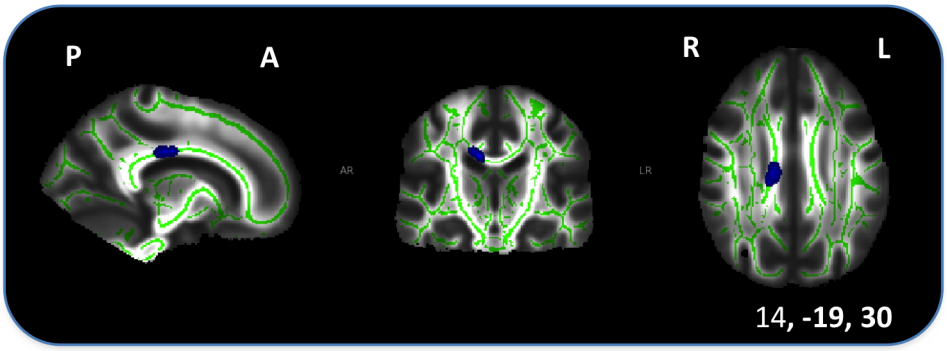


Figure 9.6 F-test 3 of unique Framingham Stroke Risk score or Metabolic Syndrome association with FA values. Results are localised in the body of corpus callosum, after controlling for Allostatic Load index, and demographic and socioeconomic factors. Significant (p < 0.05) regions are dilated for illustrative purposes, overlaid on a green skeleton.

Post-hoc tests

A significant linear association between FSRS and lower FA values was present after controlling for MetS, AL index, and demographic and socioeconomic confounders (**t5**). Significant voxels were located bilaterally in the corona radiata (anterior and superior) and corpus callosum (genu, body and splenium), forceps major, superior longitudinal fasciculus, in the right hemisphere along the anterior thalamic radiation, corticospinal tract and internal capsule, as well as in the left inferior fronto-occipital fasciculus and posterior thalamic radiation (Table 9.8, Figure 9.7). Maximum t-statistic was located in the body of corpus callosum: t (329) = 4.64, p = 0.02.

No association of higher FA values was found with FSRS, and no significant FA association was present with MetS (**t6**). In summary, secondary stress markers could be ranked in terms of unique contribution to white matter FA as follows:

AL < MetS < FSRS.

FA decrease: FSRS (+ MetS, AL index, age, sex, ethnicity, SES, education)							
Cluster	**Cluster size (voxels)**	**Max t**	**p-value**	**MNI coordinates (x, y, z)**			**Structure**
1	4110	4.64	0.02	14	-19	30	Body of corpus callosum
2	1933	4.17	0.037	-21	-51	9	Forceps major
3	1276	4.66	0.033	32	12	17	R superior longitudinal fasciculus
4	1142	4.4	0.042	-29	28	14	L inferior fronto-occipital fasciculus
5	65	2.92	< 0.05	20	8	12	R anterior thalamic radiation
6	28	1.98	< 0.05	-34	-33	25	L superior longitudinal fasciculus
7	21	2.02	< 0.05	-38	-48	17	

Table 9.8 Significant association of Framingham Stroke Risk (FSRS) with lower FA values after controlling for Metabolic Syndrome (MetS), Allostatic Load (AL) index, and demographic and socioeconomic variables (t5).

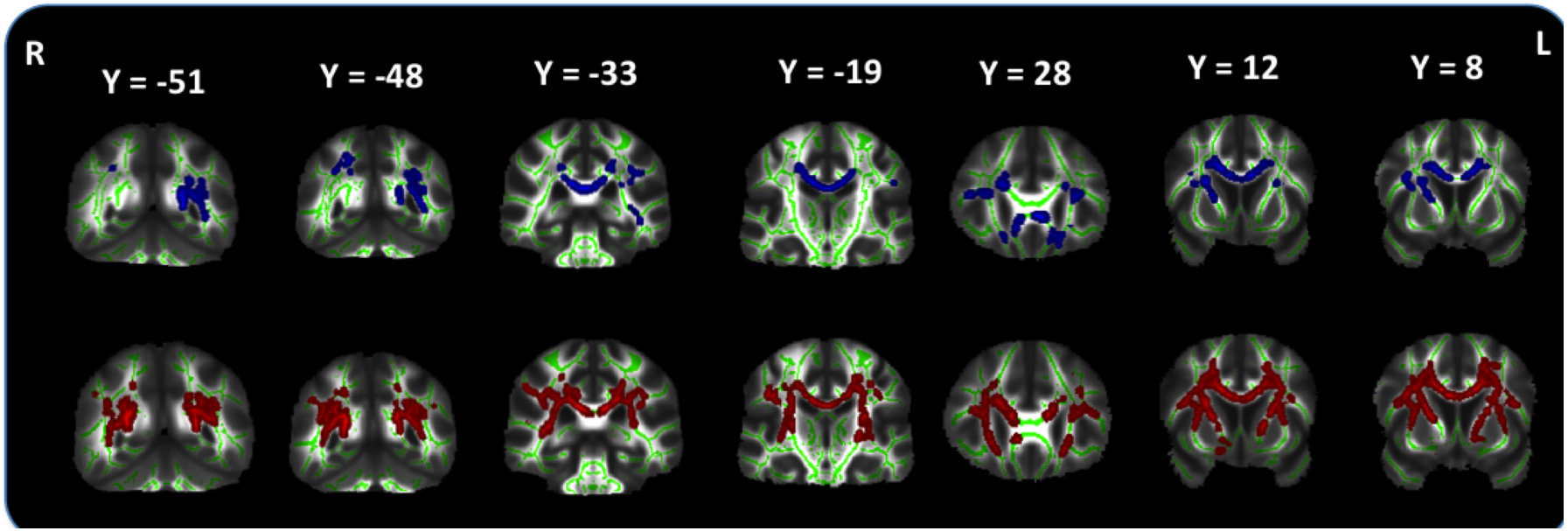


Figure 9.7 Significant association of Framingham Stroke Risk score with lower FA (t5) and higher MD (t3 = t5) values after controlling for Metabolic Syndrome, Allostatic Load index, and demographic and socioeconomic factors. Voxel locations correspond to those presented in Table 9.4. Significant regions are dilated for illustrative purposes, overlaid on a green skeleton.

Top (blue): Lower whole-brain FA values present bilaterally in the corona radiata, corpus callosum, forceps major, superior longitudinal fasciculus, in the right hemisphere along the anterior thalamic radiation, corticospinal tract and internal capsule, as well as in the left inferior fronto-occipital fasciculus and posterior thalamic radiation. **Bottom (red):** Higher whole-brain MD association was present in tracts similar to those showing reduced FA, however more widespread as well as bilateral than with FA.

9.3.3.2 Mean Diffusivity

F-test 1 showed no significant unique association with whole-brain mean diffusivity (MD). Below is a detailed presentation of significant **F-tests 2** and **3,** and follow-up post-hoc test results.

F-tests 2 and 3

The F-test of FSRS and AL index, controlling for MetS, demographic and socioeconomic confounders (**F-test 2**), and the F-test of FSRS and MetS controlling for AL index, demographic and socioeconomic confounders (**F-test 3**) revealed widespread significant unique associations between MD values and FSRS or AL index (**F-test 2**) or FSRS or MetS (**F-test 3**). Both F-tests revealed findings bilaterally in the anterior thalamic radiation, corona radiata (anterior, superior and posterior), corpus callosum (body, genu and splenium), internal capsule, external capsule and forceps major. Associations with MD values were revealed in the right tract of the superior longitudinal fasciculus in F-test 2, and bilaterally in F-test 3. Maximum F-statistic was located in the left anterior thalamic radiation for both tests. **F-test 2**: F (1,329) = 24.6, $p = 0.013$, **F-test 3**: F (1,329) = 28.8, $p < 0.05$ (Table 9.9, Figure 9.8).

MD: FSRS or AL index (+ MetS, age, sex, ethnicity, SES, education)							
Cluster	**Cluster size (voxels)**	**Max F**	**p-value**	**MNI coordinates (x, y, z)**			**Structure**
1	10760	24.6	0.013	-19	10	38	L anterior thalamic radiation

MD: FSRS or MetS (+ AL index, age, sex, ethnicity, SES, education)							
Cluster	**Cluster size (voxels)**	**Max F**	**p-value**	**MNI coordinates (x, y, z)**			**Structure**
1	11550	28.8	< 0.05	-19	10	38	L anterior thalamic radiation
2	152	7.28	< 0.05	-30	-26	4	L internal capsule
3	101	10.4	< 0.05	37	15	18	R superior longitudinal fasciculus

Table 9.9 F-test 2 (top) of unique Framingham Stroke Risk score (FSRS) or Allostatic Load (AL) index and F-test 3 (bottom) of unique Framingham Stroke Risk score (FSRS) and Metabolic Syndrome (MetS) association with Mean Diffusivity (MD) values.

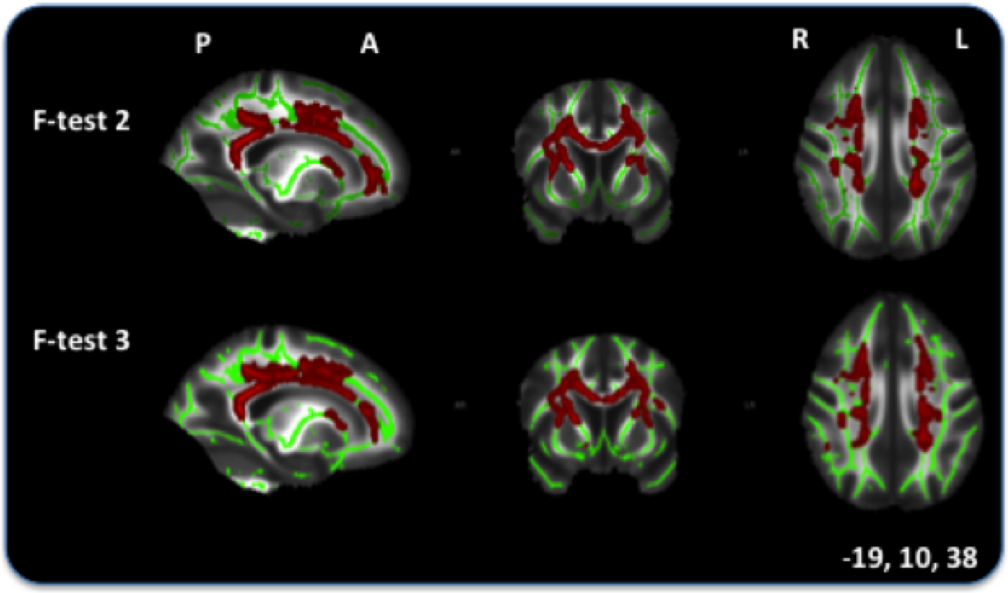


Figure 9.8 F-test 2 (top) of unique Framingham Stroke Risk score or Allostatic Load index and F-test 3 (bottom) of unique Framingham Stroke Risk score and Metabolic Syndrome association with widespread MD values. Results are primarily located in the anterior thalamic radiation, corona radiata, corpus callosum, and internal and external capsule. Significant (p < 0.05) regions are dilated for illustrative purposes, overlaid on a green skeleton.

Post-hoc tests

A significant widespread association between FSRS and higher MD values was present in regions detailed above, as well as the inferior fronto-occipital fasciculus and posterior thalamic radiation, after controlling for MetS, AL index, and demographic and socioeconomic factors (**t3** = **t5**) (Table 9.10, Figure 9.7). Maximum t-statistic was located in the left anterior thalamic radiation: t (329) = 7.01, $p < 0.05$.

Lower MD values were not found in association with FSRS, and no significant MD association was present with AL index or MetS (**t4** and **t6)**. In summary, secondary stress markers could be ranked in terms of unique contribution to white matter MD as follows: AL, MetS < FSRS.

MD increase: FSRS (+ MetS, AL index, age, sex, ethnicity, SES, education)							
Cluster	**Cluster size (voxels)**	**Max t**	**p-value**	**MNI coordinates (x, y, z)**			**Structure**
1	19561	7.01	< 0.05	-19	10	38	L anterior thalamic radiation

Table 9.10 Significant association of Framingham Stroke Risk score (FSRS) with higher MD values after controlling for Metabolic Syndrome (MetS), Allostatic Load (AL) index, and demographic and socioeconomic variables (t3 = t5).

9.4 Discussion

Chapter 9 assessed whether the three secondary stress markers, namely Framingham Stroke Risk score (FSRS), Metabolic Syndrome (MetS) and Allostatic Load (AL) index, measured the same construct. The null hypothesis could be rejected, i.e. that none of them had a unique association with structural brain integrity in older age after controlling for the effects of the other stress markers, and demographic or socioeconomic factors. However, the marker with the most unique contribution was different for grey and white matter (GM, WM respectively).

9.4.1 Whole-brain grey matter

A unique association of total Allostatic Load (AL) index measured across two study phases in mid-life was found with lower grey matter in the right hemisphere in regions along the insular cortex, opercular cortex, superior temporal gyrus, and temporal pole, after controlling for total FSRS, total MetS, and demographic or socioeconomic confounders.

In terms of grey matter, AL index has the greatest face validity for being a candidate 'stress marker', followed by MetS then FSRS. It accounts for risk that is not related to vascular risk (FSRS; e.g. (346)) or metabolic syndrome. This is the first study to provide empirical support for the theoretical concept of allostatic load, supporting the proposed link between a secondary stress marker and features of the ageing human brain (93).

Future research should aim to replicate these findings in a larger population sample (*downstream research method*). It will also have to focus on improving AL index

composition validated in relation to prior stressors, in order to reliably predict brain damage (*upstream research method*). It could take a hypothesis driven approach and compare various AL indices (e.g. (2)), or a data-driven exploratory approach to select primary stress markers that together predict the most grey matter variability.

9.4.2 Whole-brain white matter

A unique association of total Framingham Stroke Risk score (FSRS) measured across two study phases in mid-life was found with lower fractional anisotropy (FA) and higher mean diffusivity (MD) values in the corona radiata, corpus callosum, forceps major, superior longitudinal fasciculus, right anterior thalamic radiation, corticospinal tract and internal capsule, left inferior fronto-occipital fasciculus and posterior thalamic radiation, after controlling for total MetS, total AL index and demographic or socioeconomic confounders.

Vascular risk has been acknowledged widely to contribute to white matter changes appearing hyperintense on FLAIR images (226, 236, 347) and in relation to DTI measures (348-350). Therefore, in terms of white matter, FSRS has the greatest face validity for being a candidate 'stress marker', followed by MetS then AL index for FA and MetS or AL index for MD. The unique effects of MetS and AL index could not be distinguished for MD, which is likely due to the fact that MD is a more sensitive but less specific DTI measure than FA (see section 5.3.3 in detail).

Apart from the upstream method of testing the effects of AL indices that have been validated in relation to prior stress(ors), further research is needed to examine the mediating effect of FLAIR white matter hyperintensities between FSRS and FA, such as described in sections 4.3.2.3 and 5.3.2.

Chapter 10: Conclusions

This thesis examined whether there was a link between longitudinally available secondary markers of the chronic stress response and allostatic load, namely *Framingham Stroke Risk, Metabolic Syndrome and Allostatic Load index*, and cross-sectional structural brain integrity measures, namely grey and white matter, in ca. 500 community-dwelling older Whitehall II participants.

My main aims were to examine 1) whether these hypothesised markers in mid-life are able to predict patterns of abnormalities in grey and white matter in later life, 2) whether they are predictive of certain brain regions beyond the standard confounding variables such as demographic and socioeconomic factors, and 3) whether they measure and predict the same construct, or if they each have an independent role beyond the other two.

10.1 Summary of findings

10.1.1 Grey matter density

Aim 1)

As hypothesised, higher Framingham Stroke Risk, Metabolic Syndrome and Allostatic Load index measured in mid-life as early as 20 years prior to the scan, predicted lower grey matter density in older age.

Aim 2)

As hoped, unique linear relationship remained with each marker in similar areas after controlling for standard confounders, such as age, sex, ethnicity (i.e. demographic confounders) and years of education and employment grade (i.e.

socioeconomic confounders). However, the volumes significantly associated with markers were notably smaller, suggesting that some variance is shared between secondary markers and the usual correlates of general health, such as age and employment class. Higher Framingham Stroke Risk predicted lower grey matter values in the right medial temporal lobe. Metabolic Syndrome was associated with grey matter values predominantly in the right hemisphere, in neocortical areas of the temporal and parietal lobes, i.e. pre- and postcentral gyri, supramarginal gyrus, opercular cortex, and superior temporal cortex, and sub-neocortical structures, i.e. the thalamus and medial temporal lobes. Cumulative Allostatic Load index predicted lower grey matter values in the neo-cortex in the right precentral gyrus, and bilaterally in central opercular cortex and in sub-neocortical structures, i.e. the thalamus and temporal pole.

Aim 3)

Finally, higher levels of Allostatic Load index in mid-life had a unique association with lower grey matter density in the right hemisphere in regions along the insular cortex, opercular cortex, superior temporal gyrus, and temporal pole, beyond the effects of Framingham stroke risk, metabolic syndrome and demographic or socioeconomic confounders. Findings in this thesis show that allostatic load index might be the 'best' candidate 'stress marker' for grey matter integrity in older age, followed by metabolic syndrome, then Framingham stroke risk, accounting for additional risk that is not related to measured vascular risk (346) or metabolic syndrome. This is the first study to provide empirical support for the theoretical concept of allostatic load, supporting the proposed link between a secondary stress marker and features of the ageing human brain, such as grey matter atrophy (93).

10.1.2 White matter integrity

Aim 1)

Secondary stress markers measured in mid-life predicted white matter less reliably than they predicted grey matter integrity in later life. All three predicted lower white matter integrity at the time of scan. Most widespread associations were found with Framingham stroke risk, followed by Metabolic Syndrome then Allostatic Load index.

Aim 2)

After controlling for demographic and socioeconomic confounders, Framingham Stroke risk was no more associated with measures of WM integrity, apart from mean diffusivity in the right superior corona radiata. Higher metabolic syndrome predicted lower fractional anisotropy and higher mean diffusivity bilaterally in anterior thalamic radiation, external and internal capsule and right anterior corona radiata, and higher mean diffusivity in the inferior fronto-occipital fasciculus. Allostatic Load index did not predict any measures of white matter integrity after removing the effects of confounding variables.

Aim 3)

Furthermore, higher levels of Framingham Stroke risk in mid-life had a unique association with lower white matter integrity measures (fractional anisotropy and mean diffusivity) in the corona radiata, corpus callosum, forceps major, superior longitudinal fasciculus, right anterior thalamic radiation, corticospinal tract and internal capsule, left inferior fronto-occipital fasciculus and posterior thalamic radiation, beyond the effects of metabolic syndrome, allostatic load, and demographic or socioeconomic confounders. Being explicitly and empirically linked to vascular mechanisms, Framingham Stroke risk might be the best candidate 'stress

marker' for white matter integrity in older age, followed by metabolic syndrome, then allostatic load for fractional anisotropy, and metabolic syndrome or allostatic load for mean diffusivity. For mean diffusivity the unique effects of metabolic syndrome and allostatic load could not be distinguished, most likely because mean diffusivity is a more sensitive but less specific DTI measure than fractional anisotropy. This finding further shows that Framingham Stroke Risk score is not only a valid measure for predicting a stroke but might also have predictive value for white matter changes in older life. Vascular risk has been acknowledged widely to contribute to white matter changes appearing hyperintense on FLAIR images (226, 236, 347) and in relation to DTI measures (348-350), therefore this finding is little surprising.

10.1.3 Underlying mechanisms

Two neural or pathological mechanisms might underlie the findings seen in this thesis. They can be summarised as the 'glucocorticoid cascade hypothesis' and 'non-specific change in the brain's vasculature'.

Glucocorticoids trigger formation of synapses and long-term potentiation to facilitate memory. This is adaptive in the short-term (95), but can lead to neuronal damage caused by chronically elevated glucocorticoid levels (96). Chronically elevated glucocorticoid levels are associated with adverse brain changes, such as inhibition of adult neurogenesis in the hippocampus and atrophy of hippocampal neurons (35). Chronically elevated glucocorticoids can lead to a vicious circle through feedback loops, resulting in memory impairment, as well as inaccurate appraisal of and response to stressors. If the stressor is chronic, the initial surge of glucocorticoid

supplies to the hippocampus and cortex decreases, inhibiting energy storage by these neurons. Cutting back glucose supplies from neurons that are undergoing neurological insult is a stressor in its own right. Neurological insults such as hypoglycemia, hypoxia-ischemia, and seizures, can lead to neuronal death. "Glucocorticoid neurotoxicity" described above is also a feature of healthy aging in humans (97). In *rats,* additional stress in old age accelerates hippocampal degeneration and memory decline (35). In humans further research is needed.

Elevated diurnal and reactive glucocorticoid levels have been associated with white matter hyperintensities and decreased mean diffusivity, especially in anterior thalamic radiation, uncinate, arcuate and inferior longitudinal fasciculi (98). This is in line with previous in vitro post mortem studies, which suggest that "glucocorticoids potentially have negative effects on prefrontal cortex neurons' survival and function". This is due to the stimulating effects of low- and depressing effects of high glucocorticoid concentrations on axonal transport in prefrontal neurons (7).

Over time, brain-regulated sympathetic autonomic nervous system activity leads to the wear-and-tear of the cardiovascular system, which in turn affects regional brain vasodilation and vascular reactivity that are required for tasks and clearing of waste products. Mid-life vascular and stroke risk factors have been shown to predict increased rates of progression of vascular brain injury, global and hippocampal atrophy and decline of executive function over a 10-year period (98) as well as lower global cognition, memory and executive function (64). Vascular reactivity might be dysfunctional under demanding tasks among individuals with metabolic syndrome. Insulin resistance, obesity, and consequent inflammation negatively impact the

microvasculature and vascular reactivity, which may, in turn, lead to an inability to maintain energy-dependent processes and clear metabolic waste during increased demand. When coupled with other potentially damaging influences, such as HPA-axis dysregulation, dysfunctional vascular reactivity may damage the brain, particularly in vulnerable regions (73).

Metabolic syndrome is a risk factor for stroke (70, 330), presumably due to its effect on large arteries (333). It is associated with atherosclerosis, which in turn can contribute to small-vessel disease and lead to microstructural alterations (334). Lesions are presumed to arise through chronic hypoperfusion and leakage of plasma into the white matter (231, 335). White matter hyperintensities have been linked with cardiovascular risk factors, cerebrovascular disease (336) and metabolic syndrome (337), and in turn predict an increased risk of stroke, dementia and death (313).

10.1.4 Future research

Future research should consider replicating these findings in a larger population sample (195). While the general direction of *abnormalities* is known for the brain measures used (i.e. lower grey matter density and FA, higher mean and radial or axial diffusivities), the absence of repeat scans in this study makes it impossible to differentiate *changes* in brain measures from *between-subject variation* that may have pre-existed even before the accumulation of 'risk-factors'. Any interpretation of 'abnormalities' in findings of this thesis as the result of mid-life secondary stress markers is therefore to be taken with a pinch of salt.

Research is further needed to examine whether there is an effect of secondary stress markers on cognitive health and performance, and if it is, whether the effect of secondary stress markers on cognitive performance is mediated by brain structure (*upstream research method*). The best combination of allostatic load markers into a composite Allostatic Load index should be established, in order to predict structural brain changes in older age accurately and reliably. This would mean that relevant individual markers could be influenced therapeutically to keep their levels low throughout mid-life (351, 352), thus potentially contributing to resilience against stress-related disorders (353) and lower grey matter atrophy in later life (354). In terms of white matter integrity, further research is needed to examine the mediating effect of white matter hyperintensities in FLAIR images between stroke risk and fractional anisotropy changes.

Finally, the data-driven approach employed by FSL could be matched by an equally inclusive data reduction technique that takes into account all available measures on lifestyle, health and genetic information, in order to generate a 'principal component' empirically that is best placed to predict brain abnormalities or even brain changes over a limited time in older age. This would likely be possible with the very large imaging data set, collected in a number of projects, such as the UK Biobank (https://www.ukbiobank.ac.uk/) in the near future.

10.1.5 Key summary points

Key findings of this thesis can be summarised as follows:

1. Higher levels of secondary stress markers in mid-life, as early as 20 years prior to follow-up predicted lower grey and white matter integrity in older age, even after the effects of usual correlates of general health, such as age and employment class, have been removed.
2. One of the examined markers, Framingham Stroke risk, proved to be a useful predictor of brain structure in older age and grey matter integrity even after confounding variable effects have been removed. This means that the Framingham Stroke risk score predicts minor brain changes that may be precursors of a later stroke.
3. This thesis presents the first study, which provides empirical support for the theoretical concept of allostatic load, using voxel-wise grey and white matter integrity measures, supporting the proposed link between an 'everyday' secondary stress marker and features of the ageing human brain (93).
4. This thesis also presents the first examination of the relationship of three prominent secondary stress markers measured in mid-life with structural grey and white matter brain integrity in older age. Contrary to the null hypothesis prediction, the three markers do not have equal validity of being a candidate 'stress marker' of relevance to the brain.

References

1. Kabat-Zinn J. Full catastrophe living. London: Piatkus; 2004.
2. Juster RP, McEwen BS, Lupien SJ. Allostatic load biomarkers of chronic stress and impact on health and cognition. Neurosci Biobehav Rev. 2010;35(1):2-16.
3. McEwen BS, Wingfield JC. The concept of allostasis in biology and biomedicine. Horm Behav. 2003;43(1):2-15.
4. Sterling P, Eyer J. Allostasis: a new paradigm to explain arousal pathology. In: Fisher S., J. R, editors. Handbook of Life Stress, Cognition and Health New York, NY: Wiley; 1988. p. 629-49.
5. McEwen BS. Protective and damaging effects of stress mediators. N Engl J Med. 1998;338(3):171-9.
6. Zsoldos E, Ebmeier KP. Aging and Psychological Stress. In: Fink G, editor. Stress: Concepts, Cognition, Emotion, and Behavior. Handbook of Stress Series. Burlington, MA.: Academic Press; 2016. p. 311-23.
7. Lupien SJ, McEwen BS, Gunnar MR, Heim C. Effects of stress throughout the lifespan on the brain, behaviour and cognition. Nat Rev Neurosci. 2009;10(6):434-45.
8. Selye H. What is stress? Metabolism. 1956;5(5):525-30.
9. Selye H. History of the stress concept. In: Goldberger L, Breznitz S, editors. Handbook of Stress: Theoretical and Clinical Aspects. New York: NY: The Free Press; 1993.
10. Papagni SA, Benetti S, Arulanantham S, McCrory E, McGuire P, Mechelli A. Effects of stressful life events on human brain structure: a longitudinal voxel-based morphometry study. Stress. 2011;14(2):227-32.
11. Graham JE, Christian LM, Kiecolt-Glaser JK. Stress, age, and immune function: toward a lifespan approach. J Behav Med. 2006;29(4):389-400.
12. Widom CS, Horan J, Brzustowicz L. Childhood maltreatment predicts allostatic load in adulthood. Child Abuse Negl. 2015;47:59-69.
13. Barboza GE. The association between school exclusion, delinquency and subtypes of cyber- and F2F-victimizations: identifying and predicting risk profiles and subtypes using latent class analysis. Child Abuse Negl. 2015;39:109-22.
14. Friedman EM, Karlamangla AS, Gruenewald TL, Koretz B, Seeman TE. Early life adversity and adult biological risk profiles. Psychosom Med. 2015;77(2):176-85.
15. Segerstrom SC, Miller GE. Psychological stress and the human immune system: a meta-analytic study of 30 years of inquiry. Psychol Bull. 2004;130(4):601-30.
16. Bernard C. An introduction to the study of experimental medicine. New York, NY: Dover Publications; 2003.
17. Cannon WB. The wisdom of the body. New York, NY: WW Norton; 1932.
18. Brunner E, Shipley MJ, Blane D, Smith GD, Marmot MG. When does cardiovascular risk start? Past and present socioeconomic circumstances and risk factors in adulthood. J Epidemiol Community Health. 1999;53(12):757-64.

19. Chandola T, Britton A, Brunner E, Hemingway H, Malik M, Kumari M, et al. Work stress and coronary heart disease: what are the mechanisms? Eur Heart J. 2008;29(5):640-8.
20. Jones F, Bright J. Stress: Myth, theory and research. New York: NY: Pearson Education Limited; 2001.
21. Marmot MG, Smith GD, Stansfeld S, Patel C, North F, Head J, et al. Health inequalities among British civil servants: the Whitehall II study. Lancet. 1991;337(8754):1387-93.
22. Zuckerman M. Vulnerability to Psychopathology: A Biosocial Model. Washington, DC: APA; 1999.
23. Ingram RE, Luxton DD. Vulnerability-stress models. In: B.L. Hankin, Abela JRZ, editors. Development of Psychopathology: A vulnerability-stress perspective. Thousand Oaks, CA: Sage Publications; 2005.
24. Brown GW, Harris TO. Social origins of depression: a study of psychiatric disorder in women. London, UK: Tavistock Publications; 1978.
25. Hawton K, van Heeringen K. Suicide. Lancet. 2009;373(9672):1372-81.
26. Bartley M, Head J, Stansfeld S. Is attachment style a source of resilience against health inequalities at work? Soc Sci Med. 2007;64(4):765-75.
27. Goforth AN, Pham AV, and, Carlson JS. Diathesis-stress model. In: S. Goldstein, Nagheri JA, editors. Encyclopedia of Childhood Behavior and Development. New York, NY: Springer US; 2011. p. 502-23.
28. Butcher JN, Mineka S, Hooley JM. Abnormal Psychology, Core Concepts. New York, NY: Pearson Education Inc; 2010.
29. Cardenas VA, Samuelson K, Lenoci M, Studholme C, Neylan TC, Marmar CR, et al. Changes in brain anatomy during the course of posttraumatic stress disorder. Psychiatry Res. 2011;193(2):93-100.
30. Koolschijn PC, van Haren NE, Lensvelt-Mulders GJ, Hulshoff Pol HE, Kahn RS. Brain volume abnormalities in major depressive disorder: a meta-analysis of magnetic resonance imaging studies. Hum Brain Mapp. 2009;30(11):3719-35.
31. Frodl T, Reinhold E, Koutsouleris N, Reiser M, Meisenzahl EM. Interaction of childhood stress with hippocampus and prefrontal cortex volume reduction in major depression. J Psychiatr Res. 2010;44(13):799-807.
32. Cole J, Costafreda SG, McGuffin P, Fu CH. Hippocampal atrophy in first episode depression: a meta-analysis of magnetic resonance imaging studies. J Affect Disord. 2011;134(1-3):483-7.
33. MacQueen G, Frodl T. The hippocampus in major depression: evidence for the convergence of the bench and bedside in psychiatric research? Mol Psychiatry. 2011;16(3):252-64.
34. McEwen BS, Gianaros PJ. Central role of the brain in stress and adaptation: links to socioeconomic status, health, and disease. Ann N Y Acad Sci. 2010;1186:190-222.
35. Sapolsky RM. Why zebras don't get ulcers. New York, NY: Owl Books; 2004.
36. Klein LC, Corwin EJ. Seeing the unexpected: how sex differences in stress responses may provide a new perspective on the manifestation of psychiatric disorders. Curr Psychiatry Rep. 2002;4(6):441-8.
37. Chrousos GP. The hypothalamic-pituitary-adrenal axis and immune-mediated inflammation. N Engl J Med. 1995;332(20):1351-62.

38. Chrousos GP. Stress and disorders of the stress system. Nat Rev Endocrinol. 2009;5(7):374-81.
39. McEwen BS. The end of stress as we know it. Washington, DC: Joseph Henry Press; 2002.
40. Ganzel BL, Morris PA, Wethington E. Allostasis and the human brain: Integrating models of stress from the social and life sciences. Psychol Rev. 2010;117(1):134-74.
41. McEwen BS, Stellar E. Stress and the individual. Mechanisms leading to disease. Arch Intern Med. 1993;153(18):2093-101.
42. McEwen BS. Protective and damaging effects of stress mediators: central role of the brain. Dialogues Clin Neurosci. 2006;8(4):367-81.
43. Epel ES. Psychological and metabolic stress: a recipe for accelerated cellular aging? Hormones (Athens). 2009;8(1):7-22.
44. Organization WH. Mental health and older adults 2015 [Available from: http://www.who.int/mediacentre/factsheets/fs381/en/.
45. Allan CL, Zsoldos E, Ebmeier KP. Imaging and neurobiological changes in late-life depression. Br J Hosp Med (Lond). 2014;75(1):25-30.
46. Zsoldos E, Mahmood A, Ebmeier KP. Occupational stress, bullying and resilience in old age. Maturitas. 2014;78(2):86-90.
47. Akbaraly TN, Kivimaki M, Shipley MJ, Tabak AG, Jokela M, Virtanen M, et al. Metabolic syndrome over 10 years and cognitive functioning in late midlife: the Whitehall II study. Diabetes Care. 2010;33(1):84-9.
48. Kim B, Feldman EL. Insulin resistance as a key link for the increased risk of cognitive impairment in the metabolic syndrome. Exp Mol Med. 2015;47:e149.
49. Frisardi V, Solfrizzi V, Seripa D, Capurso C, Santamato A, Sancarlo D, et al. Metabolic-cognitive syndrome: a cross-talk between metabolic syndrome and Alzheimer's disease. Ageing Res Rev. 2010;9(4):399-417.
50. Gjonca E., Marmot M. Patterns of Illness and Mortality Across the Adult Lifespan. In: Johnson ML, editor. The Cambridge Handbook of Age and Ageing. Cambridge, UK: Cambridge University Press; 2005.
51. McEwen BS, Seeman T. Protective and damaging effects of mediators of stress. Elaborating and testing the concepts of allostasis and allostatic load. Ann N Y Acad Sci. 1999;896:30-47.
52. Marmot M, Brunner E. Cohort Profile: the Whitehall II study. Int J Epidemiol. 2005;34(2):251-6.
53. Seeman TE, McEwen BS, Rowe JW, Singer BH. Allostatic load as a marker of cumulative biological risk: MacArthur studies of successful aging. Proc Natl Acad Sci U S A. 2001;98(8):4770-5.
54. Valkanova V, Ebmeier KP. Vascular risk factors and depression in later life: a systematic review and meta-analysis. Biol Psychiatry. 2013;73(5):406-13.
55. McEwen BS, Gray J, Nasca C. Recognizing Resilience: Learning from the Effects of Stress on the Brain. Neurobiol Stress. 2015;1:1-11.
56. Steptoe A, Kivimaki M. Stress and cardiovascular disease. Nat Rev Cardiol. 2012;9(6):360-70.
57. Carroll D, Smith GD, Shipley MJ, Steptoe A, Brunner EJ, Marmot MG. Blood pressure reactions to acute psychological stress and future blood pressure

status: a 10-year follow-up of men in the Whitehall II study. Psychosom Med. 2001;63(5):737-43.
58. Hamer M, Steptoe A. Cortisol responses to mental stress and incident hypertension in healthy men and women. J Clin Endocrinol Metab. 2012;97(1):E29-34.
59. Gianaros PJ, Jennings JR, Sheu LK, Derbyshire SW, Matthews KA. Heightened functional neural activation to psychological stress covaries with exaggerated blood pressure reactivity. Hypertension. 2007;49(1):134-40.
60. Allan CL, Zsoldos E, Filippini N, Sexton CE, Topiwala A, Valkanova V, et al. Lifetime hypertension as a predictor of brain structure in older adults: cohort study with a 28-year follow-up. Br J Psychiatry. 2015;206(4):308-15.
61. D'Agostino RB, Wolf PA, Belanger AJ, Kannel WB. Stroke risk profile: adjustment for antihypertensive medication. The Framingham Study. Stroke. 1994;25(1):40-3.
62. Dregan A, Stewart R, Gulliford MC. Cardiovascular risk factors and cognitive decline in adults aged 50 and over: a population-based cohort study. Age Ageing. 2013;42(3):338-45.
63. Kaffashian S, Dugravot A, Elbaz A, Shipley MJ, Sabia S, Kivimaki M, et al. Predicting cognitive decline: a dementia risk score vs. the Framingham vascular risk scores. Neurology. 2013;80(14):1300-6.
64. Debette S, Seshadri S, Beiser A, Au R, Himali JJ, Palumbo C, et al. Midlife vascular risk factor exposure accelerates structural brain aging and cognitive decline. Neurology. 2011;77(5):461-8.
65. Allan CL, Sexton CE, Kalu UG, McDermott LM, Kivimaki M, Singh-Manoux A, et al. Does the Framingham Stroke Risk Profile predict white-matter changes in late-life depression? Int Psychogeriatr. 2012;24(4):524-31.
66. Grundy SM, Brewer HB, Jr., Cleeman JI, Smith SC, Jr., Lenfant C, National Heart L, et al. Definition of metabolic syndrome: report of the National Heart, Lung, and Blood Institute/American Heart Association conference on scientific issues related to definition. Arterioscler Thromb Vasc Biol. 2004;24(2):e13-8.
67. Brunner EJ, Marmot MG, Nanchahal K, Shipley MJ, Stansfeld SA, Juneja M, et al. Social inequality in coronary risk: central obesity and the metabolic syndrome. Evidence from the Whitehall II study. Diabetologia. 1997;40(11):1341-9.
68. Galassi A, Reynolds K, He J. Metabolic syndrome and risk of cardiovascular disease: a meta-analysis. Am J Med. 2006;119(10):812-9.
69. Ohaeri JU, Akanji AO. Metabolic syndrome in severe mental disorders. Metab Syndr Relat Disord. 2011;9(2):91-8.
70. Wang J, Ruotsalainen S, Moilanen L, Lepisto P, Laakso M, Kuusisto J. The metabolic syndrome predicts incident stroke: a 14-year follow-up study in elderly people in Finland. Stroke. 2008;39(4):1078-83.
71. Isomaa B, Almgren P, Tuomi T, Forsen B, Lahti K, Nissen M, et al. Cardiovascular morbidity and mortality associated with the metabolic syndrome. Diabetes Care. 2001;24(4):683-9.
72. Mortby ME, Janke AL, Anstey KJ, Sachdev PS, Cherbuin N. High "normal" blood glucose is associated with decreased brain volume and cognitive

performance in the 60s: the PATH through life study. PLoS One. 2013;8(9):e73697.
73. Yates KF, Sweat V, Yau PL, Turchiano MM, Convit A. Impact of metabolic syndrome on cognition and brain: a selected review of the literature. Arterioscler Thromb Vasc Biol. 2012;32(9):2060-7.
74. Song SW, Chung JH, Rho JS, Lee YA, Lim HK, Kang SG, et al. Regional cortical thickness and subcortical volume changes in patients with metabolic syndrome. Brain Imaging Behav. 2015;9(3):588-96.
75. Segura B, Jurado MA, Freixenet N, Falcon C, Junque C, Arboix A. Microstructural white matter changes in metabolic syndrome: a diffusion tensor imaging study. Neurology. 2009;73(6):438-44.
76. Wiley JF, Gruenewald TL, Karlamangla AS, Seeman TE. Modeling Multisystem Physiological Dysregulation. Psychosom Med. 2016;78(3):290-301.
77. Mauss D, Li J, Schmidt B, Angerer P, Jarczok MN. [Work-related Stress and the Allostatic Load Index - A Systematic Review]. Gesundheitswesen. 2015.
78. Dich N, Lange T, Head J, Rod NH. Work stress, caregiving, and allostatic load: prospective results from the Whitehall II cohort study. Psychosom Med. 2015;77(5):539-47.
79. Robertson T, Popham F, Benzeval M. Socioeconomic position across the lifecourse & allostatic load: data from the West of Scotland Twenty-07 cohort study. BMC Public Health. 2014;14:184.
80. Robertson T, Benzeval M, Whitley E, Popham F. The role of material, psychosocial and behavioral factors in mediating the association between socioeconomic position and allostatic load (measured by cardiovascular, metabolic and inflammatory markers). Brain Behav Immun. 2015;45:41-9.
81. Slopen N, Non A, Williams DR, Roberts AL, Albert MA. Childhood adversity, adult neighborhood context, and cumulative biological risk for chronic diseases in adulthood. Psychosom Med. 2014;76(7):481-9.
82. Petrovic D, Pivin E, Ponte B, Dhayat N, Pruijm M, Ehret G, et al. Sociodemographic, behavioral and genetic determinants of allostatic load in a Swiss population-based study. Psychoneuroendocrinology. 2016;67:76-85.
83. Booth T, Royle NA, Corley J, Gow AJ, Valdes Hernandez Mdel C, Munoz Maniega S, et al. Association of allostatic load with brain structure and cognitive ability in later life. Neurobiol Aging. 2015;36(3):1390-9.
84. Day TA. Defining stress as a prelude to mapping its neurocircuitry: no help from allostasis. Prog Neuropsychopharmacol Biol Psychiatry. 2005;29(8):1195-200.
85. Gruenewald TL, Kemeny ME, Aziz N. Subjective social status moderates cortisol responses to social threat. Brain Behav Immun. 2006;20(4):410-9.
86. Seeman TE, Singer B, Wilkinson CW, McEwen B. Gender differences in age-related changes in HPA axis reactivity. Psychoneuroendocrinology. 2001;26(3):225-40.
87. Gallo LC, Fortmann AL, Mattei J. Allostatic load and the assessment of cumulative biological risk in biobehavioral medicine: challenges and opportunities. Psychosom Med. 2014;76(7):478-80.

88. McEwen BS. Central effects of stress hormones in health and disease: Understanding the protective and damaging effects of stress and stress mediators. Eur J Pharmacol. 2008;583(2-3):174-85.
89. Dowd JB, Goldman N. Do biomarkers of stress mediate the relation between socioeconomic status and health? J Epidemiol Community Health. 2006;60(7):633-9.
90. Adler NE, Boyce T, Chesney MA, Cohen S, Folkman S, Kahn RL, et al. Socioeconomic status and health. The challenge of the gradient. Am Psychol. 1994;49(1):15-24.
91. Dallman MF. Stress by any other name .....? Horm Behav. 2003;43(1):18-20; discussion 8-30.
92. Ellis BJ, Del Giudice M. Beyond allostatic load: rethinking the role of stress in regulating human development. Dev Psychopathol. 2014;26(1):1-20.
93. McEwen BS. Physiology and neurobiology of stress and adaptation: Central role of the brain. Physiol Rev. 2007;87(3):873-904.
94. Sapolsky RM, Krey LC, McEwen BS. The neuroendocrinology of stress and aging: the glucocorticoid cascade hypothesis. Endocr Rev. 1986;7(3):284-301.
95. Sapolsky RM, Romero LM, Munck AU. How do glucocorticoids influence stress responses? Integrating permissive, suppressive, stimulatory, and preparative actions. Endocr Rev. 2000;21(1):55-89.
96. Lynch MA. Long-term potentiation and memory. Physiol Rev. 2004;84(1):87-136.
97. Sapolsky RM, Krey LC, McEwen BS. Prolonged glucocorticoid exposure reduces hippocampal neuron number: implications for aging. J Neurosci. 1985;5(5):1222-7.
98. Cox SR, Bastin ME, Ferguson KJ, Maniega SM, MacPherson SE, Deary IJ, et al. Brain white matter integrity and cortisol in older men: the Lothian Birth Cohort 1936. Neurobiol Aging. 2015;36(1):257-64.
99. Cavalieri M, Ropele S, Petrovic K, Pluta-Fuerst A, Homayoon N, Enzinger C, et al. Metabolic syndrome, brain magnetic resonance imaging, and cognition. Diabetes Care. 2010;33(12):2489-95.
100. Shimoji K, Abe O, Uka T, Yasmin H, Kamagata K, Asahi K, et al. White matter alteration in metabolic syndrome: diffusion tensor analysis. Diabetes Care. 2013;36(3):696-700.
101. Haley AP, Gonzales MM, Tarumi T, Miles SC, Goudarzi K, Tanaka H. Elevated cerebral glutamate and myo-inositol levels in cognitively normal middle-aged adults with metabolic syndrome. Metab Brain Dis. 2010;25(4):397-405.
102. Ansell EB, Rando K, Tuit K, Guarnaccia J, Sinha R. Cumulative adversity and smaller gray matter volume in medial prefrontal, anterior cingulate, and insula regions. Biol Psychiatry. 2012;72(1):57-64.
103. Sexton CE, Le Masurier M, Allan CL, Jenkinson M, McDermott L, Kalu UG, et al. Magnetic resonance imaging in late-life depression: vascular and glucocorticoid cascade hypotheses. Br J Psychiatry. 2012;201(1):46-51.
104. Deppermann S, Storchak H, Fallgatter AJ, Ehlis AC. Stress-induced neuroplasticity: (mal)adaptation to adverse life events in patients with PTSD--a critical overview. Neuroscience. 2014;283:166-77.

105. Gurvits TV, Shenton ME, Hokama H, Ohta H, Lasko NB, Gilbertson MW, et al. Magnetic resonance imaging study of hippocampal volume in chronic, combat-related posttraumatic stress disorder. Biol Psychiatry. 1996;40(11):1091-9.
106. Cohen RA, Grieve S, Hoth KF, Paul RH, Sweet L, Tate D, et al. Early life stress and morphometry of the adult anterior cingulate cortex and caudate nuclei. Biol Psychiatry. 2006;59(10):975-82.
107. Gianaros PJ, Jennings JR, Sheu LK, Greer PJ, Kuller LH, Matthews KA. Prospective reports of chronic life stress predict decreased grey matter volume in the hippocampus. Neuroimage. 2007;35(2):795-803.
108. Nederhof E, Schmidt MV. Mismatch or cumulative stress: toward an integrated hypothesis of programming effects. Physiol Behav. 2012;106(5):691-700.
109. Santarelli S, Lesuis SL, Wang XD, Wagner KV, Hartmann J, Labermaier C, et al. Evidence supporting the match/mismatch hypothesis of psychiatric disorders. Eur Neuropsychopharmacol. 2014;24(6):907-18.
110. Kuhn M, Scharfenort R, Schumann D, Schiele MA, Munsterkotter AL, Deckert J, et al. Mismatch or allostatic load? Timing of life adversity differentially shapes gray matter volume and anxious temperament. Soc Cogn Affect Neurosci. 2016;11(4):537-47.
111. Pell GS, Briellmann RS, Chan CH, Pardoe H, Abbott DF, Jackson GD. Selection of the control group for VBM analysis: influence of covariates, matching and sample size. Neuroimage. 2008;41(4):1324-35.
112. Del Giudice M, Ellis BJ, Shirtcliff EA. The Adaptive Calibration Model of stress responsivity. Neurosci Biobehav Rev. 2011;35(7):1562-92.
113. Sih A. Effects of early stress on behavioral syndromes: an integrated adaptive perspective. Neurosci Biobehav Rev. 2011;35(7):1452-65.
114. Kirkwood TB. A systematic look at an old problem. Nature. 2008;451(7179):644-7.
115. United Nations Population Division. Population Ageing and Sustainable Development. New York, NY.: United Nations; 2014.
116. Foresight Mental Capital and Wellbeing Project. London: The Government Office for Science; 2008.
117. Topiwala A, Patel S, Ebmeier KP. Health benefits of encore careers for baby boomers. Maturitas. 2014;78(1):8-10.
118. Matthews FE, Stephan BC, Robinson L, Jagger C, Barnes LE, Arthur A, et al. A two decade dementia incidence comparison from the Cognitive Function and Ageing Studies I and II. Nat Commun. 2016;7:11398.
119. Cabeza R. Hemispheric asymmetry reduction in older adults: the HAROLD model. Psychol Aging. 2002;17(1):85-100.
120. Davis SW, Dennis NA, Daselaar SM, Fleck MS, Cabeza R. Que PASA? The posterior-anterior shift in aging. Cereb Cortex. 2008;18(5):1201-9.
121. Dennis NA, Hayes SM, Prince SE, Madden DJ, Huettel SA, Cabeza R. Effects of aging on the neural correlates of successful item and source memory encoding. J Exp Psychol Learn Mem Cogn. 2008;34(4):791-808.

122. Filippini N, Nickerson LD, Beckmann CF, Ebmeier KP, Frisoni GB, Matthews PM, et al. Age-related adaptations of brain function during a memory task are also present at rest. Neuroimage. 2012;59(4):3821-8.
123. Brunner E. Stress and the biology of inequality. BMJ. 1997;314(7092):1472-6.
124. Wilkinson R, Marmot M. Social determinants of health. The solid facts. Denmark: WHO Library Cataloguing in Publication Data; 2003.
125. Breeze E, Fletcher AE, Leon DA, Marmot MG, Clarke RJ, Shipley MJ. Do socioeconomic disadvantages persist into old age? Self-reported morbidity in a 29-year follow-up of the Whitehall Study. Am J Public Health. 2001;91(2):277-83.
126. Singh-Manoux A, Kivimaki M, Glymour MM, Elbaz A, Berr C, Ebmeier KP, et al. Timing of onset of cognitive decline: results from Whitehall II prospective cohort study. BMJ. 2012;344:d7622.
127. Filippini N, Zsoldos E, Haapakoski R, Sexton CE, Mahmood A, Allan CL, et al. Study protocol: The Whitehall II imaging sub-study. BMC Psychiatry. 2014;14:159.
128. First MB, Gibbon, M., Spitzer, R.L., Williams, J.B.W. User's Guide for the Structured Clinical Interview for DSM-IV-TR Axis I Disorders - Research Version - (SCID-I for DSM-IV-TR). New York: Biometric Research Department, New York State Psychiatric Institute; 2002.
129. Wolf PA, D'Agostino RB, Belanger AJ, Kannel WB. Probability of stroke: a risk profile from the Framingham Study. Stroke. 1991;22(3):312-8.
130. Kivimaki M, Shipley MJ, Allan CL, Sexton CE, Jokela M, Virtanen M, et al. Vascular risk status as a predictor of later-life depressive symptoms: a cohort study. Biol Psychiatry. 2012;72(4):324-30.
131. Kaffashian S, Dugravot A, Brunner EJ, Sabia S, Ankri J, Kivimaki M, et al. Midlife stroke risk and cognitive decline: a 10-year follow-up of the Whitehall II cohort study. Alzheimers Dement. 2013;9(5):572-9.
132. Prineas R.J. CRS, Blackburn H. The Minnesota Code Manual for Electrocardiographic Findings: Standards and Procedures for Measurement and Classification. Bristol, UK.: John Wright; 1982.
133. Cooper GR. Methods for determining the amount of glucose in blood. CRC Crit Rev Clin Lab Sci. 1973;4(2):101-45.
134. Alpert L. Instrument series: model 23A Glucose Analyzer. Lab World. 1976;27:8-13.
135. Astles JR, Sedor FA, Toffaletti JG. Evaluation of the YSI 2300 glucose analyzer: algorithm-corrected results are accurate and specific. Clin Biochem. 1996;29(1):27-31.
136. Mellitus ECotDaCoD. Report of the expert committee on the diagnosis and classification of diabetes mellitus. Diabetes Care. 2003;26 Suppl 1:S5-20.
137. National Cholesterol Education Program Expert Panel on Detection E, Treatment of High Blood Cholesterol in A. Third Report of the National Cholesterol Education Program (NCEP) Expert Panel on Detection, Evaluation, and Treatment of High Blood Cholesterol in Adults (Adult Treatment Panel III) final report. Circulation. 2002;106(25):3143-421.

138. Ford ES, Giles WH, Dietz WH. Prevalence of the metabolic syndrome among US adults: findings from the third National Health and Nutrition Examination Survey. JAMA. 2002;287(3):356-9.
139. Ravaglia G, Forti P, Maioli F, Bastagli L, Chiappelli M, Montesi F, et al. Metabolic Syndrome: prevalence and prediction of mortality in elderly individuals. Diabetes Care. 2006;29(11):2471-6.
140. Hildrum B, Mykletun A, Hole T, Midthjell K, Dahl AA. Age-specific prevalence of the metabolic syndrome defined by the International Diabetes Federation and the National Cholesterol Education Program: the Norwegian HUNT 2 study. BMC Public Health. 2007;7:220.
141. Zimmet P, Boyko EJ, Collier GR, de Courten M. Etiology of the metabolic syndrome: potential role of insulin resistance, leptin resistance, and other players. Ann N Y Acad Sci. 1999;892:25-44.
142. Meigs JB. Invited commentary: insulin resistance syndrome? Syndrome X? Multiple metabolic syndrome? A syndrome at all? Factor analysis reveals patterns in the fabric of correlated metabolic risk factors. Am J Epidemiol. 2000;152(10):908-11; discussion 12.
143. Wilson PW, D'Agostino RB, Levy D, Belanger AM, Silbershatz H, Kannel WB. Prediction of coronary heart disease using risk factor categories. Circulation. 1998;97(18):1837-47.
144. Akbaraly TN, Kivimaki M, Brunner EJ, Chandola T, Marmot MG, Singh-Manoux A, et al. Association between metabolic syndrome and depressive symptoms in middle-aged adults: results from the Whitehall II study. Diabetes Care. 2009;32(3):499-504.
145. Yaffe K. Metabolic syndrome and cognitive disorders: is the sum greater than its parts? Alzheimer Dis Assoc Disord. 2007;21(2):167-71.
146. Kahn R, Buse J, Ferrannini E, Stern M, American Diabetes A, European Association for the Study of D. The metabolic syndrome: time for a critical appraisal: joint statement from the American Diabetes Association and the European Association for the Study of Diabetes. Diabetes Care. 2005;28(9):2289-304.
147. Grundy SM. Hypertriglyceridemia, insulin resistance, and the metabolic syndrome. Am J Cardiol. 1999;83(9B):25F-9F.
148. Grundy SM, Cleeman JI, Rifkind BM, Kuller LH. Cholesterol lowering in the elderly population. Coordinating Committee of the National Cholesterol Education Program. Arch Intern Med. 1999;159(15):1670-8.
149. Expert Panel on Detection E, Treatment of High Blood Cholesterol in A. Executive Summary of The Third Report of The National Cholesterol Education Program (NCEP) Expert Panel on Detection, Evaluation, And Treatment of High Blood Cholesterol In Adults (Adult Treatment Panel III). JAMA. 2001;285(19):2486-97.
150. Alberti KG, Zimmet PZ. Definition, diagnosis and classification of diabetes mellitus and its complications. Part 1: diagnosis and classification of diabetes mellitus provisional report of a WHO consultation. Diabet Med. 1998;15(7):539-53.
151. Tabak AG, Jokela M, Akbaraly TN, Brunner EJ, Kivimaki M, Witte DR. Trajectories of glycaemia, insulin sensitivity, and insulin secretion before

diagnosis of type 2 diabetes: an analysis from the Whitehall II study. Lancet. 2009;373(9682):2215-21.
152. Hamer M, Sabia S, Batty GD, Shipley MJ, Tabak AG, Singh-Manoux A, et al. Physical activity and inflammatory markers over 10 years: follow-up in men and women from the Whitehall II cohort study. Circulation. 2012;126(8):928-33.
153. Dich N, Doan SN, Kivimaki M, Kumari M, Rod NH. A non-linear association between self-reported negative emotional response to stress and subsequent allostatic load: prospective results from the Whitehall II cohort study. Psychoneuroendocrinology. 2014;49:54-61.
154. Beckie TM. A systematic review of allostatic load, health, and health disparities. Biol Res Nurs. 2012;14(4):311-46.
155. Juster RP, Sindi S, Marin MF, Perna A, Hashemi A, Pruessner JC, et al. A clinical allostatic load index is associated with burnout symptoms and hypocortisolemic profiles in healthy workers. Psychoneuroendocrinology. 2011;36(6):797-805.
156. Friedewald WT, Levy RI, Fredrickson DS. Estimation of the concentration of low-density lipoprotein cholesterol in plasma, without use of the preparative ultracentrifuge. Clin Chem. 1972;18(6):499-502.
157. Hanning I, Home PD, Alberti KG. Measurement of free insulin concentrations: the influence of the timing of extraction of insulin antibodies. Diabetologia. 1985;28(11):831-5.
158. Andersen L, Dinesen B, Jorgensen PN, Poulsen F, Roder ME. Enzyme immunoassay for intact human insulin in serum or plasma. Clin Chem. 1993;39(4):578-82.
159. Brunner EJ, Hemingway H, Walker BR, Page M, Clarke P, Juneja M, et al. Adrenocortical, autonomic, and inflammatory causes of the metabolic syndrome: nested case-control study. Circulation. 2002;106(21):2659-65.
160. WHO. Global Database on Body Mass Index 2016 [Available from: http://apps.who.int/bmi/index.jsp?introPage=intro_3.html.
161. Kirkwood BR, Sterne JAC. Essential Medical Statistics. 2nd ed. Oxford, UK.: Blackwell Science Ltd; 2003.
162. Barnes J, Ridgway GR, Bartlett J, Henley SM, Lehmann M, Hobbs N, et al. Head size, age and gender adjustment in MRI studies: a necessary nuisance? Neuroimage. 2010;53(4):1244-55.
163. Dunlop DD, Hughes SL, Manheim LM. Disability in activities of daily living: patterns of change and a hierarchy of disability. Am J Public Health. 1997;87(3):378-83.
164. Steptoe A, Fieldman G, Evans O, Perry L. Cardiovascular risk and responsivity to mental stress: the influence of age, gender and risk factors. J Cardiovasc Risk. 1996;3(1):83-93.
165. Nguyen NT, Magno CP, Lane KT, Hinojosa MW, Lane JS. Association of hypertension, diabetes, dyslipidemia, and metabolic syndrome with obesity: findings from the National Health and Nutrition Examination Survey, 1999 to 2004. J Am Coll Surg. 2008;207(6):928-34.

166. Aggarwal NT, Everson-Rose SA, Evans DA. Social Determinants, Race, and Brain Health Outcomes: Findings from the Chicago Health and Aging Project. Curr Alzheimer Res. 2015;12(7):622-31.
167. Wilson RS, Rajan KB, Barnes LL, Weuve J, Evans DA. Factors related to racial differences in late-life level of cognitive function. Neuropsychology. 2016;30(5):517-24.
168. Gurland BJ, Wilder DE, Lantigua R, Stern Y, Chen J, Killeffer EH, et al. Rates of dementia in three ethnoracial groups. Int J Geriatr Psychiatry. 1999;14(6):481-93.
169. Szanton SL, Gill JM, Allen JK. Allostatic load: a mechanism of socioeconomic health disparities? Biol Res Nurs. 2005;7(1):7-15.
170. Nuru-Jeter AM, Sarsour K, Jutte DP, Boyce WT. Socioeconomic predictors of health and development in middle childhood: variations by socioeconomic status measure and race. Issues Compr Pediatr Nurs. 2010;33(2):59-81.
171. Hall K, Murrell J, Ogunniyi A, Deeg M, Baiyewu O, Gao S, et al. Cholesterol, APOE genotype, and Alzheimer disease: an epidemiologic study of Nigerian Yoruba. Neurology. 2006;66(2):223-7.
172. Manly JJ. Deconstructing race and ethnicity: implications for measurement of health outcomes. Med Care. 2006;44(11 Suppl 3):S10-6.
173. Fitzpatrick AL, Kuller LH, Ives DG, Lopez OL, Jagust W, Breitner JC, et al. Incidence and prevalence of dementia in the Cardiovascular Health Study. J Am Geriatr Soc. 2004;52(2):195-204.
174. Alzheimer's A. 2010 Alzheimer's disease facts and figures. Alzheimers Dement. 2010;6(2):158-94.
175. Tang MX, Stern Y, Marder K, Bell K, Gurland B, Lantigua R, et al. The APOE-epsilon4 allele and the risk of Alzheimer disease among African Americans, whites, and Hispanics. JAMA. 1998;279(10):751-5.
176. Morris AA, Patel RS, Binongo JN, Poole J, Al Mheid I, Ahmed Y, et al. Racial differences in arterial stiffness and microcirculatory function between Black and White Americans. J Am Heart Assoc. 2013;2(2):e002154.
177. Chin AL, Negash S, Hamilton R. Diversity and disparity in dementia: the impact of ethnoracial differences in Alzheimer disease. Alzheimer Dis Assoc Disord. 2011;25(3):187-95.
178. Corrada M, Brookmeyer R, Kawas C. Sources of variability in prevalence rates of Alzheimer's disease. Int J Epidemiol. 1995;24(5):1000-5.
179. Fillenbaum GG, Heyman A, Huber MS, Woodbury MA, Leiss J, Schmader KE, et al. The prevalence and 3-year incidence of dementia in older Black and White community residents. J Clin Epidemiol. 1998;51(7):587-95.
180. Potter GG, Plassman BL, Burke JR, Kabeto MU, Langa KM, Llewellyn DJ, et al. Cognitive performance and informant reports in the diagnosis of cognitive impairment and dementia in African Americans and whites. Alzheimers Dement. 2009;5(6):445-53.
181. Demirovic J, Prineas R, Loewenstein D, Bean J, Duara R, Sevush S, et al. Prevalence of dementia in three ethnic groups: the South Florida program on aging and health. Ann Epidemiol. 2003;13(6):472-8.

182. Froehlich TE, Bogardus ST, Jr., Inouye SK. Dementia and race: are there differences between African Americans and Caucasians? J Am Geriatr Soc. 2001;49(4):477-84.
183. Breteler MM, van Swieten JC, Bots ML, Grobbee DE, Claus JJ, van den Hout JH, et al. Cerebral white matter lesions, vascular risk factors, and cognitive function in a population-based study: the Rotterdam Study. Neurology. 1994;44(7):1246-52.
184. Newman AB, Fitzpatrick AL, Lopez O, Jackson S, Lyketsos C, Jagust W, et al. Dementia and Alzheimer's disease incidence in relationship to cardiovascular disease in the Cardiovascular Health Study cohort. J Am Geriatr Soc. 2005;53(7):1101-7.
185. Luchsinger JA, Reitz C, Honig LS, Tang MX, Shea S, Mayeux R. Aggregation of vascular risk factors and risk of incident Alzheimer disease. Neurology. 2005;65(4):545-51.
186. Nelson KM, Reiber G, Kohler T, Boyko EJ. Peripheral arterial disease in a multiethnic national sample: the role of conventional risk factors and allostatic load. Ethn Dis. 2007;17(4):669-75.
187. Murrell JR, Price B, Lane KA, Baiyewu O, Gureje O, Ogunniyi A, et al. Association of apolipoprotein E genotype and Alzheimer disease in African Americans. Arch Neurol. 2006;63(3):431-4.
188. Evans DA, Bennett DA, Wilson RS, Bienias JL, Morris MC, Scherr PA, et al. Incidence of Alzheimer disease in a biracial urban community: relation to apolipoprotein E allele status. Arch Neurol. 2003;60(2):185-9.
189. Marmot M. Status syndrome. London: Bloomsbury; 2004.
190. Wray LA, Herzog AR, Willis RJ, Wallace RB. The impact of education and heart attack on smoking cessation among middle-aged adults. J Health Soc Behav. 1998;39(4):271-94.
191. Steptoe A, Marmot M. The role of psychobiological pathways in socio-economic inequalities in cardiovascular disease risk. Eur Heart J. 2002;23(1):13-25.
192. Steptoe A, Feldman PJ, Kunz S, Owen N, Willemsen G, Marmot M. Stress responsivity and socioeconomic status: a mechanism for increased cardiovascular disease risk? Eur Heart J. 2002;23(22):1757-63.
193. Arber S, Ginn J. Gender and inequalities in health in later life. Soc Sci Med. 1993;36(1):33-46.
194. Grundy E, Holt G. The socioeconomic status of older adults: how should we measure it in studies of health inequalities? J Epidemiol Community Health. 2001;55(12):895-904.
195. Stringhini S, Zaninotto P, Kumari M, Kivimaki M, Batty GD. Lifecourse socioeconomic status and type 2 diabetes: the role of chronic inflammation in the English Longitudinal Study of Ageing. Sci Rep. 2016;6:24780.
196. Marmot MG, Shipley MJ. Do socioeconomic differences in mortality persist after retirement? 25 year follow up of civil servants from the first Whitehall study. BMJ. 1996;313(7066):1177-80.
197. Hayes AF. Beyond Baron and Kenny: Statistical Mediation Analysis in the New Millenium. Communication Monographs. 2009;76(4):408-20.

198. Frazier PA, Tix AP, Barron KE. Testing Moderator and Mediator Effects in Counseling Psychology Research. Journal of Counseling Psychology. 2004;51(1):115-34.
199. Baron RM, Kenny DA. The moderator-mediator variable distinction in social psychological research: conceptual, strategic, and statistical considerations. J Pers Soc Psychol. 1986;51(6):1173-82.
200. Judd CM, Kenny DA. Process analysis: Estimating mediation in treatment evaluations. Evaluation Review. 1981;5(5):602-19.
201. James LR, Brett JM. Mediators, moderators, and tests for mediation. Journal of Applied Psychology. 1984;69(2):307-21.
202. Yamada K, Patel U, Shrier DA, Tanaka H, Chang JK, Numaguchi Y. MR imaging of CNS tractopathy: wallerian and transneuronal degeneration. AJR Am J Roentgenol. 1998;171(3):813-8.
203. De Vos KJ, Grierson AJ, Ackerley S, Miller CC. Role of axonal transport in neurodegenerative diseases. Annu Rev Neurosci. 2008;31:151-73.
204. Rabin BM, Hebel DJ, Salamon-Murayama N, Russell EJ. Distal neuronal degeneration caused by intracranial lesions. AJR Am J Roentgenol. 1998;171(1):95-102.
205. Coleman M. Axon degeneration mechanisms: commonality amid diversity. Nat Rev Neurosci. 2005;6(11):889-98.
206. Dewey M, Schink T, Dewey CF. Claustrophobia during magnetic resonance imaging: cohort study in over 55,000 patients. J Magn Reson Imaging. 2007;26(5):1322-7.
207. Bloch F, Hansen WW, Packard M. Nuclear Induction. Phys Rev. 1946;69(3-4):127-.
208. Purcell EM, Pound RV, Bloembergen N. Nuclear Magnetic Resonance Absorption in Hydrogen Gas. Phys Rev. 1946;70(11-1):986-7.
209. Bloch F. Nuclear Induction. Phys Rev. 1946;70(7-8):460-74.
210. Bloembergen N, Purcell EM, Pound RV. Relaxation Effects in Nuclear Magnetic Resonance Absorption. Phys Rev. 1948;73(7):679-712.
211. Hoult DI, Richards RE. Signal-to-Noise Ratio of Nuclear Magnetic-Resonance Experiment. J Magn Reson. 1976;24(1):71-85.
212. Deichmann R. Principles of MRI and Functional MRI. In: Filippi M, editor. fMRI Techniques and Protocols. Neuromethods. 41. 1 ed. New York, NY: Springer; 2009. p. 3-29.
213. Bitar R, Leung G, Perng R, Tadros S, Moody AR, Sarrazin J, et al. MR pulse sequences: what every radiologist wants to know but is afraid to ask. Radiographics. 2006;26(2):513-37.
214. Kumar A, Welti D, Ernst RR. Nmr Fourier Zeugmatography. J Magn Reson. 1975;18(1):69-83.
215. Twieg DB. The K-Trajectory Formulation of the Nmr Imaging Process with Applications in Analysis and Synthesis of Imaging Methods. Med Phys. 1983;10(5):610-21.
216. Tisdall MD, Hess AT, Reuter M, Meintjes EM, Fischl B, van der Kouwe AJ. Volumetric navigators for prospective motion correction and selective reacquisition in neuroanatomical MRI. Magn Reson Med. 2012;68(2):389-99.

217. van der Kouwe AJ, Benner T, Salat DH, Fischl B. Brain morphometry with multiecho MPRAGE. Neuroimage. 2008;40(2):559-69.
218. Smith SM, Jenkinson M, Woolrich MW, Beckmann CF, Behrens TE, Johansen-Berg H, et al. Advances in functional and structural MR image analysis and implementation as FSL. Neuroimage. 2004;23 Suppl 1:S208-19.
219. Zhang Y, Brady M, Smith S. Segmentation of brain MR images through a hidden Markov random field model and the expectation-maximization algorithm. IEEE Trans Med Imaging. 2001;20(1):45-57.
220. Smith SM. Fast robust automated brain extraction. Hum Brain Mapp. 2002;17(3):143-55.
221. Douaud G, Smith S, Jenkinson M, Behrens T, Johansen-Berg H, Vickers J, et al. Anatomically related grey and white matter abnormalities in adolescent-onset schizophrenia. Brain. 2007;130(Pt 9):2375-86.
222. Good CD, Johnsrude IS, Ashburner J, Henson RN, Friston KJ, Frackowiak RS. A voxel-based morphometric study of ageing in 465 normal adult human brains. Neuroimage. 2001;14(1 Pt 1):21-36.
223. Ashburner J, Friston KJ. Voxel-based morphometry--the methods. Neuroimage. 2000;11(6 Pt 1):805-21.
224. Andersson J, Jenkinson, M., Smith, S. Non-linear registration, aka spatial normalisation. http://www.fmrib.ox.ac.uk/analysis/techrep/ 2007/TR07JA2 2010 [
225. Filippi M. fMRI Techniques and Protocols. New York, N.Y.: Springer; 2009.
226. Debette S, Markus HS. The clinical importance of white matter hyperintensities on brain magnetic resonance imaging: systematic review and meta-analysis. BMJ. 2010;341:c3666.
227. Longstreth WT, Jr., Manolio TA, Arnold A, Burke GL, Bryan N, Jungreis CA, et al. Clinical correlates of white matter findings on cranial magnetic resonance imaging of 3301 elderly people. The Cardiovascular Health Study. Stroke. 1996;27(8):1274-82.
228. Liao D, Cooper L, Cai J, Toole JF, Bryan NR, Hutchinson RG, et al. Presence and severity of cerebral white matter lesions and hypertension, its treatment, and its control. The ARIC Study. Atherosclerosis Risk in Communities Study. Stroke. 1996;27(12):2262-70.
229. Wardlaw JM, Smith EE, Biessels GJ, Cordonnier C, Fazekas F, Frayne R, et al. Neuroimaging standards for research into small vessel disease and its contribution to ageing and neurodegeneration. Lancet Neurol. 2013;12(8):822-38.
230. Bakker SL, de Leeuw FE, de Groot JC, Hofman A, Koudstaal PJ, Breteler MM. Cerebral vasomotor reactivity and cerebral white matter lesions in the elderly. Neurology. 1999;52(3):578-83.
231. Pantoni L, Garcia JH. Pathogenesis of leukoaraiosis: a review. Stroke. 1997;28(3):652-9.
232. Li L, Simoni M, Kuker W, Schulz UG, Christie S, Wilcock GK, et al. Population-based case-control study of white matter changes on brain imaging in transient ischemic attack and ischemic stroke. Stroke. 2013;44(11):3063-70.

233. Almkvist O, Wahlund LO, Andersson-Lundman G, Basun H, Backman L. White-matter hyperintensity and neuropsychological functions in dementia and healthy aging. Arch Neurol. 1992;49(6):626-32.
234. Schmidt R, Fazekas F, Kleinert G, Offenbacher H, Gindl K, Payer F, et al. Magnetic resonance imaging signal hyperintensities in the deep and subcortical white matter. A comparative study between stroke patients and normal volunteers. Arch Neurol. 1992;49(8):825-7.
235. Kozachuk WE, DeCarli C, Schapiro MB, Wagner EE, Rapoport SI, Horwitz B. White matter hyperintensities in dementia of Alzheimer's type and in healthy subjects without cerebrovascular risk factors. A magnetic resonance imaging study. Arch Neurol. 1990;47(12):1306-10.
236. de Leeuw FE, de Groot JC, Achten E, Oudkerk M, Ramos LM, Heijboer R, et al. Prevalence of cerebral white matter lesions in elderly people: a population based magnetic resonance imaging study. The Rotterdam Scan Study. J Neurol Neurosurg Psychiatry. 2001;70(1):9-14.
237. Ylikoski A, Erkinjuntti T, Raininko R, Sarna S, Sulkava R, Tilvis R. White matter hyperintensities on MRI in the neurologically nondiseased elderly. Analysis of cohorts of consecutive subjects aged 55 to 85 years living at home. Stroke. 1995;26(7):1171-7.
238. Garde E, Mortensen EL, Krabbe K, Rostrup E, Larsson HB. Relation between age-related decline in intelligence and cerebral white-matter hyperintensities in healthy octogenarians: a longitudinal study. Lancet. 2000;356(9230):628-34.
239. de Groot JC, de Leeuw FE, Oudkerk M, van Gijn J, Hofman A, Jolles J, et al. Cerebral white matter lesions and cognitive function: the Rotterdam Scan Study. Ann Neurol. 2000;47(2):145-51.
240. O'Brien JT, Ames D. White matter lesions in depression and Alzheimer's disease. Br J Psychiatry. 1996;169(5):671.
241. O'Brien J, Desmond P, Ames D, Schweitzer I, Harrigan S, Tress B. A magnetic resonance imaging study of white matter lesions in depression and Alzheimer's disease. Br J Psychiatry. 1996;168(4):477-85.
242. Hahn EL. The Spin-Photon Echo Revisited. Nato Adv Sci Inst Se. 1994;339:75-90.
243. De Coene B, Hajnal JV, Gatehouse P, Longmore DB, White SJ, Oatridge A, et al. MR of the brain using fluid-attenuated inversion recovery (FLAIR) pulse sequences. AJNR Am J Neuroradiol. 1992;13(6):1555-64.
244. Hajnal JV, Bryant DJ, Kasuboski L, Pattany PM, De Coene B, Lewis PD, et al. Use of fluid attenuated inversion recovery (FLAIR) pulse sequences in MRI of the brain. J Comput Assist Tomogr. 1992;16(6):841-4.
245. Griffanti L, Zamboni G, Khan A, Li L, Bonifacio G, Sundaresan V, et al. BIANCA (Brain Intensity AbNormality Classification Algorithm): A new tool for automated segmentation of white matter hyperintensities. Neuroimage. 2016;141:191-205.
246. Madden DJ, Bennett IJ, Burzynska A, Potter GG, Chen NK, Song AW. Diffusion tensor imaging of cerebral white matter integrity in cognitive aging. Biochim Biophys Acta. 2012;1822(3):386-400.

247. Mori S, Zhang J. Principles of diffusion tensor imaging and its applications to basic neuroscience research. Neuron. 2006;51(5):527-39.
248. Johansen-Berg H, Behrens TEJ. Diffusion MRI. London, UK.: Academic Press, Elsevier; 2009.
249. Sullivan EV, Pfefferbaum A. Diffusion tensor imaging and aging. Neurosci Biobehav Rev. 2006;30(6):749-61.
250. Budde MD, Kim JH, Liang HF, Schmidt RE, Russell JH, Cross AH, et al. Toward accurate diagnosis of white matter pathology using diffusion tensor imaging. Magn Reson Med. 2007;57(4):688-95.
251. Song SK, Sun SW, Ramsbottom MJ, Chang C, Russell J, Cross AH. Dysmyelination revealed through MRI as increased radial (but unchanged axial) diffusion of water. Neuroimage. 2002;17(3):1429-36.
252. Billiet T, Vandenbulcke M, Madler B, Peeters R, Dhollander T, Zhang H, et al. Age-related microstructural differences quantified using myelin water imaging and advanced diffusion MRI. Neurobiol Aging. 2015;36(6):2107-21.
253. Zatorre RJ, Fields RD, Johansen-Berg H. Plasticity in gray and white: neuroimaging changes in brain structure during learning. Nat Neurosci. 2012;15(4):528-36.
254. Ennis DB, Kindlmann G. Orthogonal tensor invariants and the analysis of diffusion tensor magnetic resonance images. Magn Reson Med. 2006;55(1):136-46.
255. Douaud G, Jbabdi S, Behrens TE, Menke RA, Gass A, Monsch AU, et al. DTI measures in crossing-fibre areas: increased diffusion anisotropy reveals early white matter alteration in MCI and mild Alzheimer's disease. Neuroimage. 2011;55(3):880-90.
256. Bennett IJ, Madden DJ. Disconnected aging: cerebral white matter integrity and age-related differences in cognition. Neuroscience. 2014;276:187-205.
257. Jones DK, Cercignani M. Twenty-five pitfalls in the analysis of diffusion MRI data. NMR Biomed. 2010;23(7):803-20.
258. Jensen JH, Helpern JA. MRI quantification of non-Gaussian water diffusion by kurtosis analysis. NMR Biomed. 2010;23(7):698-710.
259. Coutu JP, Chen JJ, Rosas HD, Salat DH. Non-Gaussian water diffusion in aging white matter. Neurobiol Aging. 2014;35(6):1412-21.
260. Zhang H, Schneider T, Wheeler-Kingshott CA, Alexander DC. NODDI: practical in vivo neurite orientation dispersion and density imaging of the human brain. Neuroimage. 2012;61(4):1000-16.
261. Beaulieu C. The basis of anisotropic water diffusion in the nervous system - a technical review. NMR Biomed. 2002;15(7-8):435-55.
262. Vavasour IM, Laule C, Li DK, Traboulsee AL, MacKay AL. Is the magnetization transfer ratio a marker for myelin in multiple sclerosis? J Magn Reson Imaging. 2011;33(3):713-8.
263. Andersson JLRaS, S. Image distortion and its correction in diffusion MRI. In: D.K.Jones, editor. Diffusion MRI: Theory, Methods and Applications. Oxford, United Kingdom: Oxford University Press; 2011. p. 285-302.
264. Pierpaoli C. Artifacts in diffusion MRI. In: D.K.Jones, editor. Diffusion MRI: Theory, methods, and applications. Oxford, United Kingdom: Oxford University Press; 2011. p. 303-18.

265. Andersson JL, Sotiropoulos SN. An integrated approach to correction for off-resonance effects and subject movement in diffusion MR imaging. Neuroimage. 2016;125:1063-78.
266. Andersson JL, Graham MS, Zsoldos E, Sotiropoulos SN. Incorporating outlier detection and replacement into a non-parametric framework for movement and distortion correction of diffusion MR images. Neuroimage. 2016.
267. Andersson JLR, Skare S, Ashburner J. How to correct susceptibility distortions in spin-echo echo-planar images: application to diffusion tensor imaging. Neuroimage. 2003;20(2):870-88.
268. Andersson JLR, Sotiropoulos SN. An integrated approach to correction for off-resonance effects and subject movement in diffusion MR imaging. Neuroimage. 2016;125:1063-78.
269. Smith SM, Jenkinson M, Johansen-Berg H, Rueckert D, Nichols TE, Mackay CE, et al. Tract-based spatial statistics: voxelwise analysis of multi-subject diffusion data. Neuroimage. 2006;31(4):1487-505.
270. Rueckert D, Sonoda LI, Hayes C, Hill DL, Leach MO, Hawkes DJ. Nonrigid registration using free-form deformations: application to breast MR images. IEEE Trans Med Imaging. 1999;18(8):712-21.
271. Behrens TE, Berg HJ, Jbabdi S, Rushworth MF, Woolrich MW. Probabilistic diffusion tractography with multiple fibre orientations: What can we gain? Neuroimage. 2007;34(1):144-55.
272. Winkler AM, Ridgway GR, Webster MA, Smith SM, Nichols TE. Permutation inference for the general linear model. Neuroimage. 2014;92:381-97.
273. Freedman D, Lane D. A nonstochastic interpretation of reported significance levels Journal of Business & Economic Statistics. 1983;1(4):292-8.
274. Smith SM, Nichols TE. Threshold-free cluster enhancement: addressing problems of smoothing, threshold dependence and localisation in cluster inference. Neuroimage. 2009;44(1):83-98.
275. Jenkinson M, Smith S. A global optimisation method for robust affine registration of brain images. Med Image Anal. 2001;5(2):143-56.
276. Jenkinson M, Bannister P, Brady M, Smith S. Improved optimization for the robust and accurate linear registration and motion correction of brain images. Neuroimage. 2002;17(2):825-41.
277. Desikan RS, Segonne F, Fischl B, Quinn BT, Dickerson BC, Blacker D, et al. An automated labeling system for subdividing the human cerebral cortex on MRI scans into gyral based regions of interest. Neuroimage. 2006;31(3):968-80.
278. Wakana S, Caprihan A, Panzenboeck MM, Fallon JH, Perry M, Gollub RL, et al. Reproducibility of quantitative tractography methods applied to cerebral white matter. Neuroimage. 2007;36(3):630-44.
279. Hua K, Zhang J, Wakana S, Jiang H, Li X, Reich DS, et al. Tract probability maps in stereotaxic spaces: analyses of white matter anatomy and tract-specific quantification. Neuroimage. 2008;39(1):336-47.
280. Gorelick PB, Scuteri A, Black SE, Decarli C, Greenberg SM, Iadecola C, et al. Vascular contributions to cognitive impairment and dementia: a statement for healthcare professionals from the american heart association/american stroke association. Stroke. 2011;42(9):2672-713.

281. Glodzik L, Mosconi L, Tsui W, de Santi S, Zinkowski R, Pirraglia E, et al. Alzheimer's disease markers, hypertension, and gray matter damage in normal elderly. Neurobiol Aging. 2012;33(7):1215-27.
282. Beauchet O, Celle S, Roche F, Bartha R, Montero-Odasso M, Allali G, et al. Blood pressure levels and brain volume reduction: a systematic review and meta-analysis. J Hypertens. 2013;31(8):1502-16.
283. Rondina JM, Squarzoni P, Souza-Duran FL, Tamashiro-Duran JH, Scazufca M, Menezes PR, et al. Framingham Coronary Heart Disease Risk Score Can be Predicted from Structural Brain Images in Elderly Subjects. Front Aging Neurosci. 2014;6:300.
284. Kuper H, Singh-Manoux A, Siegrist J, Marmot M. When reciprocity fails: effort-reward imbalance in relation to coronary heart disease and health functioning within the Whitehall II study. Occup Environ Med. 2002;59(11):777-84.
285. Steptoe A, Willemsen G. The influence of low job control on ambulatory blood pressure and perceived stress over the working day in men and women from the Whitehall II cohort. J Hypertens. 2004;22(5):915-20.
286. Bastos-Leite AJ, van der Flier WM, van Straaten EC, Staekenborg SS, Scheltens P, Barkhof F. The contribution of medial temporal lobe atrophy and vascular pathology to cognitive impairment in vascular dementia. Stroke. 2007;38(12):3182-5.
287. Burton EJ, Barber R, Mukaetova-Ladinska EB, Robson J, Perry RH, Jaros E, et al. Medial temporal lobe atrophy on MRI differentiates Alzheimer's disease from dementia with Lewy bodies and vascular cognitive impairment: a prospective study with pathological verification of diagnosis. Brain. 2009;132(Pt 1):195-203.
288. den Heijer T, van der Lijn F, Koudstaal PJ, Hofman A, van der Lugt A, Krestin GP, et al. A 10-year follow-up of hippocampal volume on magnetic resonance imaging in early dementia and cognitive decline. Brain. 2010;133(Pt 4):1163-72.
289. Laakso MP, Partanen K, Riekkinen P, Lehtovirta M, Helkala EL, Hallikainen M, et al. Hippocampal volumes in Alzheimer's disease, Parkinson's disease with and without dementia, and in vascular dementia: An MRI study. Neurology. 1996;46(3):678-81.
290. Fotenos AF, Mintun MA, Snyder AZ, Morris JC, Buckner RL. Brain volume decline in aging: evidence for a relation between socioeconomic status, preclinical Alzheimer disease, and reserve. Arch Neurol. 2008;65(1):113-20.
291. Craik FI, Bialystok E. Cognition through the lifespan: mechanisms of change. Trends Cogn Sci. 2006;10(3):131-8.
292. Jack CR, Jr., Shiung MM, Weigand SD, O'Brien PC, Gunter JL, Boeve BF, et al. Brain atrophy rates predict subsequent clinical conversion in normal elderly and amnestic MCI. Neurology. 2005;65(8):1227-31.
293. Nishtala A, Preis SR, Beiser A, Devine S, Hankee L, Seshadri S, et al. Midlife cardiovascular risk impacts executive function: Framingham offspring study. Alzheimer Dis Assoc Disord. 2014;28(1):16-22.

294. Joosten H, van Eersel ME, Gansevoort RT, Bilo HJ, Slaets JP, Izaks GJ. Cardiovascular risk profile and cognitive function in young, middle-aged, and elderly subjects. Stroke. 2013;44(6):1543-9.
295. Unverzagt FW, McClure LA, Wadley VG, Jenny NS, Go RC, Cushman M, et al. Vascular risk factors and cognitive impairment in a stroke-free cohort. Neurology. 2011;77(19):1729-36.
296. Okereke OI, Kang JH, Cook NR, Gaziano JM, Manson JE, Buring JE, et al. Type 2 diabetes mellitus and cognitive decline in two large cohorts of community-dwelling older adults. J Am Geriatr Soc. 2008;56(6):1028-36.
297. Manschot SM, Biessels GJ, de Valk H, Algra A, Rutten GE, van der Grond J, et al. Metabolic and vascular determinants of impaired cognitive performance and abnormalities on brain magnetic resonance imaging in patients with type 2 diabetes. Diabetologia. 2007;50(11):2388-97.
298. Gold SM, Dziobek I, Sweat V, Tirsi A, Rogers K, Bruehl H, et al. Hippocampal damage and memory impairments as possible early brain complications of type 2 diabetes. Diabetologia. 2007;50(4):711-9.
299. van Harten B, de Leeuw FE, Weinstein HC, Scheltens P, Biessels GJ. Brain imaging in patients with diabetes: a systematic review. Diabetes Care. 2006;29(11):2539-48.
300. Manschot SM, Brands AM, van der Grond J, Kessels RP, Algra A, Kappelle LJ, et al. Brain magnetic resonance imaging correlates of impaired cognition in patients with type 2 diabetes. Diabetes. 2006;55(4):1106-13.
301. Bergmann O, Spalding KL, Frisen J. Adult Neurogenesis in Humans. Cold Spring Harb Perspect Biol. 2015;7(7):a018994.
302. Spalding KL, Bergmann O, Alkass K, Bernard S, Salehpour M, Huttner HB, et al. Dynamics of hippocampal neurogenesis in adult humans. Cell. 2013;153(6):1219-27.
303. Neurovascular Anatomy 2016 [Available from: http://www.meddean.luc.edu/lumen/meded/neuro/neurovasc/navigation/mca.htm.
304. Blood Vessels of the Brain 2016 [cited 2016 14 September]. Available from: http://www.strokecenter.org/professionals/brain-anatomy/blood-vessels-of-the-brain/.
305. Elkins JS, O'Meara ES, Longstreth WT, Jr., Carlson MC, Manolio TA, Johnston SC. Stroke risk factors and loss of high cognitive function. Neurology. 2004;63(5):793-9.
306. van Oijen M, de Jong FJ, Witteman JC, Hofman A, Koudstaal PJ, Breteler MM. Atherosclerosis and risk for dementia. Ann Neurol. 2007;61(5):403-10.
307. Troncoso JC, Zonderman AB, Resnick SM, Crain B, Pletnikova O, O'Brien RJ. Effect of infarcts on dementia in the Baltimore longitudinal study of aging. Ann Neurol. 2008;64(2):168-76.
308. Stebbins GT, Nyenhuis DL, Wang C, Cox JL, Freels S, Bangen K, et al. Gray matter atrophy in patients with ischemic stroke with cognitive impairment. Stroke. 2008;39(3):785-93.
309. Liebetrau M, Steen B, Hamann GF, Skoog I. Silent and symptomatic infarcts on cranial computerized tomography in relation to dementia and mortality: a population-based study in 85-year-old subjects. Stroke. 2004;35(8):1816-20.

310. Hofman A, Ott A, Breteler MM, Bots ML, Slooter AJ, van Harskamp F, et al. Atherosclerosis, apolipoprotein E, and prevalence of dementia and Alzheimer's disease in the Rotterdam Study. Lancet. 1997;349(9046):151-4.
311. Kuller LH, Lopez OL, Jagust WJ, Becker JT, DeKosky ST, Lyketsos C, et al. Determinants of vascular dementia in the Cardiovascular Health Cognition Study. Neurology. 2005;64(9):1548-52.
312. Jeerakathil T, Wolf PA, Beiser A, Massaro J, Seshadri S, D'Agostino RB, et al. Stroke risk profile predicts white matter hyperintensity volume: the Framingham Study. Stroke. 2004;35(8):1857-61.
313. Debette S, Beiser A, DeCarli C, Au R, Himali JJ, Kelly-Hayes M, et al. Association of MRI markers of vascular brain injury with incident stroke, mild cognitive impairment, dementia, and mortality: the Framingham Offspring Study. Stroke. 2010;41(4):600-6.
314. Kohler S, Thomas AJ, Lloyd A, Barber R, Almeida OP, O'Brien JT. White matter hyperintensities, cortisol levels, brain atrophy and continuing cognitive deficits in late-life depression. Br J Psychiatry. 2010;196(2):143-9.
315. Olesen PJ, Gustafson DR, Simoni M, Pantoni L, Ostling S, Guo X, et al. Temporal lobe atrophy and white matter lesions are related to major depression over 5 years in the elderly. Neuropsychopharmacology. 2010;35(13):2638-45.
316. Sawlani V, Gupta RK, Singh MK, Kohli A. MRI demonstration of Wallerian degeneration in various intracranial lesions and its clinical implications. J Neurol Sci. 1997;146(2):103-8.
317. Xie R, Fang M, Zhou L, Fan S, Liu J, Quan H, et al. Diffusion tensor imaging detects Wallerian degeneration of the corticospinal tract early after cerebral infarction. Neural Regen Res. 2012;7(12):900-5.
318. Puig J, Pedraza S, Blasco G, Daunis IEJ, Prats A, Prados F, et al. Wallerian degeneration in the corticospinal tract evaluated by diffusion tensor imaging correlates with motor deficit 30 days after middle cerebral artery ischemic stroke. AJNR Am J Neuroradiol. 2010;31(7):1324-30.
319. Uchino A, Sawada A, Takase Y, Egashira R, Kudo S. Transient detection of early wallerian degeneration on diffusion-weighted MRI after an acute cerebrovascular accident. Neuroradiology. 2004;46(3):183-8.
320. Gimeno D, Tabak AG, Ferrie JE, Shipley MJ, De Vogli R, Elovainio M, et al. Justice at work and metabolic syndrome: the Whitehall II study. Occup Environ Med. 2010;67(4):256-62.
321. Lakka HM, Laaksonen DE, Lakka TA, Niskanen LK, Kumpusalo E, Tuomilehto J, et al. The metabolic syndrome and total and cardiovascular disease mortality in middle-aged men. JAMA. 2002;288(21):2709-16.
322. McIntyre RS, Soczynska JK, Konarski JZ, Woldeyohannes HO, Law CW, Miranda A, et al. Should Depressive Syndromes Be Reclassified as "Metabolic Syndrome Type II"? Ann Clin Psychiatry. 2007;19(4):257-64.
323. Tillin T, and, Forouhi NG. Meabolic Syndrome and Ethnicity. In: C.D. Byrne a, Wild SH, editors. The Metabolic Syndrome. Second ed. Oxford, UK.: Wiley-Blackwell; 2011.

324. Ford ES, Li C, Zhao G. Prevalence and correlates of metabolic syndrome based on a harmonious definition among adults in the US. J Diabetes. 2010;2(3):180-93.
325. Cahana-Amitay D, Spiro A, 3rd, Cohen JA, Oveis AC, Ojo EA, Sayers JT, et al. Effects of metabolic syndrome on language functions in aging. J Int Neuropsychol Soc. 2015;21(2):116-25.
326. Gold SM, Dziobek I, Rogers K, Bayoumy A, McHugh PF, Convit A. Hypertension and hypothalamo-pituitary-adrenal axis hyperactivity affect frontal lobe integrity. J Clin Endocrinol Metab. 2005;90(6):3262-7.
327. Raji CA, Ho AJ, Parikshak NN, Becker JT, Lopez OL, Kuller LH, et al. Brain structure and obesity. Hum Brain Mapp. 2010;31(3):353-64.
328. Ward MA, Bendlin BB, McLaren DG, Hess TM, Gallagher CL, Kastman EK, et al. Low HDL Cholesterol is Associated with Lower Gray Matter Volume in Cognitively Healthy Adults. Front Aging Neurosci. 2010;2.
329. Sala M, de Roos A, van den Berg A, Altmann-Schneider I, Slagboom PE, Westendorp RG, et al. Microstructural brain tissue damage in metabolic syndrome. Diabetes Care. 2014;37(2):493-500.
330. Kurl S, Laukkanen JA, Niskanen L, Laaksonen D, Sivenius J, Nyyssonen K, et al. Metabolic syndrome and the risk of stroke in middle-aged men. Stroke. 2006;37(3):806-11.
331. de Leeuw FE, de Groot JC, Oudkerk M, Witteman JC, Hofman A, van Gijn J, et al. A follow-up study of blood pressure and cerebral white matter lesions. Ann Neurol. 1999;46(6):827-33.
332. Jagust W, Harvey D, Mungas D, Haan M. Central obesity and the aging brain. Arch Neurol. 2005;62(10):1545-8.
333. Chen HJ, Bai CH, Yeh WT, Chiu HC, Pan WH. Influence of metabolic syndrome and general obesity on the risk of ischemic stroke. Stroke. 2006;37(4):1060-4.
334. Bang OY, Kim JW, Lee JH, Lee MA, Lee PH, Joo IS, et al. Association of the metabolic syndrome with intracranial atherosclerotic stroke. Neurology. 2005;65(2):296-8.
335. O'Sullivan M, Lythgoe DJ, Pereira AC, Summers PE, Jarosz JM, Williams SC, et al. Patterns of cerebral blood flow reduction in patients with ischemic leukoaraiosis. Neurology. 2002;59(3):321-6.
336. Launer LJ. Epidemiology of white matter lesions. Top Magn Reson Imaging. 2004;15(6):365-7.
337. Portet F, Brickman AM, Stern Y, Scarmeas N, Muraskin J, Provenzano FA, et al. Metabolic syndrome and localization of white matter hyperintensities in the elderly population. Alzheimers Dement. 2012;8(5 Suppl):S88-95 e1.
338. Karlamangla AS, Singer BH, McEwen BS, Rowe JW, Seeman TE. Allostatic load as a predictor of functional decline. MacArthur studies of successful aging. J Clin Epidemiol. 2002;55(7):696-710.
339. Bizik G, Picard M, Nijjar R, Tourjman V, McEwen BS, Lupien SJ, et al. Allostatic load as a tool for monitoring physiological dysregulations and comorbidities in patients with severe mental illnesses. Harv Rev Psychiatry. 2013;21(6):296-313.

340. Crimmins EM, Johnston M, Hayward M, Seeman T. Age differences in allostatic load: an index of physiological dysregulation. Exp Gerontol. 2003;38(7):731-4.
341. Hwang AC, Peng LN, Wen YW, Tsai YW, Chang LC, Chiou ST, et al. Predicting all-cause and cause-specific mortality by static and dynamic measurements of allostatic load: a 10-year population-based cohort study in Taiwan. J Am Med Dir Assoc. 2014;15(7):490-6.
342. Karlamangla AS, Singer BH, Seeman TE. Reduction in allostatic load in older adults is associated with lower all-cause mortality risk: MacArthur studies of successful aging. Psychosom Med. 2006;68(3):500-7.
343. Karlamangla AS, Miller-Martinez D, Lachman ME, Tun PA, Koretz BK, Seeman TE. Biological correlates of adult cognition: midlife in the United States (MIDUS). Neurobiol Aging. 2014;35(2):387-94.
344. Gianaros PJ, Manuck SB. Neurobiological Pathways Linking Socioeconomic Position and Health. Psychosomatic Medicine. 2010;72(5):450-61.
345. Gianaros PJ, Horenstein JA, Cohen S, Matthews KA, Brown SM, Flory JD, et al. Perigenual anterior cingulate morphology covaries with perceived social standing. Soc Cogn Affect Neur. 2007;2(3):161-73.
346. Breteler MM, Claus JJ, Grobbee DE, Hofman A. Cardiovascular disease and distribution of cognitive function in elderly people: the Rotterdam Study. BMJ. 1994;308(6944):1604-8.
347. de Groot JC, de Leeuw FE, Oudkerk M, Hofman A, Jolles J, Breteler MM. Cerebral white matter lesions and subjective cognitive dysfunction: the Rotterdam Scan Study. Neurology. 2001;56(11):1539-45.
348. de Groot M, Ikram MA, Akoudad S, Krestin GP, Hofman A, van der Lugt A, et al. Tract-specific white matter degeneration in aging: the Rotterdam Study. Alzheimers Dement. 2015;11(3):321-30.
349. Tuladhar AM, van Norden AG, de Laat KF, Zwiers MP, van Dijk EJ, Norris DG, et al. White matter integrity in small vessel disease is related to cognition. Neuroimage Clin. 2015;7:518-24.
350. Gons RA, van Oudheusden LJ, de Laat KF, van Norden AG, van Uden IW, Norris DG, et al. Hypertension is related to the microstructure of the corpus callosum: the RUN DMC study. J Alzheimers Dis. 2012;32(3):623-31.
351. Rocha KK, Ribeiro AM, Rocha KC, Sousa MB, Albuquerque FS, Ribeiro S, et al. Improvement in physiological and psychological parameters after 6 months of yoga practice. Conscious Cogn. 2012;21(2):843-50.
352. van der Zwan JE, de Vente W, Huizink AC, Bogels SM, de Bruin EI. Physical activity, mindfulness meditation, or heart rate variability biofeedback for stress reduction: a randomized controlled trial. Appl Psychophysiol Biofeedback. 2015;40(4):257-68.
353. McEwen BS. In pursuit of resilience: stress, epigenetics, and brain plasticity. Ann N Y Acad Sci. 2016;1373(1):56-64.
354. Froeliger B, Garland EL, McClernon FJ. Yoga meditation practitioners exhibit greater gray matter volume and fewer reported cognitive failures: results of a preliminary voxel-based morphometric analysis. Evid Based Complement Alternat Med. 2012;2012:821307.

Appendix

APPENDIX A

Chapter 2. Selected literature on secondary markers of the stress response and allostatic load. Based on: (6).

Predictor / marker	Outcome / marker	Significant association?	Design	Reference	
Low Socioeconomic status (SES)	CVD	Yes	Cross	Adler NE et al., 1993	J AM Med Assoc 269, 3140-45
Low SES	Increased prevalence of stressors in the home	Yes	Review	McEwen BS and Tucker P, 2011	Am J Public Health 101, S131-139
Cortisol response to laboratory induced stress	Incident high BP	Yes	Longitudinal	Hamer M et al., 2012	J Clin Endocrinol Metab 97(1):E29-34
High BP to Psychological stress	Future BP	Modest	Longitudinal	Caroll D et al., 2001	Psychosom Med 63(5):737-43
Depression + age	Future BP	Mixed, Mostly due to age	Longitudinal	Nabi H et al., 2011	Hypertension 57(4):710-6
High BP to stress task	Functional neural reactivity to stress task in brain areas that control CV system	Yes	Longitudinal	Gianaros PJ et al., 2007	Hypertension 49: 134-40
Lifetime hypertension	Grey matter atrophy and white matter hyperintensities	Yes	Longitudinal	Allan CL et al., 2015	Br J Psychiatry 206(4):308-15
Job strain and Low decision latitude	Risk of CHD	Yes	Longitudinal	Kuper H and Marmot M, 2003	J Epidemiol Comm Health 57(2):147-53
Job strain and SES	BP + stress ratings + happiness ratings	Yes	Cross	Steptoe A and Willemsen G 2004	J Hypertens 22(5):915-20
Effort-reward imbalance	CHD + health	Moderate	Longitudinal	Kuper H et al., 2002	Occup Environ Med 59(11): 777-84

Effort-reward imbalance + job control	CHD	Yes	Longitudinal	Bosma H et al., 1998	Am J Pub Health 88(1): 68-74
Job insecurity	Incident CHD	Yes	Longitudinal	Ferrie JE et al., 2013	Atheroscl. 227(1):178-81
Unfairness and job strain	Coronary events + mental and physical health	Yes	Longitudinal	De Vogli R. et al., 2007	J Epidemiol Comm Health 61(6):513-8
Overtime work	Incident CHD	Yes	Longitudinal	Virtanen M et al., 2010	Eur Heart J 31(14):1737-44
Self-reported adverse effects of stress on health	CHD or MI risk	Yes	Longitudinal	Nabi H et al., 2013	Eur Heart J 34(34):2697-705
Cortisol secretion during the day	CVD mortality	Yes	Longitudinal	Kumari M et al., 2011	J Clin Endocrinol Metab 96(5):1478-85
Depression	Stroke and CVD	Mixed (dose-response and reverse causation	Longitudinal	Brunner EJ et al., 2014	Eur J Prev Cardiol 21(3):340-6
Cardiovascular risk and structural brain changes	Framingham CHD Risk Score	Yes + gender effects	Cross	Rondina JM et al., 2014	Front Aging Neurosci 1(6):300-14
Framingham Stroke Risk and CVD Risk scores	Cognitive decline	Yes	Longitudinal	Dregan A et al., 2012	Age and Ageing 42(3):338-45
Framingham Stroke Risk and CVD Risk scores + dementia risk score	Cognitive decline	Framingham scores better predictors	Longitudinal	Kaffashian S. et al., 2013	Neurology 80(14):1300-6
Framingham Stroke Risk score	Grey matter decline + executive function decline	Yes	Longitudinal	Debette S et al., 2011	Neurology 77(5): 461-68
Framingham Stroke Risk score in late-life depression	White matter integrity	Yes	Cross	Allan CL et al., 2012	Int Psychogeriatr. 24(4):524-31
Organizational justice	Metabolic syndrome	In men only	Longitudinal	Gimeno D et al., 2010	Occup Environ Med 67(4):256-62
Job strain	Metabolic syndrome	Yes	Longitudinal	Chandola T et al., 2006	BMJ 332(7540):521-5

SES (employment grade)	Metabolic syndrome	Central obesity + plasma fibrinogen	Cross	Brunner EJ et al., 1997	Diabetologia 40(11):1341-9
SES (house hold wealth)	Metabolic syndrome	Yes	Cross	Perel P et al., 2006	Diabetes care 29(12):2694-700
Unfairness	Metabolic syndrome	Yes but reduced after covariates	Longitudinal	De Vogli R. et al., 2007	J Psychosom Res 63(4):413-9
Metabolic syndrome	Cardiovascular disease	Yes	Meta-analysis	Galassi A et al., 2006	American J of Medicine 119(10):812-9
Metabolic syndrome	Cardiovascular disease mortality	In men only	Longitudinal	Lakka H-M et al., 2002	JAMA 288(21):2709-16
Metabolic syndrome	Telomere shortening	Yes	Review	Epel ES 2009	Hormones 8(1):7-22
Metabolic syndrome	Stroke + mortality rate	Yes	Cross	Isomaa B et al., 2001	Diabetes Care 24(4):683-9
Metabolic syndrome	Heart disease + physical functioning + mortality	Yes	Cross	Gardner AW et al., 2006	J Vasc Surg 43(6):1191-6
Cumulative Metabolic syndrome	Poor cognition	Yes	Longitudinal	Akbaraly TN et al., 2010	Diabetes care 33(1):84-9
Metabolic syndrome	Onset of depressive symptoms	Obesity + dyslipidemia	Longitudinal	Akbaraly TN et al., 2009	Diabetes care 32(3):499-504
Job strain and caring for a relative	Allostatic load (AL)	Yes	Longitudinal	Dich N et al., 2015	Psychosom Med [2015 May 15 Epub ahead of print]
Negative emotional response to stressful life events	Allostatic load	Non-linear	Longitudinal	Dich N et al., 2014	Psychoneuroendocrinol. 49:54-61
Allostatic load	Physical + cognitive decline	Yes	Longitudinal	Seeman TE et al., 1997	Arch Intern Med. 157(19): 2259-68
Allostatic load	Physical + cognitive function	AL better predictor than individual components	Longitudinal	Karlamangla AS et al., 2002	J Clin Epidemiol. 55:696-710
Allostatic load	CVD + mortality	Yes	Longitudinal	Seeman TE et al., 2001	Proc Natl Acad Sci U S A. 98(8): 4770-75

Allostatic load	Physical + general health	Yes	Longitudinal	Read S and Grundy E, 2014	Psychosom Med. 76(7):490-496
Allostatic load	Cognitive function	Yes	Cross	Karlamangla AS et al., 2014	Neurobiol Aging. 35(2):387-394
Allostatic load	Mental health	AL better predictor than individual components	Cross	Bizik G et al., 2013	Harv Rev Psychiatry 21(6):296-313
Allostatic load reduction	Mortality risk decrease	AL better predictor than individual components	Longitudinal	Karlamangla AS et al., 2006	Psychosom Med. 68(3):500-7

Chapter 2. Structural and functional studies of the brain in the stress response and allostatic load and overload. Based on (6)

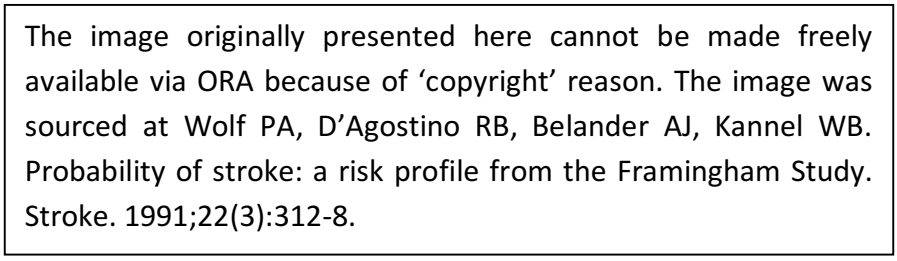
Examined Effect	Reference		Notes
Hippocampal / temporal lobe shrinkage			
Mild cognitive impairment and Alzheimer's disease	de Leon MJ et al., 1997	Neurobiol. Aging 18, 1-11	
Type-2 Diabetes (T2D)	Gold SM et al., 2007 McEwen BS et al., 2007	Diabetologia 50, 711-19 Physiol. Rev. 87, 873-904	Besides its response to glucocorticoids, the hippocampus is an important target of metabolic hormones that have a variety of adaptive actions in the healthy brain, which is perturbed in metabolic disorders, such as T2D. The hippocampus has receptors for insulin-like growth factor-1 (IGF1), which mediates exercise-induced neurogenesis.
Prolonged Major Depressive disorder (MDD)	Sheline YI et al., 2003	Biol. Psychiatry 54, 338-52	
Autopsy on MDD-suicide	Stockmeier CA et al., 2004	Biol. Psychiatry 56, 640-50	Most likely, due to glial cell loss + small soma size, which suggests shrinkage of dendritic trees in MDD.
Postnatal depression	Lupien SJ et al., 2011	Proc. Natl. Acad. Sci. 108, 14324-29	Hippocampal volume ***not*** affected
Cushing's disease	Starkman MN et al., 1999	Biol. Psychiatry 46, 1595-02	
Posttraumatic stress disorder (PTSD)	Gurvits TV et al., 1996	Biol. Psychiatry 40, 1091-99	

Chronic stress	Gianaros PJ et al., 2007	NeuroImage 35, 795-803	
Chronic inflammation	Marsland AL et al., 2008	Biol. Psychiatry 64, 484-90	
Lack of physical activity	Erickson KI et al., 2009	Hippocampus 19, 1030-39	
Jet lag	Cho K, 2001	Nat. Neurosci. 4, 567-68	
Low socioeconomic status (SES)	Hanson JL et al., 2011	PloS One 6, e18712	
Amygdala hyperactivity and enlargement			
Major depressive disorder	Sheline YI et al., 2001 Frodl T et al., 2003	Biol. Psychiatry 50, 651-58 Biol. Psychiatry 53, 338-44	Hyperactivity Enlargement
Anxiety	Drevets WC, 2000	Biol. Psychiatry 48, 813-29	Hyperactivity
PTSD	Rao RP et al., 2012 Zohar J et a.l, 2011	Bio. Psychiatry 72, 466-75 Eur Neuropsychopharmacol. 21, 796-809	Corticosteroid treatment of PTSD (characterized by low cortisol levels) alleviates symptoms in patients and increases dendritic growth and spine density in ***rat*** amygdala
Postnatal depression	Lupien SJ et al., 2011	Proc. Natl. Acad. Sci. 108, 14324-29	Enlargement in offspring
CVD	Gianaros PJ et al., 2009	Biol. Psychiatry 65, 943-50	Increased reactivity to angry & sad faces mediated by increased sympathetic activity
Traumatic event in healthy	Ganzel BL et al., 2008	NeuroImage 40, 788-95	Increased reactivity to

			angry + sad faces
Sleep deprivation	Yoo S-S et al., 2007	Curr. Biol. 17, R877-78	Increased reactivity to angry + sad faces
Upbringing in low SES environment	Gianaros PJ et al., 2008	Soc. Cogn. Affect. Neurosci. 3, 91-96	Increased reactivity to angry + sad faces
Prefrontal cortex (PFC) impairment			
Medial Prefrontal cortex (PFC)	Liston C et al., 2006	J Neurosci 26, 7870-74	Shrinkage of dendrites and loss of spines through excitatory amino acids + glucocorticoids
Orbitofrontal cortex (OFC)			Expansion of dendrites
Poor cognitive flexibility	Dias-Ferreira E et al., 2009 Liston C et al., 2006 Karatsoreos et al., 2011	Science 325, 621-25 J Neurosci 26, 7080-74 Proc. Natl. Acad. Sci. 108, 1657-62	Animal and human studies
Reduced functional connectivity	Liston C et al., 2009	PNAS 106, 912-17	
Ageing	Bloss EB et al., 2010	Exp. Neurol. 210, 109-17	Failure to reverse shrinkage of medial PFC neurons after chronic stress in rats
Low subjective SES	Gianaros PJ et al., 2007	Soc. Cogn. Affect. Neurosci. 2, 161-73	Reduction in PFC grey matter

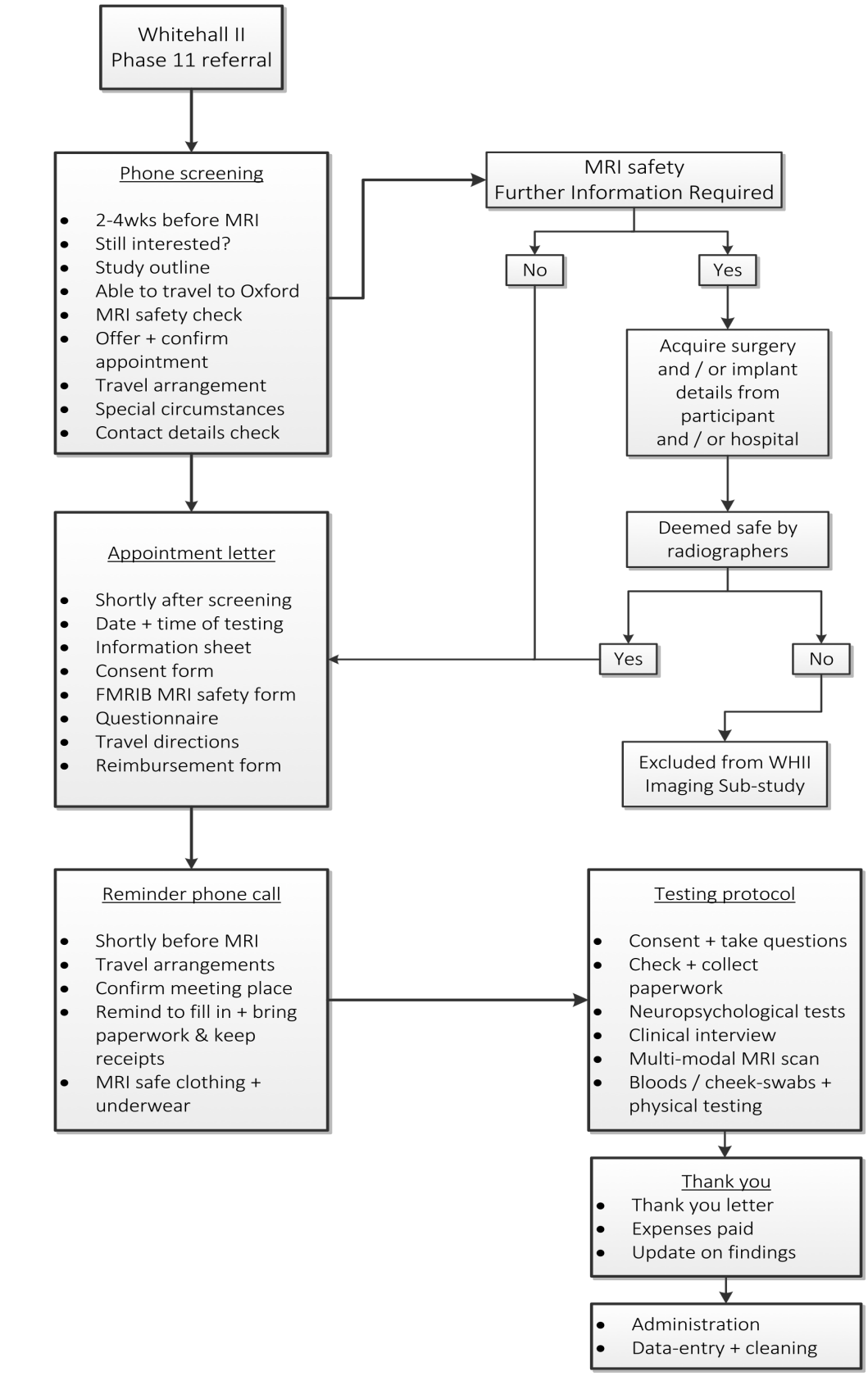
Chapter 4.

Calculation of Framingham Stroke Risk Profile in men (top) and women (bottom). Figure reused with permission (license no: 3960541387171) (129).



APPENDIX B

Flow-chart of Whitehall II Imaging Sub-study recruitment protocol (127).



.

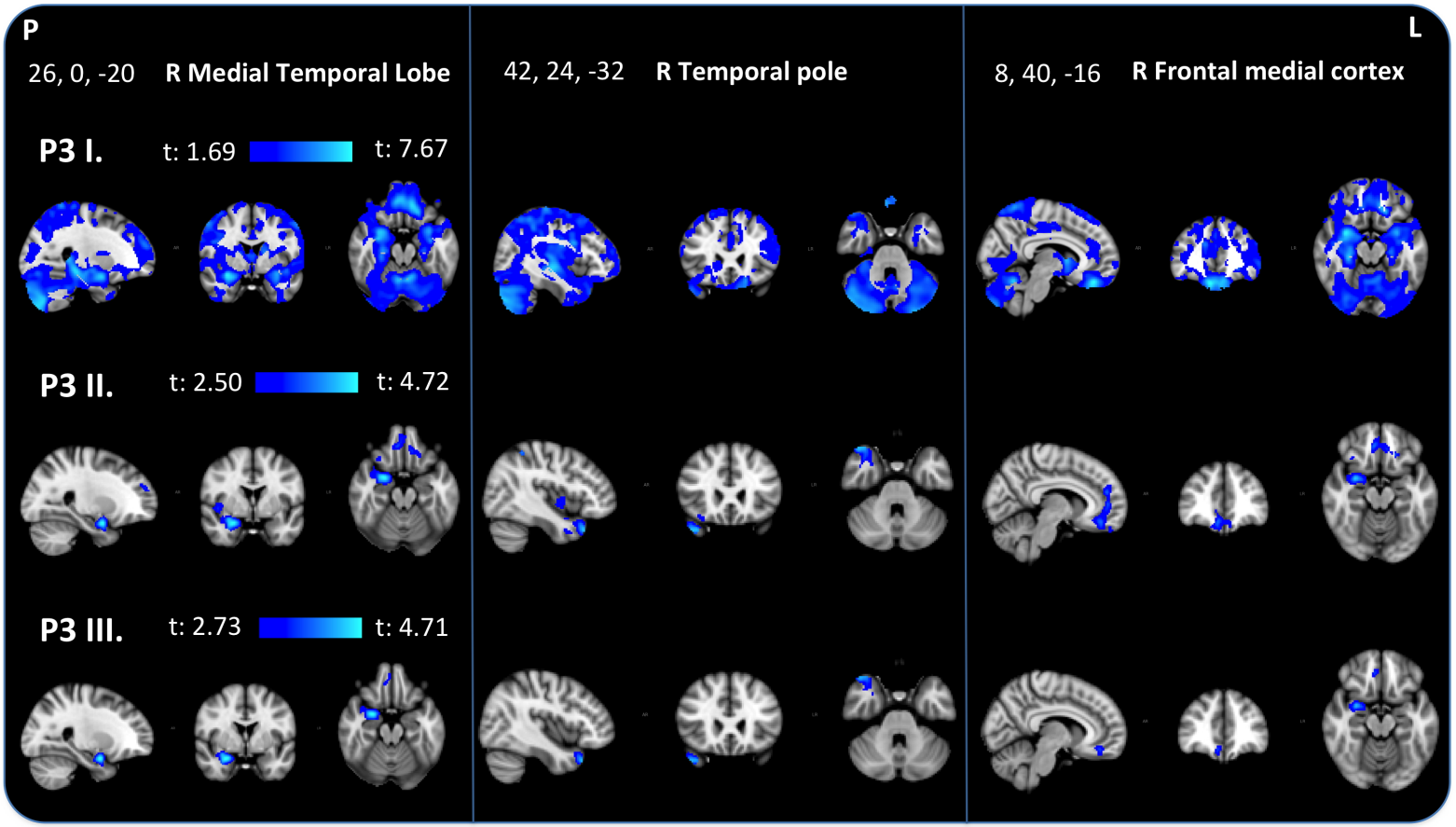
APPENDIX C

Overview of MRI sequences and parameters used in the Whitehall II Imaging Sub-study. S and T define 'sagittal' and 'transversal' orientation, respectively. Adapted from (127). TR: repetition time, TE: echo time, FoV: field of view, TI: inversion time.

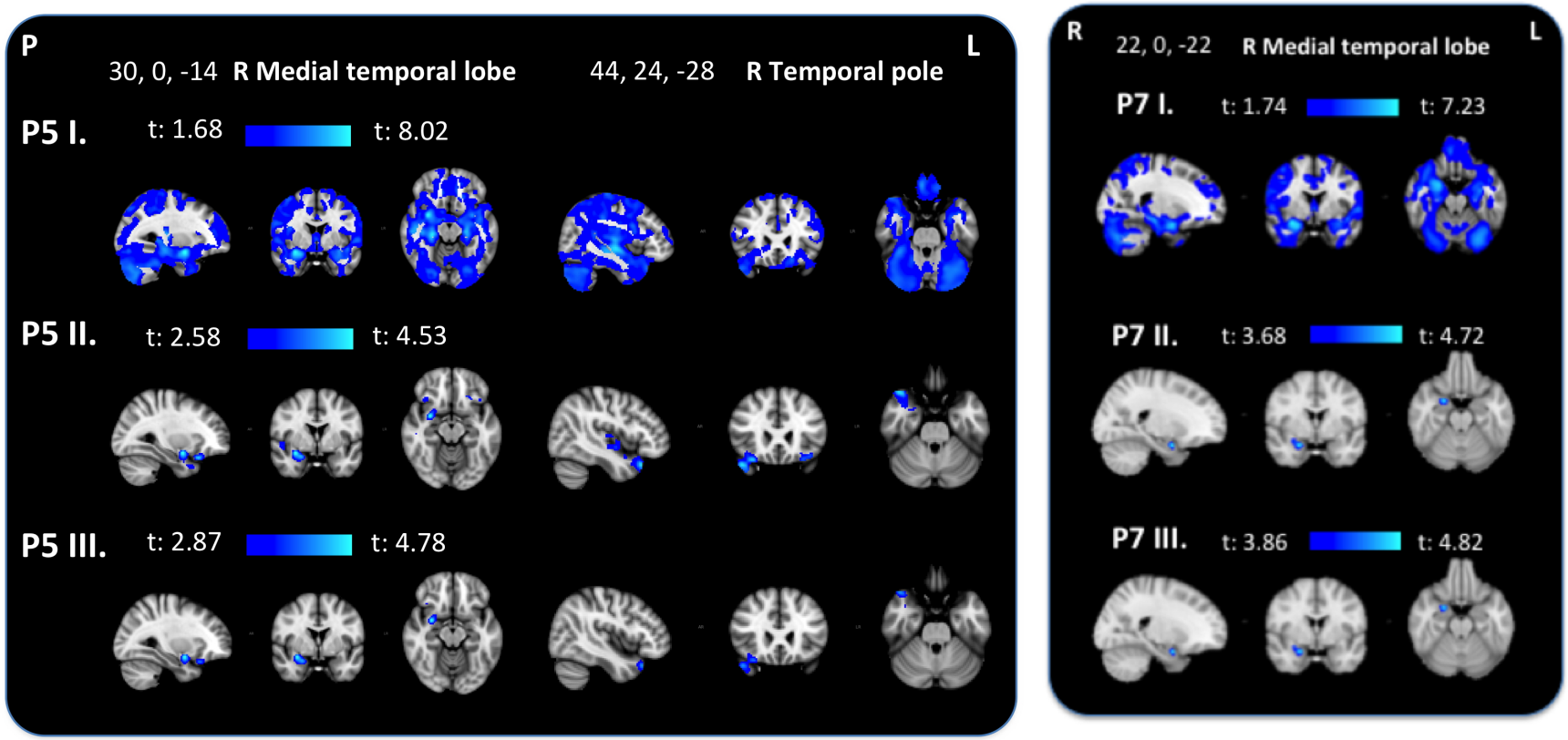
	Structural				Functional	
Sequence	MEMPR	FLAIR	T2*	dMRI	Multiband	Standard
Condition	———	———	———	———	Resting	Resting
TR in ms	2530	9000	36	8900	1300	3000
TE in ms	1.79/3.65/5.51/7.37	73	30	91.2	40	30
Flip angle	7°	150°	15°	———	66°	90°
Voxel in mm^3	1x1x1	0.9x0.9x3	0.7x0.7x1.5	2x2x2	2x2x2	3x3x3
FoV read	256	220	220	192	212	192
FoV phase	100%	100%	81.3%	100%	100%	100%
Base resolution	256	256	320	96	106	64
Phase resolution	100%	100%	100%	100%	100%	100%
TI in ms	1380	2500	———	———	———	———
Bandwidth	651 Hz/Px	283 Hz/Px	170 Hz/Px	1680 Hz/Px	1814 Hz/Px	2368 Hz/Px
Orientation	S	T	T	T	T	T
b-value	———	———	———	1500 s/mm^2	———	———
N. of volumes	———	———	———	———	460	200
N. of directions	———	———	———	60 + 5 b = 0 s	———	———
Acquisition time	6 m 12 s	4 m 14 s	4 m 17 s	9 m 56 s	10 m 10 s	10 m

APPENDIX D

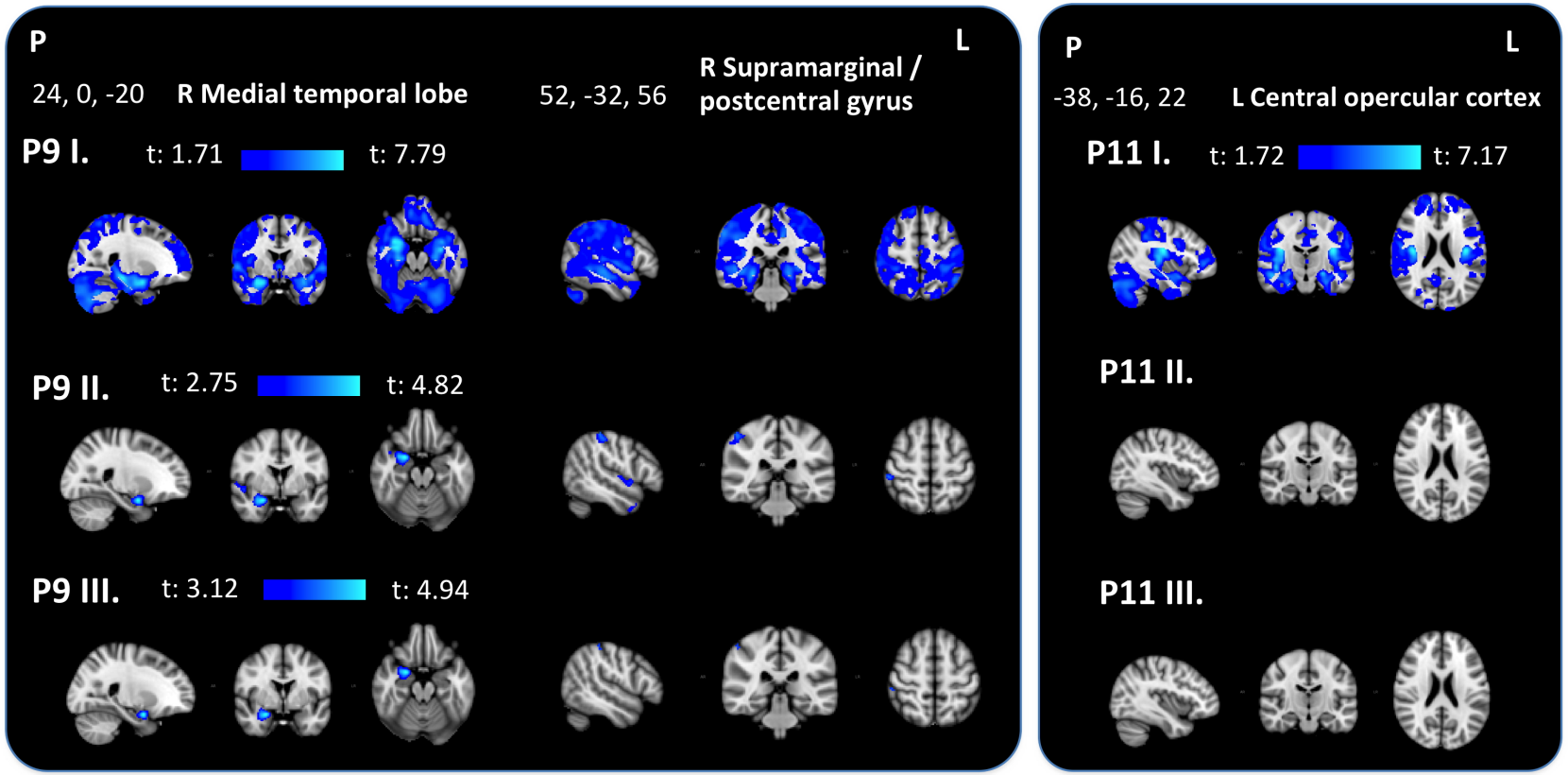
Chapter 6. Framingham Stroke Risk score measured at Phase 3 (P3) and its significant association with lower grey matter (I) and after controlling for age, sex, ethnicity (II) plus socioeconomic status (III). Locations represent maximum t values at model III. Colours represent t-values significant at $p < 0.05$, threshold free cluster enhancement and multiple comparisons corrected.



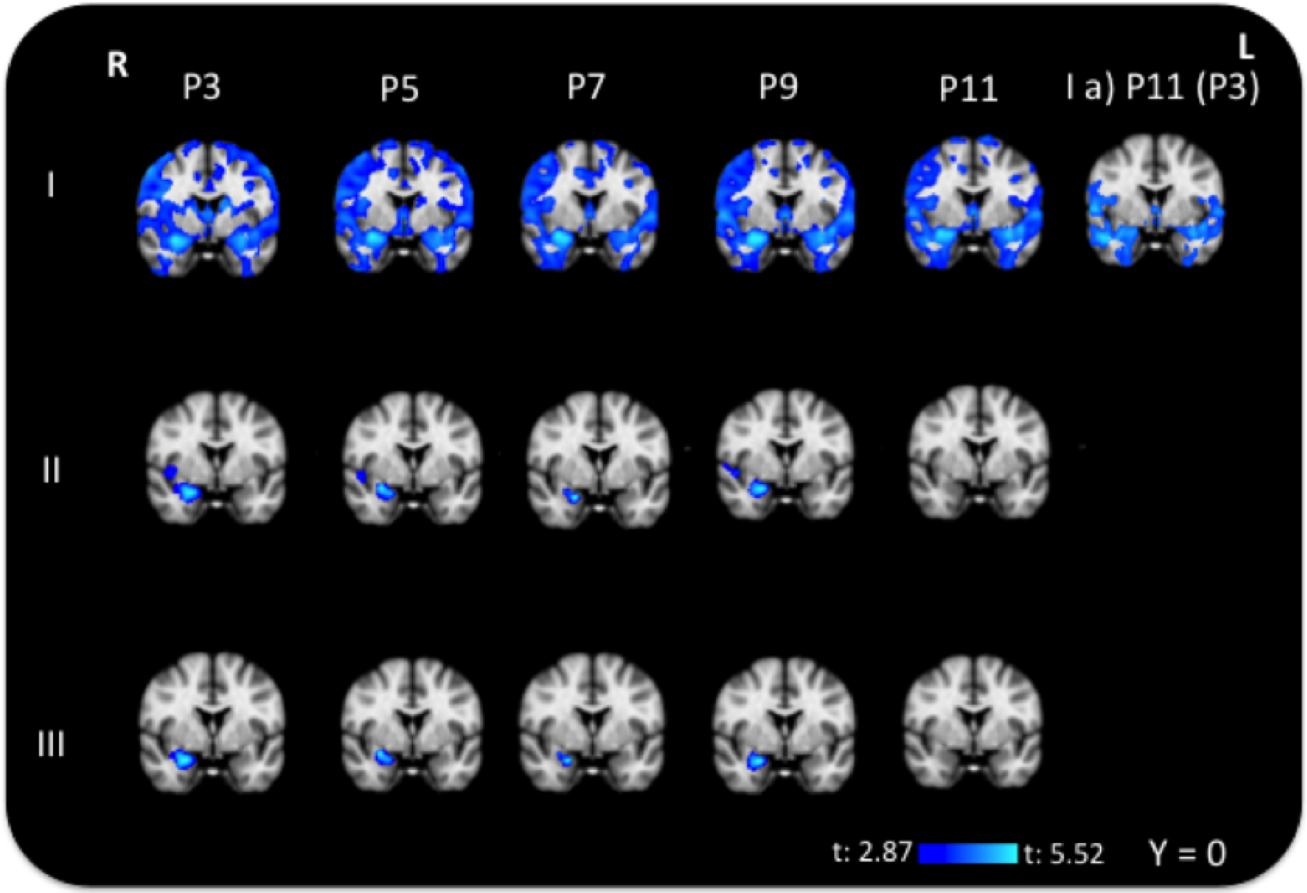
Chapter 6. Framingham Stroke Risk score measured at Phase 5 (P5, left) and at Phase 7 (P7), and its significant association with lower grey matter (I) and after controlling for age, sex, ethnicity (II) plus socioeconomic status (III). Locations represent maximum t values at model III. Colours represent t-values significant at $p < 0.05$, threshold free cluster enhancement and multiple comparisons corrected.



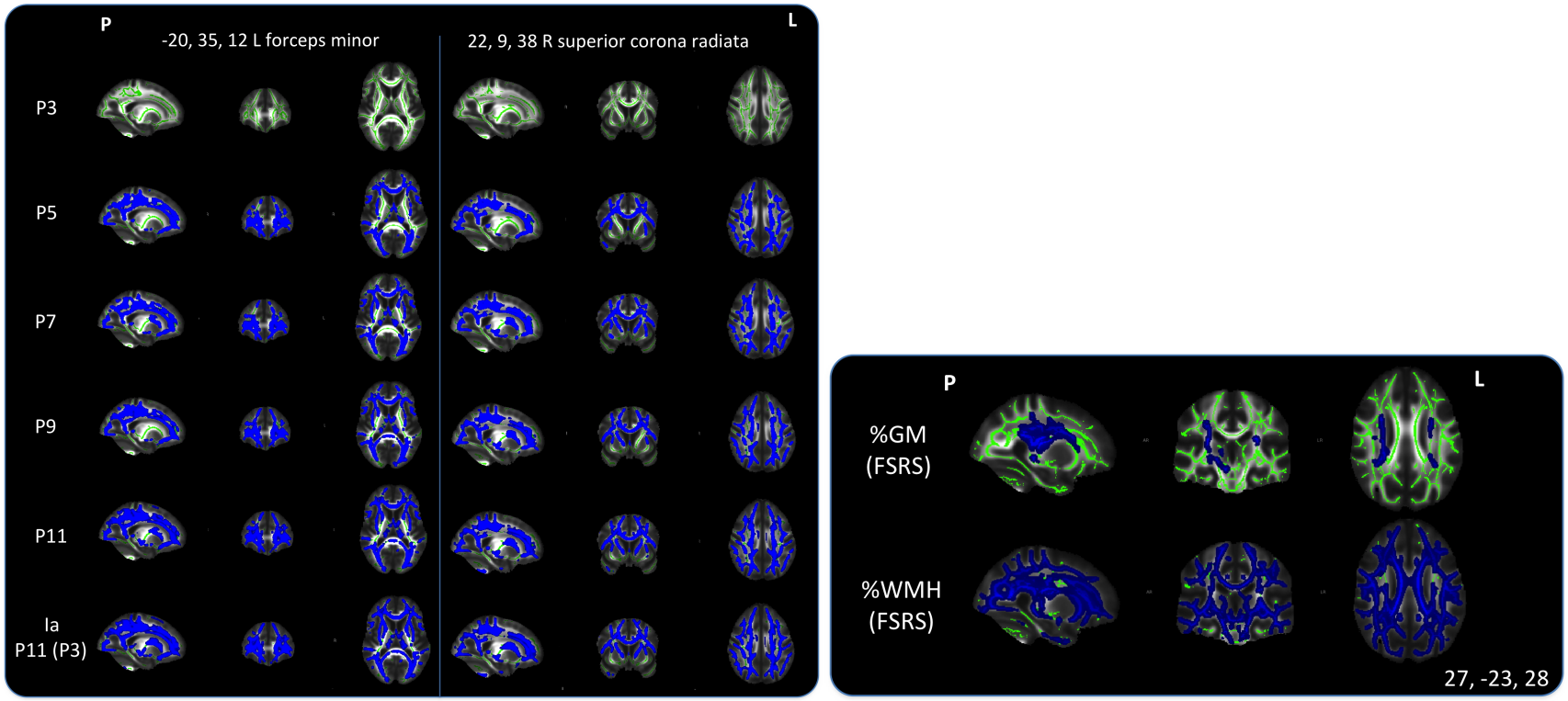
Chapter 6. Framingham Stroke Risk score measured at Phase 9 (P9, left) and at Phase 11 (P11) in older age at the time of scan, and its significant association with lower grey matter (I) and after controlling for age, sex, ethnicity (II) plus socioeconomic status (III). Locations represent maximum t values at model III. P11 model II and III associations are not significant. Colours represent t-values significant at $p < 0.05$, threshold free cluster enhancement and multiple comparisons corrected.



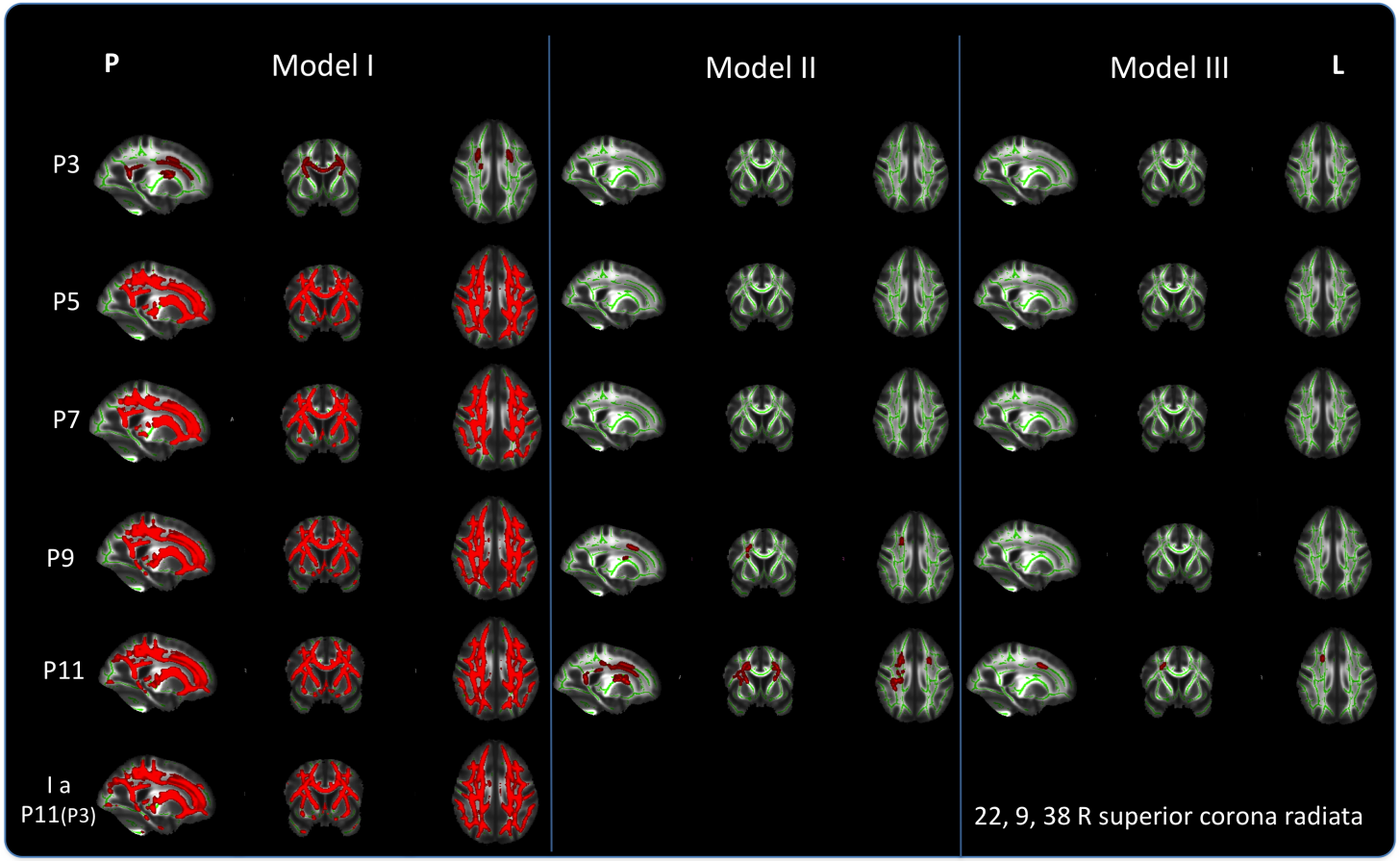
Chapter 6. Framingham stroke risk measured 20 (P3), 15 (P5), 10 (P7) and 5 (P9) years before and at scan (P11) and new risk acquired between P3 and P11 (Ia) were associated with bilateral widespread lower grey matter (GM) (Model I). Lower GM remained present with risk measured at Phases 3-9, but not at time of scan, in right medial temporal lobe, after controlling for age, sex, ethnicity (Model II) and socioeconomic factors (Model III). Colours represent t-values significant at $p < 0.05$, threshold free cluster enhancement and multiple comparisons corrected.



Chapter 6. Left: Framingham stroke risk measured 15 (P5), 10 (P7) and 5 (P9) years before and at scan (P11) and new risk acquired between P3 and P11 (Ia) were associated with bilateral widespread lower fractional anisotrop (FA) (Model I). Lower FA was not present with risk measured 20 years prior to scan (P3) or after controlling for a age, sex, ethnicity (Model II) and socioeconomic factors (Model III). Right: Significant association between percentage total GM volume (%GM) and lower FA values (top) and between white matter hyperintensities (%WMH) and lower FA (bottom), even after controlling for FSRS measured at Phase 11. Significant regions (p < 0.05, tfce) are dilated for illustrative purposes, overl aid on a green skeleton.



Chapter 6. FSRS at all Whitehall phases (P3 – P11), as well as change in stroke risk over a 20-year period is associated with widespread higher MD values. Higher MD was associated with FSRS at P9 and at time of (P11) scan after controlling for age, sex, ethnicity (Model II) in the superior corona radiata (P9: right, P11: bilaterally) and with FSRS at the time of the scan after controlling for all confounders (Model III), in right superior corona radiata. Significant regions ($p < 0.05$, tfce) are dilated for illustrative purposes, overlaid on a green skeleton.



Chapter 6. Framingham Stroke Risk score and whole-brain axial diffusivity (AD) analysis results. **Top**: FSRS at five Whitehall phases (P3 – P11) was associated with widespread higher AD values, as early as 20 years prior to scan (Model I). Change in stroke risk over the five phases was associated with widespread higher AD (Ia). **Middle & Bottom**: association remained significant with FSRS measured at P9 and at time of scan, along with change in risk over 20 years after controlling for demographic variables (model II) and in addition to socioeconomic variables (model III). No significant associations were found with lower RD values.

Model I: FSRS 10yr probability								
	Cluster	Cluster size (voxels)	Max t	p-value	MNI coordinates (x, y, z)			Structure
P3	1	17070	6.6	< 0.001	25	-5	21	R superior corona radiata
	2	973	5.97	0.028	12	-3	8	R anterior thalamic radiation
	3	86	2.62	0.049	-33	5	-2	L inferioir fronto-occipital fasciculus
	4	66	2.76	0.048	-28	-40	42	L superior longitudinal fasciculus
	5	48	2.74	0.049	36	5	25	R superior longitudinal fasciculus
P5	1	39370	7.27	< 0.001	28	-15	17	R corticospinal tract
P7	1	37855	6.39	< 0.001	26	-17	22	R corticospinal tract
P9	1	43024	8.46	< 0.001	25	-17	22	R corticospinal tract
P11	1	46836	8.6	< 0.001	-22	12	15	L anterior thalamic radiation
Ia: P11(P13)	1	51114	7.69	< 0.001	-21	11	16	L anterior thalamic radiation

Model II: Model I + age, sex, ethnicity								
	Cluster	Cluster size (voxels)	Max t	p-value	MNI coordinates (x, y, z)			Structure
P9	1	2309	4.56	0.017	-26	-21	13	L corticospinal tract
	2	2114	5.11	0.016	28	-15	17	R corticospinal tract; posterior limb of internal capsule
	3	73	3.81	0.048	34	7	19	R superior longitudinal fasciculus
	4	24	3.94	0.048	40	-10	29	R superior longitudinal fasciculus
	5	21	3.36	0.049	35	18	22	R superior longitudinal fasciculus
P11	1	3337	4.86	0.015	-21	12	15	L anterior thalamic radiation
	2	2942	4.63	0.027	22	9	38	R superior corona radiata
Ia: P11(P3)	1	1458	4.8	0.037	-21	11	16	L anterior thalamic radiation
	2	20	3.17	0.05	-31	-22	33	L superior longitudinal fasciculus

Model III: Model II + SES, education								
	Cluster	Cluster size (voxels)	Max t	p-value	MNI coordinates (x, y, z)			Structure
P9	1	2464	4.61	0.016	-25	11	32	L anterior thalamic radiation
	2	1911	5.16	0.016	25	-16	23	R corticospinal tract
	3	258	4.02	0.047	-30	-46	16	L anterior thalamic radiation
	4	43	3.83	0.047	-23	-53	20	L forceps major
P11	1	3735	5.05	0.012	-21	12	15	L anterior thalamic radiation
	2	3511	4.62	0.025	35	4	21	R superior longitudinal fasciculus
Ia: P11(P3)	1	2353	4.95	0.034	-21	11	16	L anterior thalamic radiation
	2	322	3.79	0.044	25	-17	22	R corticospinal tract
	3	117	3.74	0.047	21	13	37	R superior corona radiata
	4	85	4.26	0.046	39	-22	30	R superior longitudinal fasciculus

Chapter 6. Framingham Stroke Risk score (FSRS) and whole-brain radial diffusivity (RD) analysis results. **Top**: FSRS at four Whitehall phases (P5 – P11) was associated with widespread higher AD values (Model I). Change in stroke risk over the five phases was associated with widespread higher RD (Ia). **Bottom**: association remained significant with FSRS measured at time of scan only, after controlling for demographic variables (model II). No significant association was found with FSRS measured at any phase when controlling for all confounders (model III). No significant associations were found with lower RD values.

Model I: FSRS 10yr probability								
	Cluster	Cluster size (voxels)	Max t	p-value	MNI coordinates (x, y, z)			Structure
P5	1	61753	7.6	< 0.001	-18	8	31	Body of corpus callosum
P7	1	55088	7.83	0.001	21	13	9	L anterior thalamic radiation
P9	1	68545	7.81	< 0.001	-18	8	31	Body of corpus callosum
P11	1	73580	7.87	< 0.001	24	10	35	R superior longitudinal fasciculus
Ia: P11(P3)	1	81200	7.18	< 0.001	17	7	32	Body of corpus callosum
	2	203	4.72	0.046	-6	-51	-28	L anterior thalamic radiation

Model II: Model I + age, sex, ethnicity								
	Cluster	Cluster size (voxels)	Max t	p-value	MNI coordinates (x, y, z)			Structure
P11	1	19	4.94	0.049	-26	17	21	L superior longitudinal fasciculus

APPENDIX D

Chapter 7. Cumulative metabolic syndrome (MetS) status and whole-brain axial diffusivity (AD) analysis results. Cumulative MetS was associated with higher AD values along the forceps minor and left anterior thalamic radiation (Model I), which was no longer significant after controlling for demographic and socioeconomic variables (Models II-III).

Total Metabolic Syndrome and AD increase								
Model	**Cluster**	**Cluster size (voxels)**	**Max t**	**p-value**	**MNI coordinates (x, y, z)**			**Structure**
I	1	104	4.38	0.046	-19	30	19	forceps minor
	2	46	4.77	0.046	-30	39	9	L anterior thalamic radiation

Chapter 7. Cumulative metabolic syndrome (MetS) status and whole-brain radial diffusivity (RD) analysis results. Cumulative MetS was associated with bilaterally widespread higher AD values (Model I), which was slightly reduced but remained significant in the same regions after controlling for demographic and socioeconomic variables (Models II-III).

Total Metabolic Syndrome and RD increase								
Model	**Cluster**	**Cluster size (voxels)**	**Max t**	**p-value**	**MNI coordinates (x, y, z)**			**Structure**
I	1	36267	5.59	0.013	41	-54	46	R superior longitudinal fasciculus
II	1	30151	5.59	0.015	41	-54	46	
III	1	25019	5.72	0.016	41	-54	46	

